AD NUMBER

AD020340

NEW LIMITATION CHANGE

TO

Approved for public release, distribution unlimited

FROM

Distribution authorized to U.S. Gov't. agencies and their contractors; Administrative/Operational Use; Apr 1953. Other requests shall be referred to Wright Air Development Center, Wright-Patterson AFB, OH 45433.

AUTHORITY

AFAL ltr, 17 Aug 1979

WADC TECHNICAL REPORT 53-202

MISSILE ROLL STABILIZATION BY A FLICKER-TYPE CONTROL SYSTEM

MARTIN W. RUHNKE, PH. D.
CHARLES J. ZOET, CAPTAIN, USAF

ARMAMENT LABORATORY

APRIL 1953

WRIGHT AIR DEVELOPMENT CENTER

NOTICES

When Government drawings, specifications, or other data are used for any purpose other than in connection with a definitely related Government procurement operation, the United States Government thereby incurs no responsibility nor any obligation whatsoever; and the fact that the Government may have formulated, furnished, or in any way supplied the said drawings, specifications, or other data, is not to be regarded by implication or otherwise as in any manner licensing the holder or any other person or corporation, or conveying any rights or permission to manufacture, use, or sell any patented invention that may in any way be related thereto.

The information furnished herewith is made available for study upon the understanding that the Government's proprietary interests in and relating thereto shall not be impaired. It is desired that the Judge Advocate (WCJ), Wright Air Development Center, Wright-Patterson Air Force Base, Ohio, be promptly notified of any apparent conflict between the Government's proprietary interests and those of others.

McGregor & Werner, Inc., Wakefield, Mass.
Oct. 26, 1953 100

WADC TECHNICAL REPORT 53-202

MISSILE ROLL STABILIZATION BY A FLICKER-TYPE CONTROL SYSTEM

Martin W. Rubnke, Ph. D.
Charles J. Zoet, Captain, USAF

Armament Laboratory

April 1953

RDO No. 673-236

Wright Air Development Center
Air Research and Development Command
United States Air Force
Wright-Patterson Air Force Base, Ohio

FOREWORD

This report was prepared by Dr. Martin W. Ruhnke and Capt. Charles J. Zoet of the Armament Laboratory, Directorate of Laboratories, Wright Air Development Center and was initiated under Research and Development Order No. 673-236, "Control and Stabilization System for Guided Bombs," with Dr. Ruhnke acting as project engineer.

The authors wish to acknowledge assistance given by Mr. Jess Hoffman, formerly of the Armament Laboratory, in the form of constructive criticism and suggested methods of approach to various phases of the problem. Acknowledgement is also made of the ideas received from introductory work done by Mr. Birchard Ford, Summers Gyroscope Company and published as Air Force Memorandum Report MCREXG03, 30 October 1950.

ABSTRACT

This paper presents an analysis of a non-linear, single-axis automatic flight control system of the "flicker" type. The investigation was initiated by performing theoretical analysis of a simplified system. As a result of these approximations, it was possible to formulate generalities concerning steady state system performance. However, this method is limited by the difficulties encountered in non-linear analysis and therefore electronic simulation was applied. The results obtained from simulation not only verified the findings of the theoretical analysis, but also extended them into more difficult areas.

In the situation considered by this investigation, the controlled body acts in a normal linear manner; it is accelerated proportionally as surfaces are deflected, and it may be represented in linear transfer function terms. However, the "Flicker" type performance of the automatic control system is of a non-linear nature; its operation is preprogrammed and dependent upon airframe motion only for selection of the phase of the program to be followed. Thus the combination of control system and controlled object is non-linear in its overall performance even though most of its components are linear and may be represented by transfer functions.

A former analysis, AF Memorandum Report MCREXG03, dealt with the steady state frequency response of a "flicker" type control system in which the actuator traveled at constant speed while changing position. The investigation presented here is an extension of that study into a dual-mode type surface travel. It is an attempt to form design criteria through which system simplification and improved performance may be obtained.

PUBLICATION REVIEW

The publication of this report does not constitute approval by the Air Force of the findings or conclusions contained therein. It is published only for the exchange and stimulation of ideas.

FOR THE COMMANDER:

George L. Klingling
for JAMES H. ROTHROCK
Colonel, USAF
Chief, Armament Laboratory
Directorate of Laboratories

TABLE OF CONTENTS

LIST OF ILLUSTRATIONS

SECTION I

INTRODUCTION

1. The purpose of the following investigation was to determine:

a. the roll motion frequency response of a missile equipped with a Flicker-Type Control System for the aileron control surfaces and

b. the significance of the characteristics and the mutual relationships of the components and sub-components of the Flicker-Type Control System utilized for roll stabilization of a missile.

2.1 The three types of automatic pilots, commonly used for aircraft control, are the velocity, displacement, and force type systems described for example in pp 187-189 AF Technical Report 5677. These are linear control systems in their fundamental design, i.e., the corrective control exercised is a linear function of aircraft motion. These systems may consist of: sensing elements reacting linearly to aircraft motions - for example, angular velocity and displacement about a particular axis - actuators reacting linearly to sensing element outputs, control surfaces reacting linearly to actuators, and, for small deviations, the airframe reacting linearly to control surface deflections.

2.2 In contrast to the commonly known linear control systems as mentioned above, a Flicker Type Control System is one in which the servo response is not dependent upon the magnitude of the command signal but is programmed according to the sign of this signal. Figure 2.2.1shows a generalized block diagram of the closed loop including the missile and a flicker type control system in one of the several possible arrangements. The plots adjacent to the main components are to demonstrate their operational performances in a qualitative manner. There are other varieties which are similar to this type deviating slightly in one or more sub-components, for example, the servo response may depend upon the amplitude in a stepwise manner, including a zero bound dead zone.

The block diagram of the roll control system considered by this report is shown in Figure 2.3.1. The roll angular velocity of the motion of the missile (1) is sensed by a gyroscope (2) and its rate output signal is integrated (3) to yield the missile angular displacement. Both values, rate and displacement represented as electrical signals, are added in a predetermined proportion (4) and form the "summing command". When the sign of the combined signals (the summing command) changes, a discriminator relay (5) (sometimes called "phase detector") engages the actuator (6) to drive the surfact into one direction with a given fixed angular velocity; it continues to drive the surface in this direction until either a reversing signal is received or a physical stop is encountered. The missile reverses its direction of roll accordingly, and the whole process repeats itself continuously. For this investigation the missile is considered to be undamped in the roll axis.

In a system described later, the surfaces are released upon change in sign of the mixer signal, driven to the null position by the opposing torque of the airstream, and then motor driven to the opposite side. A system with this performance is called the "feathering type" flicker control system. Surface deflections introduce proportional torques and, since the missile is assumed to be undamped about the longitudinal axis, they can be considered in terms of missile angular roll acceleration. Because of the flip-flop or flicker characteristic of the relay, this system will have a steady state of oscillation.

It can be seen from Figure 2.3.1 that there are two major sources of non-linearities in this type of control system which do not generally exist in more conventional autopilots, namely, the so called flip-flop action of the relay and, because of certain design characteristics, the fact that the control surfaces may reach the physical limits in their travel. This, incidentally, is a necessity for the proper performance if the curve of the surface travel plotted against time is symmetrical with respect to a vertically drawn middle line. The Flicker Type System is, therefore, a basically non-linear type of the control system.

The moment at which the mixer signal changes sign is said to be the "tripping point" or "trigger point" i.e., the point at which the control surfaces should begin to move back towards the neutral position. Assuming a steady state of the missile roll oscillation, the surface motion is a periodic (non-sinusoidal) oscillation whose frequency obviously has to be the same as that of the missile. The period of this oscillation is determined by twice the time elapsed between two consecutive tripping points. The period of oscillation (for a given individual system) depends on the phase lag of the rate gyro output signal, relative to the true angular roll velocity component, and on the ratio of the gain factors by which the rate gyro signal and the displacement signal (obtained by integrating the rate signal) are amplified before being fed to the mixer. Since these two components can be easily varied to gain desired reponses, their influence, as system parameters, is of particular interest. The other components which may be adjusted are actuator speed, range of surface travel, and surface effectiveness.

It will be seen that for the feathering type system (when the curve representing the surface travel is composed of straight lines and when physical stops are not encountered) the amplitude of the oscillation is affected in a linear fashion with respect to these latter components over large performance ranges, but that these have no effect upon the frequency of missile oscillation. However, when physical stops are encountered, both the range of travel and the actuator speed become factors in determining frequency. The absolute magnitude of the summing command signal (velocity component plus position component) has no significance as long as it is appreciably greater than the threshold value of the relay. Hence only parameters which affect the change of sign in this mixer signal (summing command), in respect to time, are to be considered.

SECTION II

REAC SIMULATION DESCRIPTIONS

3.1 It is well known that an attempt to perform an analysis of any system, which includes pronouncedly non-linear functions, is necessarily tedious, difficult, and time consuming. Certain problems involving simple, periodic, non-linear functions sometimes lend themselves readily to a solution. However, the non-linearities involved in the control system under consideration do not fit into this category and, hence, mathematical analysis of this problem in its entirety will be highly complex; the final solution would very likely be in a form which would render applications difficult.

However, some mathematic solution of the problem is desirable as a guide by which other investigations may be gauged. Mathematical analysis is therefore performed for a simplified system and yields certain valuable approximations to the problem. For more complete and quick information on missile behavior, an electronic analogue computer was used for simulation. Most of the complexities of the system were included in this solution. The varying of parameters, to investigate resulting system changes, which prove difficult by mathematical means, is easily accomplished on the simulator. Hence the burden of this investigation was borne by electronic analogue simulation. In addition, the results obtained from simulation research were frequently a helpful guide in the attempt to find generalized mathematical formulations or graphs for approximate solutions of problems resulting from the changing of parameters. Such graphs can be used advantageously for design work.

3.2 The generalized system, as it is considered for simulation on a Reeves Electronic Analogue computer, has been represented in Figure 2.3.1. For simulation, the missile body is treated in the manner given in Figure 3.2.1. The input δ_a representing the roll acceleration due to surface deflection is integrated twice by the missile. The first integration yields the missile angular roll rate component to which the rate gyro (block #2 in Figure 2.3.1) is sensitive. The second integration by the missile yields the missile angular roll displacement which is not directly utilized for control purposes.

The characteristics of the rate gyro (block #2, Figure 2.3.1) are described in detail by Figure 3.2.2 (upper part). The gain of the gyro system, i.e., volts output per degree sec^{-1} input, is of no significance in determining the zero points of the mixer signal; the zeros are determined only by the ratio of the rate signal amplitude to the displacement signal amplitude, as will be shown. However, in order to obtain a comparison between true roll angular velocity (input) and indicated angular roll velocity (output) for evaluation purposes, this gain factor, as well as certain characteristics of the simulator setup must be considered. By assuming, in the classical representation of a gyro,

$$(1) \qquad \ddot{D} + B\dot{D} + KD = -G_1\dot{\varphi}$$

a steady state related to a step input, it is seen that

$$(2) \qquad D = -\frac{G_1}{K}\dot{\varphi}$$

In the REAC setup for a rate gyro, seen in Figure 3.2.2, (lower part)

$$\dot{\varphi}^* = abD \qquad B = ac \qquad K = abd$$

and the input is $G_1\dot{\varphi}$; substituting these values in

equation (2) yields, (3) $\varphi'^{*} = -\frac{G_1}{d}\varphi'$. Hence, in this setup, true and indicated angular roll velocities are related by the factor d/G_1 . For example, consider a gyro which has a frequency of 5.033 cps and a damping ratio (ξ) = 0.316; then

$$\omega_n = 31,623 \quad K = \omega_n^2 = 1000 \quad \text{and} \quad B = 2\xi\omega_n = 20.$$

It can be seen that the gains of the setup, which determine B and K, are the individual gain factors a and c, and a, b, and d respectively. The operator will choose a reasonable combination of a, b, c, d, for the purpose of simulation. If, for instance,

$$G_1 = 8 \quad a = 10 \quad b = 10 \quad c = 2 \quad d = 10, \text{ then } B = 20 \quad K = 1000$$

and the factor by which φ'^{*} is to be multiplied to obtain a steady state output signal of unity magnitude for a step input signal of unity magnitude is d/G_1.

It has been previously stated that the signals utilized for control of the missile are "indicated angular roll rate" and "indicated roll angle" obtained from the former by an integrating motor (block #3, Figure 2.3.1). The sole purpose of the mixing device (block #4, Figure 2.3.1) is to sum these signals continuously in a predetermined proportion. Schematic details of this operation are shown in Figure 3.2.3 with its REAC simulation. Since only the relative magnitude of these signals and not their absolute values affect the operation of the control system, the gain of the rate signal is arbitrarily considered to be unity. Thus in this setup the ratio of

$\frac{\text{Gain factor of the rate signal}}{\text{Gain factor of the displacement signal}}$ is simply $1/G_2$.

The phase detector (block #5, Figure 2.3.1) is shown with two different types of simulation by which it was represented in Figure 3.2.4. In spite of a comparatively large time delay inherent in the computer, the REAC simulation for the discriminator proved satisfactory for the non-feathering type control system; it was not satisfactory for the faster operating feathering control system for which the discriminator was simulated by an Armour Special Function Generator which has less time delay. The output of the discriminator has a very good rectangular wave form with frequency identical to that of the mixer signal and a constant amplitude.

The motor actuator (block #6, Figure 2.3.1) drives the control surfaces as programmed by the relay output. The motor runs at constant speed, and hence the position of the ailerons, until they arrive at physical stops, is the integral of the relay signal. In some systems (non-feathering type) the surfaces will contact stops in normal, steady state oscillation; in others (some of the feathering type) they may contact stops only when the missile is subjected to disturbing torques. The motor actuator is prevented from operating at constant speed by the varying torque of the airstream and, also initially, by the inertia of the body, Thus, while the deflection of the aileron is considered here to be graphically represented by a straight line, in reality it will be slowed slightly, as deflection increases, by the increasing opposing torque of the airstream. However, because the actuator output is large with respect to any load placed upon it, a general picture of system operation is gotten without considering the time delays in the actuator. A later, detailed analysis

is made in which the effect of including the time delay due to inertia is investigated. However, wind tunnel tests indicate that the loading effect caused by the airstream is negligibly small.

The REAC simulations for non-feathering and feathering actuators appear in Figures 3.2.5 and 3.2.6 respectively. The following paragraphs are a detailed description of their operation:

A. Non-feathering actuator: The REAC setup (Figure 3.2.5) simulating a non-feathering actuator, with no time lag, is an integrating amplifier connected with a limiting device. Their combined effect is as follows:

a. To simulate the control surfaces being driven by the constant speed motor; the relay signal is integrated.

b. This integration continues until the voltage output of the amplifier is equal to a preset value in the limiter at which time the integration stops and the output voltage holds constant, simulating the action of the control surface as it contacts a physical stop.

c. When the relay signal changes sign, the integration process resumes and the output voltage of the amplifier, which has been held at a preset level, changes accordingly, thus simulating the surface being driven back to zero and deflected to the opposite side.

B. Feathering System:

A flicker-type system in which the deflected control surface is allowed to "free-wheel" back to the neutral position propelled only by the opposing torque of the airstream is called a Feathering Flicker Type System. A simplified analysis of the feathering system is made by consi-

dering it to be the equivalent of a non-feathering system in which the outbound actuator speed is slower than the inbound speed.

No accurate data relating to the aerodynamic performance of the control surfaces when free-wheeling are available. Even if such data were available the coefficients involved would assume different values under various conditions such as different airspeeds and densities; also, the clutch, by which the surface is engaged to and released from the actuator, by its very nature, introduces a variable delay. Hence, because of the uncertainty as to the exact dynamic characteristics of these surfaces during the feathering period, it was found that the results of this investigation would not be changed significantly if this second order system were replaced by a first order system. The errors introduced by such a simplification are not greater than those which would originate in selecting one particular fixed quadratic as representative of the entire range of surface operation.

A graphic representation of the "free-wheeling" control surface would very likely show it to be a nearly critically damped oscillation. The spring constant supplied by the airstream, and the moment of inertia of the control surfaces are such that the surface system has a high natural frequency. Thus, the time taken by the "free-wheeling" surfaces in reaching the neutral position when returning from a deflection is comparatively small and independent of the amplitude of deflection. However, this time determines the point at which the surfaces are again engaged to the actuator. Because of the high frequency by which the surface system feathers, the integral of the curve representing the surface travel versus time during

the feathering time will be relatively small compared with the integral of the preceding portion covered by the outbound curve; in other words, there will be only a small change of the roll velocity during the feathering operation. Consequently the system may be simulated, without sacrifice to accuracy, by any other system which has a relatively small integral and would reproduce the time required in returning to the null position. Consider, for example, an exponential of the form $f(t) = (\delta_a + \frac{a}{q}) e^{-qt} - \frac{a}{q}$ where δ_a = surface deflection at the reversing point, a = constant, and $q = \frac{1}{T}$; T = Time constant. Such a function may be made to be zero at any reasonable desired time for a given deflection. The amplitude of the surface at the reversing point was found to be from 10^o- 20^o for most conditions considered by this investigation. For a fixed value of q the time consumed for the surface travel from δ_a to zero will differ only by a few milliseconds as the amount of deflection under different flight conditions varies. This variation, however, can be considered negligible for the purposes of this investigation.

Until the relay signal changes sign the simulation of the feathering system isequal or similar to that for the non-feathering system. Then, rather than returning to zero along a straight line, the signal returns along an exponential path and after that follows a straight line outbound. This simulation is accomplished in the manner shown in Figure 3.2.6 which is described as follows:

The output of the Special Function Generator "A" representing the discriminator relay (Block #5 in Figure 2.3.1) has been previously described to be dependent for sign upon the summing command and of fixed absolute

amplitude $G_3 \frac{\psi}{|\psi|}$. Assume this sign to be positive; it is fed into both the limiting integrating amplifier and into a summing amplifier. The integrating amplifier output is connected to a second special function generator "B". Its output $G_3 \cdot \frac{\delta_a}{|\delta_a|}$ has the same amplitude as "A" but its sign depends on the integrating amplifier output. The output from generator "B" is also fed to the summing amplifier. If $G_3 \frac{\psi}{|\psi|}$, as assumed, has been positive for some time, $G_3 \frac{\delta_a}{|\delta_a|}$ will be negative and, as their amplitudes are equal but of opposite sign, the summing amplifier output is zero and the relay controlling the integrating amplifier feedback remains open. Suppose the summing command changes the sign and consequently "A" changes its sign. Then the output of the summing amplifier becomes suddenly negative and closes the relay in the integrating amplifier feedback thus, according to the above equation, causing an exponential decay of the integrating amplifier signal which passes through the null position to a signal of opposite polarity. However, the very instant when the integrating amplifier output signal changes its polarity the output of generator "B" changes its sign, too, thus producing again a zero output of the summing amplifier and the opening of the feedback circuit allowing the integrating amplifier to resume its integrating function starting from zero. Figure 3.2.7 is a graphic representation of the signal sent to the missile. At time 0 the integrating amplifier begins its output; at T_1 generator "A" changes sign resulting in the exponential decay; at T_2 the exponential decay has reached the null position and generator "B" changes sign causing the relay to open; at T_3 the generator "A" changes sign again, etc.

Several components of the Flicker Type System have inherent time delays. Some of these, even though they are relatively small, could be significant. Therefore, the REAC setup shown in Figure 3.2.8 was used to investigate this possibility. A desired time delay could be introduced at any point in a setup by merely inserting this arrangement of amplifiers into the circuitry. The setup is similar to that normally used to simulate a first order system. Consider the time delay effect for example on an integrating motor. If the motor is assumed to have negligible moment of inertia so that it may be represented as a pure integrator its transfer function may be expressed in standard La Place terminology as $\frac{1}{s}$. When a step voltage is applied to this motor the result is such that $\mathcal{L}[\Theta_o] = \frac{K}{s^2}$; where K is the magnitude of the step; in the time domain $\Theta_o = K \cdot t$. If the moment of inertia of the motor is considered significant, a time delay results. By introducing the time delay the transfer function of the motor becomes $\frac{q}{s(s+q)}$. When a step is applied the result is such that $\mathcal{L}[\Theta_o] = \frac{K \cdot q}{s^2(s+q)}$ or in the time domain: $\Theta_o = K[t - \frac{1}{q}(1-e^{-qt})]$.

Question may be raised concerning the factor q in the setup (i.e., the q in the numerator of the transfer function). If this factor was omitted the result would be $\Theta_o = \frac{K}{q}[t - \frac{1}{q}(1-e^{-qt})]$. It can be seen that such an arrangement would introduce a change in steady state value of the motor output speed. Since it is desired only to intorduce a time delay, the "q factor" is accordingly included in the setup.

The Discriminator Relay has been mentioned as sensing a change in sign with ideal accuracy. In reality, a certain magnitude of change must occur before the relay becomes cognizant of the change. This magnitude,

necessary to obtain a response from the relay, is said to be its dead space. A similar dead space (due to play in the actuator linkage) often occurs in mechanical systems possessing a restoring force. This dead space was simulated by the REAC setup shown in Figure 3.2.9 with Z_o being the mixer signal as it is sensed by the relay. The change of sign of this signal occurs somewhat later than the true change.

SECTION III

THEORETICAL CONSIDERATIONS

4.1 A brief comparison between the performance of an airframe equipped with a conventional autopilot and a missile controlled by a flicker type control system will help to clarify the problem of investigating the performance of a flicker type system. A conventional autopilot in an airframe reacts to a disturbance in the manner shown in Figure 4.1.1. A disturbance occuring at t_o results in displacing the airframe from its original position. The surface is deflected instantaneously by the autopilot so as to counteract this deviation. However, before the airframe reaches its zero position, t_2, the influence of the velocity signal causes the control surface to pass through its zero position thus producing a lead of control surface deflection relative to airframe displacement. The airframe overshoot during the next half cycle is then greatly reduced. This is repeated for perhaps one more oscillation (as at t_3 and t_4) until both vehicle and control surface are again in their original positions. During this entire process the action of the control surface was continuously dictated by outputs of sensing elements reacting to various components of airframe motion. A vehicle equipped with such

a control system is said to have a quiescent zero position.

A system consisting of a missile with a flicker type control has no such quiescent zero position. It is continuously in oscillation even when in the undisturbed state. The magnitude and frequency of this oscillation are well defined and maintained. The reason for this behavior is that the surface motion is dependent on the missile motion in a discontinuous stepwise manner. It responds to missile travel on one side or the other of a zero position by surface travel to an extreme position. There is no provision for the surface to remain in a neutral position and, hence, even if the missile were to assume a zero position by pure accident, it would be forced from this state by the surface travel.

4.2 From what has been said previously one might conclude that only a signal which is a linear function of missile position is necessary for a flicker type control. However, a system using only an angular position signal is shown by the following consideration to be unworkable. Consider a system in which a sensing device detects change of missile position to either side of a zero position. This activates an actuator to drive the control surface at a constant speed to the extreme position which tends to return the missile to the opposite side of zero. Assume that such a system be workable. It would result in the periodic acceleration curve shown in Figure 4.2.1. Such an acceleration curve would yield the position curve also shown in Figure 4.2.1. The operating condition, i.e., the position = zero at tripping, is shown to be feasible only if the surface travels from one extreme to the other in zero time as shown in Figure 4.2.2. This is practically unworkable and is rendered more so by the fact that any detector used would contribute

a phase lag to the position signal.

Assume next a system which triggers on zeros of velocity only. Such a system if workable must present a periodic acceleration which would yield the velocity curve shown in Figure 4.2.3. It can be seen that the velocity zero must occur in the middle of the surface dwell period. Hence, such a system can work only if the trigger line, i.e., zero point of velocity, coincides with the midpoint of the surface dwell; this is possible only if surface dwell time is zero, as shown in Figure 4.2.4. However, such a system does not sense minor deviations which occur at a very low rate, and the system will drift from the zero line.

Since angular velocity and position are the most reliably obtained components of missile motion, one next considers a possibility of using a combination of roll angular velocity and angular position to trigger the system. Consider a system which triggers whenever:

Gain factor (g_1) x Velocity Signal + Gain

Factor (g_2) x Position Signal = 0.

If such a system were to operate ideally, the components of missile motion would have the relationship shown in Figure 4.2.5. The operation of this system is not as immediately obvious as were the two preceding systems but can be ascertained only by analysis. Hence, a theorectical analysis of this system is presented in paragraph 4.3.

4.3 The following is a theoretical analysis of a somewhat generalized flicker type control system. The system considered operates as follows: The control surface is driven out from the neutral position at K_1 degrees per second; it continues outbound until (1) it reaches physical limits or (2)

it reaches a position at which the velocity component is some predetermined fraction of and opposite in sign to the position component. In either case when gain terms, in a ratio inverse to this fraction, are applied to the angular velocity and position signals, and when the sum of the resulting signals equals zero, the system triggers. At this moment the control surface returns to neutral at K_2 degrees per second, is driven to the opposite side at K_1 degrees per second, and the cycle repeats. The following nomenclature is used for this analysis:

K_1 = Outbound surface velocity. (Deg/Sec)

K_2 = Inbound surface velocity. (Deg/Sec)

g_1 = Gain term on the velocity signal. (1)

g_2 = Gain term on the position signal. (1/Sec)

$R = g_2/g_1$. $\left[\frac{1}{sec}\right]$

τ = Time to drive surfaces from neutral to stops. (Sec)

$M\tau$ = Time surface spends at stops in each half cycle. (Sec)

$P = K_1/K_2$. (1)

V = Missile Angular Velocity. (Deg/Sec)

V* = Indicated Missile Angular Velocity (Deg/Sec)

D = Missile Angular Position (Deg)

D* = Indicated Missile Angular Position (Deg)

V_{max} = Maximum velocity. (Deg/Sec)

D_{max} = Maximum displacement (Deg)

V_τ = Velocity when system triggers (Deg/Sec)

D_τ = Position when system triggers (Deg)

t_o = Time at which velocity is zero. (Sec)

T = Time at which tripping occurs (Sec)

This analysis is based upon the following assumptions:

1. The system is in steady state oscillation.

2. The missile is assumed to have no damping about the roll axis.

3. At tripping: $V_T = RD_T$ or $g_1 V_T = g_2 D_T$.

4. $K_2 \geq K_1$ *i.e.* $P \leq 1$

5. Surface effectiveness is assumed to be $1^o/sec^2$ per degree surface deflection.

Effectiveness may be introduced into these considerations by multiplying the surface velocities K_1 and K_2 by the effectiveness factor. Missile response will be investigated with respect to missile frequency and amplitude of oscillation as they are related to P, R, V, and τ .

Surface deflections, in the system described above, will impart a torque to the missile which is proportional to the amount of deflection; the missile roll acceleration is proportional to this torque. Disregarding time delays, a single cycle of roll acceleration may be represented as shown in Figure 4.3.1. Roll acceleration is obtained by multiplying surface deflection by effectiveness. Symbolic representation of a cycle of surface deflection is given in the following six equations:

1. $A = K_1 t_1$ if $0 \leq t \leq \tau$

2. $A = K_1 \tau$ if $\tau \leq t \leq (1+M)\tau$

3. $A = K_1 \tau - K_2 t_3$ if $(1+M)\tau \leq t \leq (1+M+P)\tau$

4. $A = -K_1 t_4$ if $(1+M+P)\tau \leq t \leq (2+M+P)\tau$

5. $A = -K_1\tau$ if $(2+M+P)\tau \leq t \leq (2+2M+P)\tau$

6. $A = -K_1\tau + K_2 t_6$ if $(2+2M+P)\tau \leq t \leq 2(1+M+P)\tau$

The time intervals listed above are hereafter designated interval 1, 2, 3, etc. in the order listed: $t_1 = 0$ at the beginning of interval 1, $t_2 = 0$ at the beginning of interval 2, etc. "t" represents continuous time from the beginning of the cycle.

The roll velocity is the integral of roll acceleration which is symmetrical about the time axis (A = 0). Hence, the roll velocity will be symmetrical about an axis parallel to the time axis and since the missile is assumed to be controlled about a given point, this axis must be the line V = 0. Roll velocity is described by the following equations:

7. $V = \int K_1 t_1\, dt_1 + C = \frac{K_1 t_1^2}{2} - V_{max}$ if $0 \leq t \leq \tau$

(Where it is assumed that A(o) = 0 and hence V(o) = V_{max} or V_{min} and is arbitrarily taken as V_{min} which by symmetry is - V_{max})

8. $V = K_1\tau t_2 + \frac{K_1\tau^2}{2} - V_{max}$ if $\tau \leq t \leq (1+M)\tau$

9. $V = K_1\tau t_3 - \frac{K_2 t_3^2}{2} + \frac{K_1\tau^2}{2} + K_1 M\tau^2 - V_{max}$ if $(1+M)\tau \leq t \leq (1+M+P)\tau$

10. $V = V_{max} - \frac{K_1 t_4^2}{2}$ if $(1+M+P)\tau \leq t \leq (2+M+P)\tau$

11. $V = V_{max} - \frac{K_1\tau^2}{2} - K_1\tau t_5$ if $(2+M+P)\tau \leq t \leq (2+2M+P)\tau$

12. $$V = V_{max} - \frac{K_1 \tau^2}{2} - K_1 M \tau^2 - K_1 \tau t_6 + \frac{K_2 t_6^2}{2}$$

if $$(2+2M+P)\tau \leq t \leq (2+2M+2P)\tau$$

When $t = (1+M+P)\tau$, $V = V_{max}$ (See Figure 4.3.1) which when substituted in (9) yields:

$$V_{max} = \tfrac{1}{2} K_1 \tau^2 + K_1 M \tau^2 + \tfrac{1}{2} K_1 P \tau^2 - V_{max}$$

from which: (13) $$V_{max} = \tfrac{1}{4} K_1 \tau^2 (1+2M+P)$$

Also from Figure 4.3.1, it can be seen that tripping occurs at $t = (1+M)\tau$ which when substituted in (8) yields:

$$V_T = K_1 M \tau^2 + \tfrac{1}{2} K_1 \tau^2 - V_{max}$$

from which: (14)
$$V_T = \tfrac{1}{4} (K_1 \tau^2)(1+2M-P)$$

t_o is defined as the point at which $V = 0$. This is the point at which the area under the acceleration curve, from $t = 0$ to $t = (1+M+P)\tau$ is divided in half. Examination of the curve and considering a previous assumption that $K_2 \geq K_1$ reveals that t_o could lie in either the first or second time interval.

Case I If t_o is in the first time interval, it may be substituted for t_1 in (7). This yields: $$0 = \tfrac{1}{2} K_1 t_o^2 - V_{max} \quad \text{or}$$

(15) $$t_o = \tau \sqrt{\tfrac{1}{2}(1+2M+P)}$$

Case II If t_o is in the second time interval it can be substituted in (8) for t_2. This yields:

$$0 = \tfrac{1}{2} K_1 \tau^2 + K_1 \tau t_o - V_{max}$$

or: (16) $t_o = \frac{\tau}{4}(-1+2M+P)$ where "t_o" is calculated from the beginning of the second time interval so that the actual time is $t = t_o + \tau$.

The Displacement is the Intergral of Velocity with its minimum and maximum at zero velocity. Therefore the greatest change in displacement $D_{max} - D_{min}$ is represented by:

$$D_{max} - D_{min} = \int_{t_o}^{(1+M+P)\tau + t_o} V(t)\,dt$$

Velocity, a function symmetrical about V = 0 and since the missile is assumed to be in a steady state of undisturbed oscillation it may be assumed that the point about which it oscillates is D = 0 and that displacement will be symmetrical about this point. Therefore:

17. $$D_{max} = -D_{min} = \frac{1}{2}\int_{t_o}^{(1+M+P)\tau + t_o} V(t)\,dt$$

Displacement at the tripping point will therefore be:

18. For Case I:
$$D_{T_1} = -\frac{1}{2}\cdot\int_{t_o}^{(1+M+P)\tau+t_o} V(t)\,dt + \int_{t_o}^{\tau} V(t_1)\,dt_1 + \int_0^{M\tau} V(t_2)\,dt_2$$

19. For Case II:
$$D_{T_2} = -\frac{1}{2}\int_{t_o}^{(1+M+P)\tau+t_o} V(t)\,dt + \int_{t_o}^{M\tau} V(t_2)\,dt_2$$

These are shown to be identical by the following considerations:

Expanding equation (18): $D_{T_1} = -\frac{1}{2}\int_{t_o}^{\tau} V(t_1)\,dt_1 - \frac{1}{2}\int_0^{M\tau} V(t_2)\,dt_2$

$$-\frac{1}{2}\int_0^{P\tau} V(t_3)\,dt_3 - \frac{1}{2}\int_0^{t_o} V(t_4)\,dt_4 + \int_{t_o}^{\tau} V(t_1)\,dt_1 + \int_0^{M\tau} V(t_2)\,dt_2$$

Gathering terms and using the fact that $V(t_4) = -V(t_1)$

20. $$D_{T_1} = \frac{1}{2}\int_0^{\tau} V(t_1)\,dt_1 + \frac{1}{2}\int_0^{M\tau} V(t_2)\,dt_2 - \frac{1}{2}\int_0^{P\tau} V(t_3)\,dt_3$$

Expanding (19) in a similar manner $D_{T_2} = -\frac{1}{2}\int_{t_o}^{M\tau} V(t_2)\,dt_2 - \frac{1}{2}\int_{0}^{P\tau} V(t_3)\,dt_3$

$-\frac{1}{2}\int_{0}^{\tau} V(t_4)\,dt_4 - \frac{1}{2}\int_{0}^{t_o} V(t_5)\,dt_5 + \int_{t_o}^{M\tau} V(t_2)\,dt_2$

and using the fact that $V(t_4) = -V(t_1)$ and $V(t_5) = -V(t_2)$

$$(21)\quad D_{T_2} = \frac{1}{2}\int_{0}^{\tau} V(t_1)\,dt_1 + \frac{1}{2}\int_{0}^{M\tau} V(t_2)\,dt_2 - \frac{1}{2}\int_{0}^{P\tau} V(t_3)\,dt_3$$

(20) = (21) i. e., $D_{T_1} = D_{T_2}$

Evaluating for D_T by substituting values for $V(t_1)$ etc. in equation (20)

$$D_T = \frac{1}{2}\int_{0}^{\tau}\left(\frac{K_1 t_1^2}{2} - V_{max}\right)dt_1 + \frac{1}{2}\int_{0}^{M\tau}\left(K_1\tau t_2 + \frac{K_1\tau^2}{2} - V_{max}\right)dt_2$$

$$-\frac{1}{2}\int_{0}^{P\tau}\left(K_1\tau t_3 - \frac{K_2 t_3^2}{2} - \frac{K_1\tau^2}{2} + K_1 M\tau^2 - V_{max}\right)dt_3$$

$$D_T = -\frac{V_{max}\,\tau(1+M-P)}{2} + \frac{K_1 M\tau^3}{4} + \frac{K_1 P\tau^3}{4} - \frac{K_1 MP\tau^3}{2}$$

$$+ \frac{1}{2}\left|\frac{K_1 t_1^3}{6}\right|_0^{\tau} + \frac{1}{2}\left|\frac{K_1\tau t_2^2}{2}\right|_0^{M\tau} - \frac{1}{2}\left|\left(\frac{K_1\tau t_3^2}{2} - \frac{K_2 t_3^3}{6}\right)\right|_0^{P\tau}$$

$$D_T = -\frac{K_1\tau^3}{4}\left[\frac{(1+2M+P)(1+M-P)}{2} - M - P - 2MP - \frac{1}{3} - M^2 + \frac{P^2}{6}\right]$$

$$(22)\quad D_T = -\frac{K_1\tau^3}{4}\left(\frac{1}{6} + \frac{M}{2} + \frac{3MP}{2} + P + \frac{P^2}{6}\right)$$

The introductory description of the system contains the condition for tripping $V_T = -RD_T$. Substituting from equation (14) and (22):

$$\frac{K_1\tau^2}{4}(1+2M-P) = \frac{RK_1\tau^3}{24}(1+3M+9MP+6P+P^2)$$

(23) From which $M = \frac{R\tau + 6R\tau P + R\tau P^2 - 6 + 6P}{12 - 9R\tau P - 3R\tau}$ and $\tau = \frac{6(1+2M-P)}{R(1+3M+9MP+6P+P^2)}$

It is of considerable interest to note here that, while surface speeds were significant in calculating actual values of velocity and displacement, they enter into frequency considerations only insofar as they determine the time taken in reaching physical stops (τ). Two cases of particular interest are the case involving no physical stops, i. e., $M = 0$, and the case where outbound surface velocity equals inbound surface velocity i.e.,

$$K_1 = K_2 \quad or \quad P = 1$$

Case where M = 0 (no physical stops)

(24) $$\tau = \frac{6(1-P)}{R(1+6P+P^2)}$$

Here it can be seen that if M = 0 and P = 1 the system cannot operate. Case where P = 1 (one inbound and outbound surface velocity)

(25) $$M = \frac{2R\tau}{3(1-R\tau)} \quad or \quad \tau = \frac{3M}{R(2+3M)}$$

The period of oscillation in the general case is, from inspection of Figure 4.3.1, $2(1+M+P)\tau$. For the special cases: if P = 1 the period is $2(2+M)\tau$ and if M = 0 the period = $2(1+P)\tau$. The maximum oscillation of the missile is shown in (17) to be:

$$D_{max} = -D_{min} = \frac{1}{2}\int_{t_o}^{(1+M+P)\tau + t_o} V(t)\,dt$$

where t_o is the time at which the angular roll velocity is zero. As has been discussed earlier in this analysis $t_o = t_1$ or t_2. t_o has been calculated in equation (15) and (16). In Case I, if $t_o \leq \tau$, $t_o = \tau\sqrt{\frac{1+2M+P}{2}}$ But since t_o is not easily determined it is desirable to state these conditions without reference to t_o. Using the condition for Case I that $t_o \leq \tau$ we have

26. $$\tau \geq \tau\sqrt{\frac{1+2M+P}{2}} \quad or \quad 1 \geq 2M+P$$

Similarly for Case II, $t_o = t_2$, and from equation (16) $t_o = (-1+2M+P)\frac{T}{4}$

To have any meaning $t_o \geq 0$ and hence:

27. $1 \leq 2M+P$

Calculating the maximum amplitude for Case I

$$D_{max} = -D_{min} = \frac{1}{2} \cdot \int_{t_o}^{(1+M+P)\tau} V(t)\,dt$$

$$D_{max} = \frac{1}{2}\int_{t_o}^{\tau} V(t_1)\,dt_1 + \frac{1}{2}\int_{0}^{M\tau} V(t_2)\,dt_2 + \frac{1}{2}\int_{0}^{P\tau} V(t_3)\,dt_3 + \frac{1}{2}\int_{0}^{t_o} V(t_4)\,dt_4$$

28. $$D_{max} = \frac{K_1\tau^3}{24}\left[2\sqrt{2}(1+2M+P)^{3/2} - 1 - 3M + 3MP + P^2\right]$$

Likewise determining the maximum amplitude for Case II in which

$1 \leq 2M+P$ and $t_o = (-1+2M+P)\frac{\tau}{4}$

$$D_{max} = \frac{1}{2}\int_{t_o}^{(1+M+P)\tau+t_o} V(t)\,dt = \frac{1}{2}\int_{t_o}^{M\tau} V(t_2)\,dt_2 + \frac{1}{2}\int_{0}^{P\tau} V(t_3)\,dt_3$$

$$+ \frac{1}{2}\int_{0}^{\tau} V(t_4)\,dt_4 + \frac{1}{2}\int_{0}^{t_o} V(t_5)\,dt_5$$

29. $$D_{max} = \frac{K_1\tau^3}{96}\left(7 + 24M + 18P + 24MP + 7P^2 + 12M^2\right)$$

Now consider the system to have a steady state in which the surface dwells in its extreme position for part of the cycle, i.e., $M \geq 0$. If we consider the two extreme values for P, $P = 1$ or $P = 0$, we get the following equalities:

30. From equation (25) if $P = 1$ $\quad M = \frac{2R\tau}{3(1-R\tau)}$

31. And substituting $P = 0$ in 23. $\quad M = \frac{R\tau - 6}{3(4-R\tau)}$

in 30. $M > 0$ only if $0 < R\tau \leq 1$

Consider τ to be some fixed time as it will be in the practical case; then, as R varies from 0 to $\frac{1}{\tau}$, M increases in value and the frequency decreases. In 31. $M>0$ only if $4<R\tau\leq 6$ or $\frac{4}{\tau}<R\leq\frac{6}{\tau}$. Again considering τ fixed it is seen that varying R from $\frac{4}{\tau}$ to $\frac{6}{\tau}$ results in decreasing M and increasing the frequency. If one considers that the effect of varying R is exactly reversed for extreme values of P, it occurs that there must be some sort of a crossover value of P. Considering $\tau=\frac{1}{6}$ sec the values of R which yield $M=\infty$ or 0 c.p.s., and M = 0 or no dwell time, are plotted against varying values of P in Figure 4.3.2. It is seen that the "infinite dwell" line and "no dwell" line intersect at about P = 0.13. This is superficially interpreted to indicate a condition in which, if the surface does contact its stop prior to reaching a triggering condition, the system will not operate. Granting that this value of P may be considerably altered for practical cases, it can be assumed that the point still exists and will be a critical point in system operation. It is noted that for the value $\tau=\frac{1}{6}$ sec this point occurs very near to the value of P which could be yielded by a feathering system; the symmetrical case, i.e., P = 1 is far away from this point. Furthermore, by differentiating in

(23) $$\frac{\partial M}{\partial R}=\frac{6\tau(11P^2+6P-1)}{(12-9R\tau P-3R\tau)^2}$$

from which it can be seen that, while varying τ does vary the magnitude of $\frac{\partial M}{\partial R}$ for any given value of R, varying τ does not change the value of P for which $\frac{\partial M}{\partial R}=0$ i.e., the changeover point. Since the investigation of the subject under discussion has not been carried any farther in an extensive manner, it should be kept in mind that the picture may change significantly when practical limitations are considered. However, there is a certain

indication that even in the practical case such a point might exist and should be approached with caution.

Reference to equation (24) shows that, for the "no dwell" condition, τ decreases as R increases. That is: increasing R increases frequency. It is noted that the condition placed upon the overall system, $V_T = -RD_T$ eliminates the symmetrical case with no dwell.

The following are the more important equations developed by these considerations where the surface effectiveness is $1^o/sec^2$ per degree surface deflection. Only equations involving K_1 will be affected by changing the effectiveness. This would be accomplished by substituting C for K_1 where $C = EK_1$; E being the effectivity factor.

$$V_{max} = \frac{1}{4} K_1 \tau^2 (1+2M+P)$$

$$D_{max} = \frac{K_1 \tau^3}{24} \left[2\sqrt{2} (1+2M+P)^{3/2} - 1 - 3M + 3MP + P^2 \right] \quad \text{if } 1 \geq 2M+P$$

$$D_{max} = \frac{K_1 \tau^3}{96} (7 + 24M + 18P + 24MP + 7P^2 + 12M^2) \quad \text{if } 1 \leq 2M+P$$

$$V_T = \frac{1}{4} K_1 \tau^3 (1+2M-P)$$

$$D_T = -\frac{K_1 \tau^3}{24} (1+3M+9MP+6P+P^2)$$

$$V = 0 \quad \text{when } t = \tau \sqrt{\frac{1+2M+P}{2}} \quad \text{if } 1 \geq 2M+P$$

$$\text{when } t = (3+2M+P)\frac{\tau}{4} \quad \text{if } 1 \leq 2M+P$$

$$M = \frac{R\tau + 6R\tau P + R\tau P^2 - 6 + 6P}{12 - 9R\tau P - 3R\tau} \quad \text{Generally.}$$

$$M = \frac{R\tau - 6}{3(4 - R\tau)} \quad \text{if } P=0 \qquad M = \frac{2R\tau}{3(1-R\tau)} \quad \text{if } P=1$$

$$\tau = \frac{6(1-P)}{R(1+6P+P^2)} \quad \text{if } M=0$$

Note: $P=0 \equiv$ ideal feathering; $P=1 \equiv$ symmetrical case; $M=0 \equiv$ no physical stops.

By the method of approach used here, it appears that, for the feathering case, the frequency increases as the gain ratio is increased. This is shown by the formula (24) (when M = 0) but it is more clearly seen by reference to Figures 4.3.3, 4.3.4, and 4.3.5 which show an approximation of the Feathering Case at 0.5 cps, 1 cps and 2 cps. These calculations assumed ideal sensing. For the symmetrical case this assumption ignored only a phase lag introduced by the sensing device; this will be readily remedied in paragraph 4.4. However, in the feathering case practical sensing devices will not merely contribute a phase lag to the velocity signal but will also modify the wave form significantly. Hence, one must be careful in drawing conclusions from this analysis concerning the feathering case. It is believed that good results could be obtained by analyzing this case by Fourier methods. Once an approximation has been made of the acceleration curve by a Fourier series, the velocity and displacement series are gotten through termwise integration of the original series. The fundamental term and all significant harmonic terms of the angular velocity are subjected to the dynamics of a rate gyro, and the rate gyro output is obtained as a series. This, when integrated, yields the indicated position signal. These indicated components of missile motion are the controlling factors in missile oscillation; just as a group of curves are assembled later in the report for the VPR chart, in Figure 4.4.4, curves representing several frequencies for the feathering system could be assembled. The focal point of such a drawing would again be the triggering line, which could be moved as described in 4.4 to represent other phase lags in the system. In this case however, the gyro used would be an integral part of the chart which for the feathering system would differ in uniformity of appearance from the VPR chart, but should be at least as useful for design purposes.

4.4 The analysis in 4.3 shows the final system proposed in paragraph 4.2 to be workable within the stated operating limitation. This analysis assumed subcomponents without time lags. Practically, however, such a system is not feasible. If one is to establish design criteria on this system a means must be devised for including these phase lags.

In order to obtain a clearer picture of the system analyzed in paragraph 4.3 by equating P = 1, graphic representation is made of the ideal system action at three operating frequencies. In Figures 4.4.1, 4.4.2, and 4.4.3 the angular acceleration, angular velocity, and angular displacement imparted by a so-called symmetrical flicker type system, are shown in their relationship to each other. The figures represent frequencies of 1.25 c.p.s., 1 c.p.s., and 0.833 c.p.s. respectively.

These curves were drawn from theoretical considerations presented in paragraph 4.3. Surface stops were arbitrarily set at $\pm 15^{\circ}$ with surface velocity taken as 120°/sec. Evaluation of the angular velocity and displacement at the time the system is triggered reveals ratios of displacement to velocity to be 1:5, 1:4.32, and 1:333 for frequencies 0.833, 1, and 1.25 respectively. Hence the ratios of the gain applied to these signals as they enter the mixer must be the inverse of this to obtain triggering at this point. The broken curve represents a comparison of the rate and displacement signals entering the mixer if these gain ratios are applied. It can be seen that as the "gain in displacement" is increased for a given gain in velocity, the frequency decreases.

Any component which tends to delay these signals simultaneously, without distorting them significantly (for example the rate gyro), can be

represented by shifting the "trigger line", on these graphs a comparable distance to the left. A component which delays one signal can be shown by shifting the trigger line only for that signal; if this is accompanied by an attenuation the graph signal must also be attenuated accordingly. These statements are meant to be indicative of approximations which can be made; they ignore filtering actions of the rate gyro which change the shape of the velocity curve and, hence, of the position curve. A time delay in the integrating motor component makes the position curve even more sinusoidal. For the symmetrical case, the curves are already very close to a sinusoid, thus, (apart from the shift due to phase lag) the error made by utilizing the original velocity and position curves instead of corrected ones is, for the purposes under consideration, negligibly small. These methods should prove very advantageous in system design problems.

The only truly significant parts of Figures 4.4.1, 4.4.2, and 4.4.3 are those quarter cycles immediately preceeding the triggering line. A graph comparing angular velocity and positions in this region for the several listed frequencies is shown in Figure 4.4.4. For these curves, aileron stops were placed at $\pm 20^{o}$. The acceleration curve is omitted because it is not directly significant to these considerations. The scales for velocity and displacement are different to facilitate closer approximations. Since the acceleration curve preceeding the trigger line is of constant value, i.e.; $20^{o}/sec^{2}$ (for the surface is dwelling at its stop), the velocity curve from its zero point to the trigger line is a straight line with a slope $20^{o}/sec/sec$. From the trigger line on the acceleration curve is a straight line with a slope of $-120^{o} \cdot sec^{-2}/sec$. Therefore from this point to its maximum the velocity

curve is parabolic, increasing over its trigger position by 1.67 degrees. The zero point of the displacement occurs at the point of maximum velocity and the position values at maximum and triggering points may be obtained by reference to formulas No. 29 and 22 in paragraph 4.3.

The major sources of phase lag and attenuation are the following:

1. Rate gyro which results in delaying and amplifying both signals.
2. Integrating motor which delays and attenuates and position signal only.
3. Time lag in the relay motor - time taken by the relay signal to change from one extreme to that of opposite polarity. This results in delaying actuator action and thus causes triggering to occur after the time at which triggering conditions exist i.e., after $V_T^* = -RD_T^*$.
4. Dead space in relay sensing - results in a delay in beginning the reverse of relay signal and hence also delays the actual triggering.
5. Time lag in the actuator - results in a delay of the trigger line, in the same manner as 3 and 4 above.

The only one of these delays which deals with one signal by itself is that in the integrating motor. The amount of phase lag and attenuation of the position signal caused by the integrating motor is frequency dependent as indicated by Figure 4.4.4.1.

The actual sensing device producing the control signal for the missile ailerons is a rate gyro yielding the indicated angular roll velocity signal. This signal serves a dual purpose; it is first fed into the summing

or mixing device and secondly it controls an integrating motor whose output is also fed into the summing device. Computer study reveals that the introduction of relatively large time delays into the integrating motor component has a comparatively small effect on the frequency of missile oscillation. In certain instances improvements in system performance result from the introduction of a time delay. These results are rather surprising and demand an explanation.

For the following considerations the indicated angular roll velocity signal is the basic signal. Furthermore, the velocity is assumed to have a true sinusoidal nature. The Figure 4.4.5 is drawn in such a way that the velocity component is represented by a vertical vector V lying in the positive imaginary axis. Then, an ideal integrating motor component with no time delay would yield a signal represented by a horizontal vector P lying in the positive real axis. To simplify the representation of the components relationship, this vector shall be of unity length. For a given frequency (ω in radians/sec) by which the missile oscillates, the vector V then has the length of ω/k units if the gain ratio of velocity component over position component is 1:k. (The diagram in Figure 4.4.5 is drawn for a ratio 1:2 and $\omega = 8$.) The resultant vector R represents a summing command, whose zeros determine the trigger points of the control system. The "time line" t-t rotates in a clockwise direction about the origin of the complex coordinates O. If the position of this time line is chosen such that it is perpendicular to the resultant vector R, the projections of the vectors V and P on this time line are of equal length and opposite in sign. This is the condition necessary for triggering the system. The angle between t-t and OP which is the same as between OR and OV is the

phase angle between the zero of the velocity component and the instant when triggering occurs. Consider now the case in which the integrating motor has a noticeable moment of inertia represented by a certain time constant in its response transfer function. The integrating motor output signal then lags behind the true integral of the velocity component. If the frequency of missile oscillation is assumed not to change appreciably, the locus of the position vector, as the time constant varies from zero to infinite, is very nearly the semicircle PP_1P_2O. The phase lag angle is given as $\tan^{-1}\frac{\omega}{q}$. where $\frac{1}{q} = T$ is the time constant of the motor integrator. As can be seen by graphical representation, for a relatively large change in q there is only a very slight change in the angle VOR. The locus of the vector R, as q varies from ∞ to 0, is the semicircle RR_1R_2V. Expressed in a qualitative manner: as to the response of the system, for an increasing Time Constant the increase of phase lag (between the time integral of the indicated angular velocity component and the actual delayed position signal) will be cancelled by the attenuation of the position vector thus resulting in only a small change of the overall missile performance. If, for example, the time delay in the rotor integrator is such that the position vector OP_1 lies in the direction of the time line t-t, as drawn in the figure, it can be seen that the resultant vector has exactly the same direction as it had when no time delay was encountered i.e., when the position vector was O P. As can be found this occurs when $q = \frac{\omega^2}{k}$. Since the velocity vector in the systems under consideration is appreciably greater than the position vector, and for cases where $0 \leq T = \frac{1}{q} \leq \frac{K}{\omega^2}$ the trigger point is only slightly shifted.

As the analysis proves and as can be seen by comparing the three plots

presenting the velocity curve in its relative position to the trigger point within a whole cycle (Figures 4.4.1, 4.4.2, and 4.4.3) the following fact becomes apparent:

The smaller the phase angle (in radians) between the zero of the velocity component and the trigger point, the higher the frequency of the missile oscillation. Let δ be this phase angle (in radians). Then, the relation exists $\frac{\pi}{2} - \delta = C \cdot f \cdot \pi$, C is the time taken for the surface to travel from one stop to the other stop.

If a noticeable integrator time lag is introduced into the vector plot (position vector being OP_2), the time line, t* - t*, representing the moment when triggering occurs for this system, advances relative to the triggering time line for a system with no time delay at all. In other words: the angle δ becomes smaller. From the equation above δ can become smaller only if f increases. The vector diagram, Figure 4.4.5 is drawn for a given frequency ($\omega = 8$). At higher frequencies the velocity vector will have a greater magnitude relative to the true position vector (OP). The result of this change would be a slight additional advance of the triggering time line which would in turn increase the frequency. Although this appears to have a cascaded effect, in the practical case the phase shifting influence of the rate gyro opposes such a development by increasing the phase lag between true angular velocity and the trigger point; this prevents the system from a further advance in this direction and keeps the shift of the triggering time line relatively small.

Consider the case in which the Time Constant is just large enough that the position vector in question (let it be P_m) together with the velocity

vector (V) forms a summing vector (R_m) which has the same direction as the vector R in a system with no time lag. When the system has no time lag the projection of the position vector P on to the trigger time line t-t is smaller than its actual length. Since the time line rotates clockwise it can be seen that triggering occurs after the time line passed the maximum of the position component. However, in the case under consideration, the trigger time line and the vector P_m are in coincidence thus indicating that triggering occurs exactly at the maximum amplitude of the position component. Any larger time delay in the integrating motor component connected with a further advance of the trigger time line causes the system to trigger before the maximum of the position component appears.

With increasing values of the time delay the trigger point advances on the position curve from a point behind the maximum through the peak of the position component to points ahead of the maximum. As far as the velocity curve is concerned the trigger point travels only on the ascending linear portion of the curve ahead of a maximum point.

The foregoing explanations were made by assuming the velocity component to be a sinusoid and hence are approximative. In an ideal symmetrical case the component sensing the actual missile roll velocity produces an output signal which represents the angular velocity without delay; its graphical picture in the time plot is composed of straight lines and parts of a parabola hence, the deviation from a sinusoid is of minor magnitude. In addition, if a component simulating the actual rate gyro performance is included, the output signal then assumes a shape which, due to the filter effect of the second order component, differs from a sinusoid still less.

The vector plot, furthermore, reveals the fact that the frequency decreases if the gain of the position component is increased. The vector V in such a case has to be reduced (since the position vector is assumed to be of unity length). This rotates the resulting vector R and consequently the trigger time line t-t clockwise yielding a larger angle δ and therefore a smaller value for the frequency.

For very large time lags where the position vector almost disappears, the response should be similar to a system with only a velocity signal resulting in an almost triangular surface motion (see general remarks in introduction).

The deadspace in the relay sensing is jointly dependent on the frequency of oscillation and the magnitude of the signal $g_1 V + g_2 P$; this is immediately apparent from the graphic representation of this deadspace in Figure 4.4.6. It can be seen from careful examination of the mixer signal in the vicinity of the relay deadspace in this figure that the delay due to relay deadspace is a function of the mixer signal $(g_1 V + g_2 P)$ slope in the deadspace. This is in turn a function of the frequency and amplitude of the mixer signal and can be calculated for individual cases.

The delay in relay signal due to relay time lag is not frequency dependent. For the relay used in computer analysis it was approximately 0.02 second.

The time lag in the actuator is also not frequency dependent but is characteristic of the actuator itself. It results physically in a delay in the time taken by the surfaces in comcing up to speed. Once a constant speed is reached the surfaces continue until encountering physically stops or until the relay reverses.

Auxiliary lines which contribute to the ease of application have been added to Figure 4.4.4. In the velocity curves, lines showing the phase lag caused by a rate gyro, f_n = 5 c.p.s., with four values for the damping ratio, are plotted against the various frequencies. It is characteristic of the plot that these lines are nearly straight and parallel to the trigger line. These phase lags apply to related position curves in the same manner.

Another set of lines has been added in the position half of the plot to indicate phase shifts of 10°, 20°, 30°, and so on from the trigger line for the various frequencies. These will be used with Figure 4.4.4.1 to consider the effects of time lags in the integrating motor.

The utilization of Figure 4.4.4 can be best demonstrated by considering some related problems.

Example No. 1. Consider a system, having ideal sensing, in which because of delay in the discriminator relay 0.02 sec time delay occurs in the triggering mechanism. It is desired to maintain the system at 1 c.p.s. What gain ratio is necessary?

(1) The delay results in a relative shift of velocity and position curves with respect to the acceleration curve and hence the triggering line. This may be represented in Figure 4.4.4 as a shift of the trigger line equal to 0.02 seconds to the left.

(2) Then reading the ratio of velocity to position signals on the 1 c.p.s. curve yields velocity/position equals 1.3/0.49 or 1:0.377.

(3) The necessary gain ratio of velocity/position, to be adjusted in a physical setup, therefore, equals 1:2.65.

Example No. 2. Consider a system with the same time delay in the relay and a rate gyro with f_n = 5 c.p.s. and ζ = 0.3; which is to oscillate at 0.7 c.p.s.

(1) Phase lag by the rate gyro at 0.7 c.p.s. is seen to be represented by the line labeled ζ = 0.3.

(2) Time delay treated as in Example No. 1, except that it is now added to the delay contributed by the gyro.

(3) Attenuation or amplification of the true velocity signal by the gyro is unimportant in that it results in proportional changes for both position and rate signal.

(4) Referring to the 0.7 c.p.s. curves and reading the ratio of velocity/position under the shifted trigger line reveals a ratio of approximately 3:1.

(5) Hence the gain ratio of velocity/position necessary in the physical set-up to maintain 0.7 c.p.s. under these conditions is 1:3.

Example No. 3. Consider a system with .02 second delay in the discriminator as before but this system is preset at a gain ratio of 1:2. At what frequency will it oscillate if the rate gyro ζ = 0.3 and f_n = 5 c.p.s. is used?

(1) Treat the time delay again as a shift of the trigger line to the left, and as the time shift by the rate gyro is approximately the same for all frequencies treated here, add the shift indicated for a rate gyro having ζ = 0.3.

(2) Looking under the new trigger line find the frequency which has the desired ratio at triggering in this case approximately 0.95 c.p.s.

Example No. 4. Analogue simulator results reveal that increasing the time delay in the integrating motor does not have a detrimental effect on the steady state. Explanation for this property was given earlier in this section. The conclusion drawn can be substantiated by using the VPR chart in Figure 4.4.4. Consider a system operating with the following characteristics:

(1) Angular roll rate is sensed by a rate gyro $f_n = 5$ c.p.s. and $\zeta = 0.3$.

(2) The gain ratio of rate to displacement is 1:1.

(3) The time taken for the Discriminator Relay signal to change sign from an extreme position is 0.02 sec. (Time delay in the relay).

(4) The time delay in the integrating motor is 0.1 sec.

Steps in determining the system characteristic oscillation are as follows:

(1) The effect of the rate gyro is to move the ideal tripping line into the position of the line $\zeta = 0.3$.

(2) A 0.02 sec. delay in the relay results in a further trigger line shift of 0.02 sec. (see time scale) to the left.

(3) By comparing the frequency-related pairs of lines at this new trigger line it is found that, with no time delay in the integrator and for a gain ratio 1:1, the system would oscillate at 1.1 c.p.s.

(4) Reference to the associate time delay chart (Figure 4.4.4.1) reveals that a time delay of 0.1 sec at 1.1 c.p.s. results in a phase shift of 35 degrees and an attenuation of 0.83 for the

position signal.

(5) The new tripping line maintains its position in the velocity plane but, since the time delay is in the integrator, moves an additional 35 degrees to the left in the displacement plane. Now comparing reading at the new tripping point yields an attenuated displacement of 0.32° and a value of 0.42°/sec, for the velocity component the gain ratio thus being 1:1.3 at this point.

(6) However, if the ratio at tripping is to remain at 1:1, a rule of thumb established for this system can be applied: the lower the ratio the higher the frequency. Hence, the ratio being lower than 1:1.3, a frequency of more than 1.1 has to be chosen.

(7) Resorting now to the method of iteration yields for each new frequency considered a new phase and attenuation due to the integrator time lag. The rule of thumb in paragraph (6) above eliminates most of the guess work from this process.

(8) Each new frequency also means a new phase lag due to the rate gyro effects. However, since the lines referring to the gyro effect on the VPR chart are represented by straight line, nearly parallel to the trigger line, a small change in frequency results in only a negligible shift of the trigger line.

(9) At an estimated frequency of 1.15 c.p.s. the phase lag is 36 degrees and the attentuation 0.81. Apparent tripping displacement at this point is (0.34 degrees X 0.81) 0.28 degrees as compared to an apparent tripping velocity of approximately 0.25

degrees yielding an apparent gain ratio of 1:0.9, this being now lower than the previously found ratio of 1:1, indicating that the correct frequency will be slightly below 1.15 c.p.s. An estimate of 1.14 c.p.s. would be very close; increased accuracy could be obtained by extending the scales of the VPR chart. Thus the introduction of this integrator time lag resulted in an increase in frequency from 1.1 to 1.14 c.p.s.

(10) The analogue simulator results for this situation yield a frequency of approximately 1.13 c.p.s. Allowance which must be made for VPR chart accuracy limitations are such that this agreement is as good as it might be anticipated. For most practical purposes, this degree of accuracy is sufficient.

The VPR chart is used here as a graph with a supporting graph to represent attenuation and phase lag by the integrating motor. However, this chart would be much more convenient for practical use if it were designed as a computer similar in appearance to the E-4 navigation computer or to a slide rule. Such an instrument, applicable to a specific system could be designed quite easily and, while generalization would present some difficulty, it could be accomplished at a comparatively small cost.

4.5 Up to this point only the steady state operation of the system has been considered. If the system is workable it must also maintain a stable condition when subjected to outside disturbances. It would appear that the system could react to a disturbance by varying the relative time of dwell at the surface stops. However, to determine the details of system performance in the disturbed condition by theoretical means, it would be necessary to conduct

an additional long-time investigation on the subject. This has been approached only superficially in order to have a basis to obtain a comparison for analogue results. A good similarity existed and it was decided that this study would be completed by the faster analogue methods.

Consider first a well mannered system of this type in which the center line about which it oscillates, is being displaced by some undetermined force. Assume only that when displaced in such a manner the system maintains its frequency and is returned to its neutral position. Figure 4.5.1 shows the missile position in the hypothetical situation. On the same figure velocity and acceleration curves were built up in a stepwise manner from the fact that $V = \int A\,dt + c$ and that at the tripping point velocity is equal to displacement. Examination of the figure shows that this disturbance would then be counteracted by varying the relative dwell time.

Disturbances are referred to as percentages of full surface deflection. An external disturbance is called 100% if a 100% steady state surface deflection will exactly counterbalance it. It can be seen that if the system is to be stable under the influence of a disturbance applied in a stepwise manner the resultant acceleration (disturbance plus surface deflection expressed as acceleration) must equal zero. Hence the average acceleration delivered by the control surface must be equal in magnitude and in the opposite direction from that due to the disturbance. Then the line of average acceleration caused by surface deflection is merely biased from the original zero by a percentage of maximum surface displacement equal to the percentage disturbance considered. Figure 4.5.2 assumes $V = \int A\,dt + C$ and $P = \int V\,dt + C_1$ and shows the relation which must exist in a stable system subjected to a light disturbance of

constant magnitude. It is of particular importance to note that the missile oscillates past its old zero position but the average position is now somewhat changed.

Figure 4.5.3 shows the result of applying any disturbance strong enough so that the surface dwells on only one side. It is of interest to note that in this condition the theoretical velocity signal is zero at the second tripping point T_2. Because of the triggering condition and the fact that position maximum occurs at $V(t) = 0$ it must be concluded that, in the theoretical case the missile will always return to its original zero. Practically speaking the velocity signal would include a phase lag and its value would differ somewhat from zero at the tripping point. Since this point is not far from the peak of the position curve, it must be surmised that the bomb will no longer return to its original zero position. The external disturbance condition which will cause the surface to dwell at only one of the stops is determined by the following parameters: frequency by which the missile oscillates, surface stops, surface speed, and surface effectiveness. These are related by simple geometric considerations.

SECTION IV

SIMULATION RESULTS

5.1 The system first simulated was one in which the actuator output was of an isosceles, trapezoidal wave form. It is assumed that the actuator output is independent of any load placed upon it in the form of an external hinge moment and that the surfaces will be limited to ± 20 degrees deflection. Due to the method of simulation used for the actuator the surface dwelling at

the stops is represented as a high frequency, low amplitude vibration whose mean value is the constant output representing true surface dwelling. A comparison of the desired actuator travel to the actuator travel taken from an oscillogram recording of the simulated actuator appears in Figure 5.1.1.

As has been mentioned earlier in this report, acceleration is directly proportional to aileron deflection. This being the case the angular velocity is obtained by integrating the acceleration curve. A comparison between theoretical angular velocity and angular velocity taken from oscillogram recording of the simulation is shown in Figure 5.1.2. Similarly the angular displacement, obtained by integrating angular velocity appears as Figure 5.1.3, with that taken from an oscillogram recording of simulation.

5.2 The setup shown in Figure 5.2.1 was used to evaluate the effects of varying the surface angular velocity on the frequency and amplitude of missile oscillation. Since this case was investigated under the assumption of an ideal sensing device the excellent agreement between the results of the simulation and the theoretical evaluation was anticipated. The results are presented graphically in Figure 5.2.2 showing frequency and amplitude of oscillation vs aileron speed. Change in aileron effectiveness (missile roll acceleration (deg/sec^{-2}) per degree aileron deflection) is seen in the theoretical analysis to have no effect on frequency but it effects amplitude of oscillation directly.

A rate gyro f_n = 5 c.p.s. and ζ = 0.316 was next introduced into the system as the means of obtaining angular roll rate of the missile. The setup used for the following investingation is shown in Figure 5.2.3. The effect of varying the gain ratio under this condition is shown in Figure 5.2.4 which yields frequency and amplitude of missile oscillation and dwelling time of the

ailerons at their stops. It can be seen that increasing the gain of the positional signal results in a decrease in frequency as in the ideal system considered theoretically in paragraph 4.3; the mode of the change is, however, somewhat altered.

This setup was also used to check the system reaction to the application of an external disturbance. Figure 5.2.5 reveals the upper and lower oscillation peaks of the system, operating at 3 different gain ratios, to varying amounts of external disturbance expressed as percentages. Obviously disturbances of 100% will result in complete system failure and hence, no accelerations in excess of 90% were considered. The frequency of oscillation as a function of external disturbance is shown in Figure 5.2.6 for the same three different gain ratios. Figure 5.2.6 reveals that the frequency reaches a partial minimum, increases and finally drops off toward zero as the disturbance is increased. Even in these extreme conditions, increasing the gain factor of the positional signal decreases frequency (Figure 5.2.6).

It may be noted that the displacement curve differs more and more from a sinusoid as the size of the external disturbance is increased as shown in the recordings in Figure 5.2.6.1 and 5.2.6.2 for 63% and 80% disturbance respectively. This is to be expected since the symmetry of the acceleration is progressively more distorted as the disturbance increases. First the dwell time at the stops is no longer equal, then the surfaces dwell at only one stop but travel past the neutral position, and finally, as the disturbance becomes quite large, the surface no longer returns to the opposite side of neutral but completes its entire oscillation deflected on the one side of neutral which is in opposition to the disturbance. It is possible to compute

the mean value of surface deflection for each test with various parameters by evaluating the records. For a disturbance of approximately 50%, one would expect the mean value of surface deflection to be 10° (= 50% of total surface deflection). Figure 5.2.7 yields the curve for computed mean deflection compared to expected mean deflection. However, determination of the mean deflection from the computed records is difficult since in all cases the width of the trace itself is quite significant in the final results. Hence, the deviation between expected and computed mean deflection in Figure 5.2.7 is, in all probability, one in either evaluation or the recording mechanism. This viewpoint is substantiated by the fact that there is no apparent shift in the angular velocity signal; a drift in this signal is inherently related to a realistic deviation of the type shown. Since the error is consistently in one direction and appears only when the surface travel becomes asymmetrical to the point that the surface dwells on only one side it appears to be an error in recording rather than evaluation. This error, probably a time lag in the pen motor of the Recorder, apparently cancels out in more symmetrical recordings but in asymmetrical cases yields a larger apparent dwell time than the system actually has.

The effect of varying the damping ratio in the rate gyro, on overall system performance, was investigated for undisturbed and disturbed flight conditions; a 25% acceleration was used as representative of a disturbance. Damping ratios were varied from 0.1 - 1.6; the results are plotted in Figure 5.2.8 showing amplitude of upper and lower peaks of missile oscillation in terms of amplitude/aileron effectiveness and also showing frequency plotted against damping ratio for the undisturbed case. Figure 5.2.9 presents the same

data for the system reacting to a disturbing acceleration.

5.3 It has been revealed by previous analysis (4.4) that a time delay in the integrating motor should have a very small effect on the overall system performance. This conclusion is supported by the simulation represented in Figure 5.3.1. Results of the simulation appear in Figures 5.3.2 and 5.3.3. 5.3.2 shows maximum and minimum peaks plotted against percentage disturbance for q (q = 1/T) of 1, 2, 5, and 10 for a gain ratio of 1:1. Figure 5.3.3 shows the same plot for q = 1,5, and 15 if the gain ratio is 1:0.5. Figure 5.3.2.1 and 5.3.2.2 are recordings for q = 1 and q = 10 and for gain ratio 1:1. Superimposed on the trace for external disturbance is a continuous sequence of time marks indicating periods of 1 sec each. These records reveal that no great change in system performance results from the introduction of even relatively large time delays in the integrating motor. The magnitude of change which can be tolerated is dictated by the desired accuracy and hence must be determined for individual missile control system combinations.

A time delay in the actuator has a greater effect on system performance. The computer setup showing how this delay was simulated is presented in Figure 5.3.4. Time delays of 0.1 second and 0.05 second were introduced into the actuator and the results are plotted in Figure 5.3.5 which represents the results for q = 10 (T = 0.1) and q = 20 (T = 0.05 sec) and shows maximum and minimum peak values, and frequency vs percentage disturbance. A comparison of Figure 5.3.5 with 5.2.5 reveals that a time delay of 0.1 sec introduced into the actuator has a very noticeable effect on system performance. For a time delay of 0.1 sec and a gain ratio of 1:05, the maximum mean deviation from the original missile neutral position is 10 times the aileron effectiveness factor

as compared with 2.4 times the aileron effectiveness factor for no time delay. The peak deviation in the first case occurs at a 25-30% disturbance and in the latter at 63% disturbance. Hence if a system is expected to operate through the entire disturbance range such a time delay is very detrimental to system performance; however, for limited disturbance conditions the time delay has much less influence.

5.4 The setup in Figure 5.4.1 was used to determine the effects of a dead zone in the sensitivity of the flip-flop relay. A dead zone in a sensing device is taken to be a region of insensitivity within its range of operation. The dead zone for the relay is electrically considered as a region symmetrical about the zero point, which has a width of ±10V in the simulator setups; this would correspond to a signal representing 10 degrees/sec angular velocity. More specifically this means that at any time, the mixer signal is within this dead zone, the relay senses zero; when the signal changes sign, the flip-flop action will be delayed according to the width of the dead zone and the rate at which the signal is changing as it passes through zero.

Since the dead zone in the relay results in phase-shifting the tripping point an amount determined by the slope of the mixer signal, and, hence, by its magnitude, the response of a particular system is dependent on system gain from the rate gyro to the actuator. Therefore, the term amplitude per effectiveness has no meaning as used in previous graphs; for Figures 5.4.2 and 5.4.3 the actual amplitude of displacement and frequency of oscillation vs percent disturbance is shown for an effectiveness of 8 degrees/sec^2/degree surface deflection. These tests also included integrator time delays of .05 and .20 sec respectively. Since a time delay in the integrator has been shown to have only

a small effect on system response, the similarity between Figures 5.4.2 and 5.4.3 was anticipated. These figures also show that, although amplitude of oscillation and displacement become relatively large, the system is still well natured for disturbances of up to 40 percent. The recording shown in Figure 5.4.2.1 presents the manner in which the dead space influences the system operation. It would appear that the relay dead space might have a considerably greater influence upon the transient reponse of the missile. The nature of the transient resulting from a time gust would differ considerably from that resulting from the step input used here. Hence, conclusions concerning the transient would be subject for further study. It is of interest to note that the nature of the transient for "step like" disturbances besides being dependent on the disturbance will also be dependent upon the position of the control surfaces at the time of its application. Since the control surfaces are in constant oscillation, the results of a study concerning the transient would be limited to placing upper and lower limits upon the system output during the transient. Figure 5.4.2.2 through 5.4.2.4 show a number of transient responses for the symmetrical system operating under various conditions.

5.5 The influence of component characteristics which usually cause a phase lag have been discussed. It is also likely that certain components may have a slightly asymmetrical response to a symmetrical forcing function. These non-symmetrical tendencies can be present in the sensing components (rate gyro and integrating motor) and in the controlling or actuating components (discriminator, actuator, control surfaces, and the missile itself).

Consider the case where there is an asymmetry in the rate gyro, If the missile were in a symmetrical steady state oscillation, with no

aerodynamical feedback from the controlling elements, the signal of the rate gyro would be an asymmetrical oscillation with respect to its original null position. In other words, the mean angular velocity yielded by the gyro output would have a steady state error determined by the degree of asymmetry involved. However, for the closed loop the system is to minimize an error indicated by the rate gyro, so that an indicated mean steady state angular velocity of zero results. Consequently, the missile must have a fixed rate of rotation superimposed on its oscillatory roll motion. This fixed rate exactly balances the asymmetry of the gyro. This results in the indicated and true angular velocity and position relationship shown in Figure 5.5.1. Thus, the amount of this type of error which can be tolerated in any given situation, is merely such that: rate gyro error x time = allowable displacement error. This situation has been investigated by a REAC simulation which supported both qualitatively and quantitatively the conclusions just drawn. The results of this simulation are recorded in Figure 5.5.1.1. The system for which the recording was made had the following characteristics: surface speed $120^{\circ}/sec$, surface stops at $\pm 20^{\circ}$, surface effectiveness $14^{\circ}/sec^2$ per degree aileron deflection, rate gyro $f_n = 5$ c.p.s., $\zeta = 0.316$. The asymmetrical output of the gyro is assumed to be such that the signal is amplified by 1.3 when it is of one polarity and attenuated by 0.7 when the signal is of the opposite polarity. To calculate the effect of any asymmetry in the rate gyro, one must merely determine the true angular velocity which results in an indicated angular velocity whose integral over one cycle is zero. Since they do not contribute to the asymmetry to the indicated angular velocity, the ordinary phase lag and attenuation of the rate gyro system have no significance in these calculations.

Consequently, by assuming a missile angular velocity of the form " $A \sin(\omega t) - D$ ", the following condition exists:

$$(32) \qquad -\int_{\frac{\sin^{-1} D/A}{\omega}}^{\frac{\pi}{2\omega}} \alpha(A \sin \omega t - D)\,dt = \int_{\frac{\pi}{\omega} - \frac{\sin^{-1} D/A}{\omega}}^{\frac{3\pi}{2\omega}} (A \sin \omega t - D)\,dt$$

Where: D is the average missile angular velocity

A is the amplitude of missile angular velocity oscillation.

The amplification of rate gyro signals of opposite polarity has the ratio 1:a.

When this is reduced it yields:

$$(33) \qquad \frac{D}{A} = \sin\left[\frac{a+1}{2(a-1)} - \frac{\sqrt{A^2 - D^2}}{D}\right]$$

from which D may be calculated for a specific case.

For the case represented by Figure 5.5.11, A was 35° and a = 1.85 which when substituted into equation (33) yields $D \sim 6.8$. This indicates a rate of missile drift of about 6.8°/sec as compared to a simulated drift of 7.2°/sec. Each type of asymmetry would require special consideration to establish its effect on system performance. Generally speaking, asymmetry in a rate sensing element will result in error in missile angular velocity while asymmetry in position sensing devices will result in errors in missile angular position.

If controlling components such as actuators, control surfaces, surface stops, discriminators, etc, are asymmetrical in their performance, the result of the asymmetry will be apparent at the sensing element outputs causing the system to take corrective action in such a manner that for the

steady state oscillation the average indicated missile angular velocity is zero (if the rate sensing element itself does not have an asymmetrical output). Thus the mean value of the true missile angular velocity will also be zero. In terms of missile motion, the final result will be a steady position error. In any of these cases the introduction of an asymmetry would be likely to result in a change in frequency as well. However, since it was only desired to determine the steady state positional changes brought about by the introduction of asymmetries into the system, the changes in frequency and amplitude of oscillation were not investigated.

6.1 As has been previously mentioned (2.3) it is possible to improve the performance of the flicker control system to a certain extent by designing the surface actuating component so that a feathering operation results. For the feathering type the outbound surface motion occurs, as before, with constant angular velocity. The inbound motion, however, is independent of the systems performance inasmuch as the surface is released from the driving parts of the servo actuator as soon as the summing command changes its sign. At this moment the surface swings back into the neutral (streamlined) position due to the force of the airstream. From this point it is motor driven again into the outbound direction until it hits the stop or is released once more. Details relating to the specific kind of motion and the manner by which it has been simulated on the REAC computing machine, have been explored in 3.2B and by Figure 3.2.6.

The sensing device (rate gyro) used in the Feathering Case is the same as that used in the symmetrical case. However, because of the manner in which the surface is returned to neutral in the feathering case it is an inherently faster system than the other. This results in system frequencies

nearer the natural frequency of the rate gyro. As can be seen from a particular feathering performance graphically represented in Figure 4.3.4, the angular velocity curve for the missile differs considerably from a sinusoid. However, because of filtering action of the gyro, the indicated angular velocity signal which appears at the mixer and the integrator is more nearly sinusoidal. Since the mixer signal is a major component in the determination of system performance, this filtering effect becomes very significant in the overall picture.

It is necessary to determine the manner in which the system performance is altered by the introduction of a rate gyro as a sensing device; particularly the phase lag and distortion of the signals entering the integrator and mixer will be significant since they change the apparent ratio of velocity signal to position signal at the time the system triggers. A very good approximation of missile motion and gyro response to such motion may be gotten by Fourier methods. Fourier representation of the acceleration of the symmetrical type system, shown in Figure 4.4.1 and discussed by paragraph 4.3 by equating P = 1, is given by the following approximation:

$$(34) \quad f''(t) \cong \frac{4A}{\pi\alpha}\left(\sin\alpha \sin\omega t + \frac{1}{9}\sin 3\alpha \sin 3\omega t + \frac{1}{25}\sin 5\alpha \sin 5\omega t\right)$$

Where $\alpha = \omega T$ and A is the physical limit to aileron travel in degrees if aileron effectivity is $1^{o}/sec^{2}$/degree aileron travel.

Fourier representation of the acceleration of the Feathering System, shown in Figure 4.3.4 and discussed in paragraph 4.3 by equating M = 0, is given by the following approximation:

$$(35)\quad f''(t) \cong \frac{2}{\pi^2 \lambda(1-\lambda)}\left[\sin \lambda\pi \sin \omega t - (1-2\lambda-\cos\lambda\pi)\cos\omega t + \frac{1}{9}\sin 3\lambda\pi \sin 3\omega t - \frac{1}{9}(1-2\lambda-\cos 3\lambda\pi)\cos 3\omega t\right]$$

Where " λ " is the fraction of a half cycle during which the surfaces travel outbound, i.e., $\frac{K_2}{K_1 + K_2}$.

In order to obtain a clearer picture of the gyro effect on the two systems, a comparison of missile motion to motion indicated by the sensing device is made in Figure 6.1.1, 6.1.2, 6.1.3, and 6.1.4. In figure 6.1.1 and 6.1.2 missile angular velocity and position are plotted on the same graph with indicated angular velocity and position for the symmetrical system at $\omega = 3$ and $\omega = 6$. In Figure 6.1.3 and 6.1.4, a similar comparison is made for the feathering system at $\omega = 6.28$ and $\omega = 12.56$.

The symmetrical system shown in 6.1.1 and 6.1.2 was based upon the following consideration:

1. Physical surface stops at $\pm 20^\circ$
2. Surface velocity between stops 120° per sec
3. Surface effectiveness $1^\circ/\text{sec}^2/\text{deg}$ surface travel
4. The rate gyro utilized had $f_n = 5$ c.p.s. and $\zeta = 0.316$.
5. The integrating motor operated ideally.

Such a system has a theoretical maximum frequency of 1.5 c.p.s. and it is slowed down by the phase lag in the rate gyro. True missile motion was gotten from the formulae in 4.3. Indicated missile velocity was gotten by integrating termwise the Fourier equation (No. 34) and applying the dynamics of the rate gyro to the results of this integration by means of frequency response

charts. Indicated angular position is then obtained by termwise integration of indicated angular velocity.

The ratio of position to velocity at the triggering point, taken from 6.1.1 and 6.1.2 for $\omega = 3$, and $\omega = 6$, is 1:5 and 1:3.9 respectively for true missile motion and is 1:4.6 and 1:3.2 respectively for indicated missile motion. This reflects a decrease in the magnitude of velocity relative to position when the gyro is introduced; however, when frequency is increased, the ratio of position to velocity at the tripping point decreases for both true and indicated missile motions. Hence, approximations made by the V.P.R. chart in Figure 4.4.4 yield qualitatively correct results. Further examination shows that the slopes of both indicated and actual missile angular velocity in the region of the triggering point are nearly the same. Hence, the method of delaying the actual missile motion, relative to the triggering line, to obtain the indicated missile motion gives reasonably accurate results.

Similar examination was made of the feathering system in Figure 6.1.3 and 6.1.4 for $\omega = 6.28$ and $\omega = 12.56$ respectively. Ratios of position to velocity were taken at the triggering point and found to be 1:4.5 and 1:9 respectively for actual missile motion and 1:2.9 and 1:2.3 respectively for indicated missile motion. Again the introduction of the rate gyro results in a decrease of velocity signal relative to position signal at the triggering point. However, in this system, as the frequency increases the ratio of missile true velocity to position increases at the triggering point while the ratio of indicated missile velocity to indicated position decreases. These frequencies were intentionally held below those at which the feathering system tends to operate and hence present the best gyro representation likely for this case.

Comparing these missile angular velocity curves to indicated angular velocity in the triggering region reveals that no amount of shifting of the true curve relative to the trigger line could render it a passable approximation for the indicated curve. This is true, basically, for two reasons: (1) because the feathering system operates at a higher frequency and thus nearer the natural frequency of the rate gyro than the non-feathering and (2) because of the lack of symmetry in missile motions for this system, the harmonics play a more significant part in gyro outputs. Hence, a chart utilizing theoretically true missile motion as is done by the VPR chart, is not feasible. However, a workable chart could be prepared for a given gyro by using Fourier approximations as they have been used here, to obtain theoretical indication missile motion. Preparation of such a chart would obviously have to be made in conjunction with a particular system.

6.2 Tests have been conducted simulating a missile equipped with a rate gyro and a surface actuator with a dynamic performance as described above.

The setup on the REAC for simulating a missile with a feathering type control system is given in Figure 6.2.1. As can be seen, the general outline (except the surface motion component) is the same as was used in the so called symmetrical (non-feathering) case. This setup represents the simulation of the missile performance involving no components which cause time delays or dead zones or other similar influences. The setup consists of practically the same circuitry used for the symmetrical system, with the feathering component, described by Figure 3.2.6, substituted for the inbound surface actuator component.

It seemed necessary to extend the investigation in such a manner that

the influence of a time delay in the integrating motor or in the actuator could be studied. The same subcomponents (representing the simulation of such an influence) were used and placed within the general circuit diagram as has been done in the symmetrical (non-feathering) case. Therefore, no specific circuit diagrams are presented as their arrangement can easily be composed from the diagrams for the corresponding cases relating to the non-feathering type.

In order to obtain information on the missile response and the performance of certain individual components in close correlation with the developmental progress of the missile, all tests were run with an outbound surface angular velocity of $120^{\circ}/sec$, an inbound return following the equation as given in 3.2.B, and a surface effectiveness of $15^{\circ}/sec^2$ missile roll acceleration for 1° surface deflection.

6.3 One apparent characteristic of the missile "feathering" flicker-type-control combination is the rather high frequency of oscillation and consequently a smaller amplitude of displacement.

Preliminary investigation revealed that the frequency is markedly influenced by the phase lag existing between true roll angular velocity and indicated angular velocity as yielded by the output signal of the rate gyro. Since, for frequency ranges below the natural frequency of the rate gyro, the phase angle becomes larger for higher ratios of the rate gyro damping and since, for a given rate sensitive device, the damping ratio is a part of the system which can be easily adjusted within a certain range, it was of interest to investigate the influence of the damping ratio on missile response. The rate gyro investigated had a natural frequency of 5 c.p.s. the same as in

previous investigations concerning the non-feathering case.

Figure 6.3.1 shows curves representing the frequency of the missile roll motion plotted against the gain ratio (velocity component: position component) as it has been done for the non-feathering type. There are four curves, three of which represent the frequency dependency on gain ratio for different damping ratios. The fourth curve pertains to a test in which the gyro with a relatively high damping ratio ($\zeta = 0.316$) was used in combination with a lead network, Figure 6.3.2. The output of this combination was then utilized in the same manner as the gyro output in the systems without the lead network. The purpose of this lead network is to compensate for the phase lag of the rate gyro output and thus to shift the missile frequency closer to the natural frequency of the rate gyro. The transfer function of the network has been found to be:

$$\frac{E_o}{E_{in}} = \frac{(0.84p+1)(0.0001p+1)}{5.8(0.145p+1)(0.0001p+1)}$$

Insertion of the lead network results in lessening the dependency of missile frequency upon the gain ratio. The missile frequency which is relatively high varies only a small amount for large changes in gain ratio.

Corresponding to the frequency curves are those for the amplitude of the missile roll oscillation. Utilization of a rate gyro with a natural frequency of 5 c.p.s. and a damping ratio of $\zeta = 0.316$ in combination with a proper lead network results in a large reduction of the amplitude for the steady state oscillation and a lesser degree of dependency on the gain ratio (gain of velocity/gain of position) as shown in Figure 6.3.3.

In respect to design work connected with the rate gyro it is of importance to obtain information about the magnitude of the angular velocity

encountered during the missile performance. Under the assumption that the missile oscillation is of an almost sinusoidal nature the response characteristic of the rate gyro gimbal can be computed if both the missile roll oscillation and the transfer function of the rate gyro are known. Such an assumption, however, is justified only as an approximation; reference to Figures 6.1.3 and 6.1.4 shows that less accurate approximations may be also made by the formulae in 4.3. The graphical representation of the half cycle of the roll acceleration (originated by the surface motion) is a rather asymmetrical and distorted triangle, and the integral of it yielding the missile roll velocity also differs somewhat from a true sinusoid.

The evaluation of tests simulating the missile behavior for different parameters of the damping ratio in the rate gyro component is represented in Figure 6.3.4; the amplitude curves for true angular velocity and angular velocity indicated by the rate gyro are plotted against the gain ratio.

It may also become necessary to determine peak values of angular velocity. These peaks may be approximated by assuming the velocity wave form to be sinusoidal and basing calculations on this assumption. This can be seen by evaluating the records to determine velocity peak amplitude as function of frequency. Figure 6.3.5 shows three plots of the amplitude ratio of a rate gyro (rate gyro output/rate gyro input or in other words: indicated angular velocity/true angular velocity) versus frequency ratio. Parameters are again three different values for the damping ratio of the rate gyro. The curves represent the analytical computation for the amplitude ratio versus frequency ratio of a rate gyro (second order system) excited by a sinusoidal forcing

function. The corresponding values taken from the records are marked by crosses. There is a relatively good agreement between the computed response for sinusoidal oscillation and the actual values as yielded by REAC simulations.

In order to obtain a complete picture of how the amplitude of roll angle, true and indicated roll angular velocity, and the frequency of the missile response change if the damping ratio in the rate gyro is varied over a large range, the results of corresponding tests are compiled in Figure 6.3.6.1, 6.3.6.2, and 6.3.6.3 respectively. A specific adjustment for the gain ratio (velocity/position) of 1:1 has been chosen for this investigation after it became apparent that under certain conditions this ratio (or a similar one in this neighborhood) would likely produce the best results with regard to the stabilization problems involved. However, the qualitative overall picture as revealed by these figures will remain basically the same for other gain ratios.

Assuming the missile oscillation in undisturbed flight may be approximated by a sinusoid, it could be expected that values for the damping ratio above 0.7 would produce a curve for indicated roll velocity that lies below the curve for the true angular velocity (Figure 6.3.6.2); such a rate gyro system is in or beyond the critically damped condition and no amplitude amplification takes place. On the other hand, the phase lag (produced by the second order system characteristic of the rate gyro) increases relatively fast with frequency, thus forcing the missile control system to oscillate with a lower frequency. The actual attentuation of the rate gyro output is insignificant since the system is sensitive only to the zeros of the summing command which is composed of both the indicated angular velocity signal and its integral thus eliminating the influence of absolute magnitude of the summing command.

For rather small values of the damping ratio in the rate gyro a higher frequency can be anticipated since in this case the phase lag increases slowly with frequency until the natural frequency of the rate gyro is approached. However, this being the case, the amplification of the output signal is comparatively large.

With the damping ratio continuously increasing, the mutual influence between phase lag increase and change in amplification or attenuation with decreasing frequency causes the curve of the indicated angular velocity to first decrease, pass a minimum, and then climb up and cross the curve of true angular velocity; the curve for the frequency steadily descends and those for true angular velocity and the roll position ascend. These curves could be of considerable significance in design work with this type of system.

To study the missile response to external disturbances, a step roll acceleration of different magnitudes has been applied to the system. Again, the amount of the external acceleration is given in percent of the product of surface deflection (in degrees) and the effectiveness (degree sec^{-2} angular acceleration per degree surface deflection). The results as obtained by a simulation for which a rate gyro with a natural frequency of 3.16 c.p.s. and a damping ratio of 0.25 was used, are presented in Figure 6.3.7.1, 6.3.7.2, and 6.3.7.3 for gain ratios of 1:1, 1:2, and 1:4 respectively. No time lags or dead spaces were assumed to be present.

Markedly better results were obtained by utilizing a rate gyro with a higher natural frequency (5 c.p.s.) in which the damping ratio was 0.316. The results as evaluated from simulation tests are given in Figure 6.3.8.1, 6.3.8.2, 6.3.8.3, 6.3.8.4 and 6.3.8.5 for gain ratios 1:05, 1:1, 1:2, 1:4, and

1:8 respectively. Recordings for ratios 1:1 and 1:4 are shown in Figure 6.3.8.2.1 and 6.3.8.4.1 respectively. Comparison of these graphical plots with those as obtained for corresponding conditions in the non-feathering (symmetrical) case presented in Figure 5.2.5 exhibits two major significant differences.

1. As to the course of the mean value of displacement, there exists no peak in the curves for the feathering case. Generally, an increase of external acceleration results in a larger amount of missile roll deviation. Such a peak, however, is always present in the symmetrical (non-feathering) case.

2. For a given parameter (gain ratio of velocity/position) and a value of external acceleration for which the non-feathering system has not yet reached the peak of mean displacement, the oscillation amplitude is much smaller in the feathering case, as is the mean deviation. However, since the curves for the non-feathering system pass through a maximum whose absolute value and location relative to external acceleration vary with the parameter, i.e., the gain ratio, there are regions of large external disturbance where the non-feathering system yields a smaller mean deviation from zero position than does the feathering type.

The extent to which the missile performance is influenced by a time delay introduced in the integrating motor component, has been explained in paragraph 4.4. There it became evident that an integrating motor with a relatively large time constant has no detrimental effect, but improves performances inasmuch as the mean deviation of the missile in response to external accelerations becomes smaller than in the case of an ideal integrating motor.

The simulation dealing with a symmetrical case applying different values for the time constant yielded results which were in agreement with considerations previously made on a more qualitative basis. This can be seen by comparing the Figure 5.2.5 with 5.3.2. A similar response with respect to binding of the missile nearer to its zero position was observed in the feathering case. Results obtained from simulation tests with a time delay of 100 m sec and for different gain ratios are presented in Figure 6.3.9.1, 6.3.9.2, and 6.3.9.3 for gain ratios of 1:1, 1:2, and 1:4 respectively which compare favorably with those given in Figure 6.3.8.2, 6.3.8.3, 6.3.8.4 respectively. However, it should be kept in mind that all these curves represent only the steady state of missile oscillatory deviation. There are more or less noticeable differences in both the frequency by which the missile oscillates and its transient behavior; a few examples are demonstrated in Figure 6.3.9.4, 6.3.9.5 for gain ratios of 1:1 and 1:4 respectively.

In agreement with results obtained from the investigation of the non-feathering type, a time delay in the actuator pushes the response curve of the missile into the region of larger deviations; however, the difference in system response between a time delayed actuator and an ideal one is not as big as it is in the case of the corresponding investigation on the non-feathering type. An example of this shift is given in Figure 6.3.10.1, 6.3.10.2, 6.3.10.3 and 6.3.10.4 for the time delays of .01, 0.02, 0.05, and 0.1; a gain ratio of 1:4 was used for each of these figures. Recordings representing various components of a system using a time delayed actuator are shown in Figure 6.3.10.1.1 and 6.3.10.2.1 for gain ratio 1:4 and disturbances of 40% and time delays of 0.1 and 0.01 sec respectively.

SECTION V

CONCLUSIONS

The Flicker Type Control System is particularly adapted to pilotless flight vehicles. It is quite versatile and maintains well controlled oscillations with components upon which it places liberal requirements. Despite its non-linear features it resembles linear systems in many respects. In addition, it lends itself very well to electronic simulation. On a single REAC unit, complete simulation (for one axis) was performed with a small amount of supporting equipment.

The faster operating feathering method of returning the surface to neutral position by the force of the airstream results in higher system frequencies and consequently smaller amplitudes than the aymmetrical system which has equal velocities for surface outbound and inbound travel. It seems reasonable that this feathering system would yeld better overall system performance. However, if the larger amplitude of oscillation appears to be acceptable, the simpler symmetrical system will actually yield better results in response to gust conditions which are large with respect to maximum surface effectiveness. (See Figure 5.2.5, 6.3.8.1, 6.3.8.2 and 6.3.8.3)

The steady state operation of a flicker type system may be approximated by simplified graphic methods which permit the introduction of many of the practically difficult component characteristrics. (See paragraph 4.4. and Figure 4.4.4)

The frequency of oscillation for a system in which the surfaces contact stops depends in a linear manner upon the surface angular velocity and upon the limitations to surface travel. The amplitude of oscillation for this

system depends linearly upon surface effectiveness. (See Figure 5.2.2)

The frequency of a system whose surfaces do not contact stops is not dependent upon surface travel velocity. However, the amplitude of oscillation for this system depends in a linear manner on both surface speed and effectiveness.

Controlling the ratio of position signal gain to angular velocity signal gain provides an effective means for controlling system frequency within its limits of operation. It serves as a means of obtaining desirable system performance in response to external disturbance. (See Figure 5.2.4 and 6.3.3)

Although the system performance depends on rate gyro characteristics in an expectable manner, the rate gyro performance is a point of particular interest. There exists a range of rate gyro damping ratios for each missile control system combination, which by minimizing gimbal deflection offers a desirable gyro response. (See Figure 6.3.6.2)

In general, time delays in the system have the usual deteriorating effect. However, a certain range of time delays in the position sensing device tends to improve system performance. (Compare Figure 6.3.8.3 with 6.3.9.3, and Figure 5.3.3 with 5.2.5)

The system remains well mannered in spite of relatively large time delays in any of its components. However, if the components introduce errors of an asymmetry, the result is a steady state error in either angular position or velocity depending on the nature of the asymmetry and the component in which it is located. (See paragraph 5.5)

GENERALIZED DIAGRAM OF A FLICKER TYPE SYSTEM

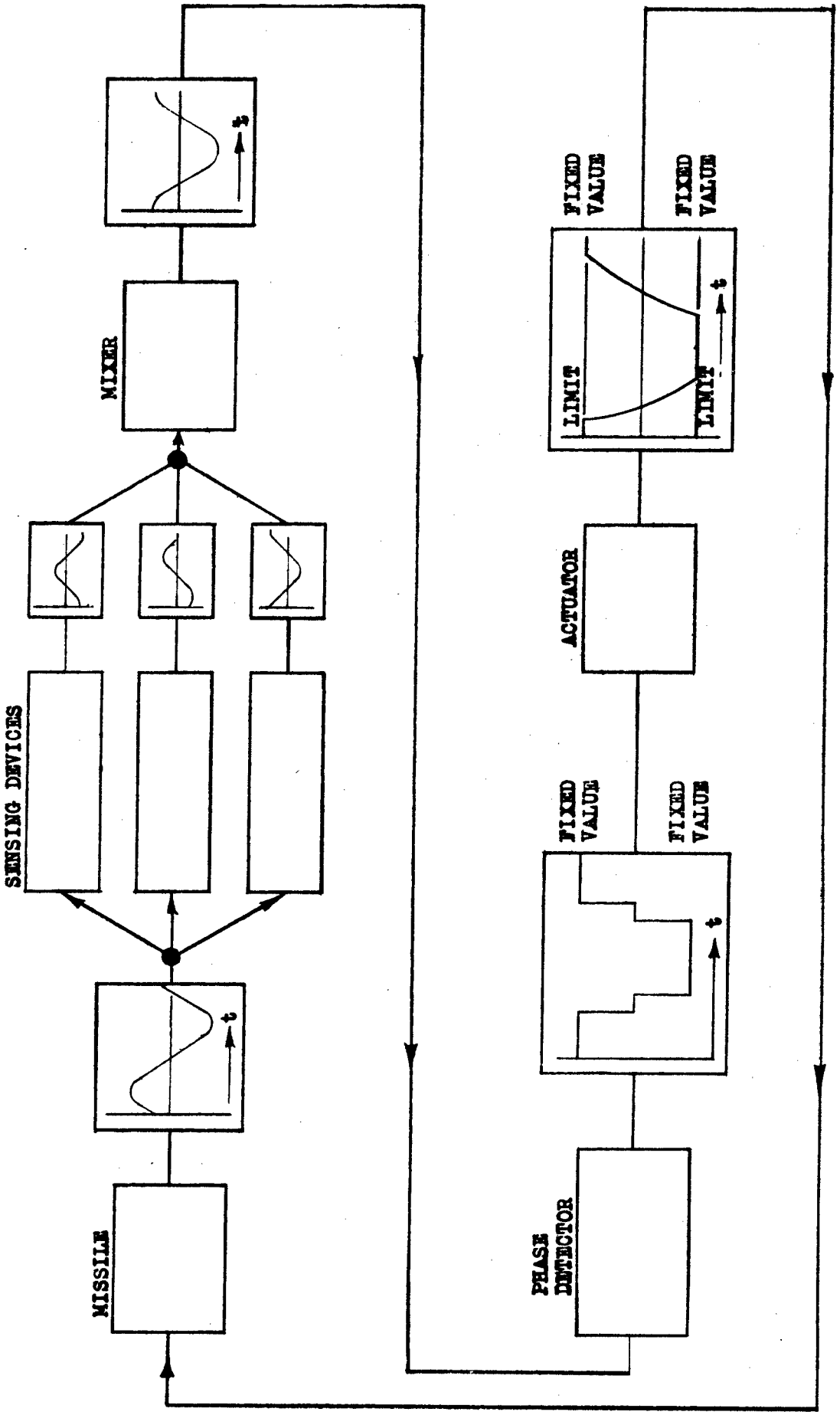

FIGURE 2.2.1

FLICKER-TYPE SYSTEM INVESTIGATED

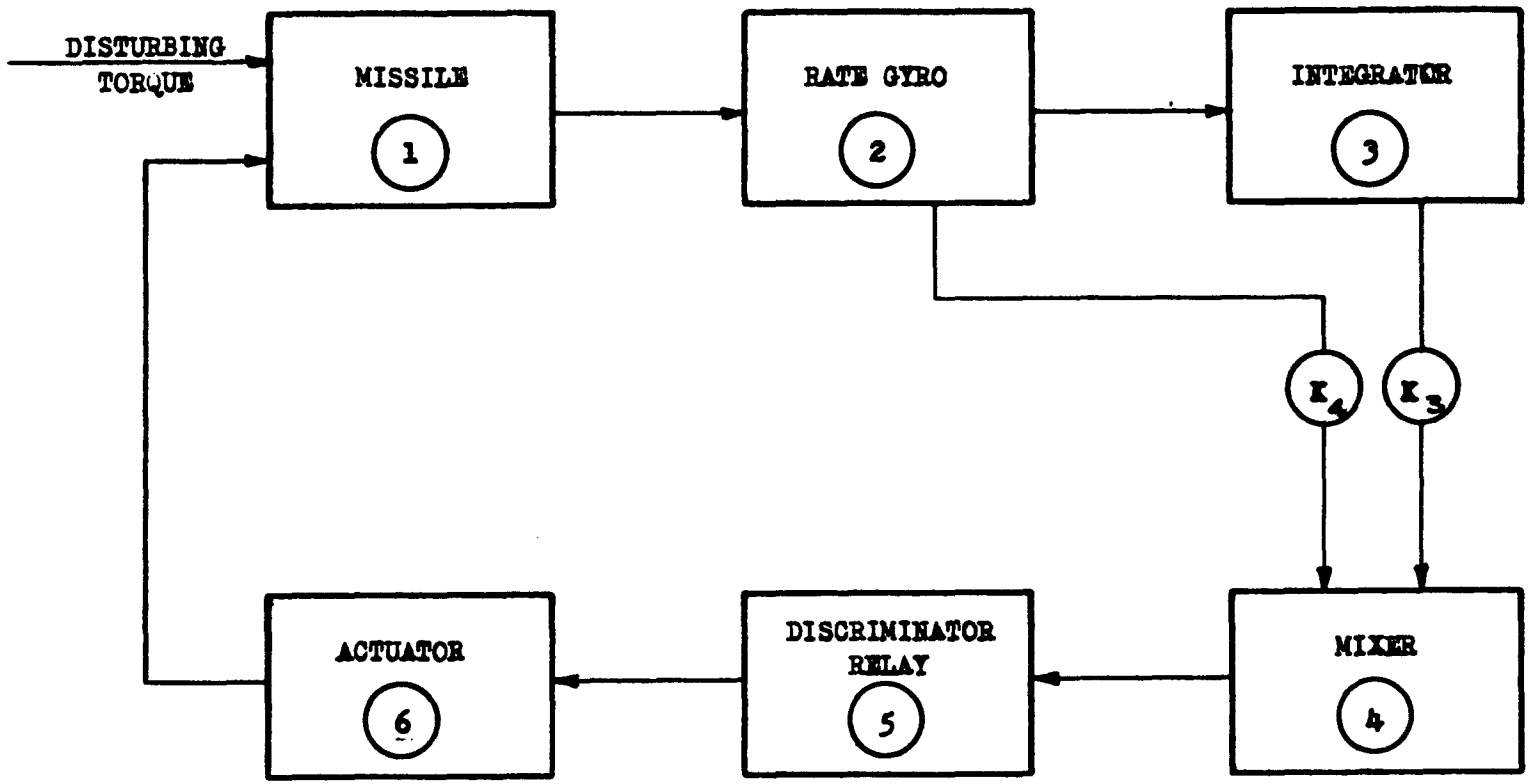

FIGURE 2.3.1

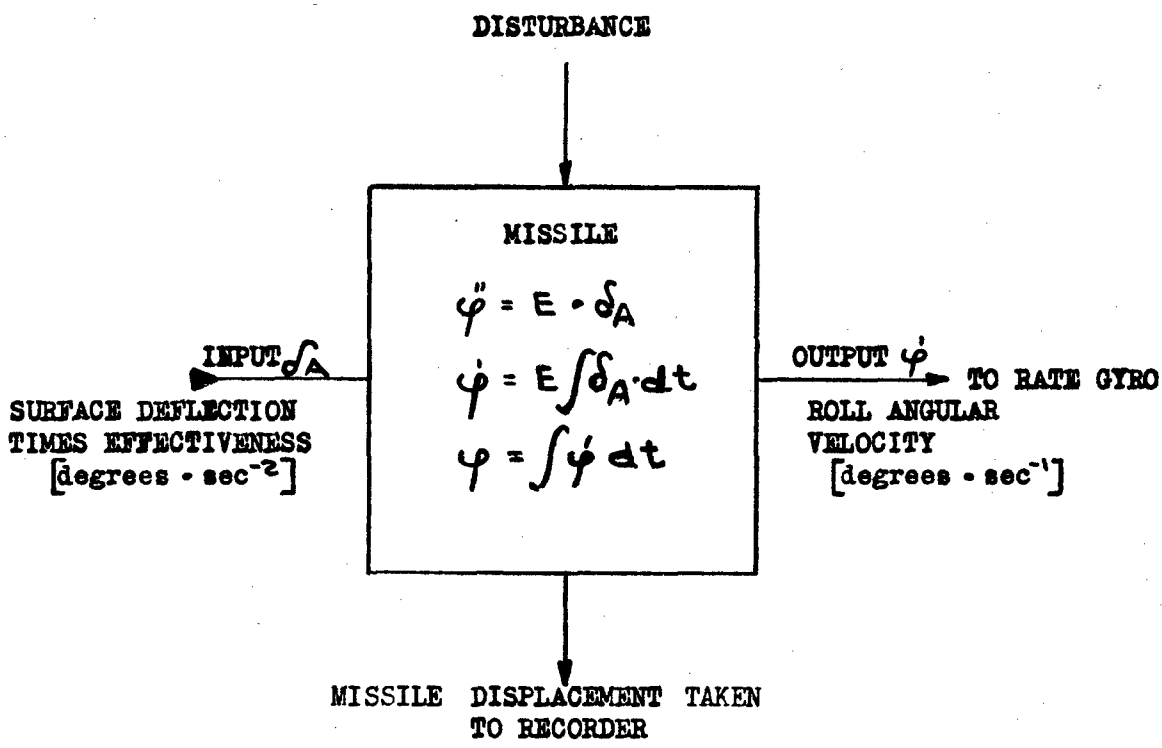

DETAILED BLOCK DIAGRAM OF MISSILE

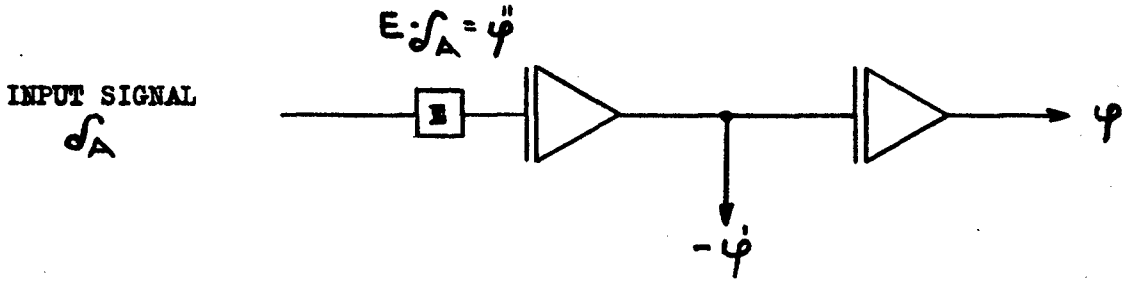

REAC DIAGRAM OF MISSILE SIMULATION

FIGURE 3.2.1.

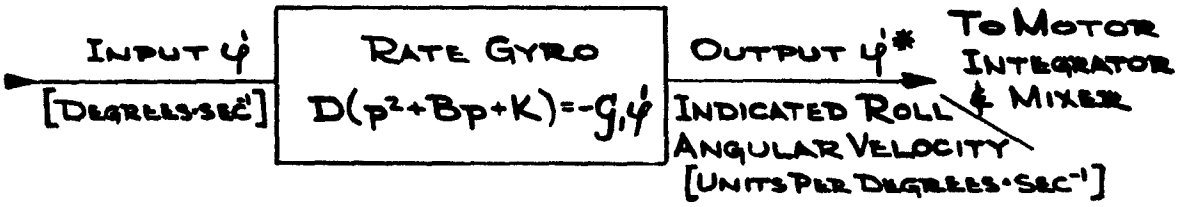

D = RATE GYRO GIMBAL DISPLACEMENT = OUTPUT SIGNAL = $\frac{\text{UNITS}}{(\text{DEGREE}\cdot\text{SEC}^{-1})\text{INPUT}}$

$B = 2\zeta\omega_n \left[\frac{1}{\text{SEC}}\right]$

ζ = DAMPING RATIO [1]

$K = \omega_n^2 \left[\frac{1}{\text{SEC}^2}\right]$

ω_n = NATURAL FREQUENCY OF THE UNDAMPED SYSTEM $\left[\frac{1}{\text{SEC}}\right]$

$p = \frac{d}{dt}$

g_1 = GAIN FACTOR [1]

$\dot{\varphi} = f(t)$ FORCING FUNCTION

DETAILED BLOCK DIAGRAM OF RATE GYRO

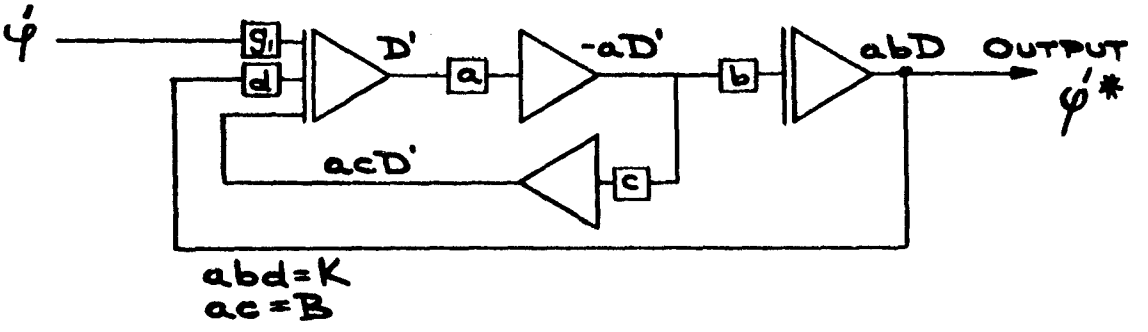

REAC DIAGRAM OF RATE GYRO SIMULATION

FIGURE 3.2.2

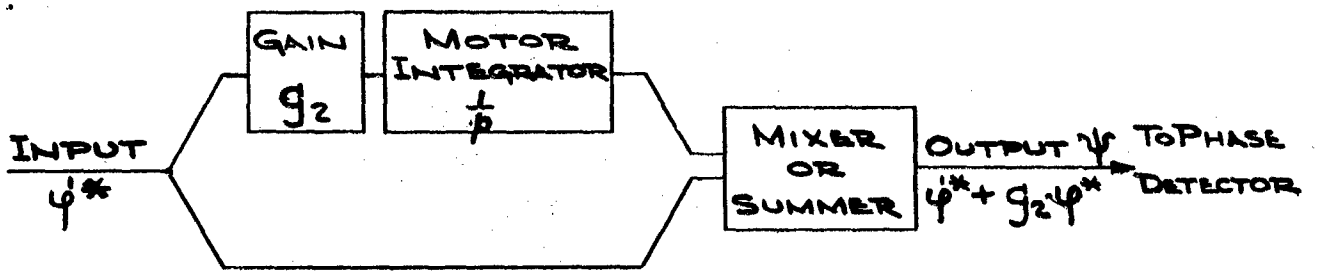

$$\varphi^* = \frac{g_2}{p} \cdot \dot{\varphi}^* = \text{INDICATED ROLL ANGLE}$$

$$\dot{\varphi}^* + g_2\varphi^* = \text{SUMMING COMMAND} = \psi$$

DETAILED BLOCK DIAGRAM OF MOTOR INTEGRATOR AND MIXER

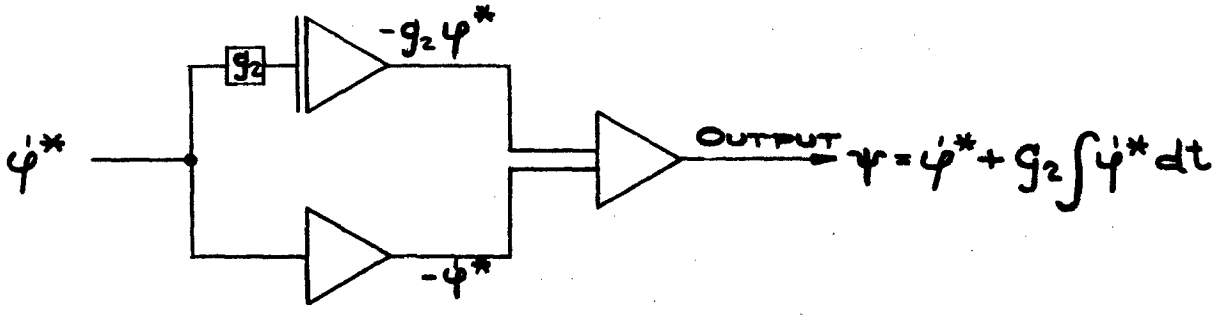

$$\text{GAIN RATIO } \frac{\text{VELOCITY COMPONENT}}{\text{POSITION COMPONENT}} = \frac{1}{g_2}$$

REAC DIAGRAM OF MOTOR INTEGRATOR AND MIXER SIMULATION

FIGURE 3.2.3

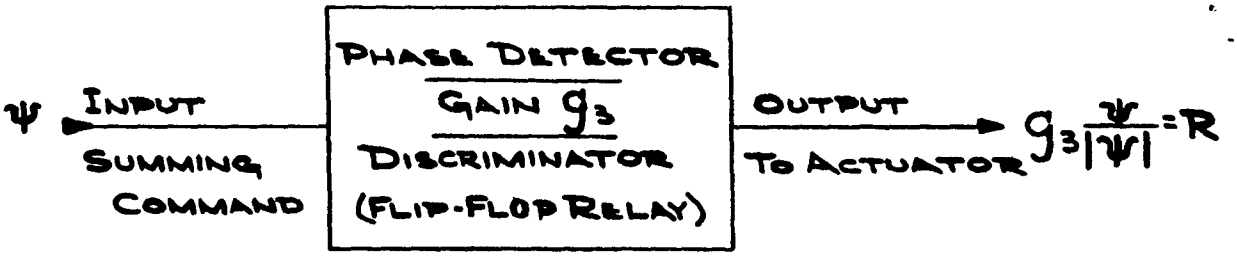

DETAILED BLOCK DIAGRAM OF PHASE DETECTOR

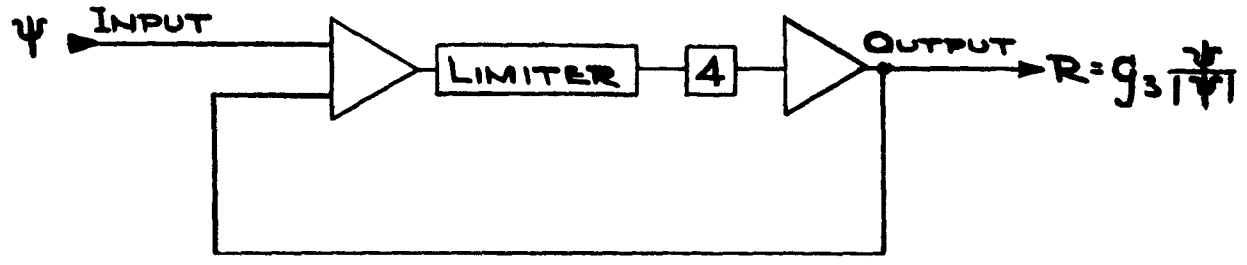

REAC DIAGRAM OF PHASE DETECTOR SIMULATION

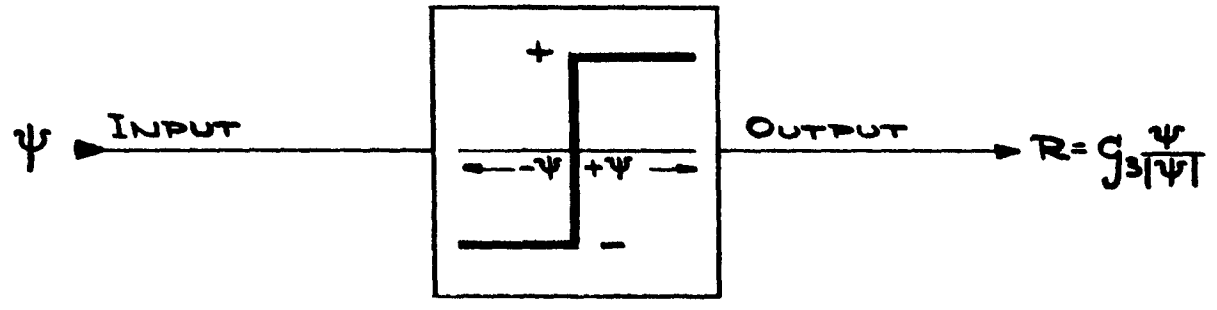

DIAGRAM OF PHASE DETECTOR SIMULATION
USING THE ARMOUR SPECIAL FUNCTION GENERATOR

FIGURE 3.2.4

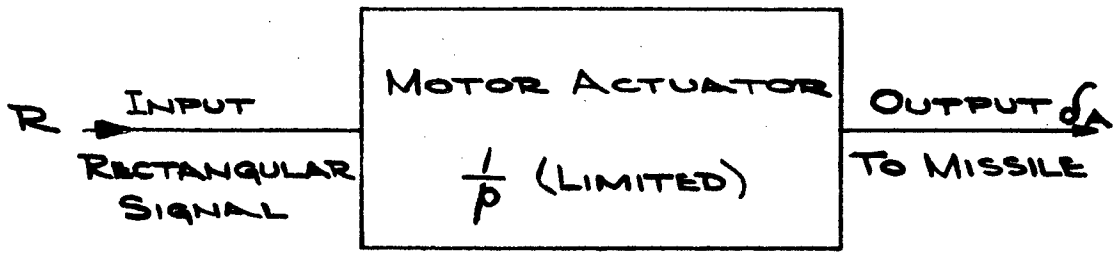

DETAILED BLOCK DIAGRAM OF MOTOR ACTUATOR

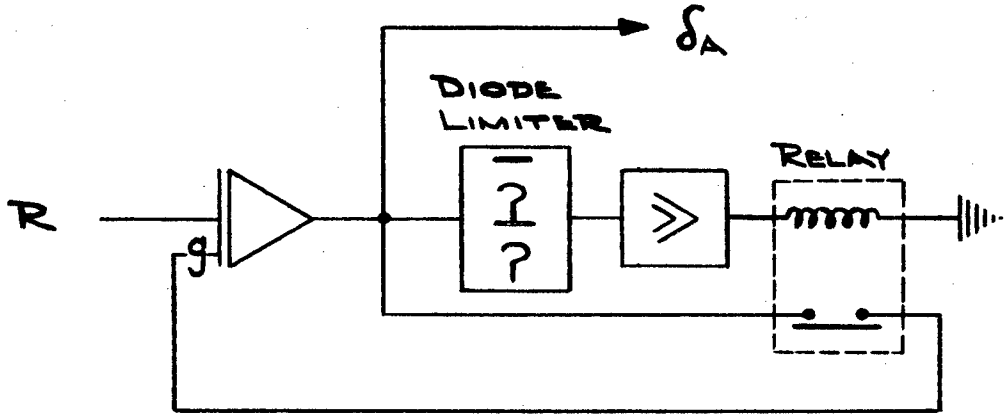

(g = High Gain)

REAC DIAGRAM OF MOTOR ACTUATOR SIMULATION
(NON-FEATHERING)

FIGURE 3.2.5

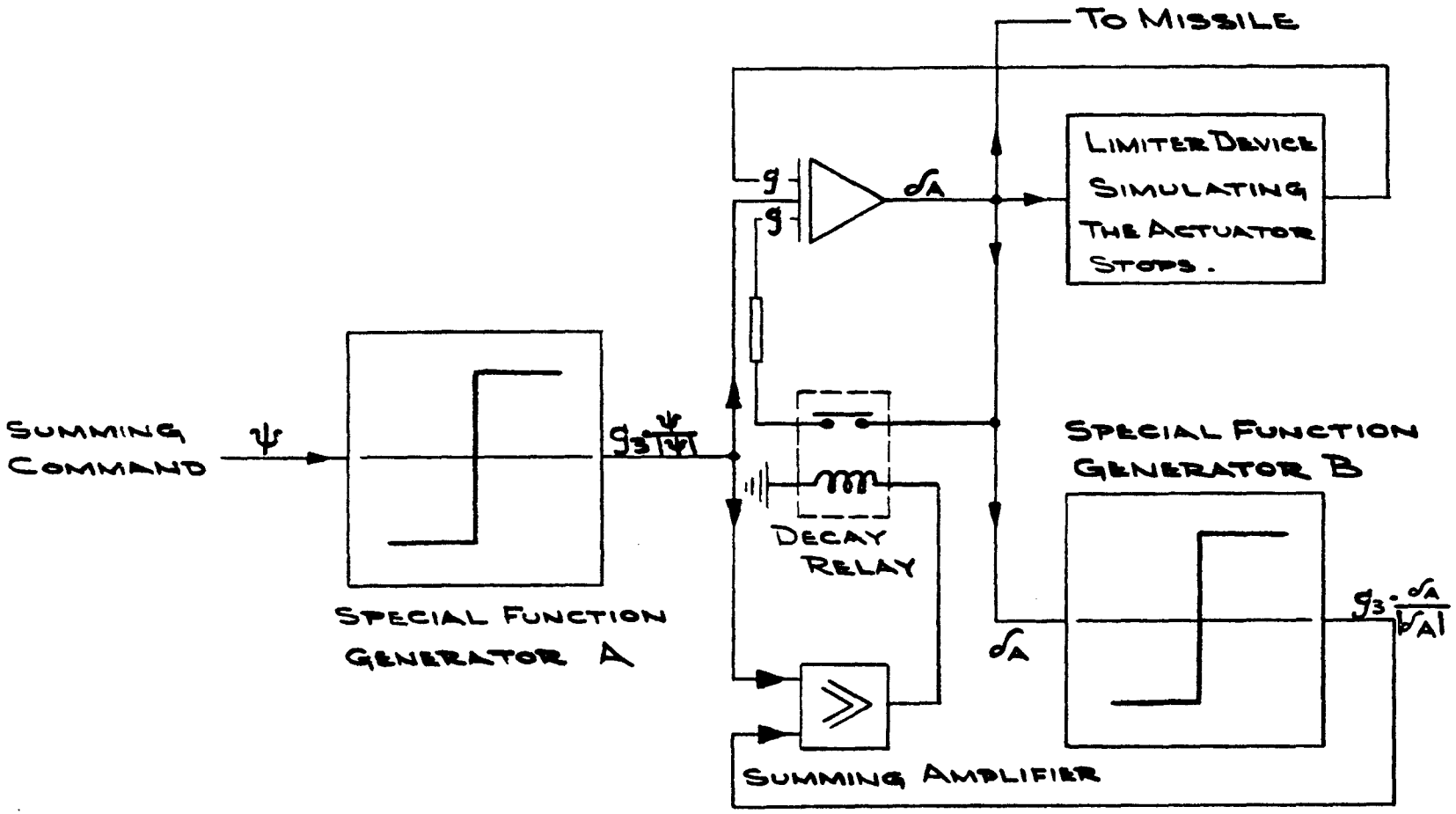

REAC DIAGRAM OF FEATHERING CONTROL SURFACE SIMULATION

FIGURE 3.2.6

ACTUATOR CUTPUT FOR FEATHERING TYPE SYSTEM

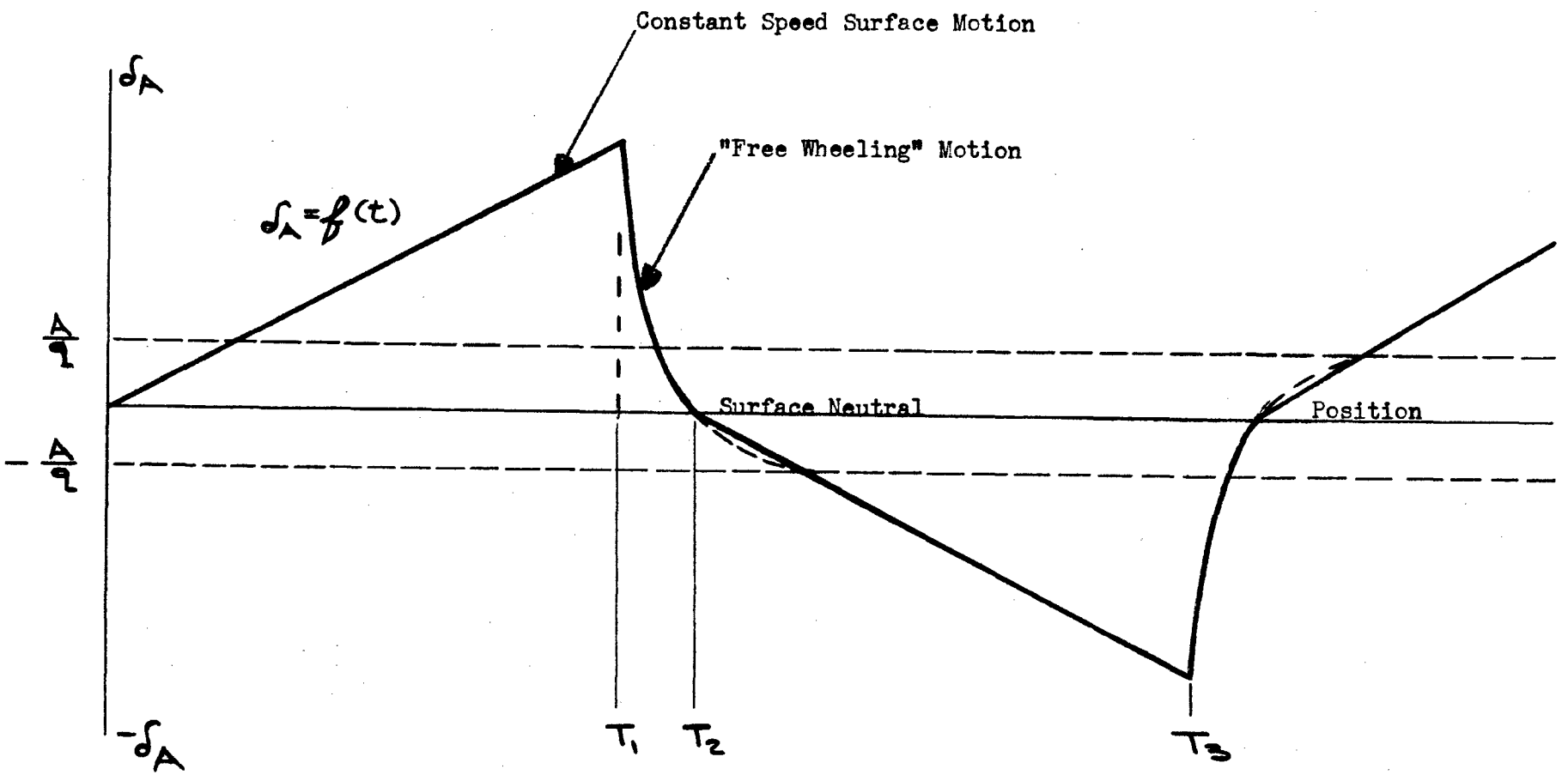

FIGURE 3.2.7

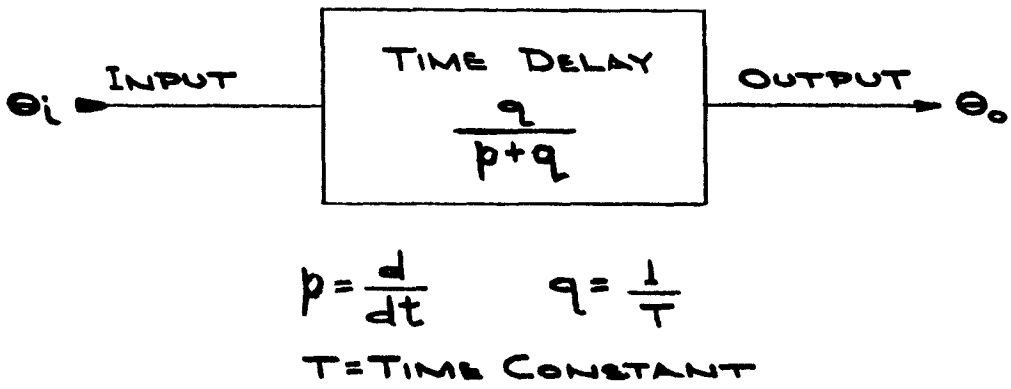

DIAGRAM OF A COMPONENT PRODUCING A TIME DELAY

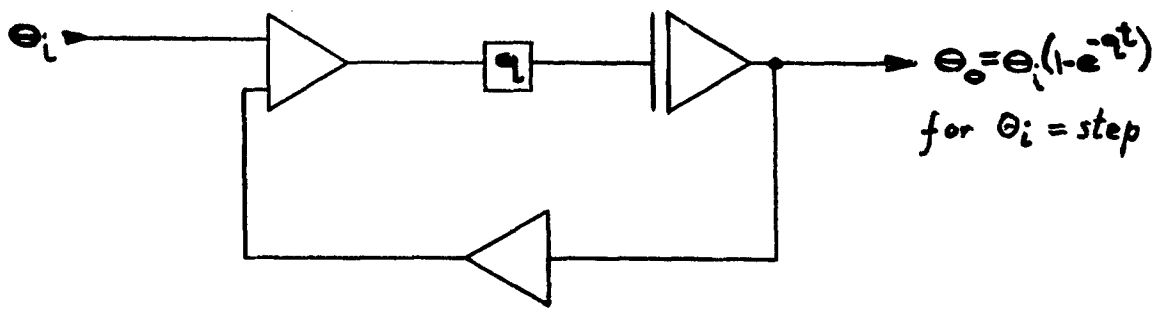

REAC DIAGRAM OF TIME DELAY SIMULATION

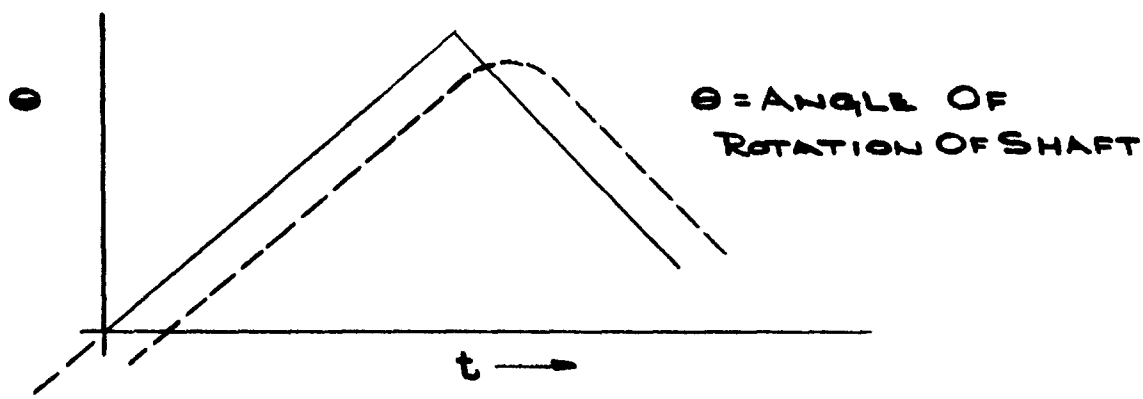

MOTOR INTEGRATOR WITH (---) AND WITHOUT (——) TIME DELAY

FIGURE 3.2.8

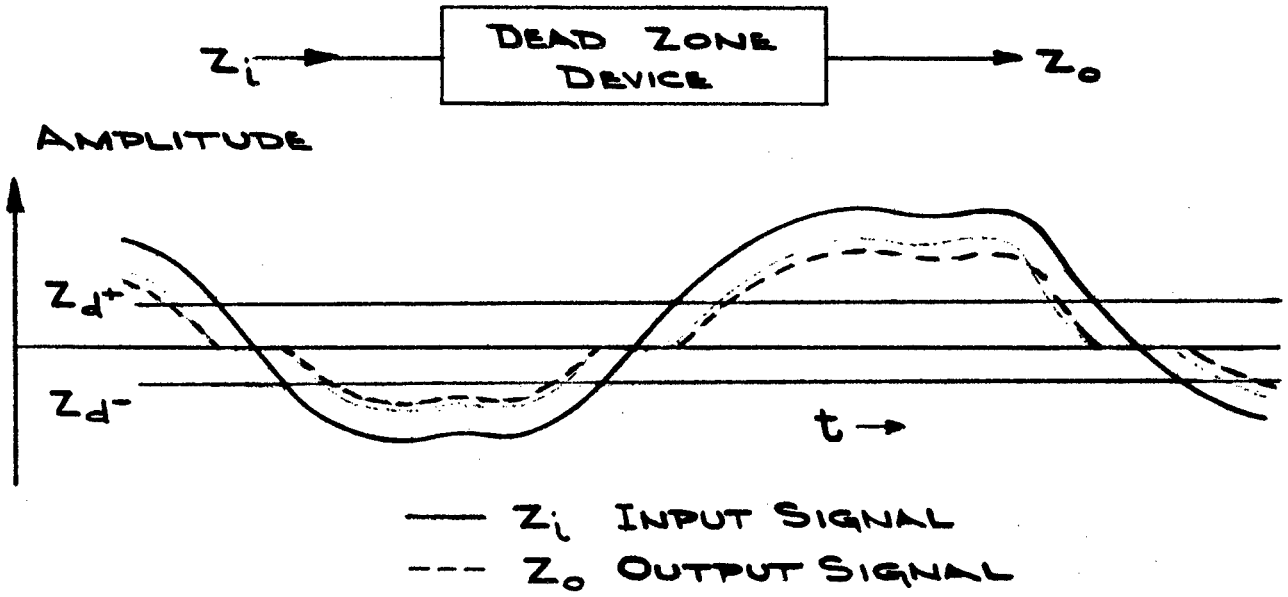

DETAILED BLOCK DIAGRAM OF DEAD ZONE DEVICE

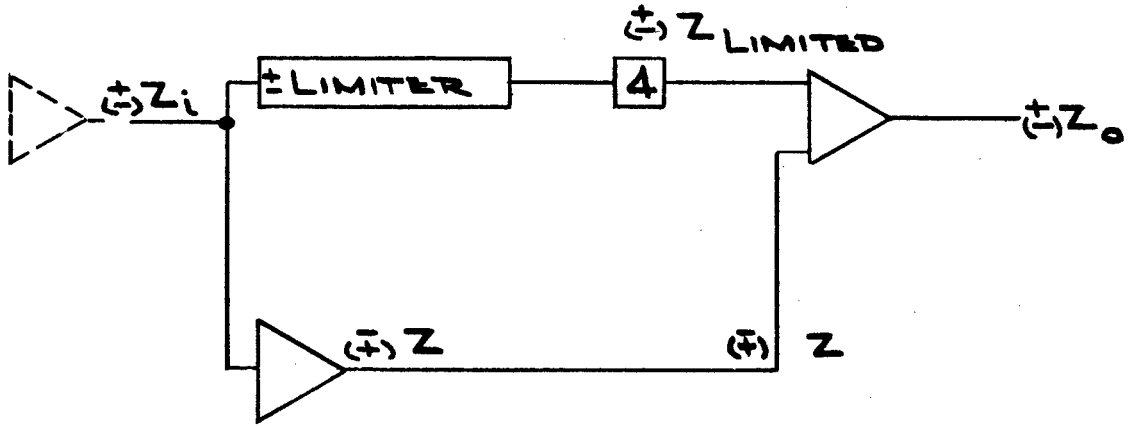

$$Z_o = 0 \quad \text{IF } Z_{d^-} \leq Z_i \leq Z_{d^+}$$

$$Z_o = Z_i - Z_{d^+} \quad \text{IF } Z_i \geq Z_{d^+}$$

$$Z_o = Z_i + Z_{d^-} \quad \text{IF } Z_i \leq Z_{d^-}$$

REAC DIAGRAM OF DEAD ZONE SIMULATION

FIGURE 3.2.9

AIRFRAME CONTROL BY CONVENTIONAL TYPE AUTOPILOT

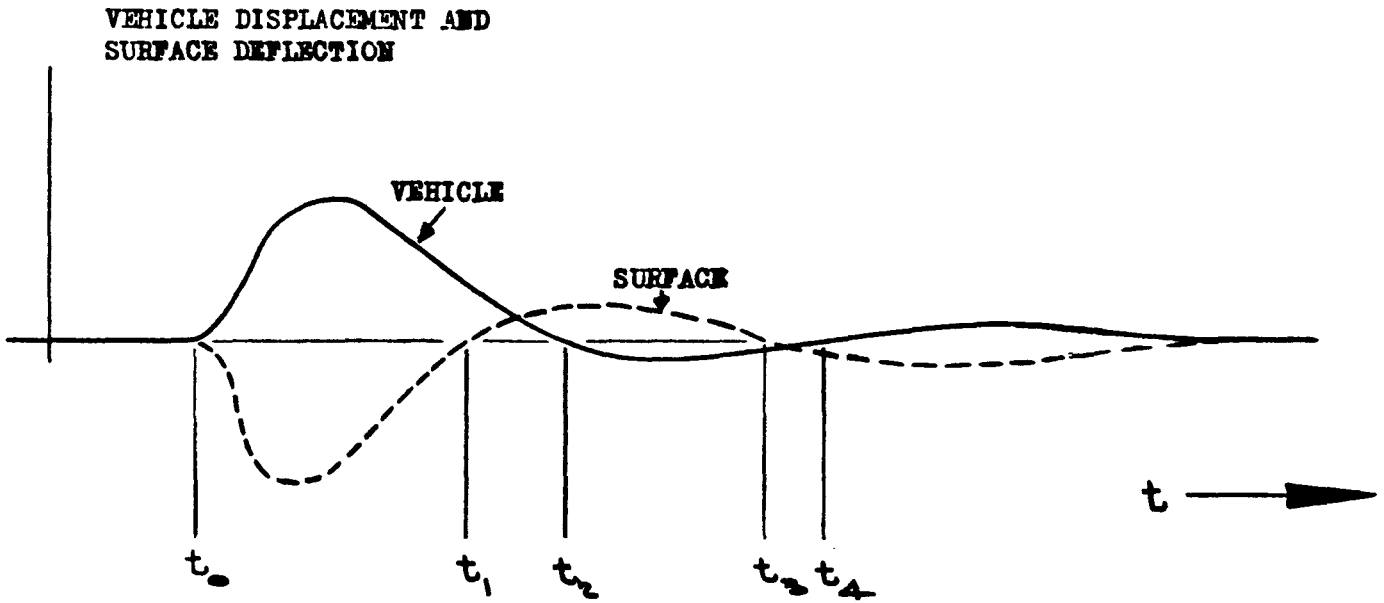

FIGURE 4.1.1

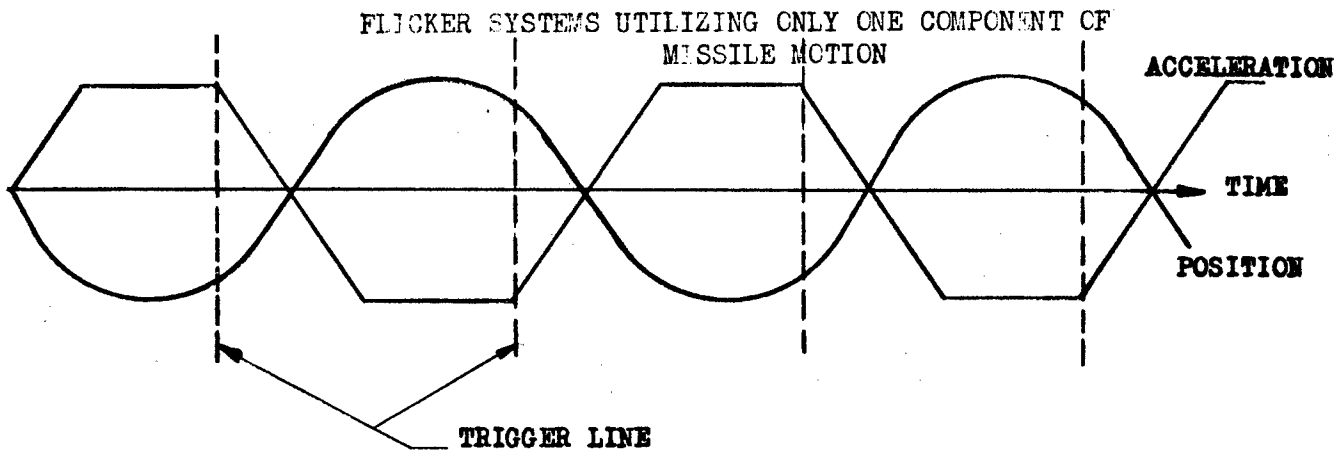

FIGURE 4.2.1

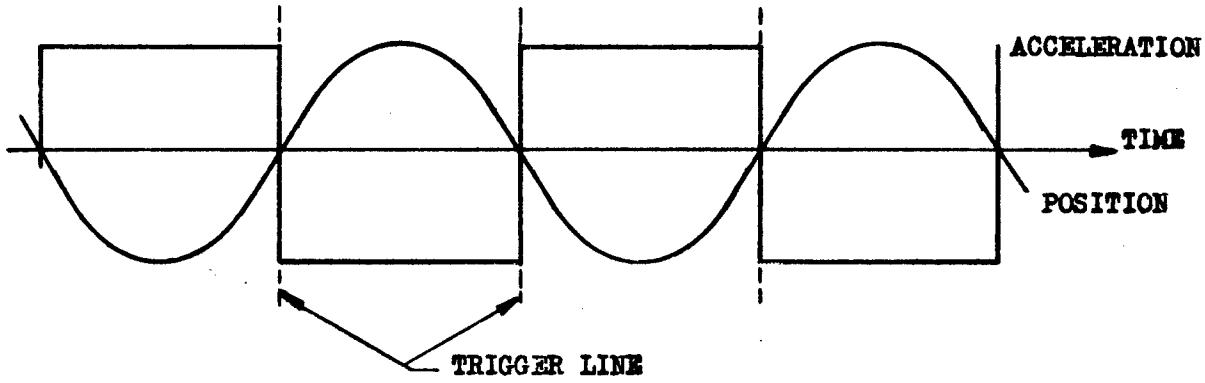

FIGURE 4.2.2

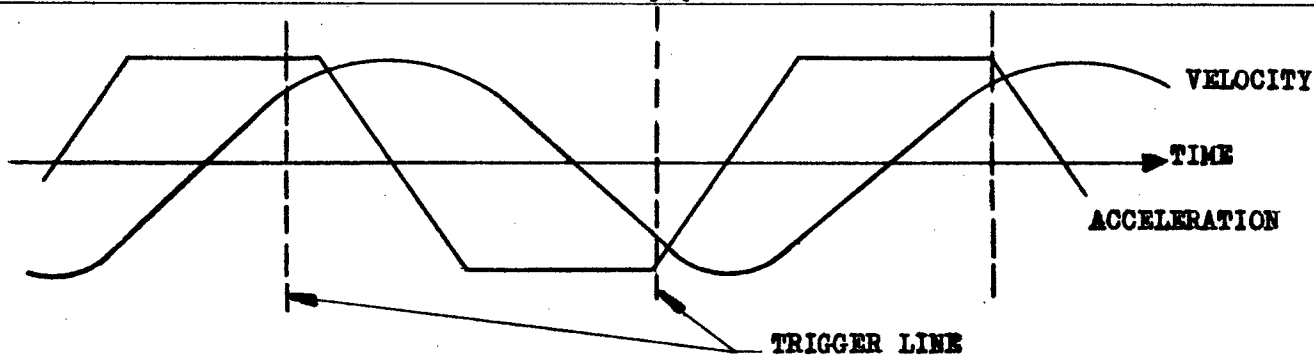

FIGURE 4.2.3

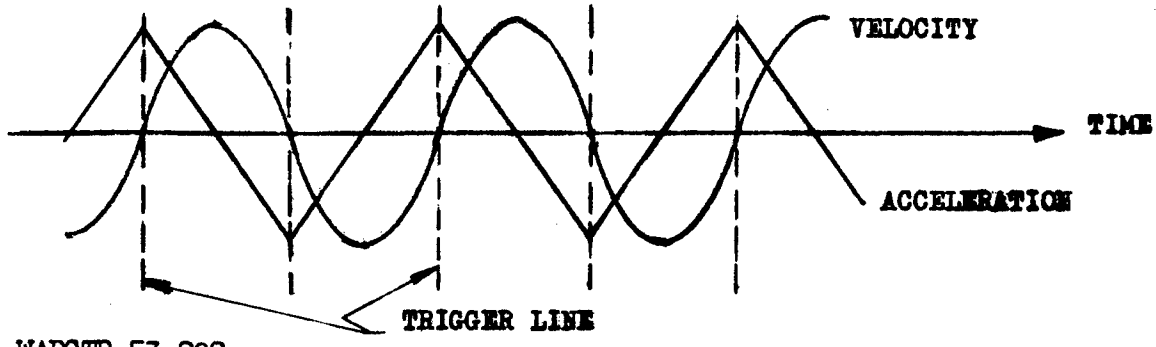

FIGURE 4.2.4

RELATIONSHIP OF MISSILE MOTION COMPONENTS
FOR A SYSTEM UTILIZING A COMBINATION OF ANGULAR
VELOCITY AND ANGULAR POSITION

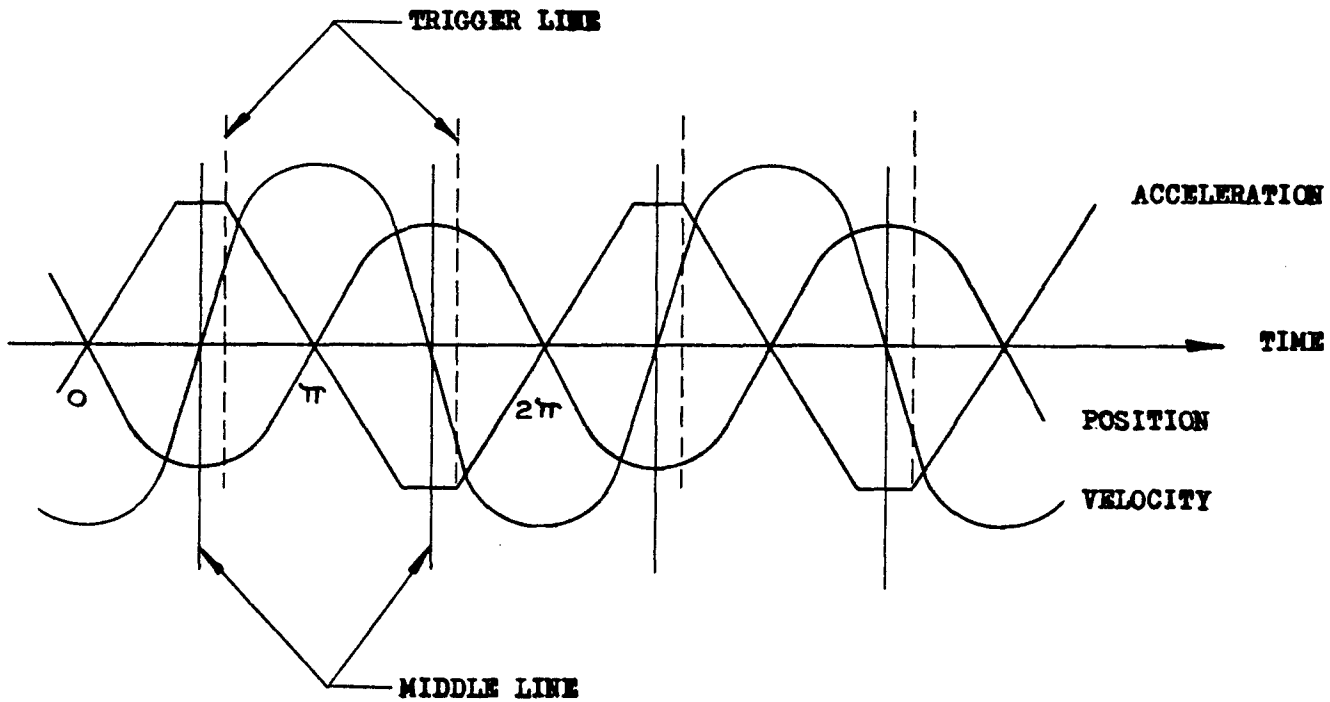

FIGURE 4.2.5

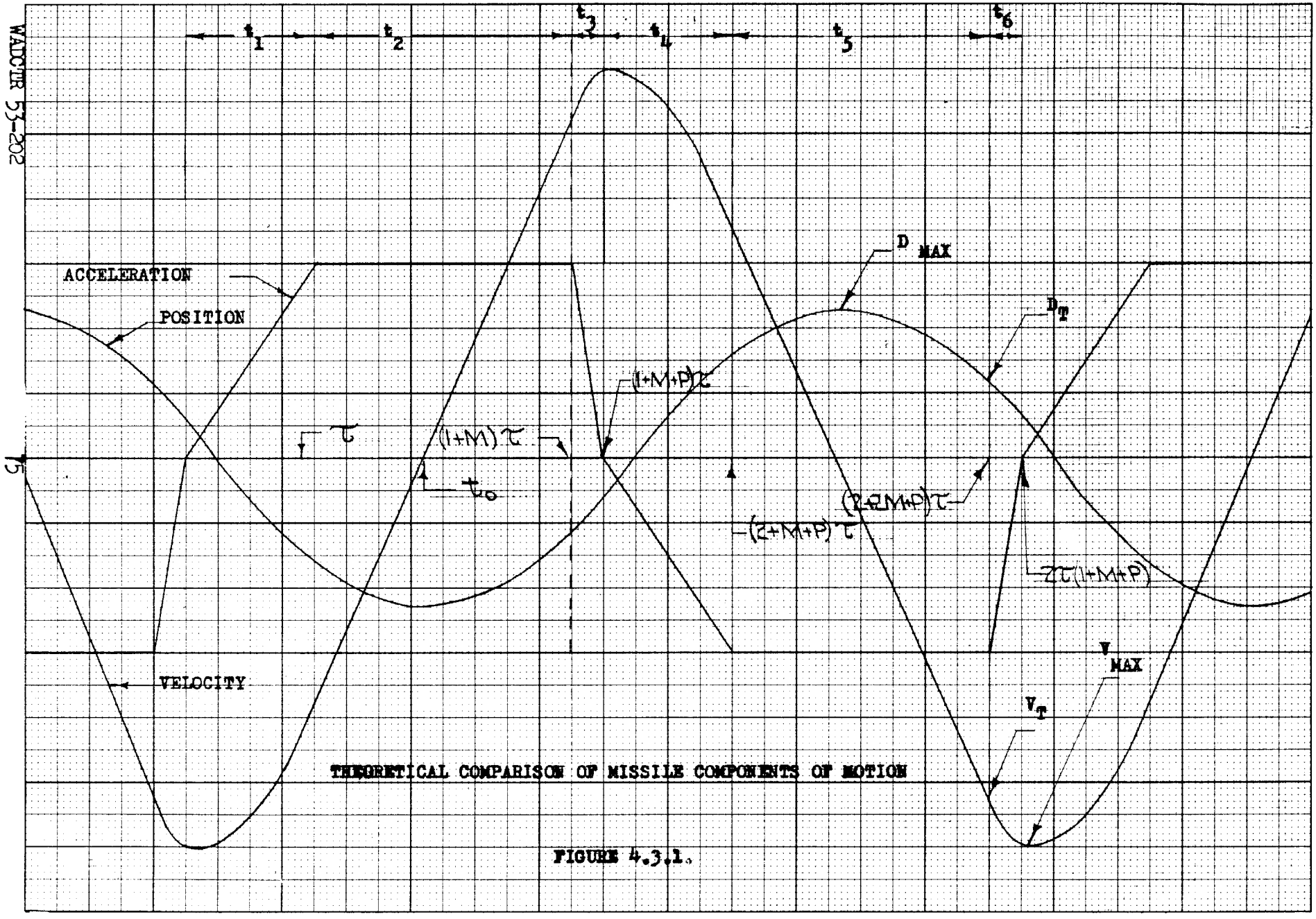

THEORETICAL COMPARISON OF MISSILE COMPONENTS OF MOTION

FIGURE 4.3.1.

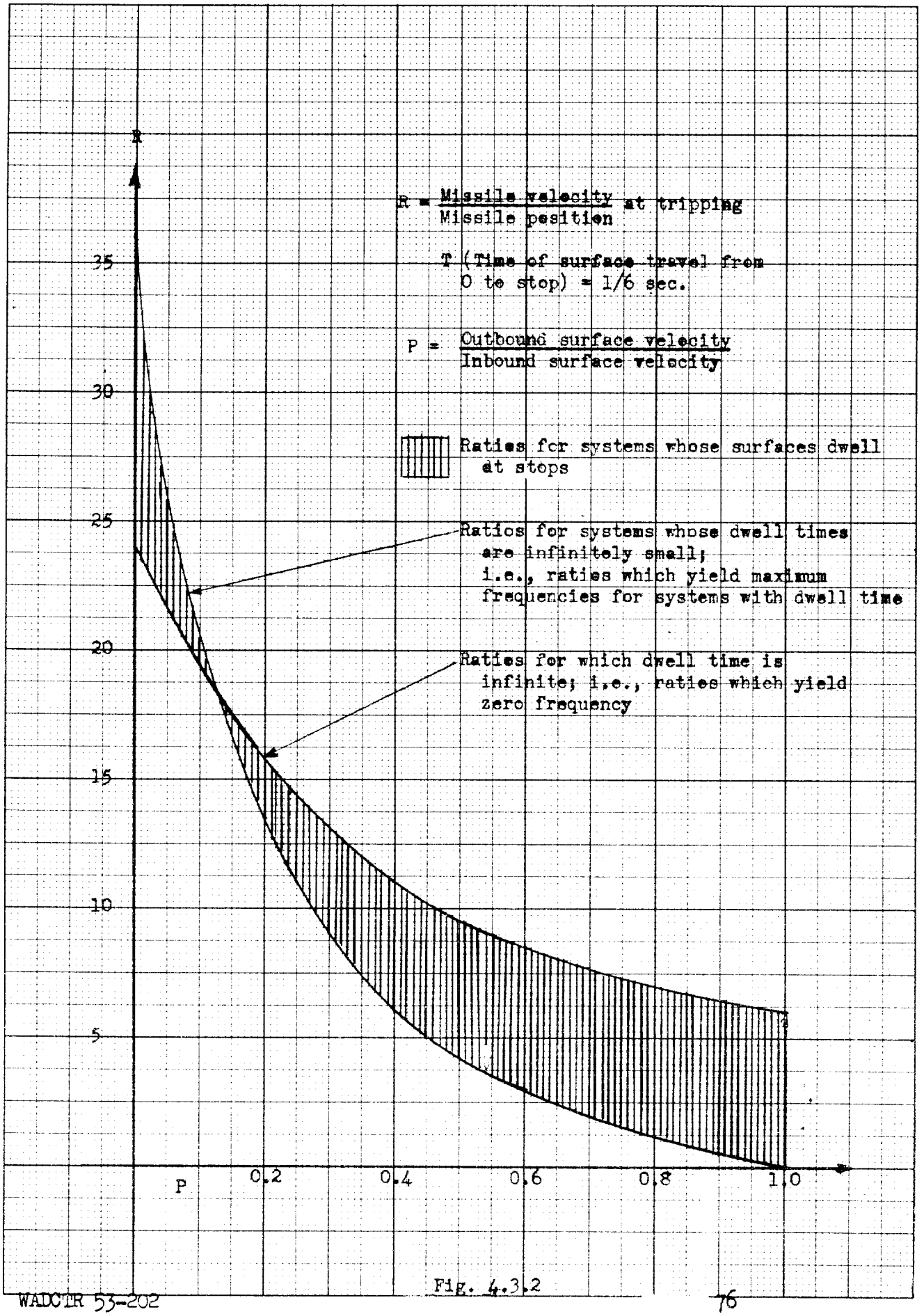
R
35
30
25
20
15
10
5
P
0.2
0.4
0.6
0.8
1.0
R = Missile velocity at tripping / Missile position
T (Time of surface travel from 0 to stop) = 1/6 sec.
P = Outbound surface velocity / Inbound surface velocity
Ratios for systems whose surfaces dwell at stops
Ratios for systems whose dwell times are infinitely small; i.e., ratios which yield maximum frequencies for systems with dwell time
Ratios for which dwell time is infinite; i.e., ratios which yield zero frequency

Fig. 4.3.2

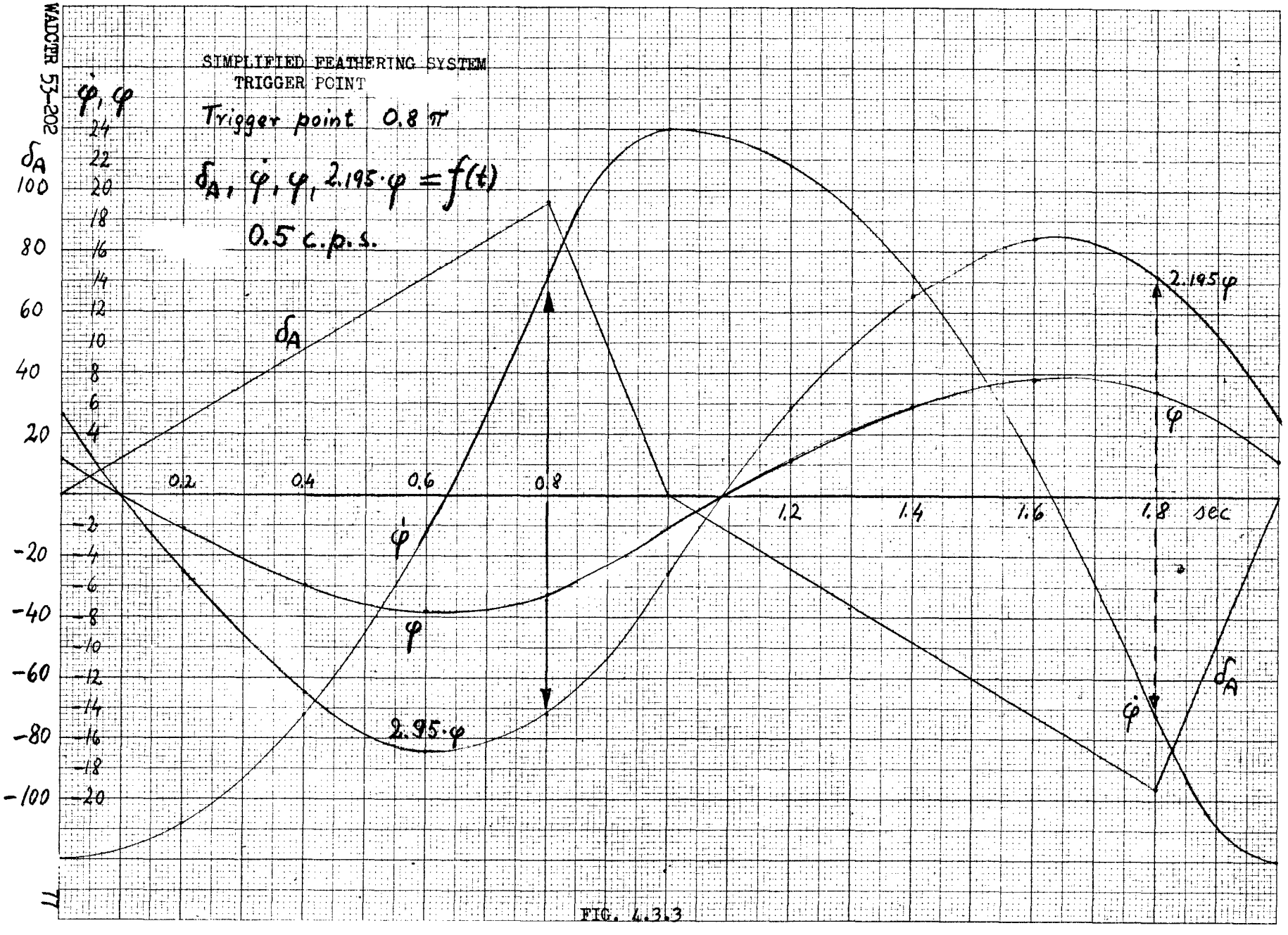
WADCTR 53-202
SIMPLIFIED FEATHERING SYSTEM
TRIGGER POINT
Trigger point 0.8 π
δA, φ̇, φ, 2.195·φ = f(t)
0.5 c.p.s.
φ̇, φ
δA
100
80
60
40
20
-20
-40
-60
-80
-100
24
22
20
18
16
14
12
10
8
6
4
-2
-4
-6
-8
-10
-12
-14
-16
-18
-20
0.2
0.4
0.6
0.8
1.2
1.4
1.6
1.8 sec
δA
φ̇
φ
2.195φ
φ
φ̇
δA
2.95·φ

FIG. 4.3.3

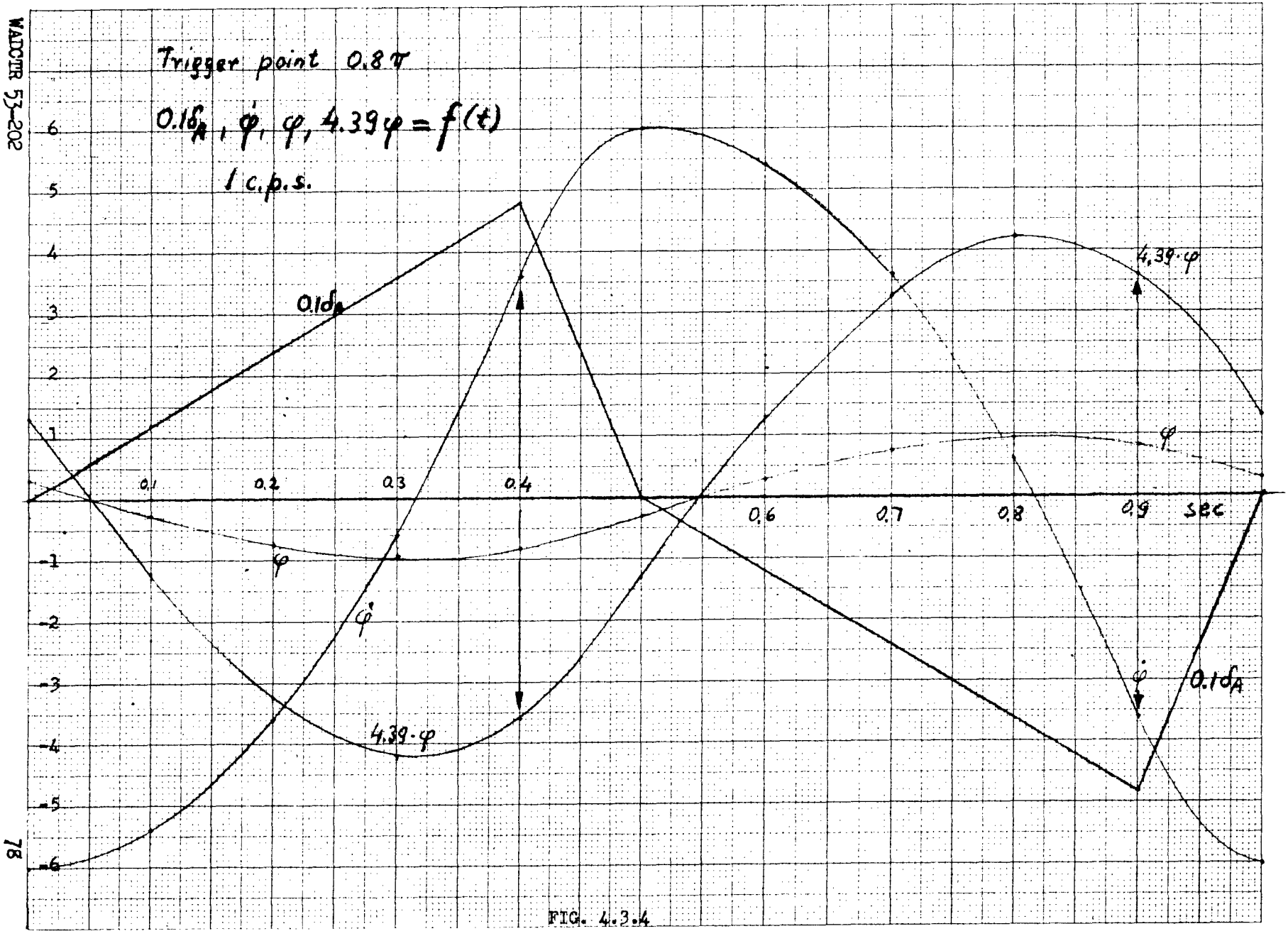
Trigger point 0.8 τ
0.1δA, φ̇, φ, 4.39φ = f(t)
1 c.p.s.
0.1δA
4.39·φ
φ
φ̇
0.1δA
4.39·φ
φ̇
0.1
0.2
0.3
0.4
0.6
0.7
0.8
0.9
sec
6
5
4
3
2
1
-1
-2
-3
-4
-5
-6

FIG. 4.3.4

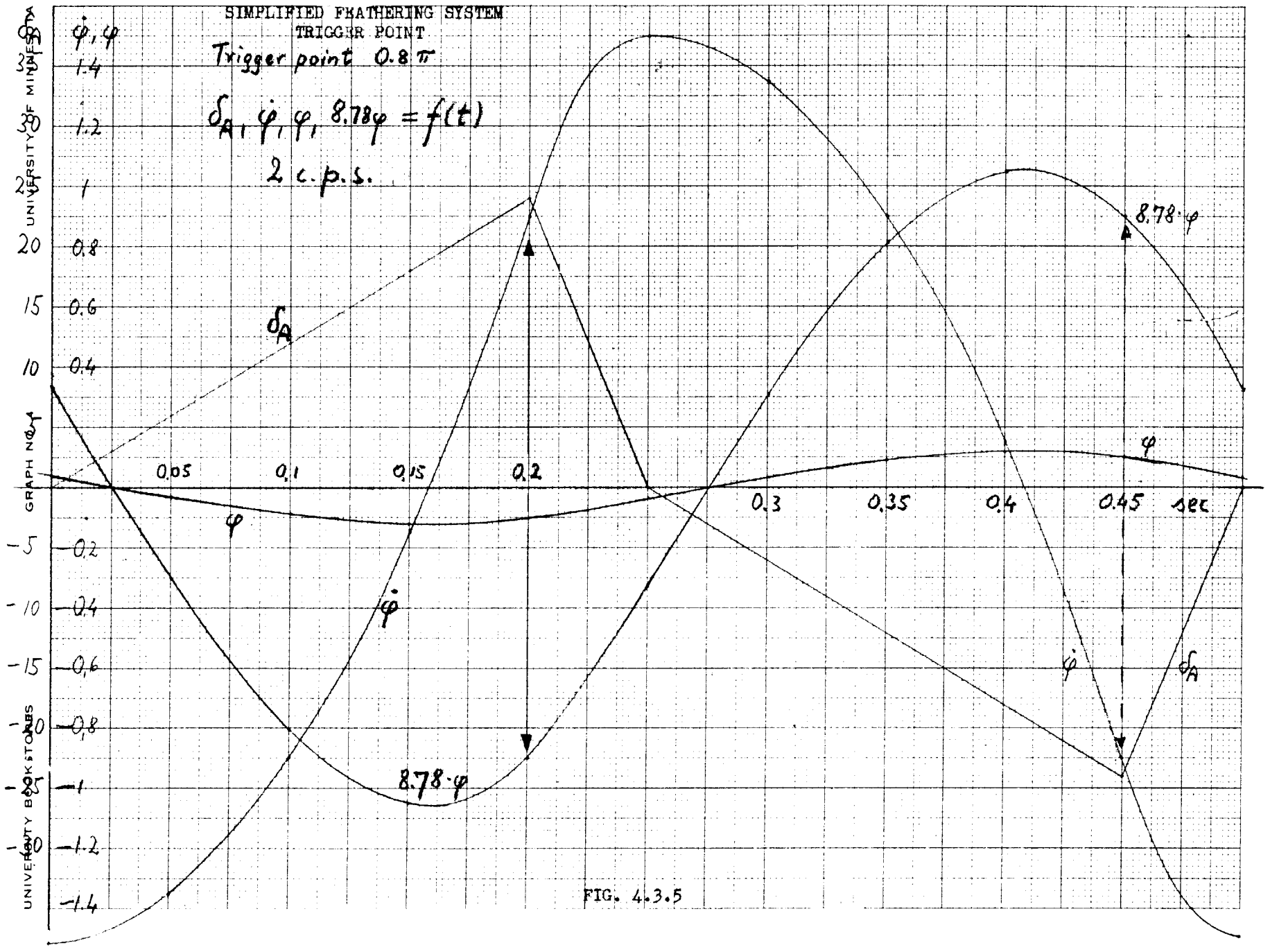

FIG. 4.3.5

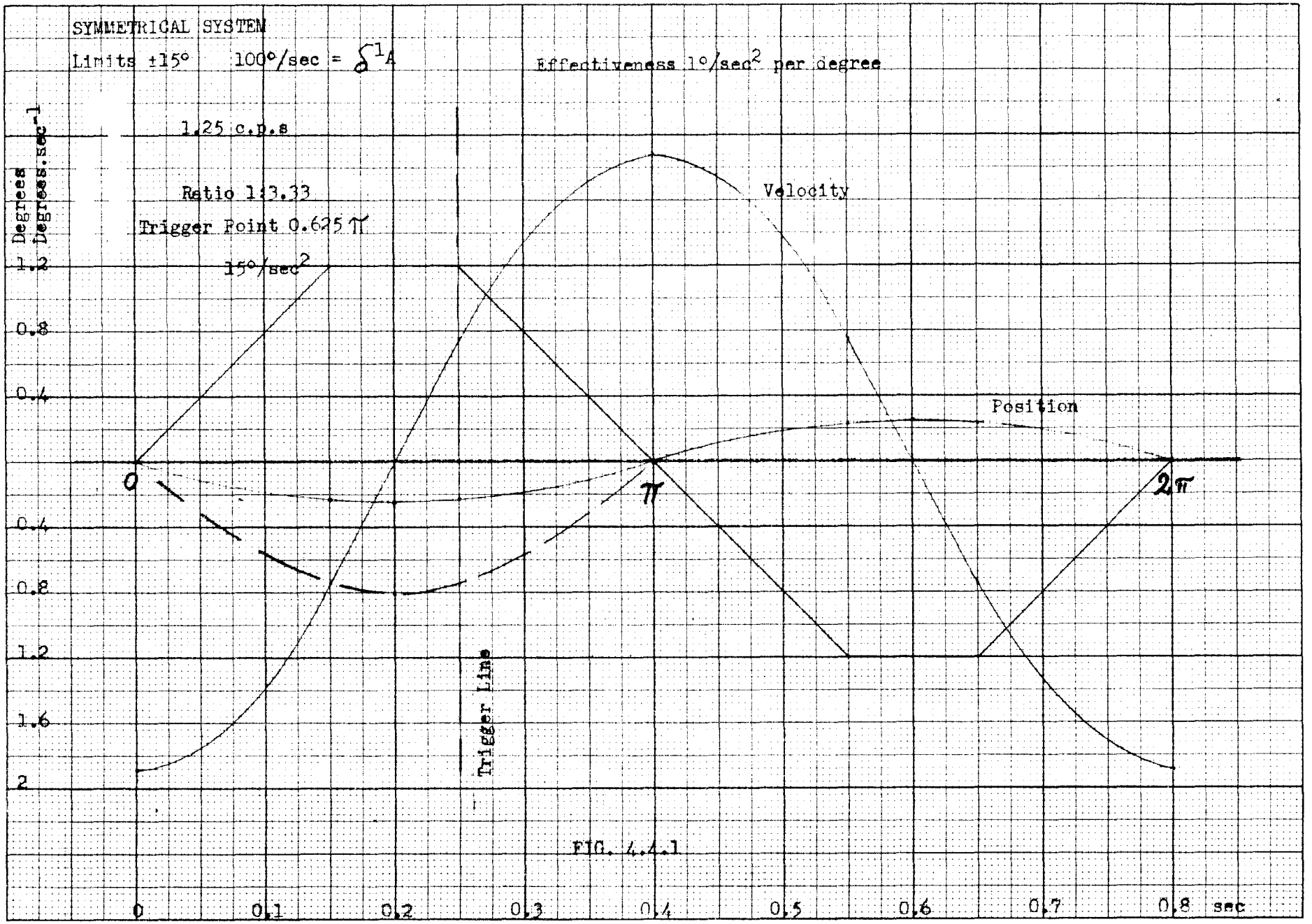
SYMMETRICAL SYSTEM
Limits ±15°
100°/sec = $\delta^1 A$
Effectiveness 1°/sec² per degree
1.25 c.p.s
Ratio 1:3.33
Trigger Point 0.625 π
15°/sec²
Degrees
Degrees.sec⁻¹
Velocity
Position
0
π
2π
Trigger Line
0
0.1
0.2
0.3
0.4
0.5
0.6
0.7
0.8 sec

FIG. 4.4.1

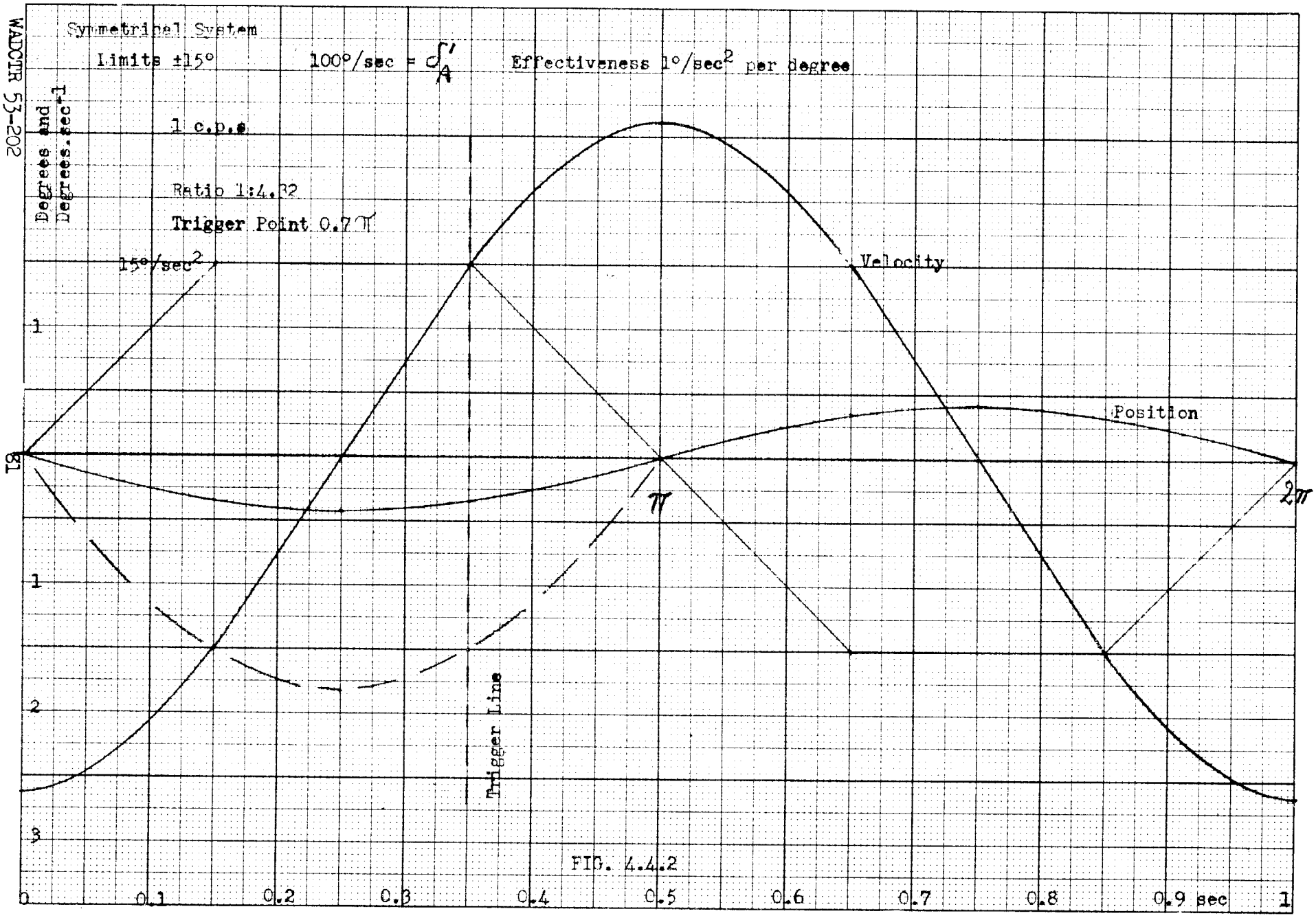
Symmetrical System
Limits ±15°
100°/sec = δ_A'
Effectiveness 1°/sec² per degree
Degrees and Degrees.sec⁻¹
1 c.p.s
Ratio 1:4.32
Trigger Point 0.7 π
15°/sec²
Velocity
Position
81
π
2π
Trigger Line
0
0.1
0.2
0.3
0.4
0.5
0.6
0.7
0.8
0.9 sec
1

FIG. 4.4.2

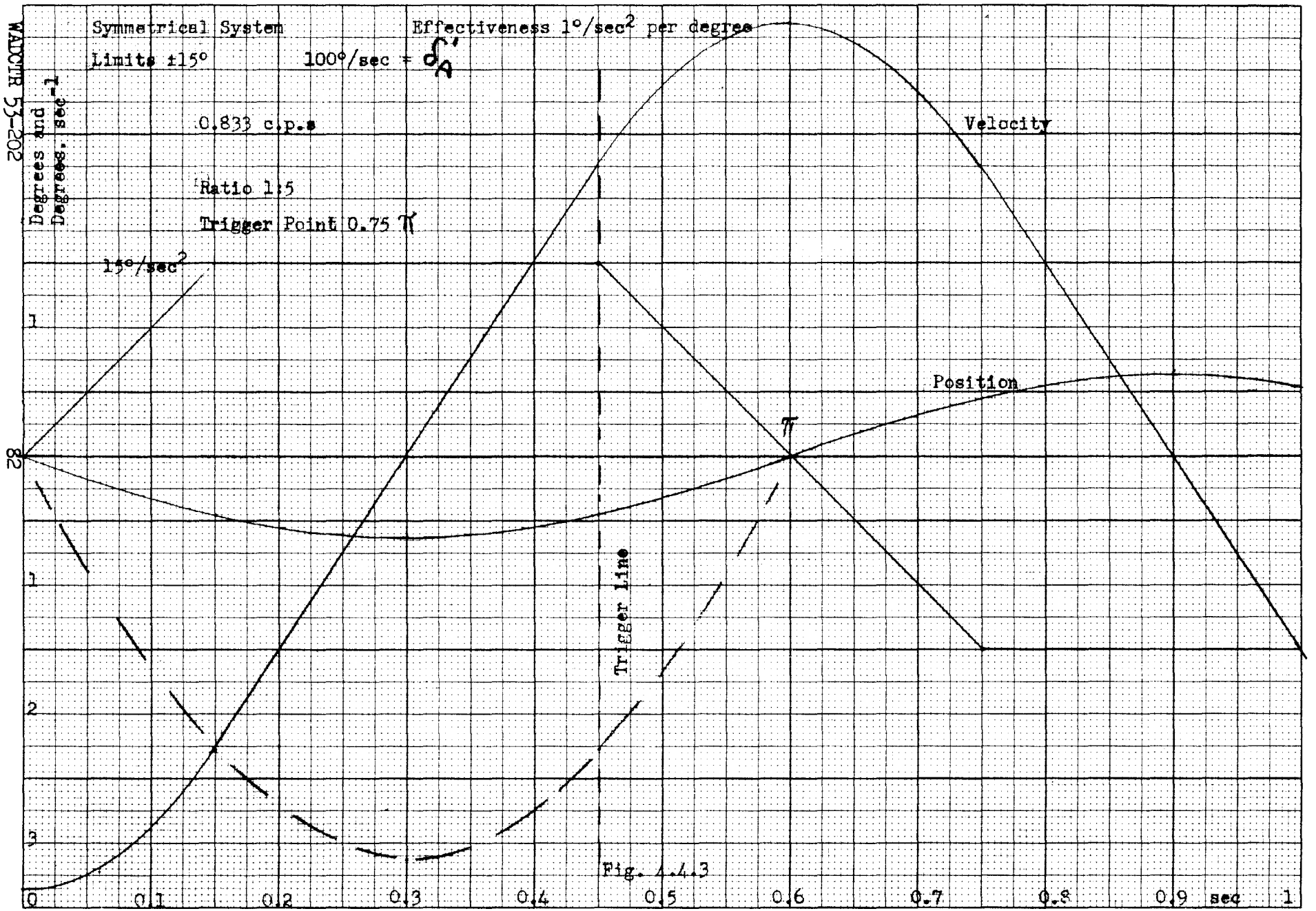
Symmetrical System
Effectiveness 1°/sec² per degree
Limits ±15°
100°/sec = δ'
0.833 c.p.s
Ratio 1:5
Trigger Point 0.75 π
Degrees and Degrees. sec-1
15°/sec²
Velocity
Position
π
Trigger Line
82
0
0.1
0.2
0.3
0.4
0.5
0.6
0.7
0.8
0.9
sec
1
2
3

Fig. 4.4.3

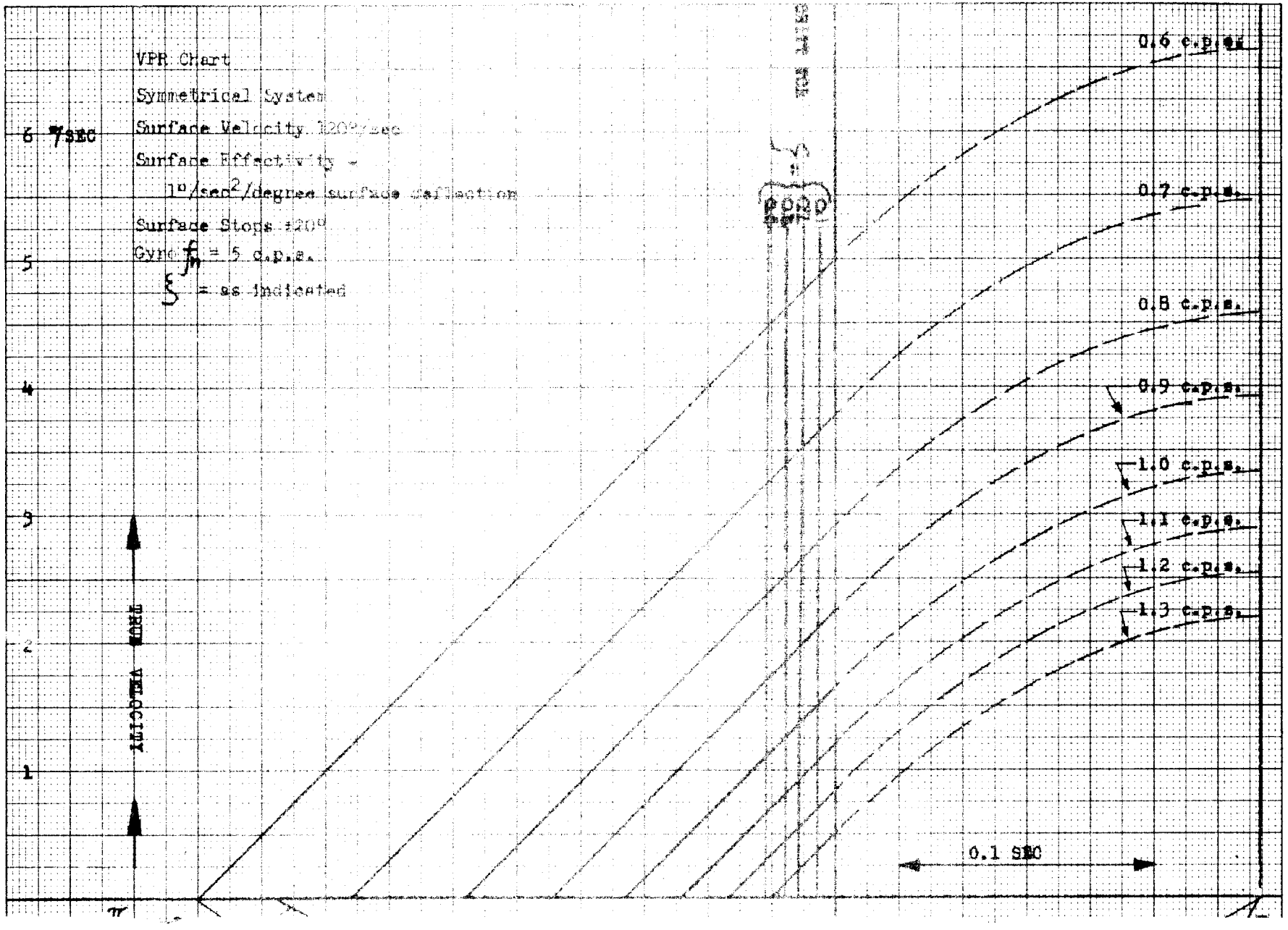
VPR Chart
Symmetrical System
Surface Velocity 1200°/sec
Surface Effectivity -
1°/sec²/degree surface deflection
Surface Stops ±20°
Gyro f_n = 5 c.p.s.
ζ = as indicated
6 TSEC
5
4
3
2
1
VELOCITY
0.6 c.p.s.
0.7 c.p.s.
0.8 c.p.s.
0.9 c.p.s.
1.0 c.p.s.
1.1 c.p.s.
1.2 c.p.s.
1.3 c.p.s.
0.1 SEC

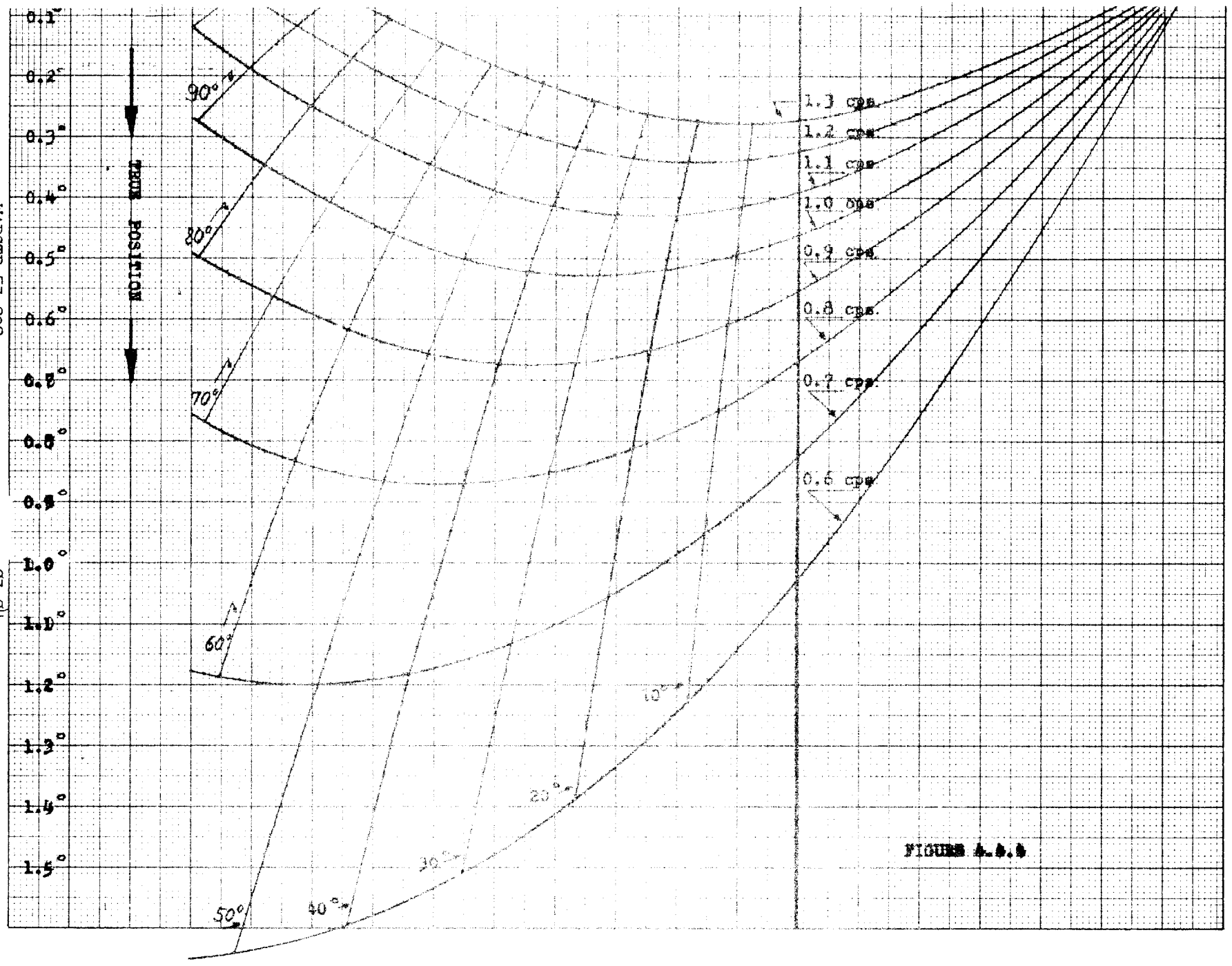
WADC TR 53-202
83-84
TRUE POSITION
0.1°
0.2°
0.3°
0.4°
0.5°
0.6°
0.7°
0.8°
0.9°
1.0°
1.1°
1.2°
1.3°
1.4°
1.5°
90°
80°
70°
60°
50°
40°
30°
20°
10°
1.3 cps.
1.2 cps.
1.1 cps.
1.0 cps.
0.9 cps.
0.8 cps.
0.7 cps.
0.6 cps.

FIGURE 4.4.4

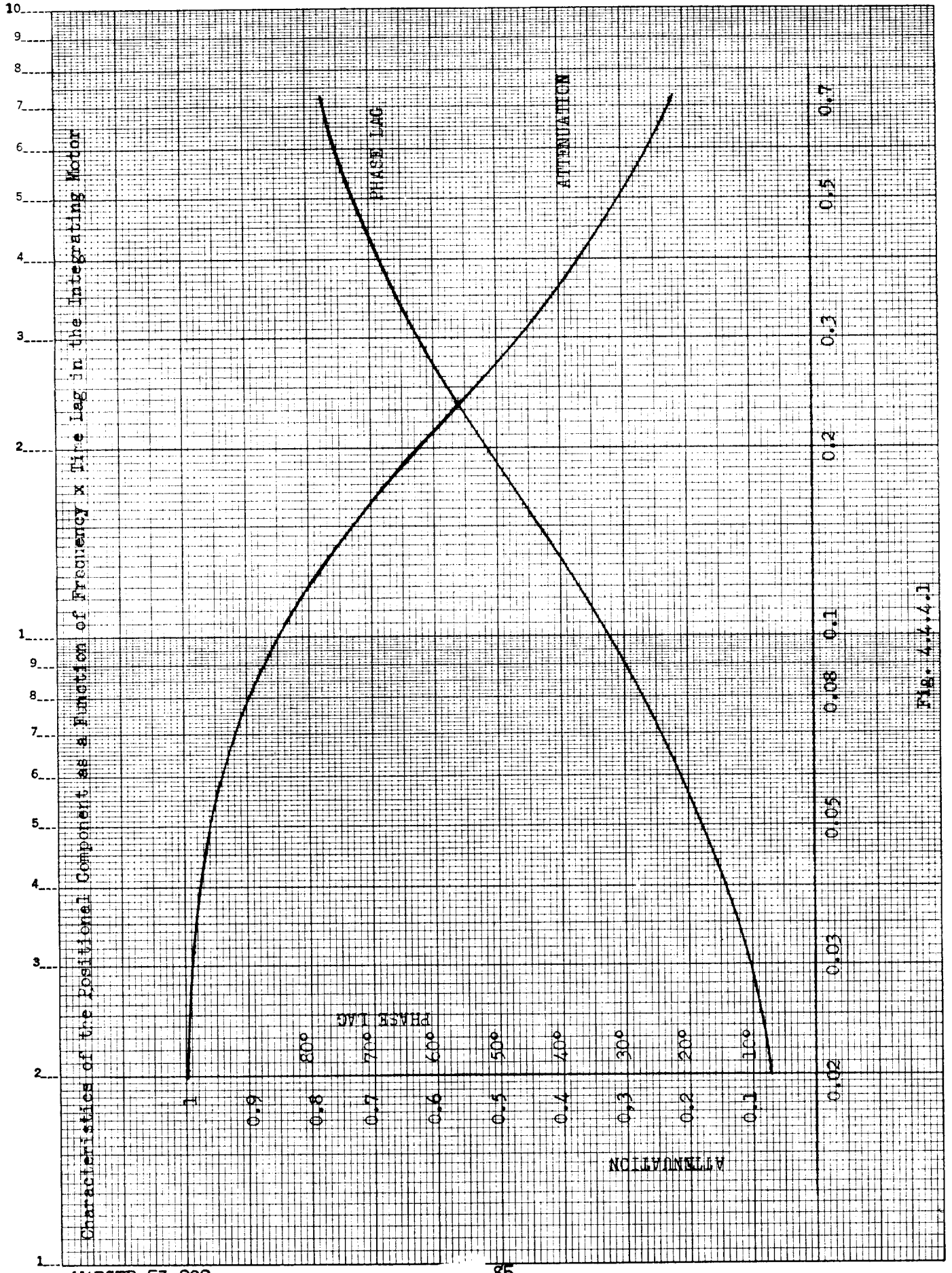
Characteristics of the Positional Component as a Function of Frequency x Time Lag in the Integrating Motor
PHASE LAG
ATTENUATION
PHASE LAG
ATTENUATION

Fig. 4.4.4.1

Velocity - Position

Vector Diagram for

a Time Delay in the

Integrating Motor

Gain Ratio $(\frac{\text{Velocity}}{\text{Position}})$ = 1:2

Frequency = 8

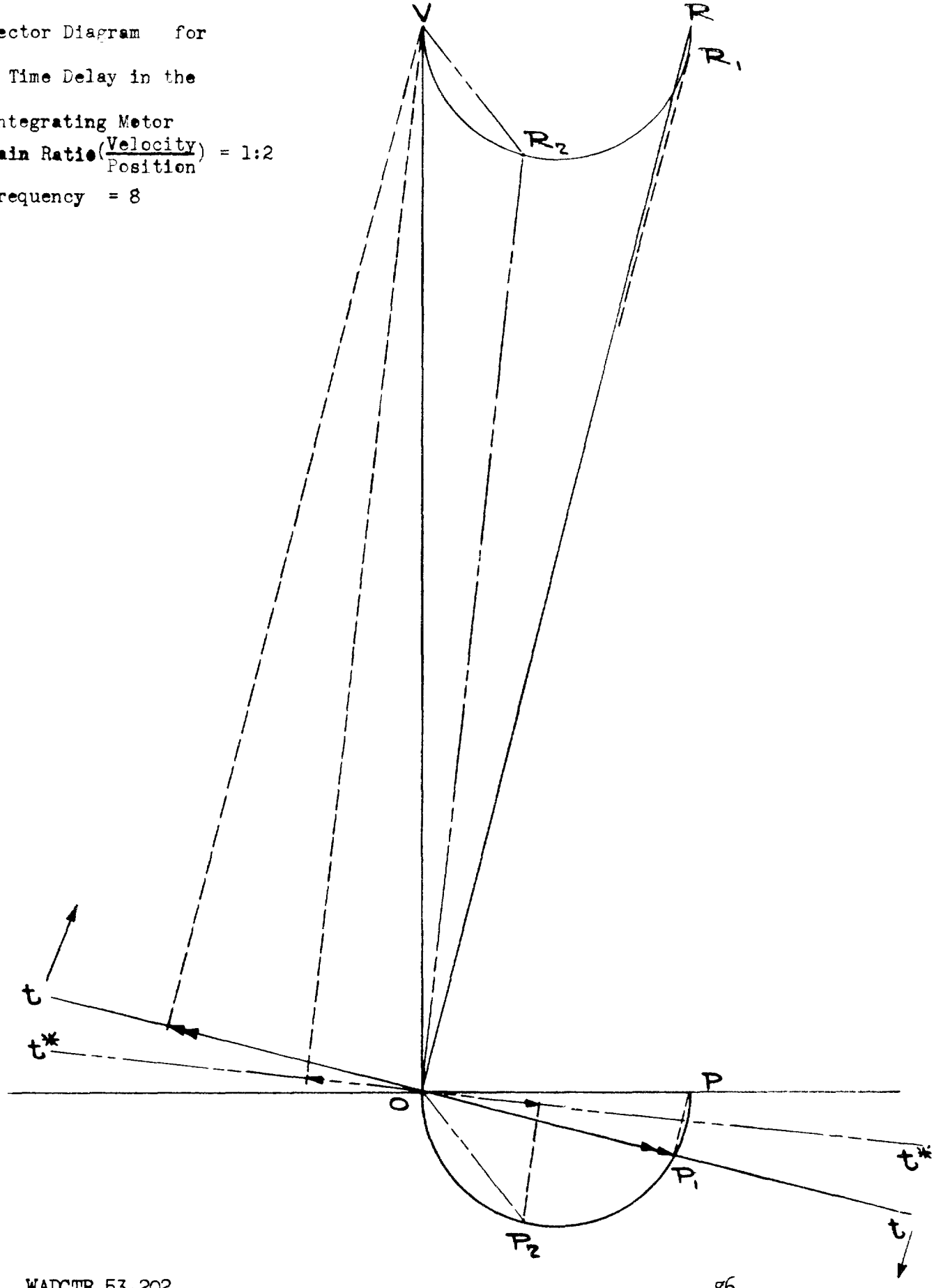

Figure 4.4.5

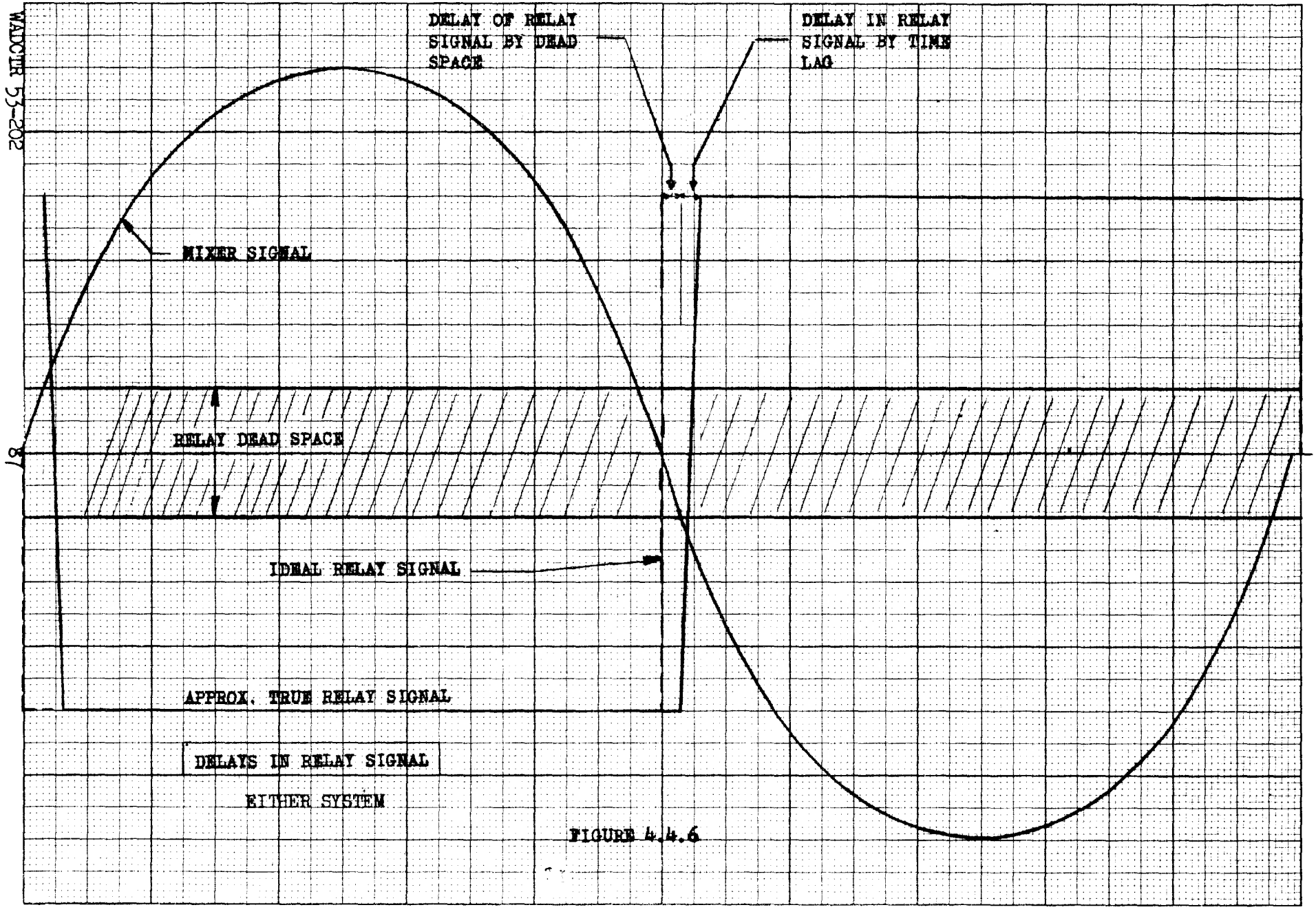
DELAY OF RELAY SIGNAL BY DEAD SPACE
DELAY IN RELAY SIGNAL BY TIME LAG
MIXER SIGNAL
RELAY DEAD SPACE
IDEAL RELAY SIGNAL
APPROX. TRUE RELAY SIGNAL
DELAYS IN RELAY SIGNAL
EITHER SYSTEM

FIGURE 4.4.6

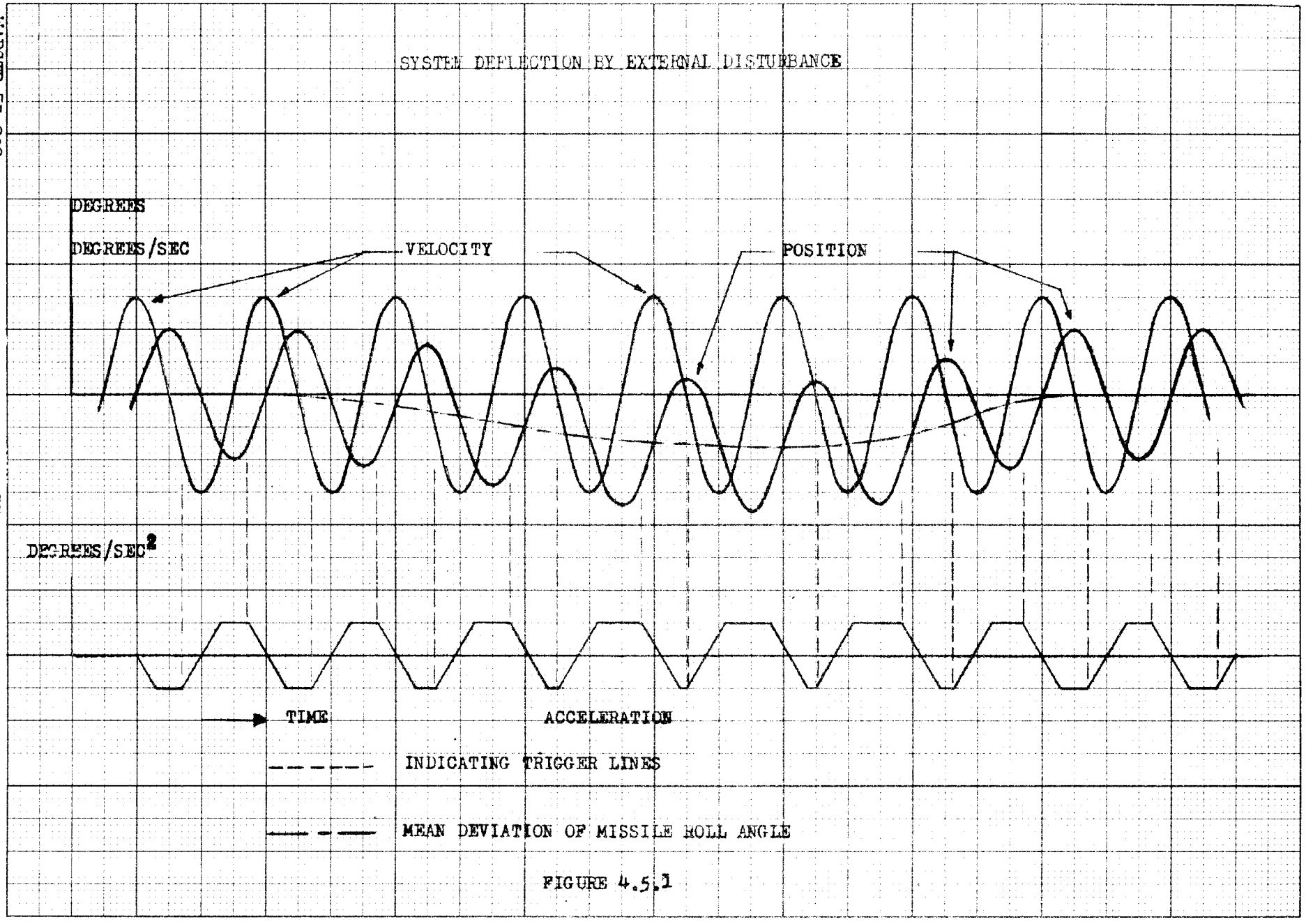
SYSTEM DEFLECTION BY EXTERNAL DISTURBANCE
DEGREES
DEGREES/SEC
VELOCITY
POSITION
DEGREES/SEC²
TIME
ACCELERATION
INDICATING TRIGGER LINES
MEAN DEVIATION OF MISSILE ROLL ANGLE

FIGURE 4.5.1

MISSILE COMPONENTS OF A SYMMETRICAL SYSTEM OPPOSING A SMALL EXTERNAL DISTURBANCE

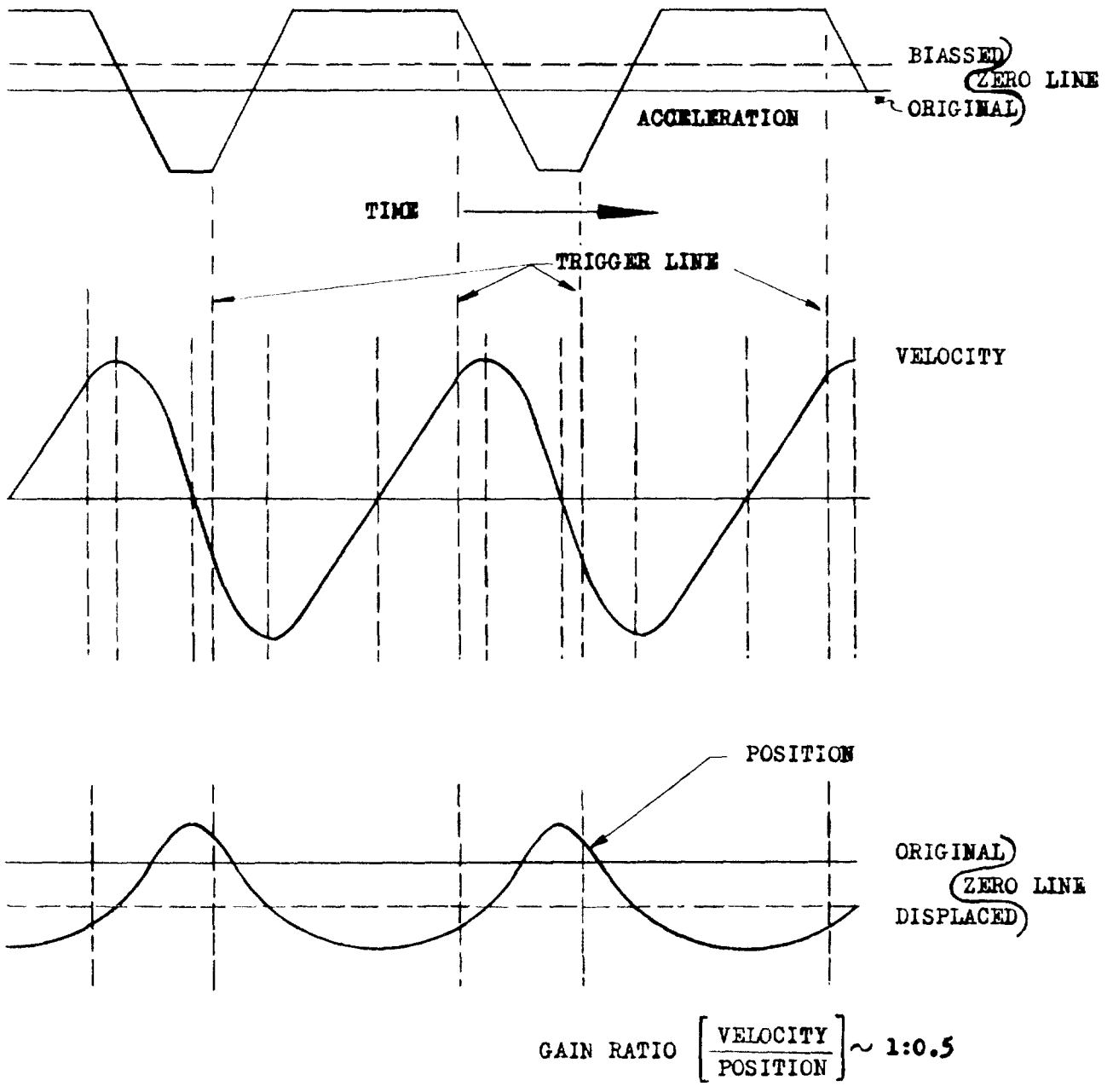

FIGURE 4.5.2

SYMMETRICAL SYSTEM SUBJECTED TO LARGE EXTERNAL DISTURBANCE

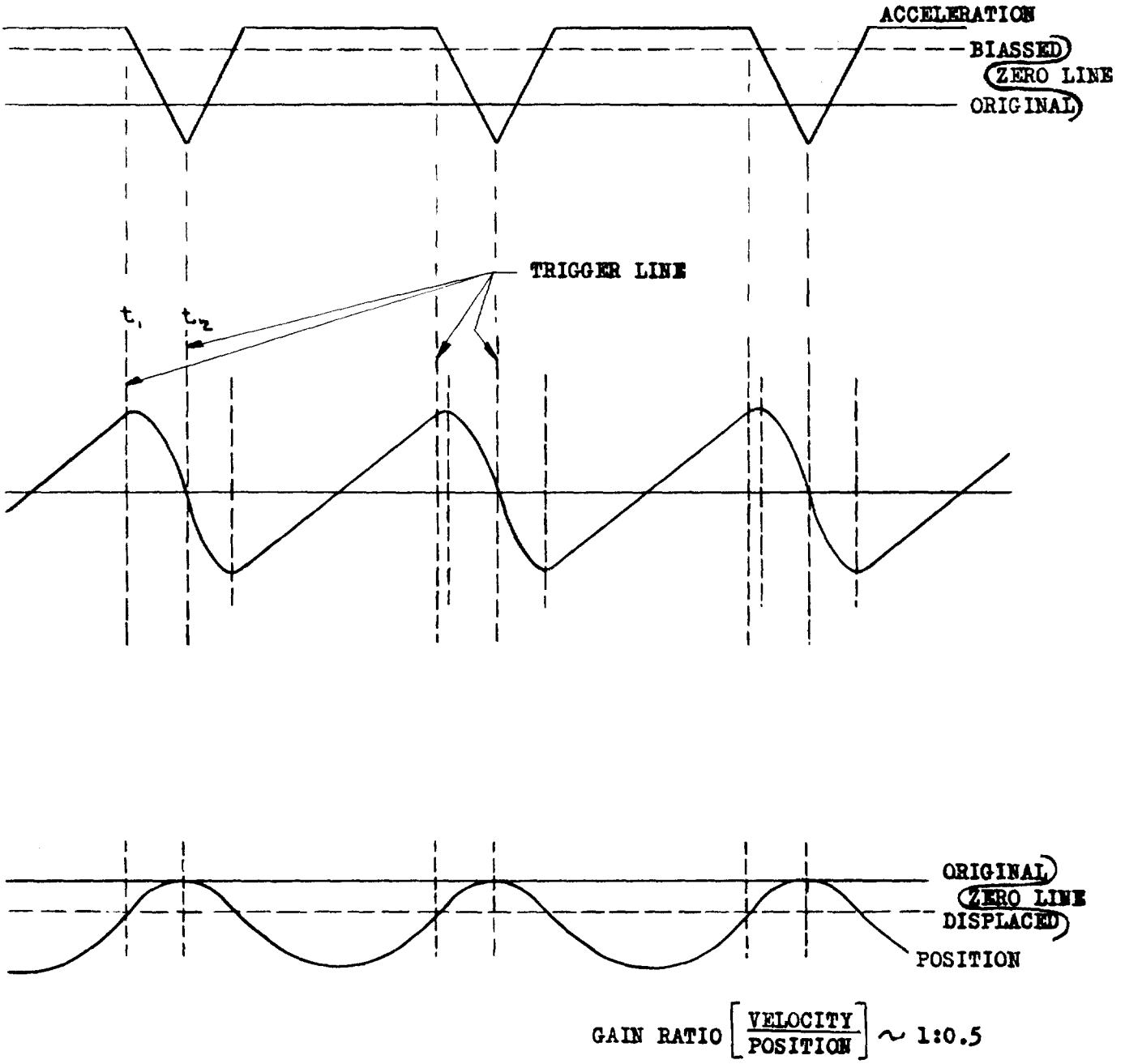

FIGURE 4.5.3

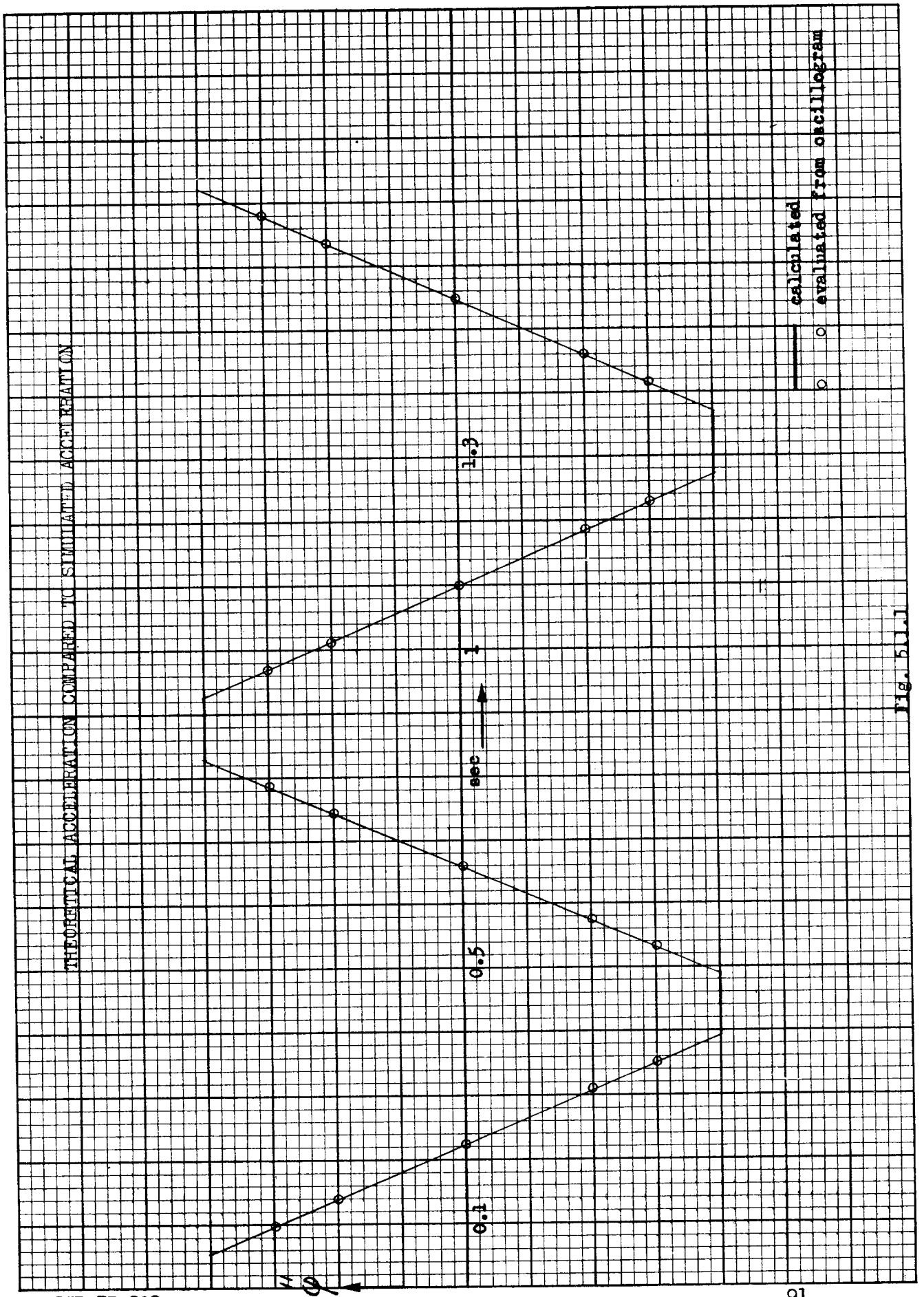
THEORETICAL ACCELERATION COMPARED TO SIMULATED ACCELERATION
calculated
evaluated from oscillogram
1.3
1
0.5
0.1
sec

Fig. 5111

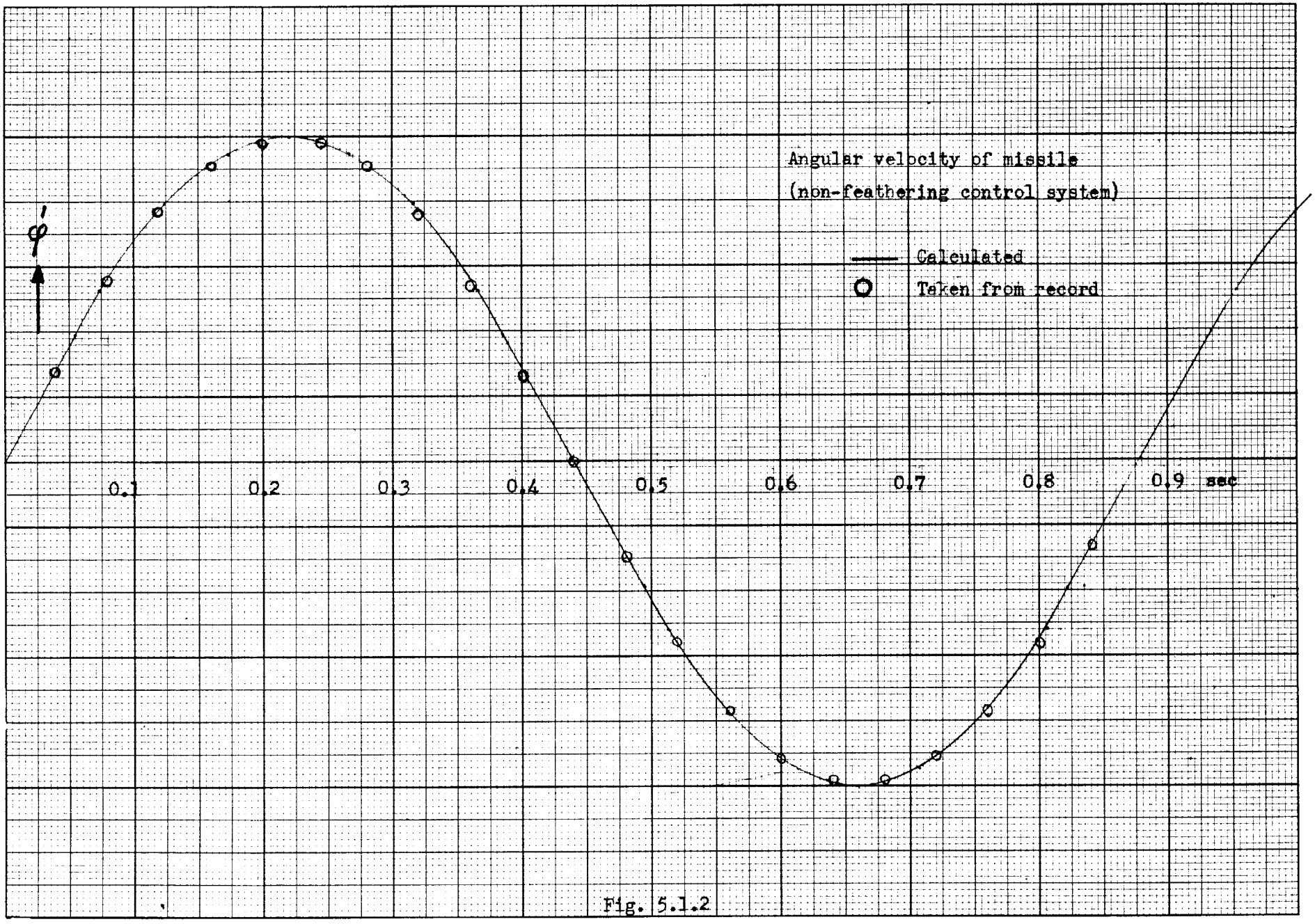
Angular velocity of missile
(non-feathering control system)
Calculated
Taken from record
$\dot{\varphi}$
0.1
0.2
0.3
0.4
0.5
0.6
0.7
0.8
0.9 sec

Fig. 5.1.2

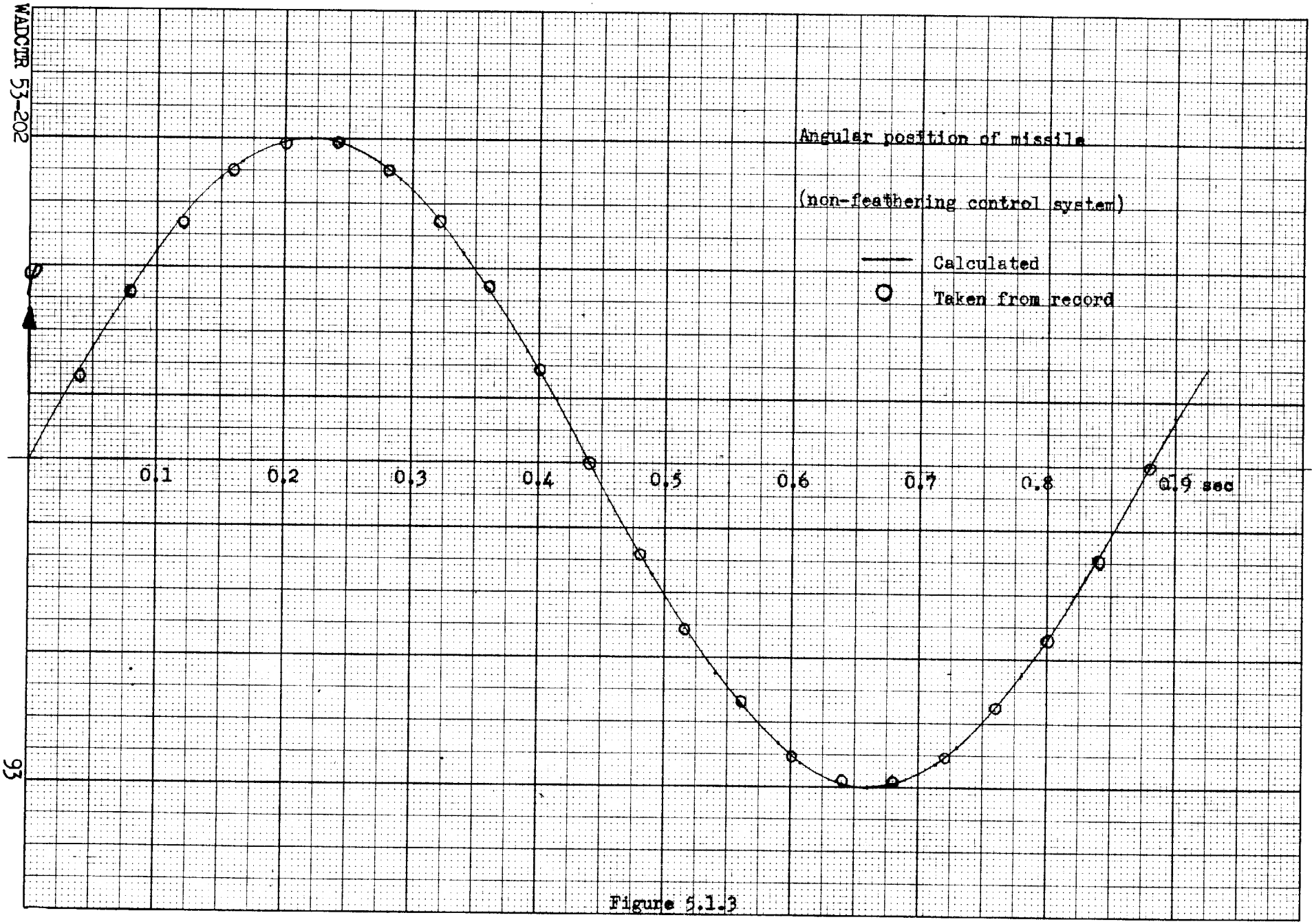
Angular position of missile
(non-feathering control system)
Calculated
Taken from record
0.1
0.2
0.3
0.4
0.5
0.6
0.7
0.8
0.9 sec

Figure 5.1.3

SIMULATOR SETUP REPRESENTING SYMMETRICAL SYSTEM WITH IDEAL SENSING

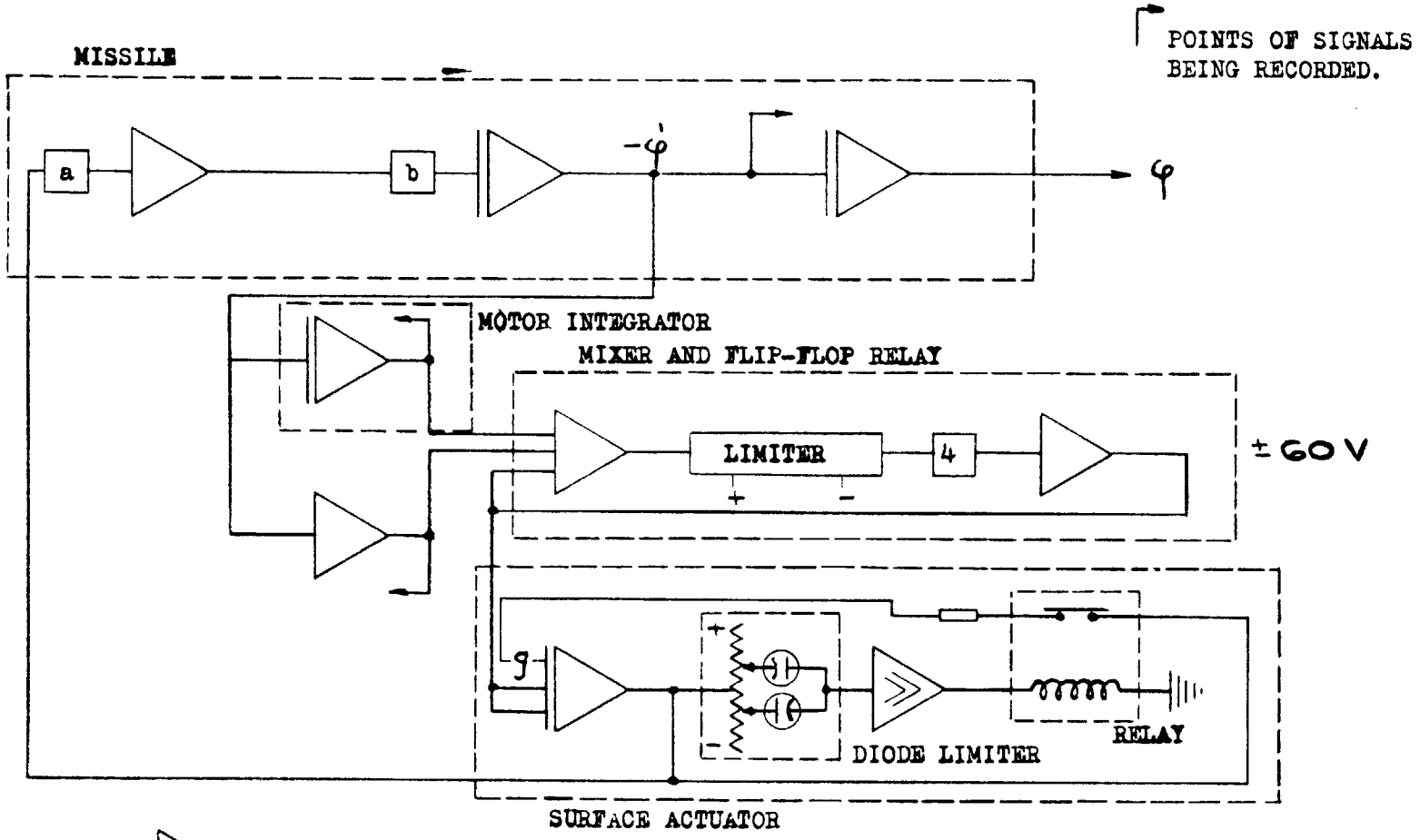

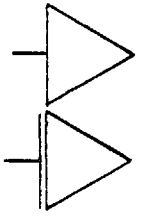

SUMMING OR INVERTING AMPLIFIER

INTEGRATING AMPLIFIER

[a] GAIN FACTOR = a

g CONNECTION TO GRID

FIGURE 5.2.1

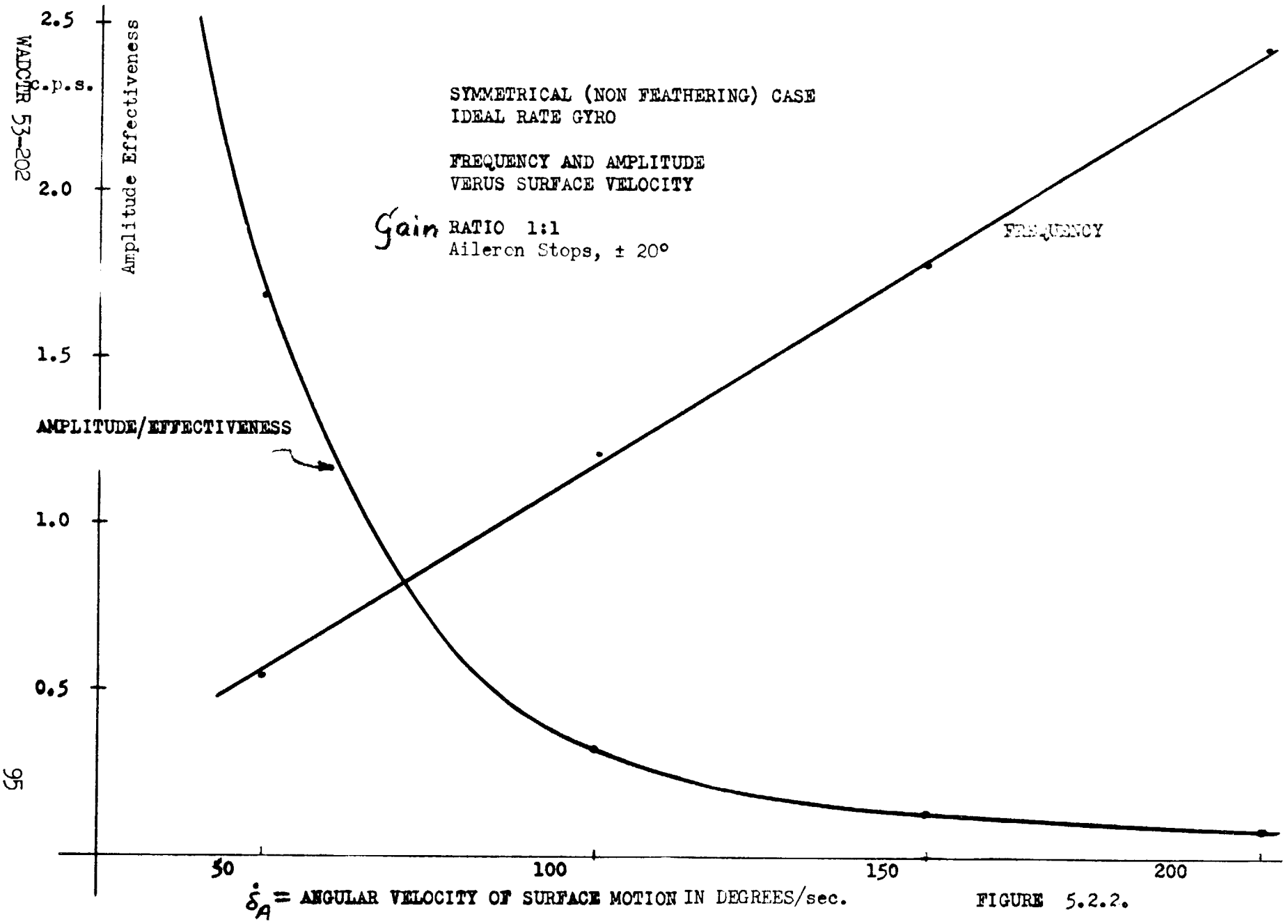
2.5
c.p.s.
2.0
1.5
1.0
0.5
Amplitude Effectiveness
AMPLITUDE/EFFECTIVENESS
SYMMETRICAL (NON FEATHERING) CASE
IDEAL RATE GYRO
FREQUENCY AND AMPLITUDE
VERUS SURFACE VELOCITY
Gain RATIO 1:1
Aileron Stops, ± 20°
FREQUENCY
50
100
150
200
$\dot{\delta}_A$ = ANGULAR VELOCITY OF SURFACE MOTION IN DEGREES/sec.

FIGURE 5.2.2.

SIMULATOR SET REPRESENTING SYMMETRICAL SYSTEM WITH RATE GYRO SENSING

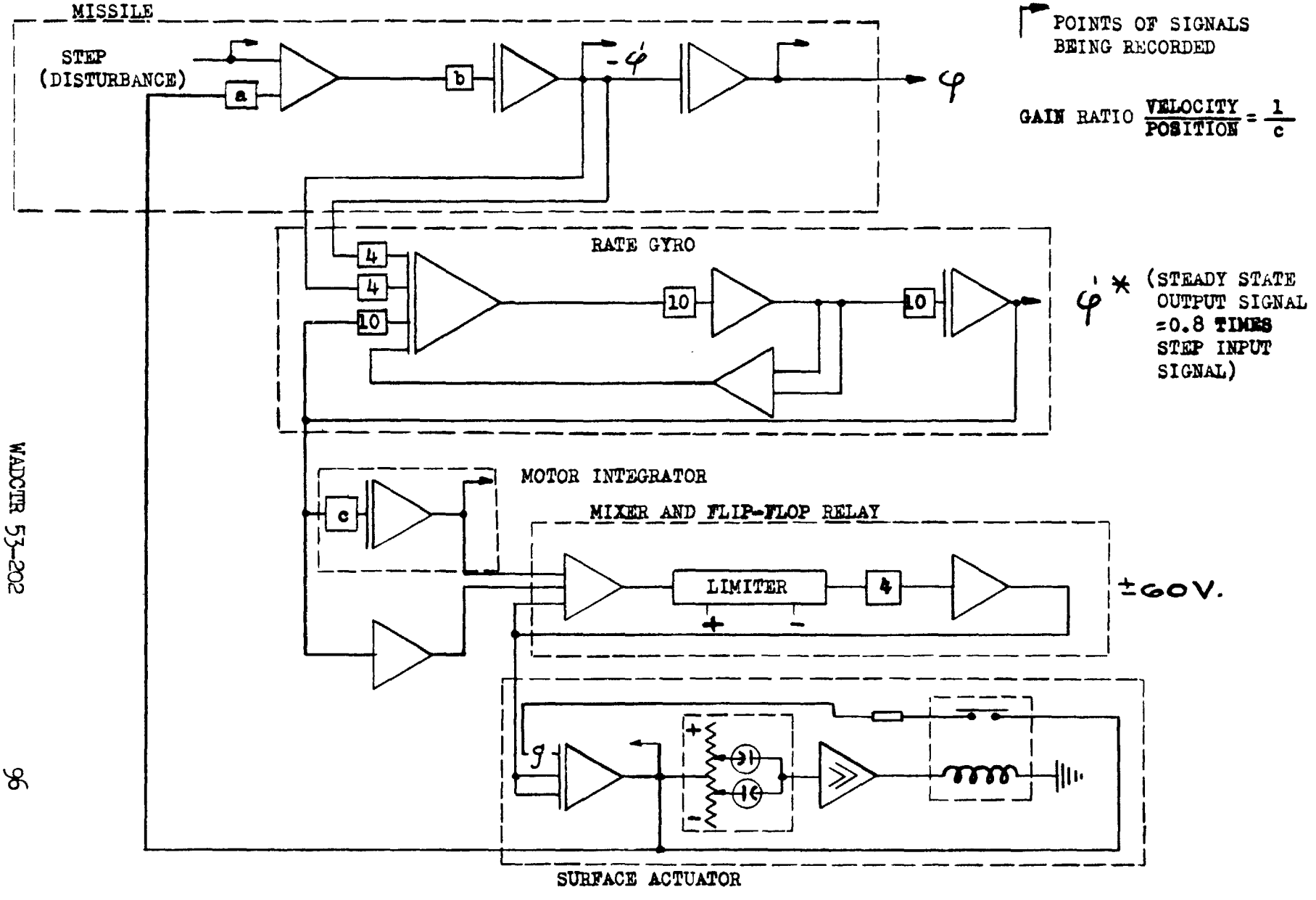

FIGURE 5.2.3

SYMMETRICAL SYSTEM
DEPENDENCE ON GAIN RATIO
RATE GYRO f_n = 5 c.p.s
ζ = 0.716

FIGURE 5.2.4

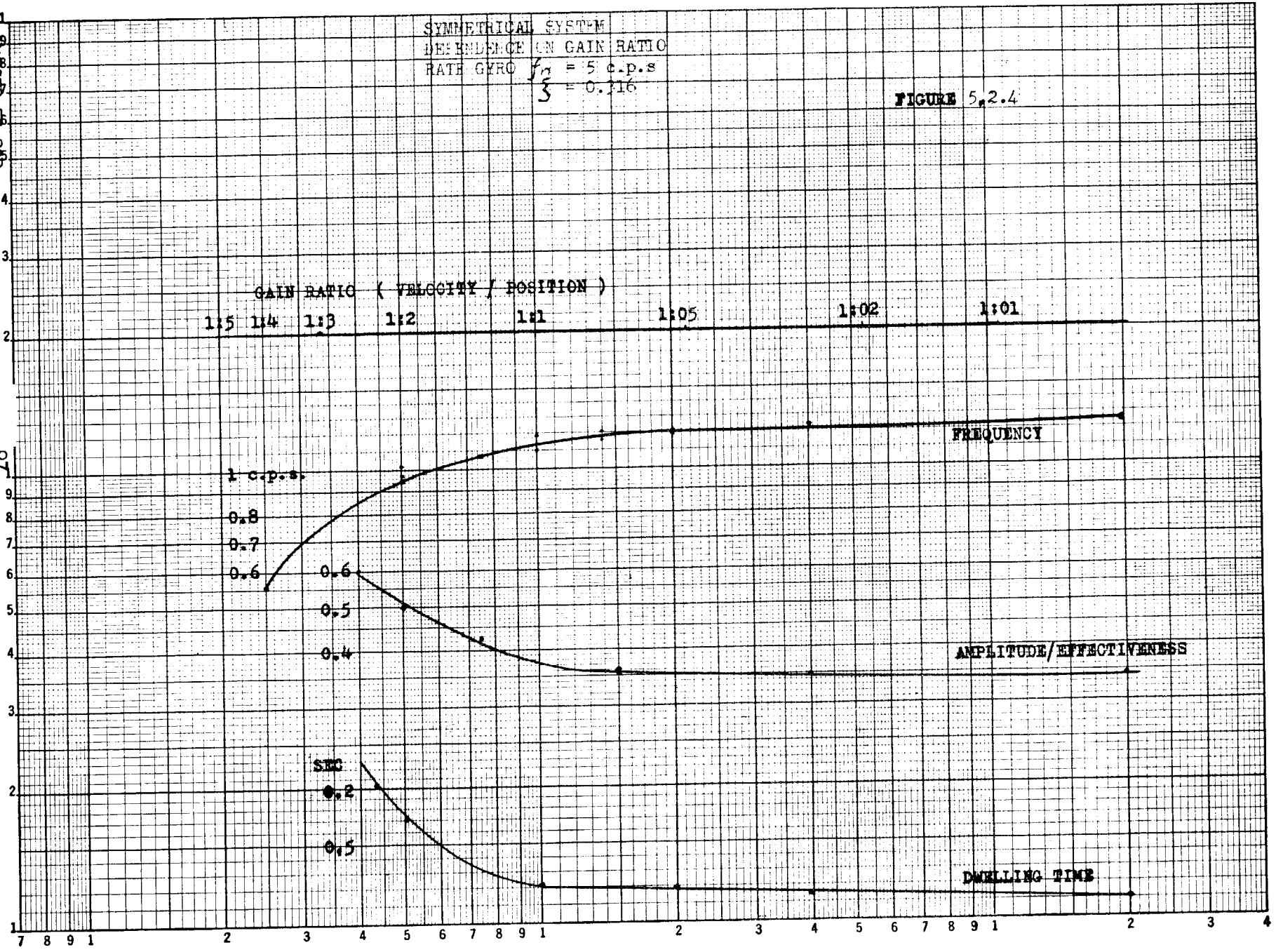

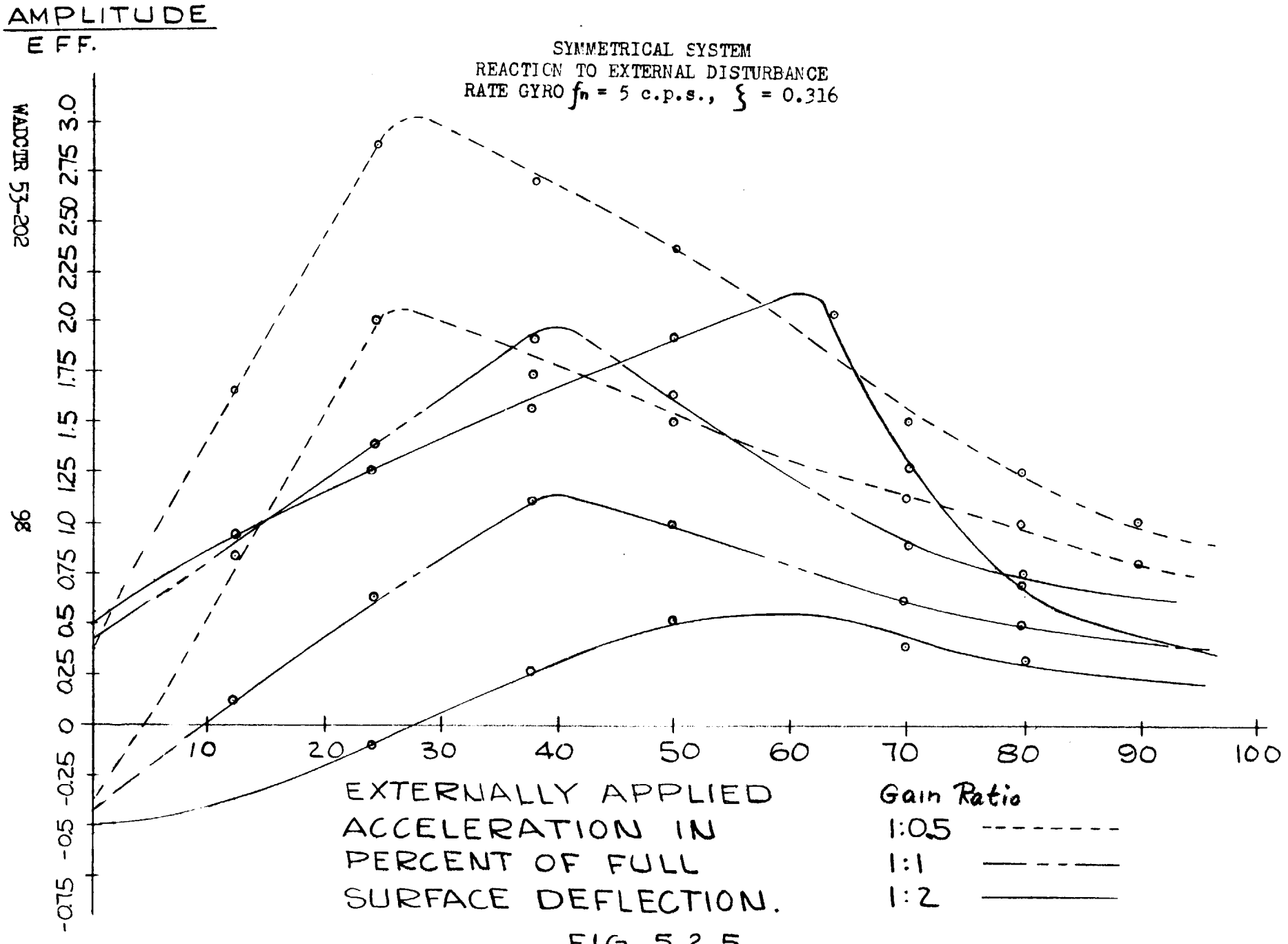
AMPLITUDE
EFF.
SYMMETRICAL SYSTEM
REACTION TO EXTERNAL DISTURBANCE
RATE GYRO f_n = 5 c.p.s., ζ = 0.316
-.075 -.05 -.025 0 .025 .05 .075 .10 .125 1.5 1.75 2.0 2.25 2.50 2.75 3.0
10 20 30 40 50 60 70 80 90 100
EXTERNALLY APPLIED ACCELERATION IN PERCENT OF FULL SURFACE DEFLECTION.
Gain Ratio
1:0.5
1:1
1:2

FIG. 5.2.5

SYMMETRICAL SYSTEM REACTION
TO EXTERNAL DISTURBANCE
RATE GYRO f_n = 5 c.p.s., ζ = 0.316

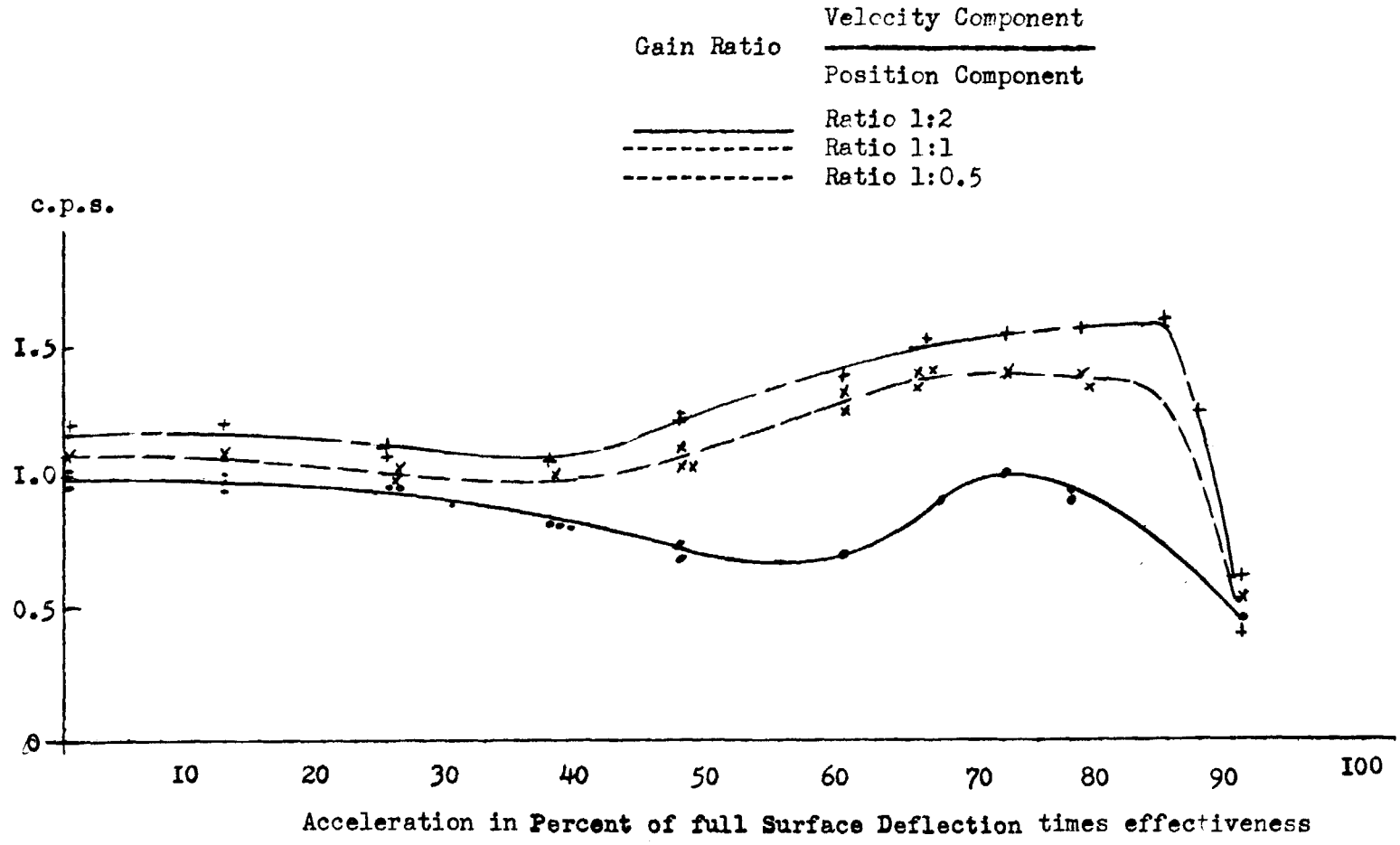

Fig. 5.2.6

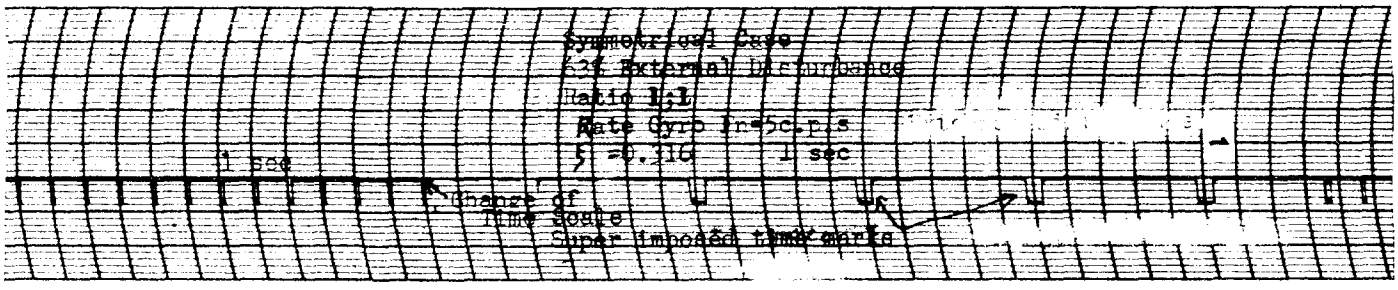
Symmetrical Case
(3% External) Disturbance
Ratio 1:1
Rate Gyro 1=5c.p.s
ζ =0.316
1 sec
1 sec
Change of
Time Scale
Super Imposed time marks
1

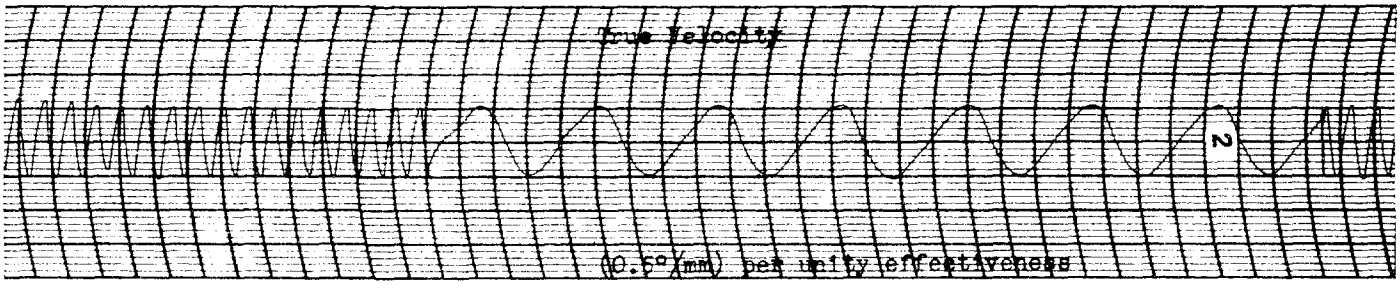
True Velocity
2
(0.5°/mm) per unity effectiveness

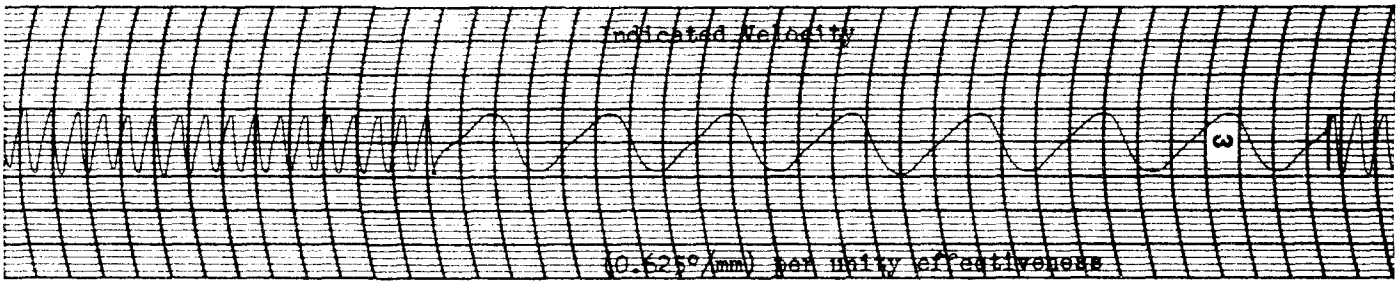
Indicated Velocity
3
(0.625°/mm) per unity effectiveness

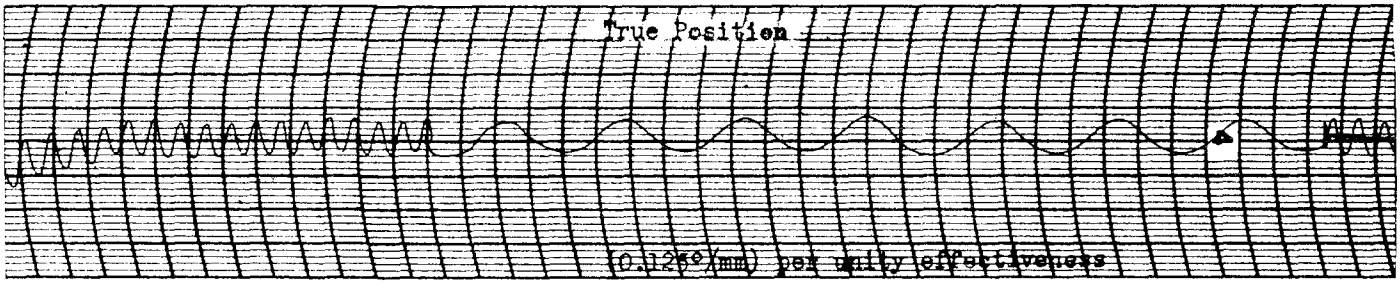
True Position
4
(0.125°/mm) per unity effectiveness

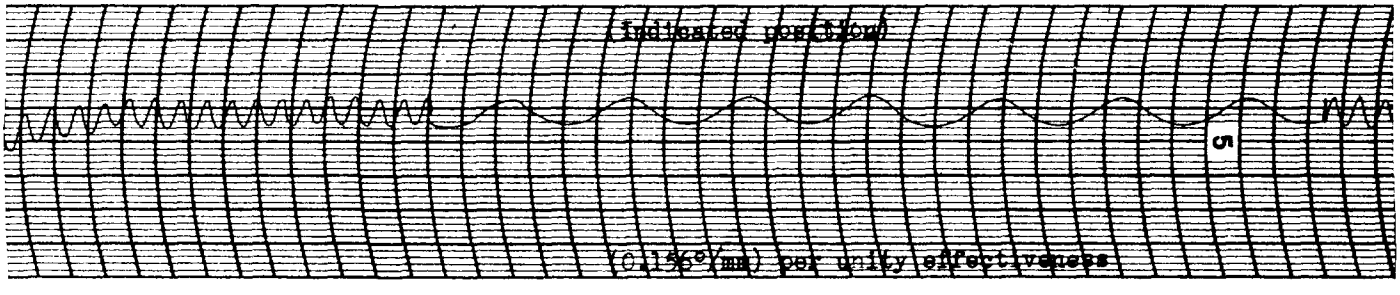
Indicated position
5
(0.156°/mm) per unity effectiveness

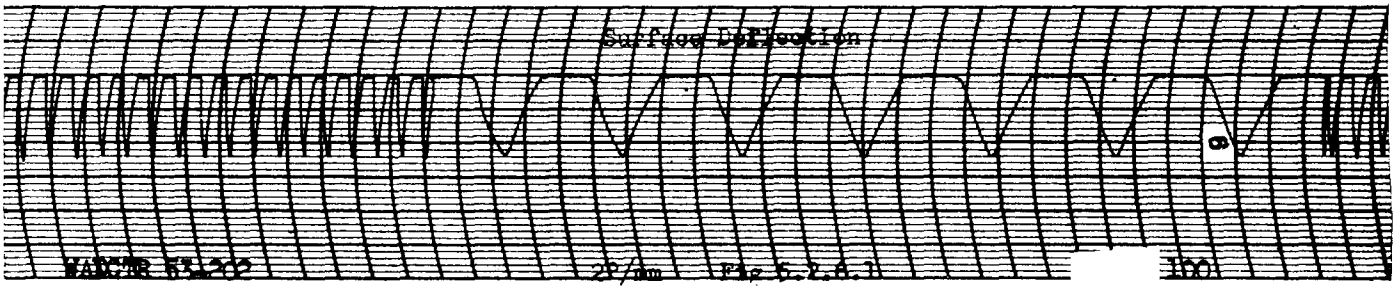
Surface Deflection
6
2°/mm
Fig 6.2.6.1

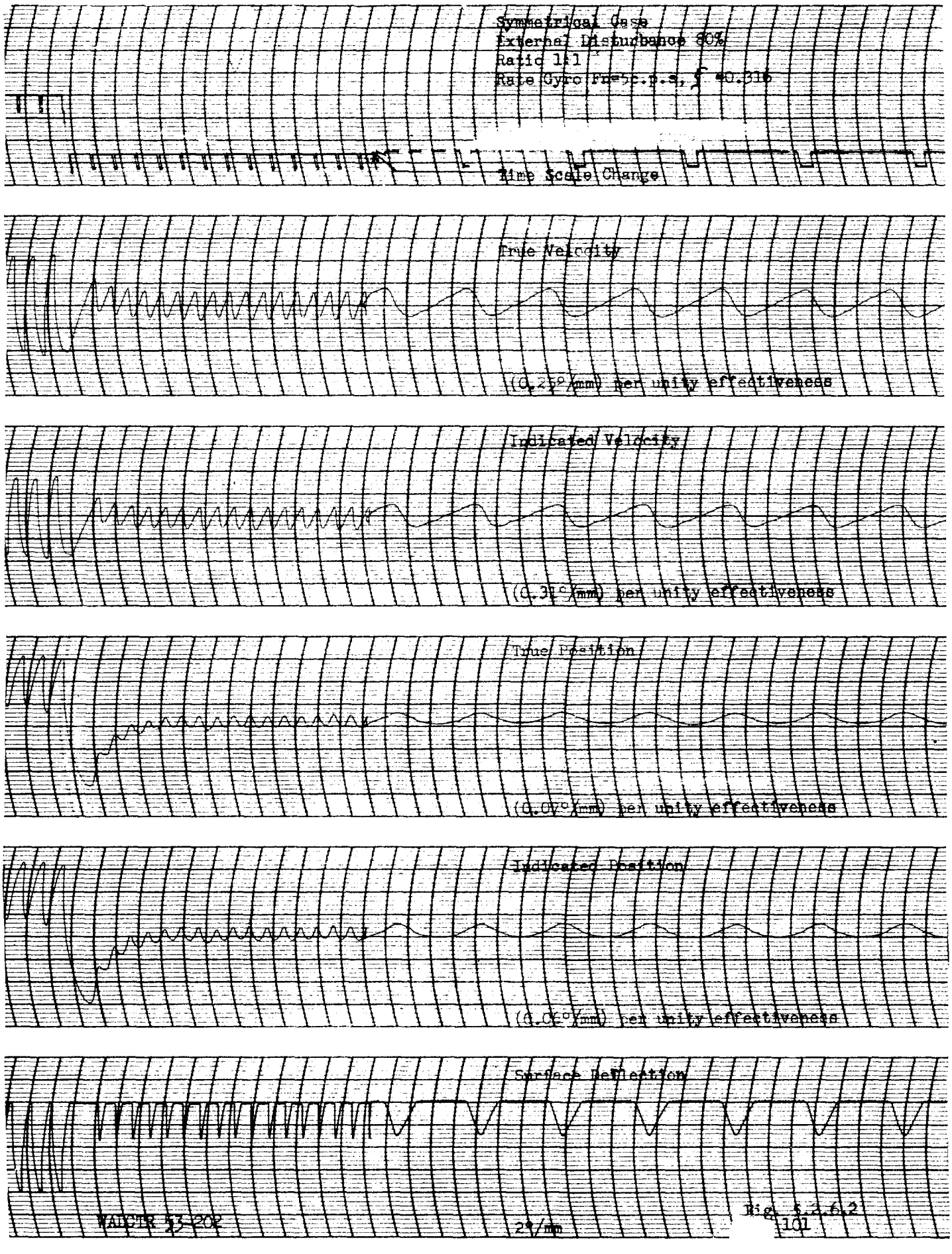
Symmetrical Case
External Disturbance 80%
Ratio 1:1
Rate Gyro Fn=5c.p.s, ζ =0.316
Time Scale Change
True Velocity
(0.25°/mm) per unity effectiveness
Indicated Velocity
(0.3[illegible]°/mm) per unity effectiveness
True Position
(0.0[illegible]°/mm) per unity effectiveness
Indicated Position
(0.0[illegible]°/mm) per unity effectiveness
Surface Deflection
WADC TR 53-202
2°/mm
Fig. 5.3.6.2
101

COMPARISON OF MEAN SURFACE DEFLECTION TO EXPECTED MEAN SURFACE DEFLECTION

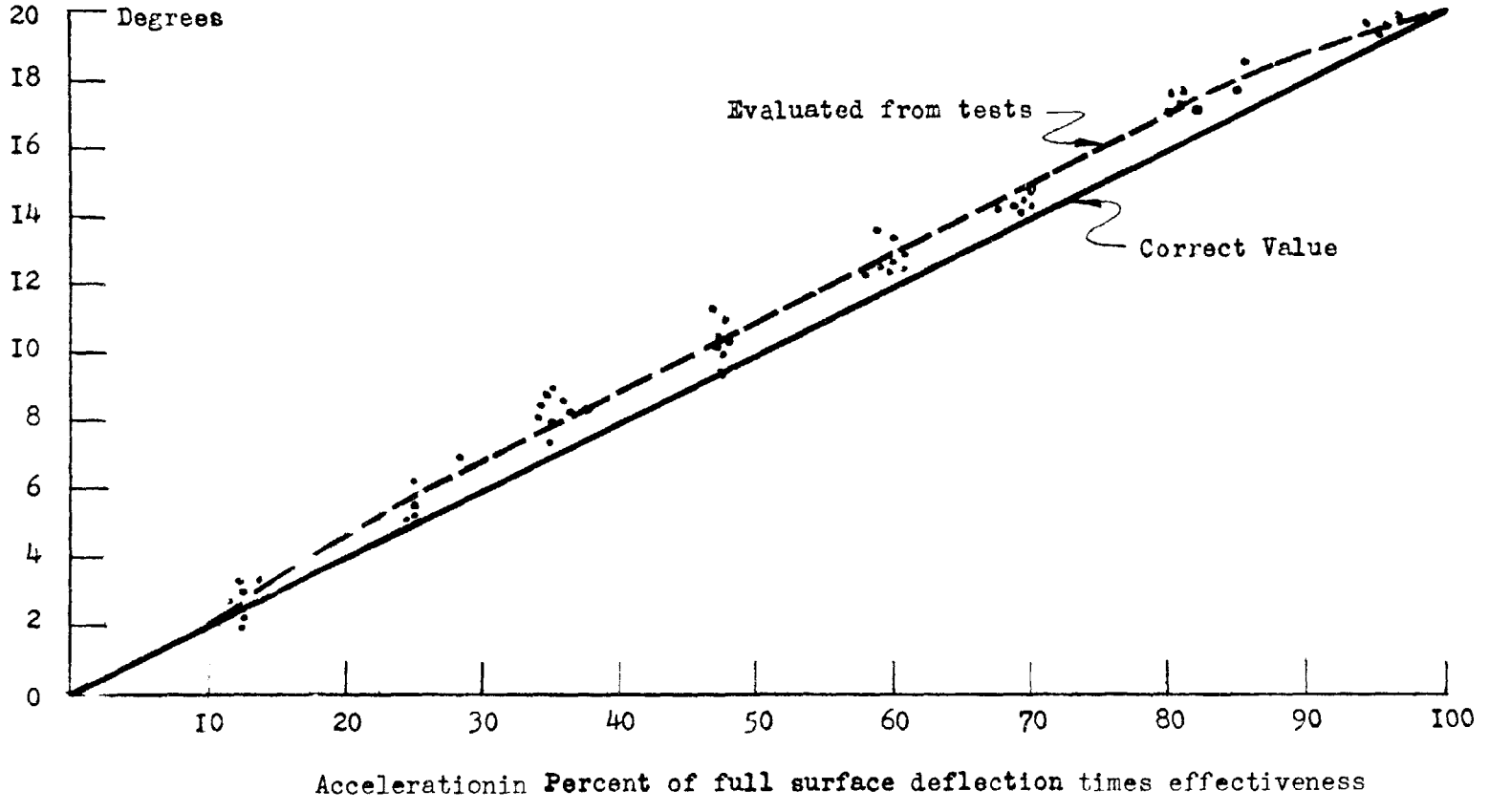

Fig. 5.2.7

SYMMETRICAL SYSTEM OPERATION
UNDER VARIOUS RATE GYRO DAMPING RATIOS
f_n = 5 c.p.s.

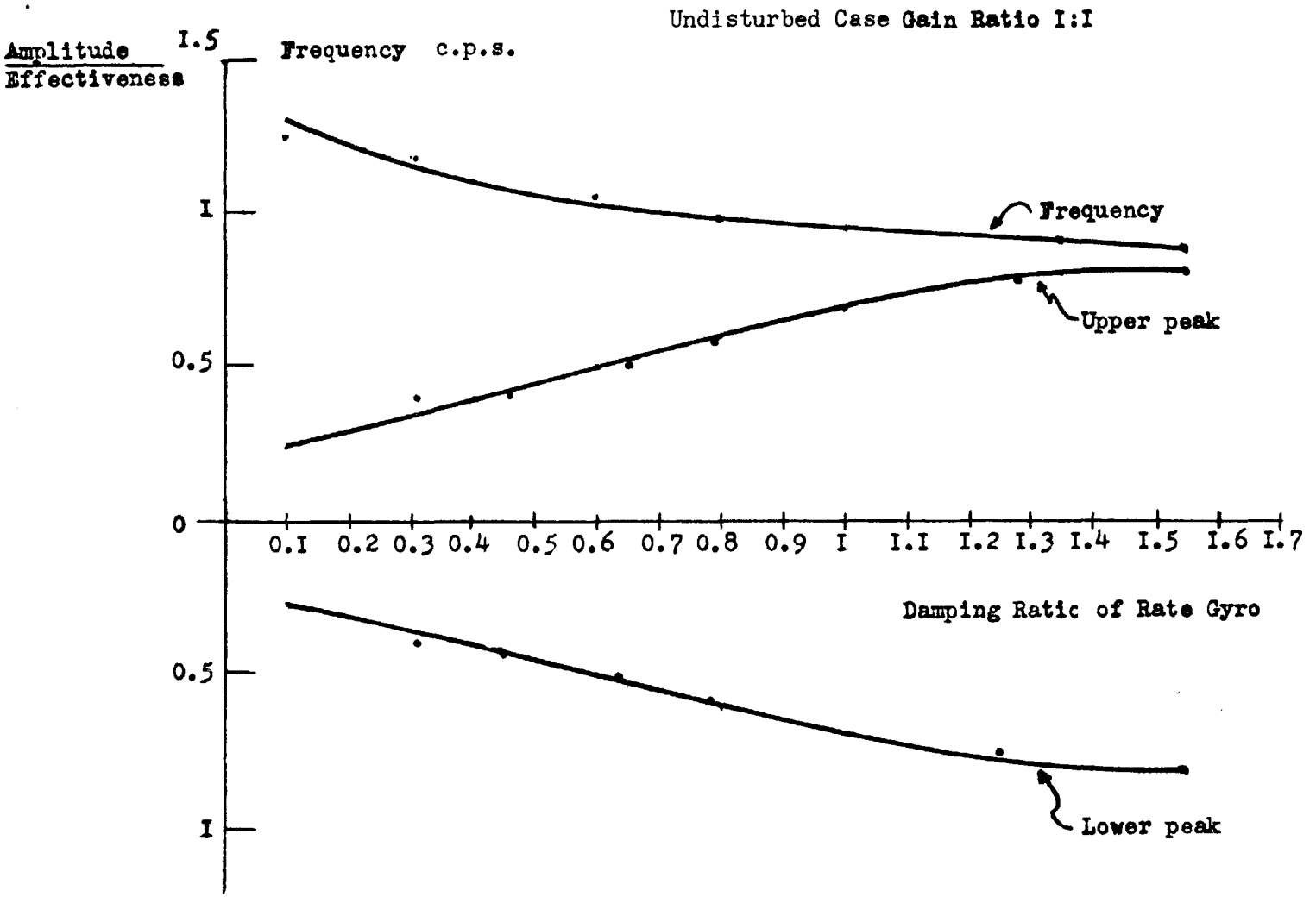

Fig. 5.2.8

SYMMETRICAL SYSTEM OPERATION
FOR VARIOUS RATE GYRO DAMPING RATIOS

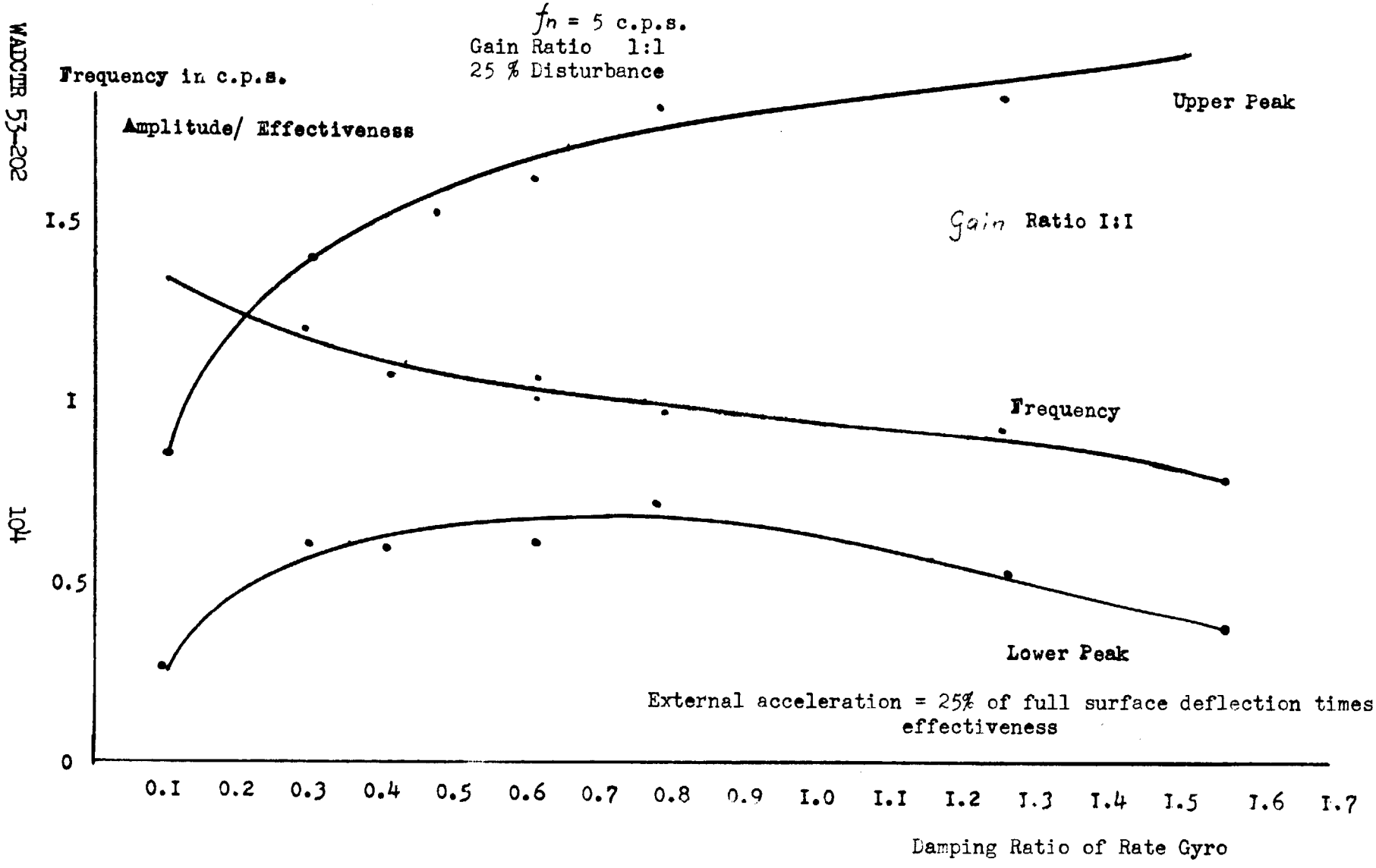

Fig. 5.2.9

REAC SIMULATION OF SYMMETRICAL
SYSTEM WITH A TIME DELAY IN THE INTEGRATING MOTOR

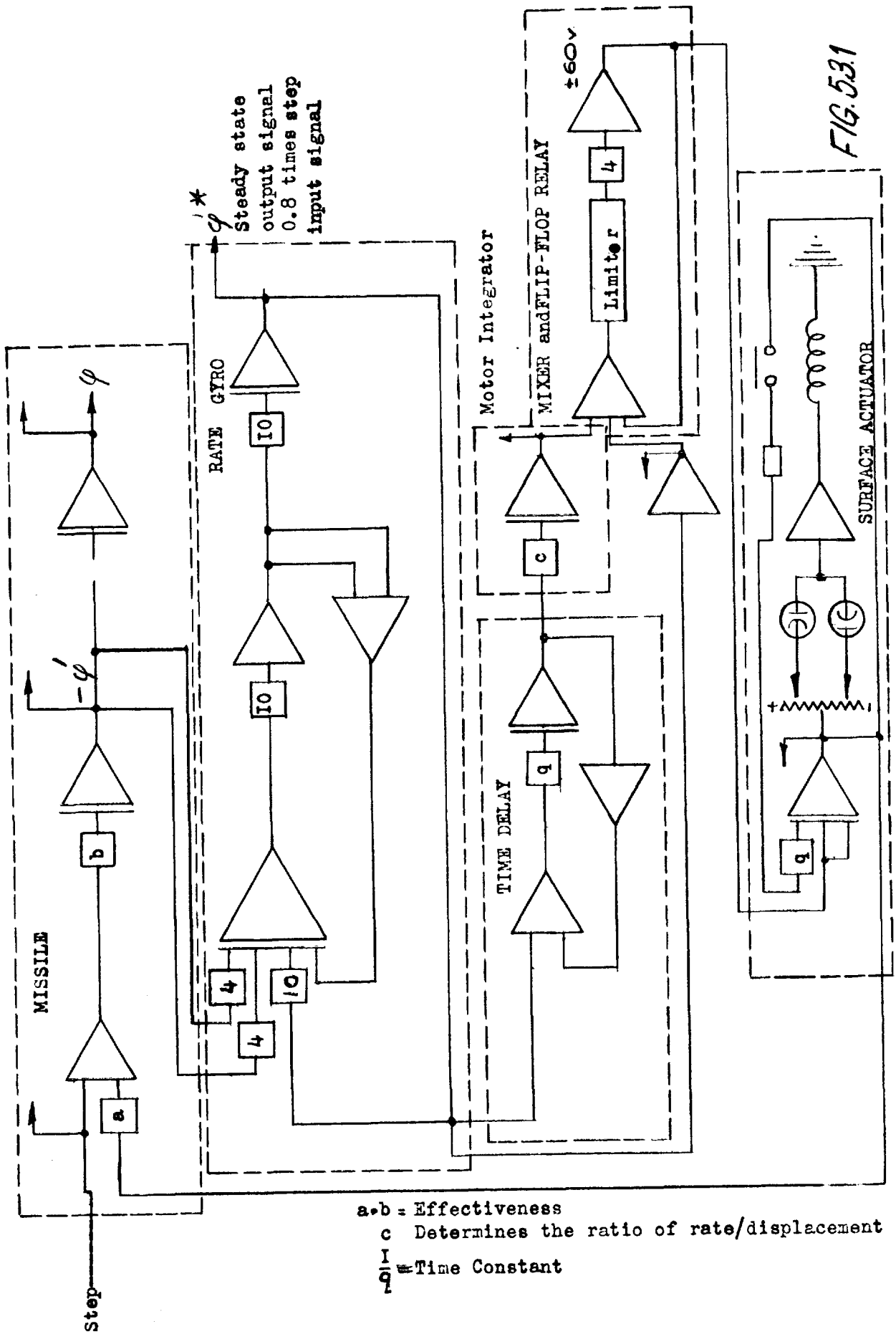

FIG. 531

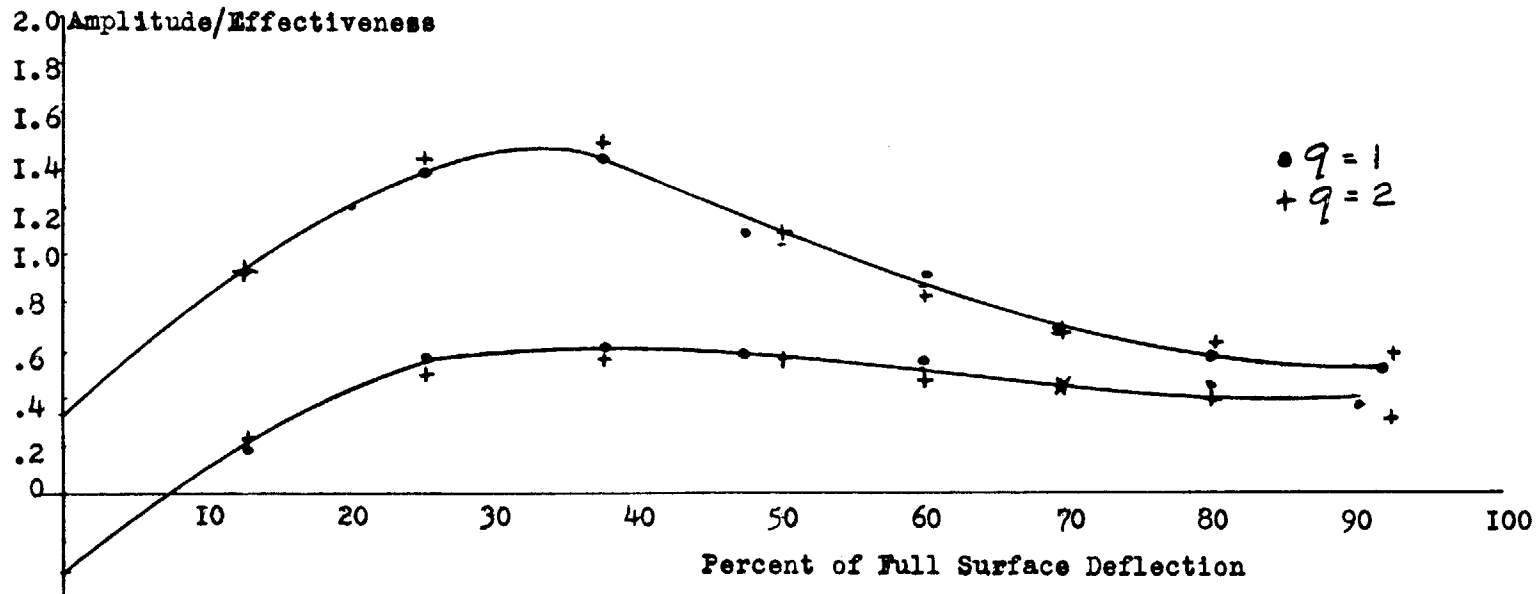
2.0 Amplitude/Effectiveness
I.8
I.6
I.4
I.2
I.0
.8
.6
.4
.2
0
10
20
30
40
50
60
70
80
90
100
Percent of Full Surface Deflection
• q = 1
+ q = 2

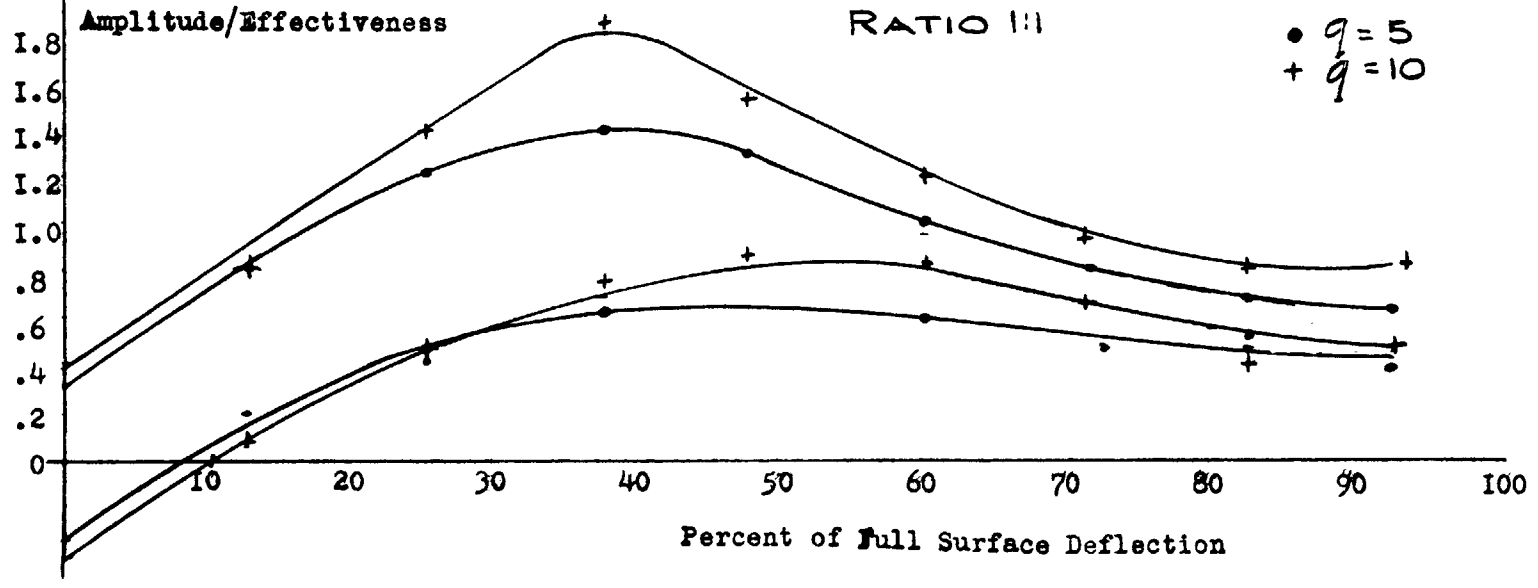
Amplitude/Effectiveness
RATIO 1:1
I.8
I.6
I.4
I.2
I.0
.8
.6
.4
.2
0
10
20
30
40
50
60
70
80
90
100
Percent of Full Surface Deflection
• q = 5
+ q = 10

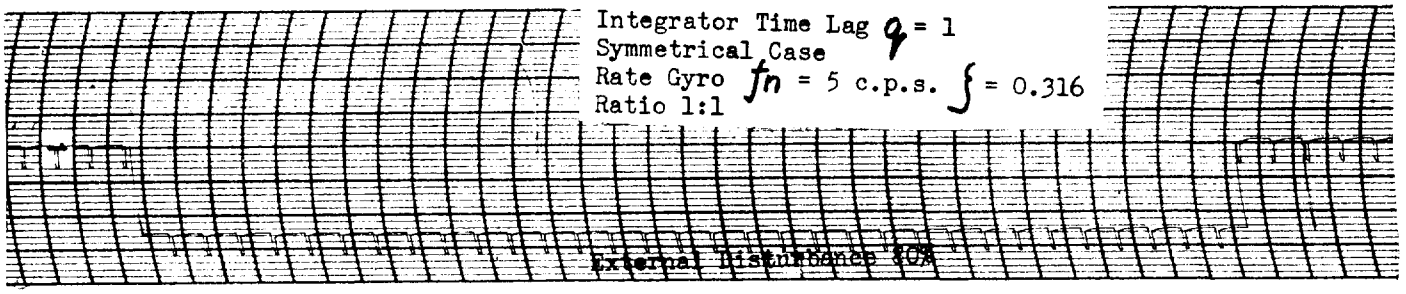
Integrator Time Lag $q = 1$
Symmetrical Case
Rate Gyro f_n = 5 c.p.s. $\zeta = 0.316$
Ratio 1:1
1
External Disturbance 30A

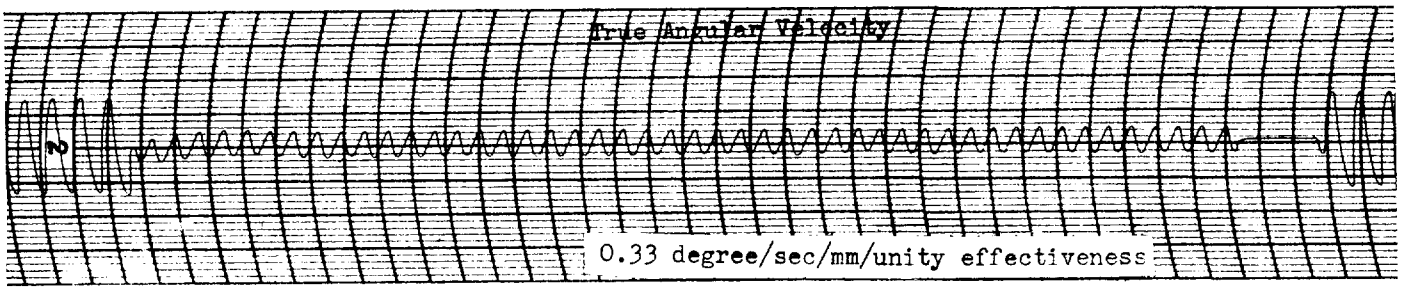
True Angular Velocity
2
0.33 degree/sec/mm/unity effectiveness

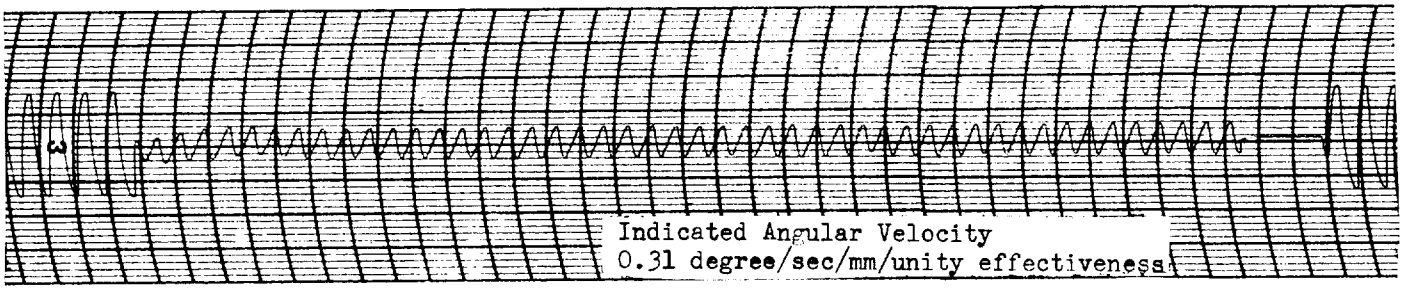
3
Indicated Angular Velocity
0.31 degree/sec/mm/unity effectiveness

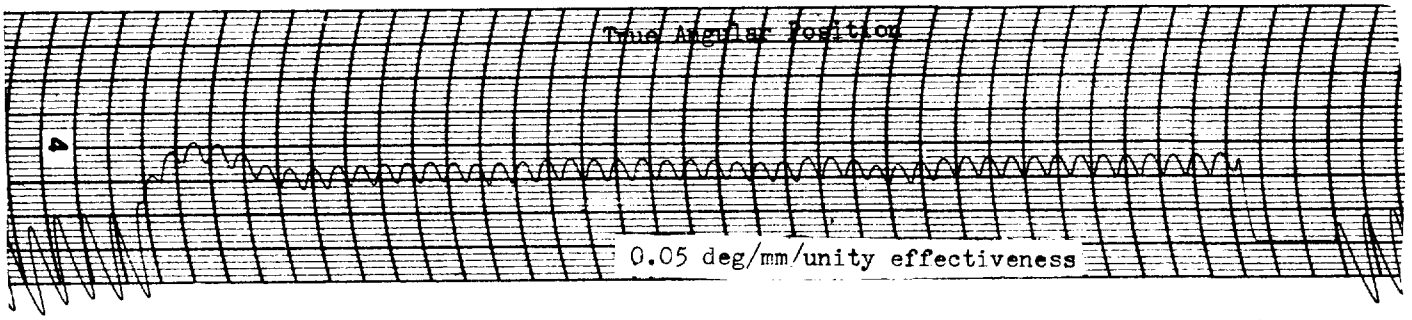
True Angular Position
4
0.05 deg/mm/unity effectiveness

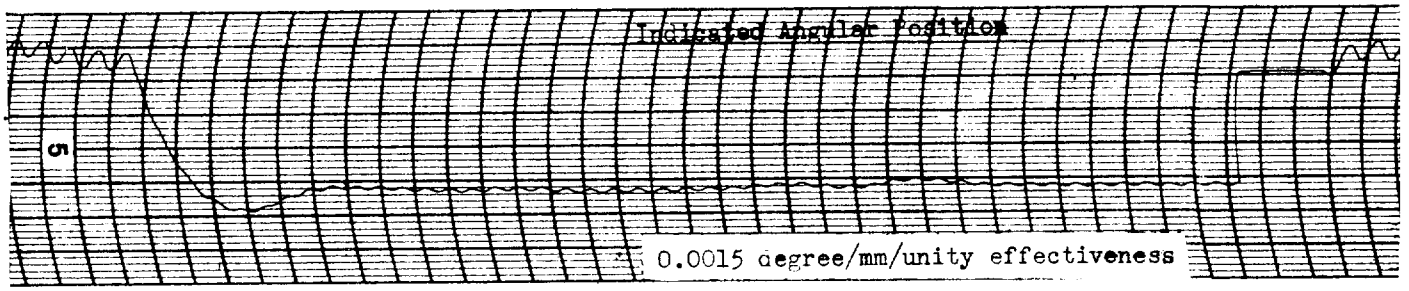
Indicated Angular Position
5
0.0015 degree/mm/unity effectiveness

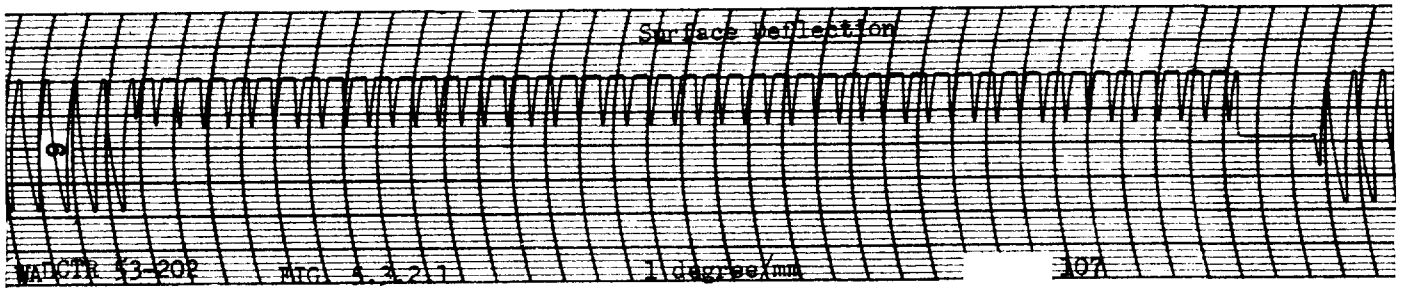
Surface Deflection
6
1 degree/mm

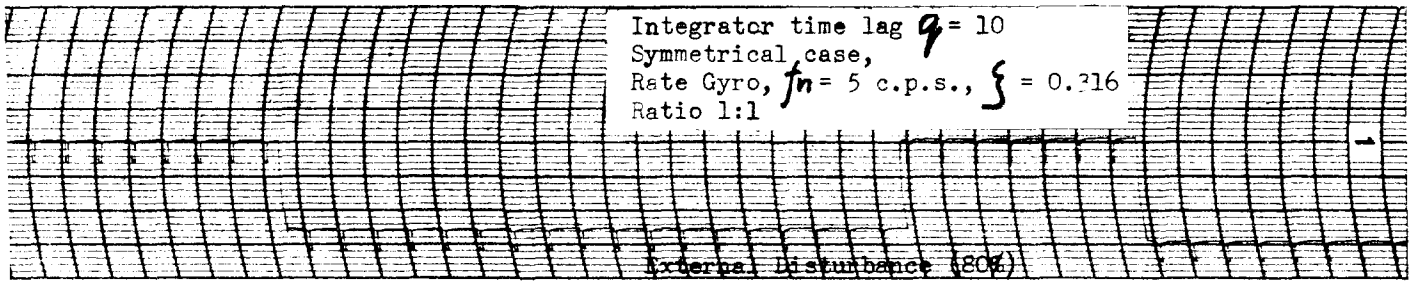
Integrator time lag q = 10
Symmetrical case,
Rate Gyro, f_n = 5 c.p.s., ζ = 0.216
Ratio 1:1
1
External disturbance (80%)

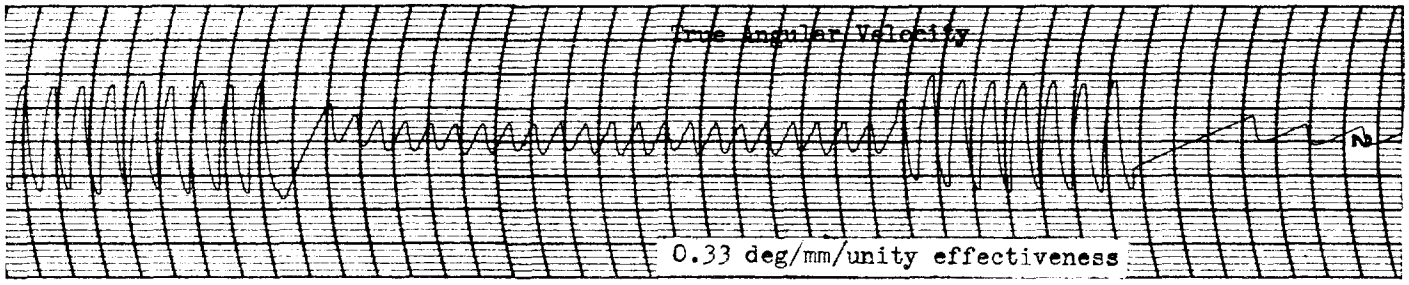
True Angular Velocity
2
0.33 deg/mm/unity effectiveness

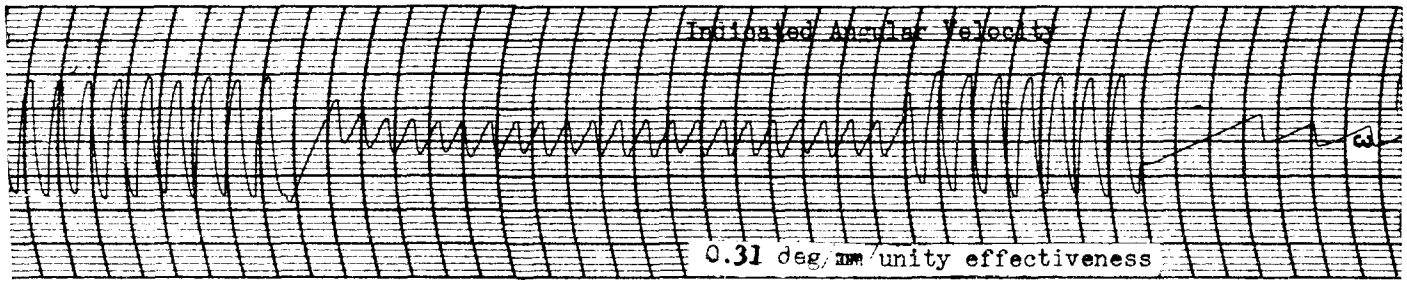
Indicated Angular Velocity
3
0.31 deg/mm/unity effectiveness

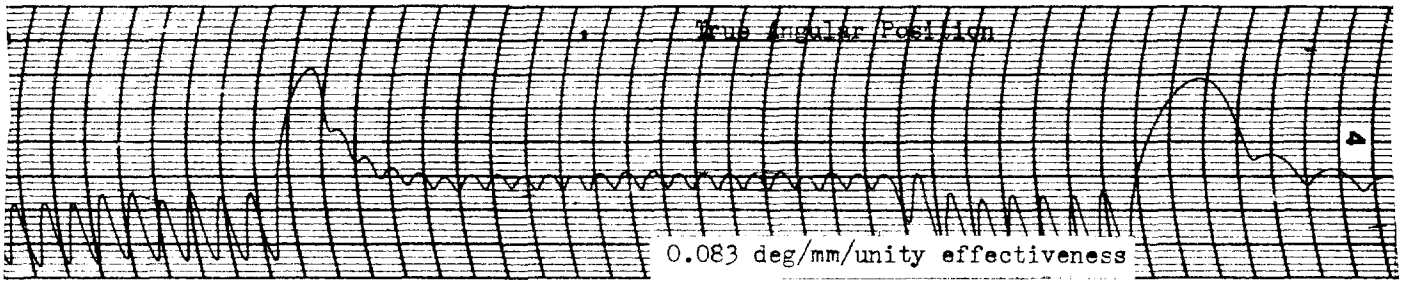
True Angular Position
4
0.083 deg/mm/unity effectiveness

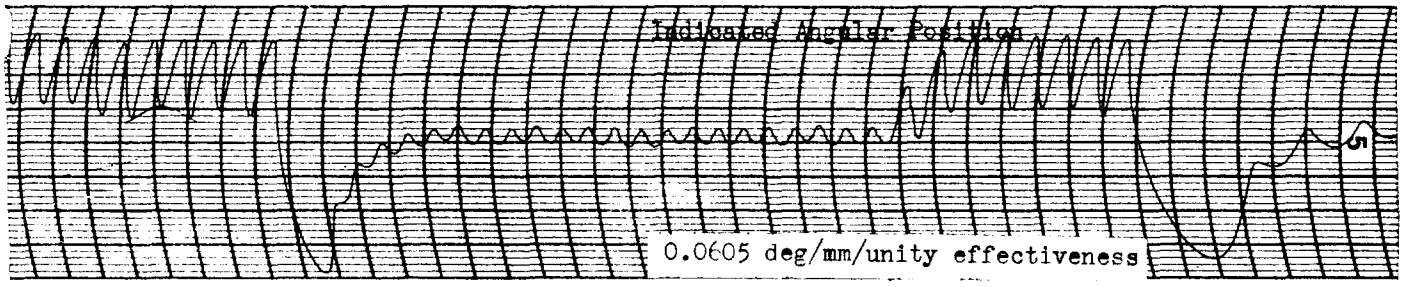
Indicated Angular Position
5
0.0605 deg/mm/unity effectiveness

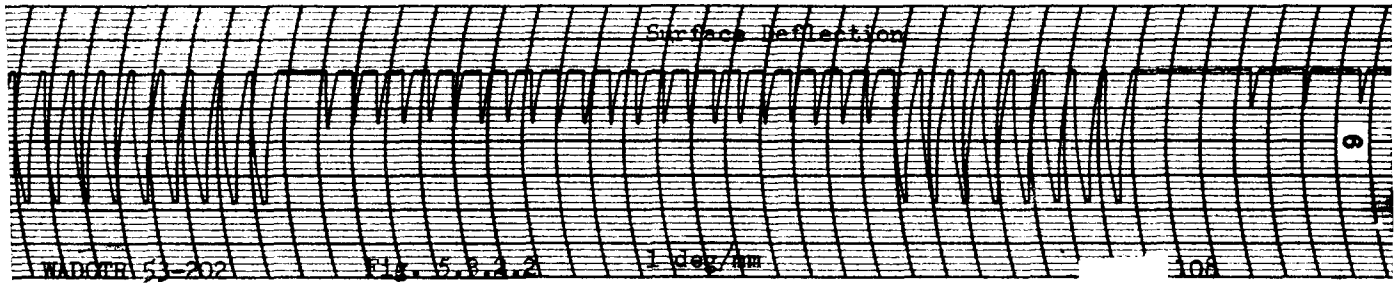
Surface Deflection
6

SYMMETRICAL SYSTEM RESPONSE TO EXTERNAL
DISTURBANCE FOR VARIOUS TIME DELAYS IN INTEGRATING MOTOR

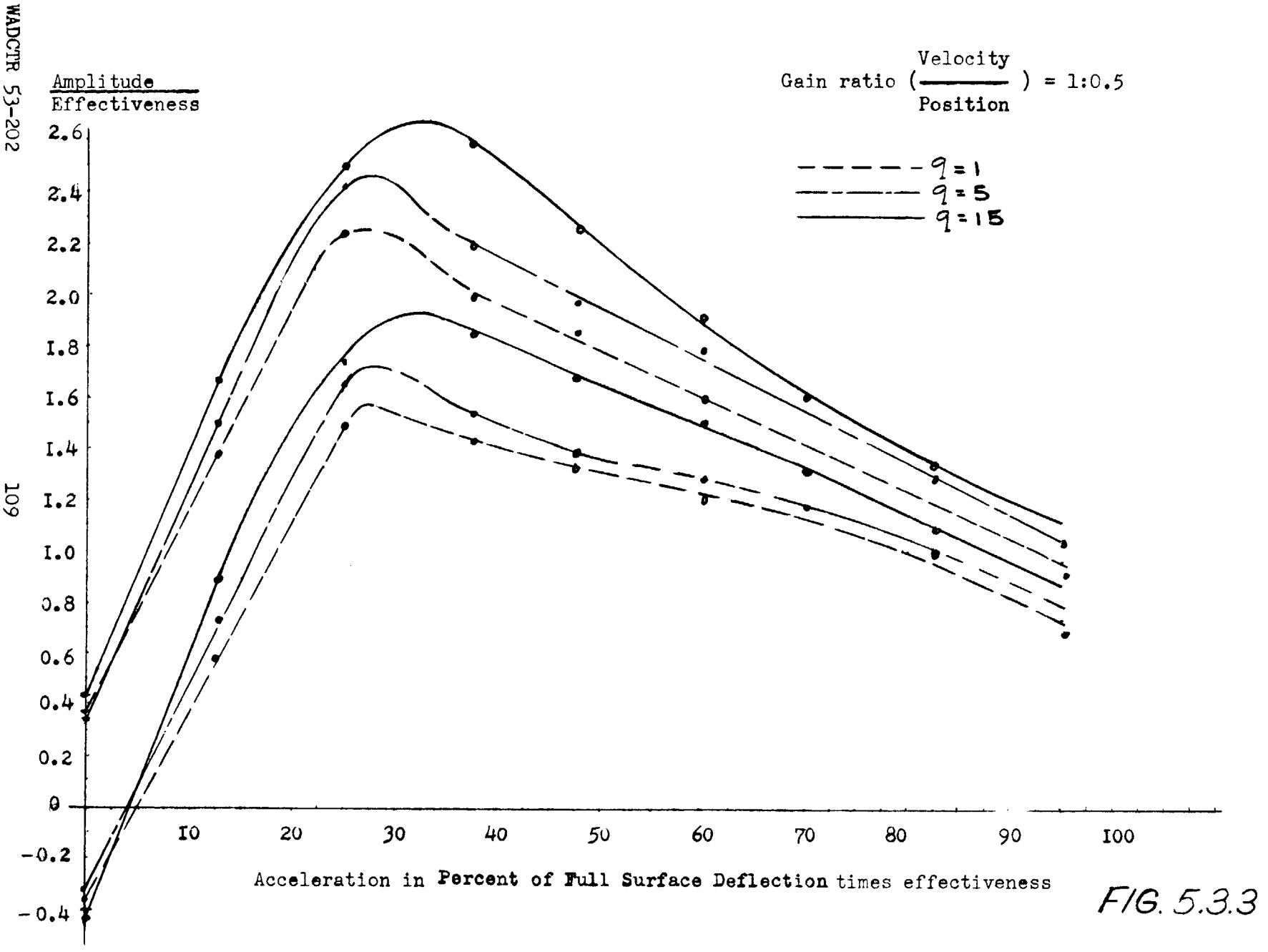

FIG. 5.3.3

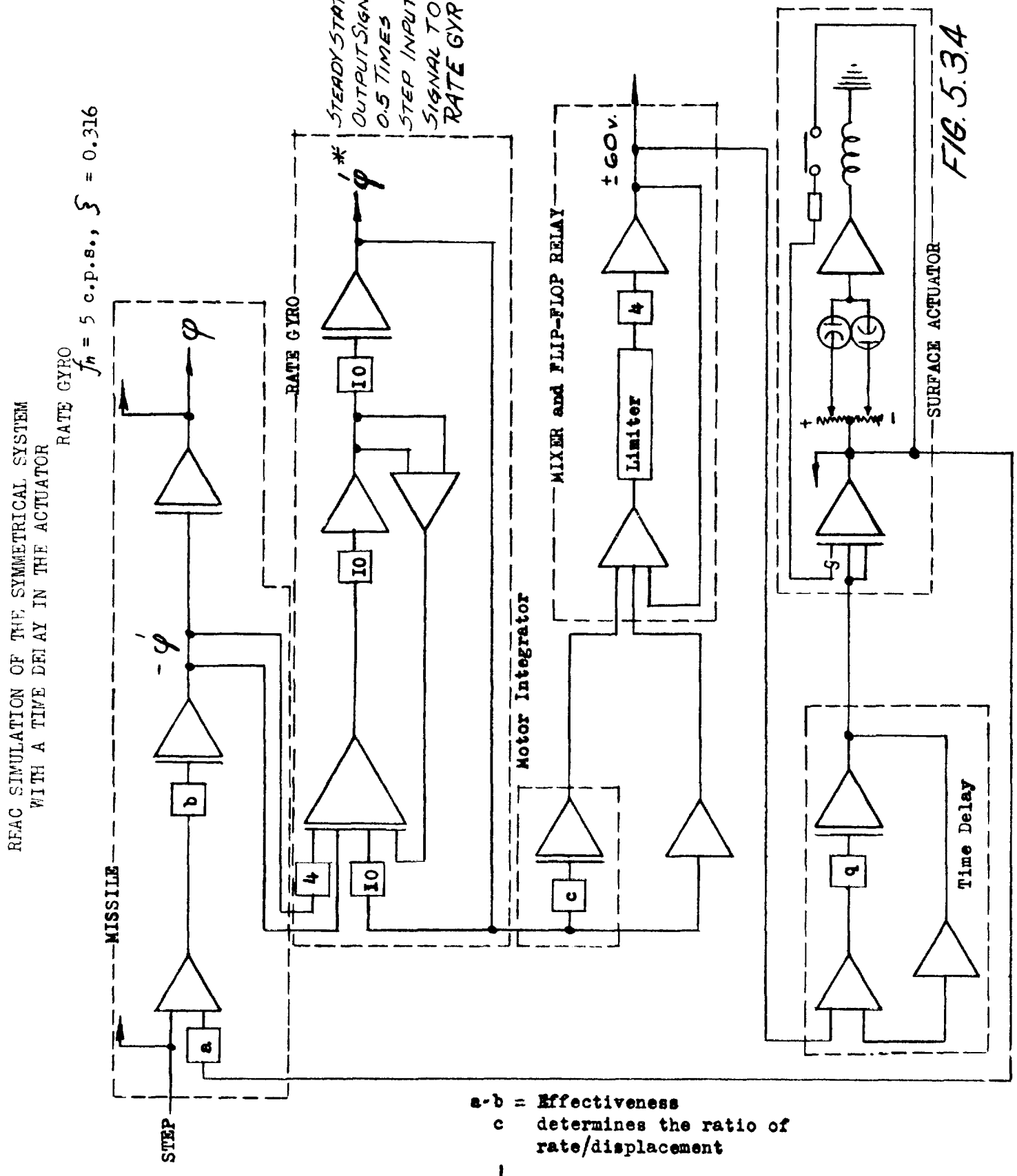
REAC SIMULATION OF THE SYMMETRICAL SYSTEM
WITH A TIME DELAY IN THE ACTUATOR
RATE GYRO
f_n = 5 c.p.s., ζ = 0.316
STEADY STATE OUTPUT SIGNAL = 0.5 TIMES STEP INPUT SIGNAL TO RATE GYRO
RATE GYRO
MISSILE
STEP
Motor Integrator
MIXER and FLIP-FLOP RELAY
±60v.
Limiter
SURFACE ACTUATOR
Time Delay
a
b
c
q
4
10
a-b = Effectiveness
c determines the ratio of rate/displacement
$\frac{1}{q}$ = Time constant

FIG. 5.34

SYMMETRICAL SYSTEM PERFORMANCE WITH TIME DELAYS IN THE ACTUATORS
RATE GYRO f_n = 5 c.p.s.
ζ = 0.316

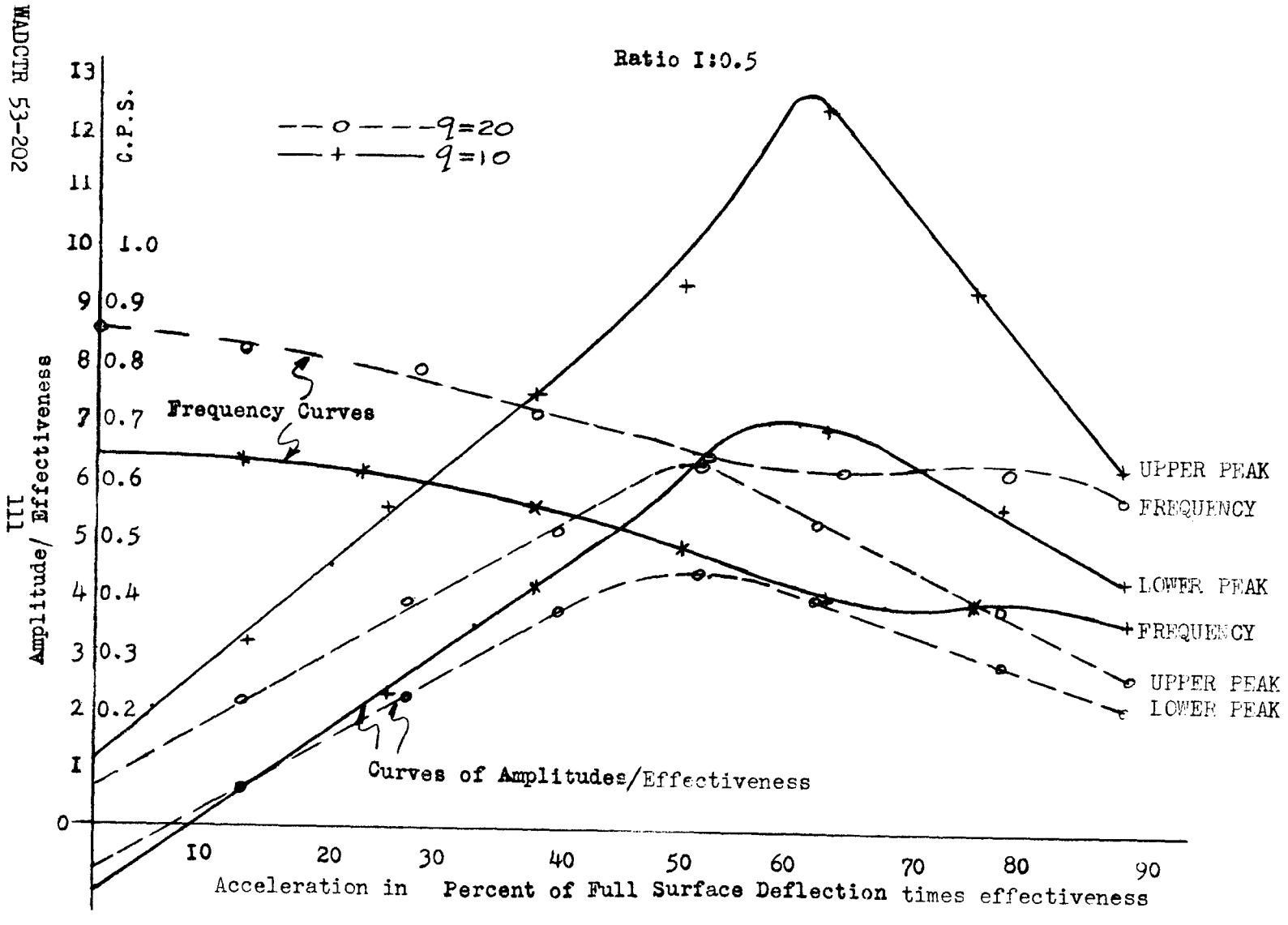

FIG. 5.3.5

REAC SIMULATION OF A DEAD ZONE IN THE SENSITIVITY OF THE "FLIP-FLOP" RELAY OF A SYMMETRICAL SYSTEM

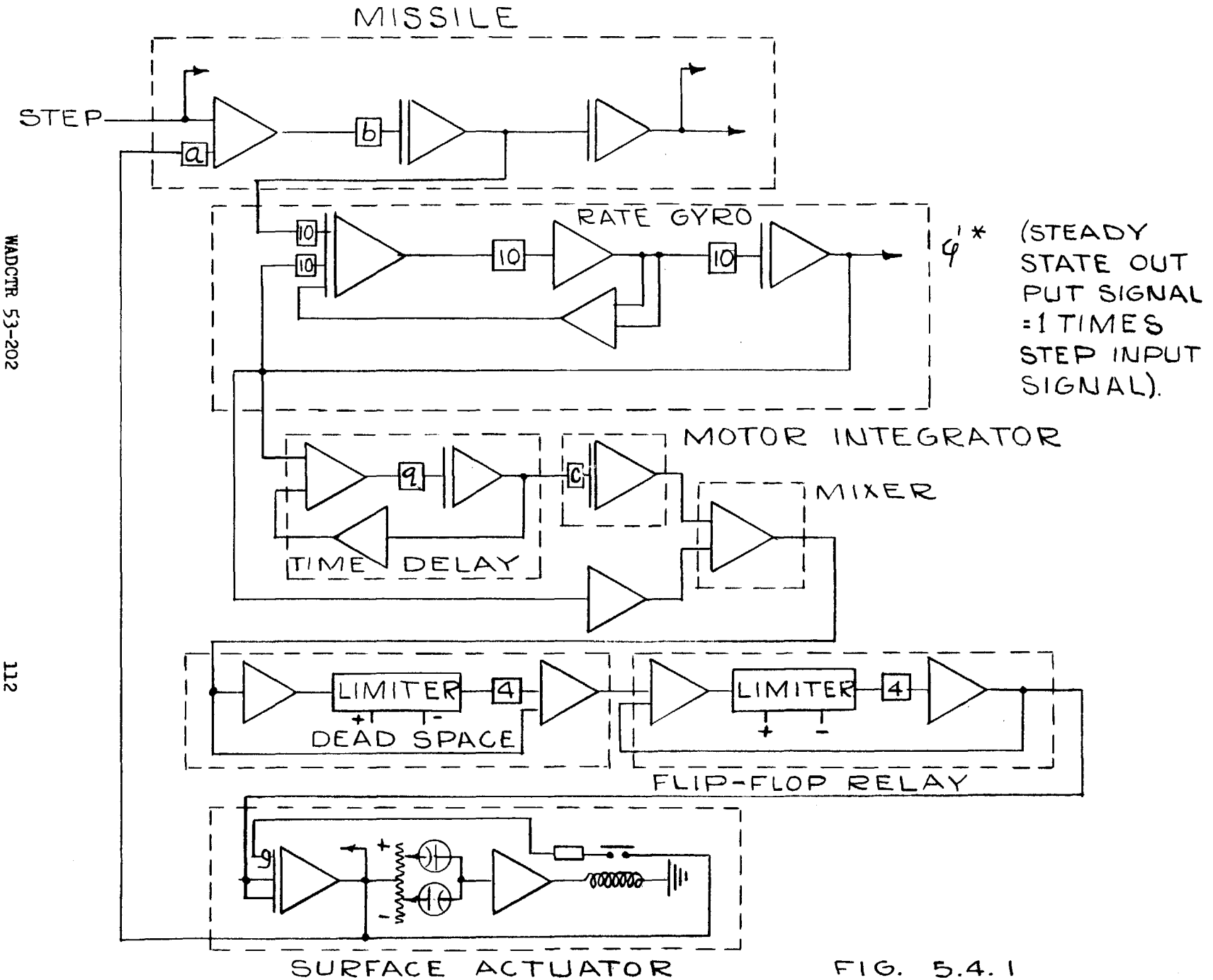

FIG. 5.4.1

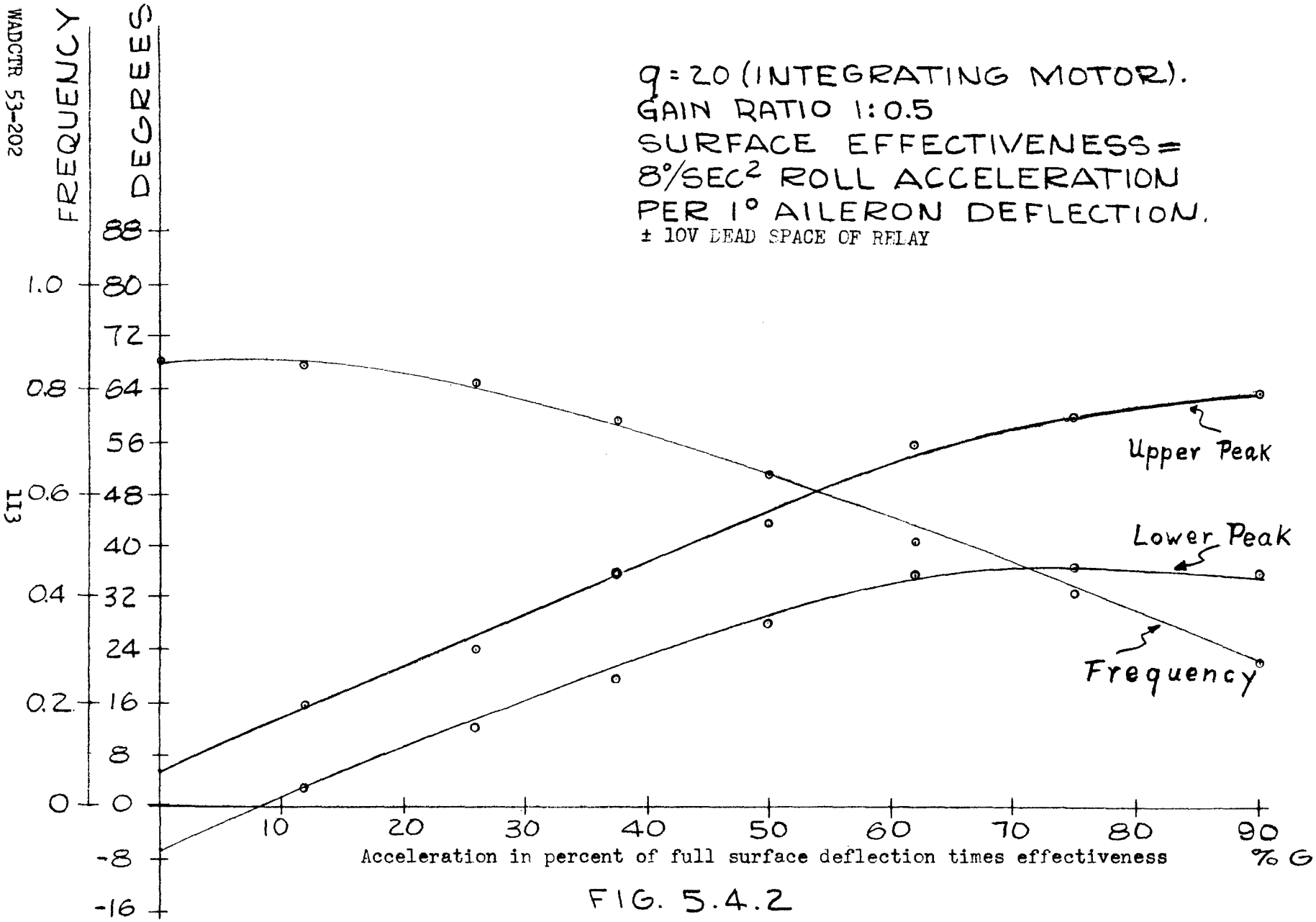
FREQUENCY
DEGREES
1.0
0.8
0.6
0.4
0.2
0
88
80
72
64
56
48
40
32
24
16
8
0
-8
-16
q = 20 (INTEGRATING MOTOR).
GAIN RATIO 1:0.5
SURFACE EFFECTIVENESS =
8°/SEC² ROLL ACCELERATION
PER 1° AILERON DEFLECTION.
± 10V DEAD SPACE OF RELAY
Upper Peak
Lower Peak
Frequency
10
20
30
40
50
60
70
80
90
Acceleration in percent of full surface deflection times effectiveness
% G

FIG. 5.4.2

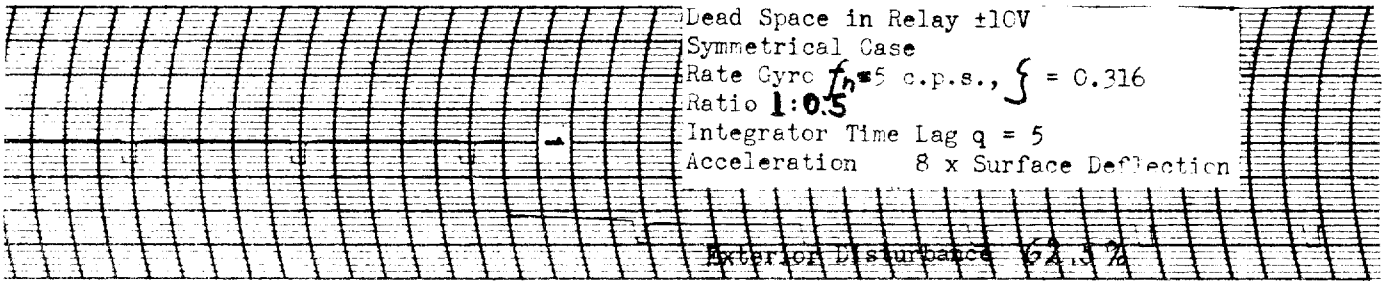
Dead Space in Relay ±1CV
Symmetrical Case
Rate Gyro f_n=5 c.p.s., ζ = 0.316
Ratio 1:0.5
Integrator Time Lag q = 5
Acceleration 8 x Surface Deflection
1
Exterior Disturbance 62.5%

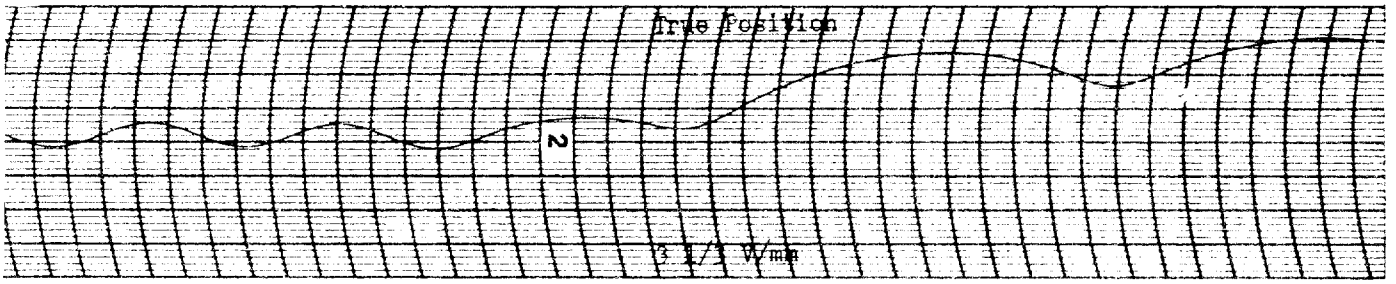
True Position
2
3 1/1 W/mm

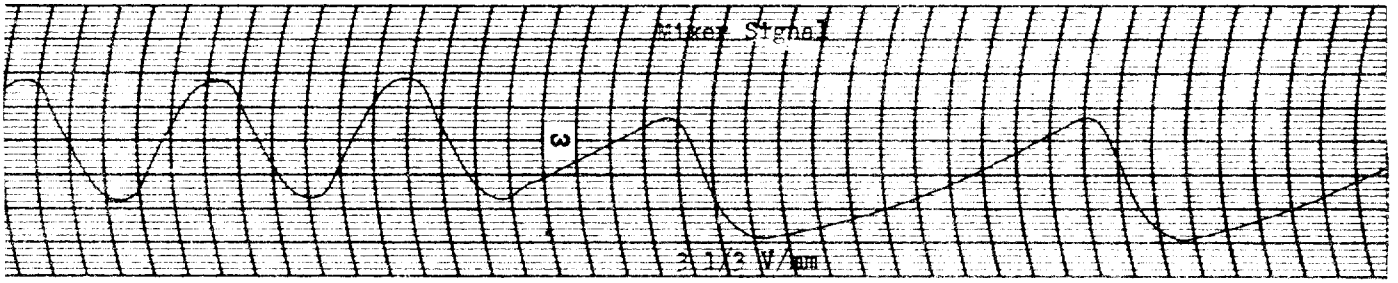
Aileron Signal
3
3 1/2 W/mm

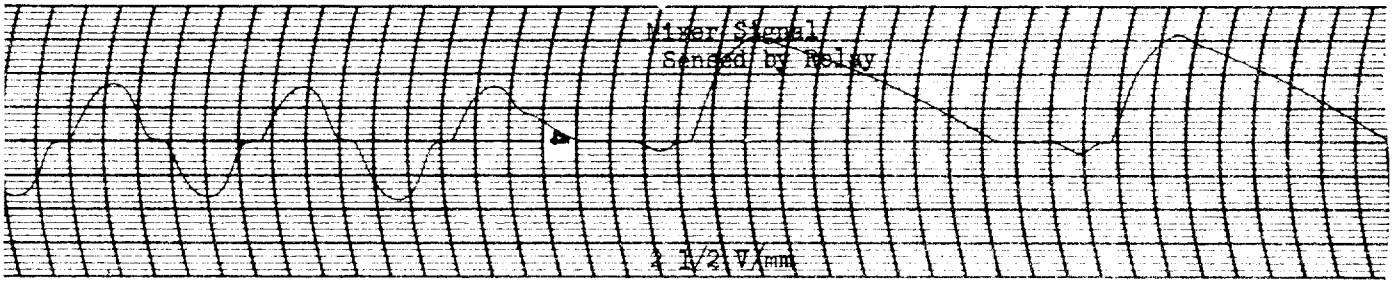
Aileron Signal
Sensed by Relay
4
2 1/2 V/mm

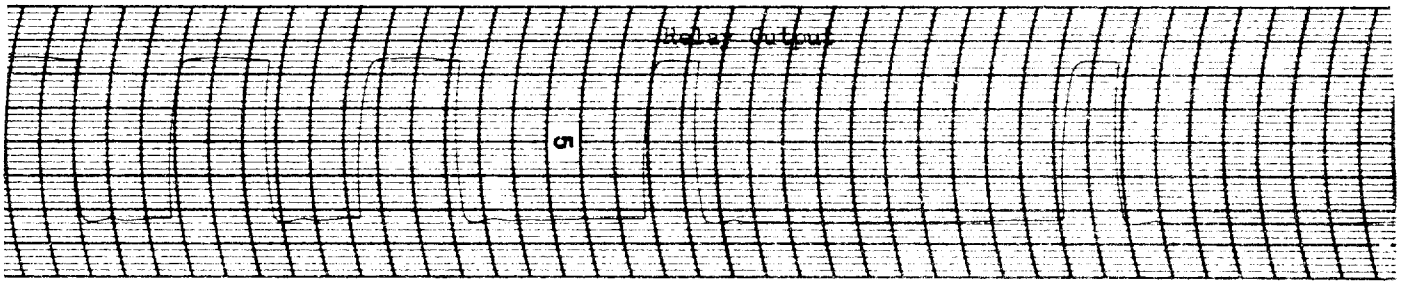
Relay Output
5

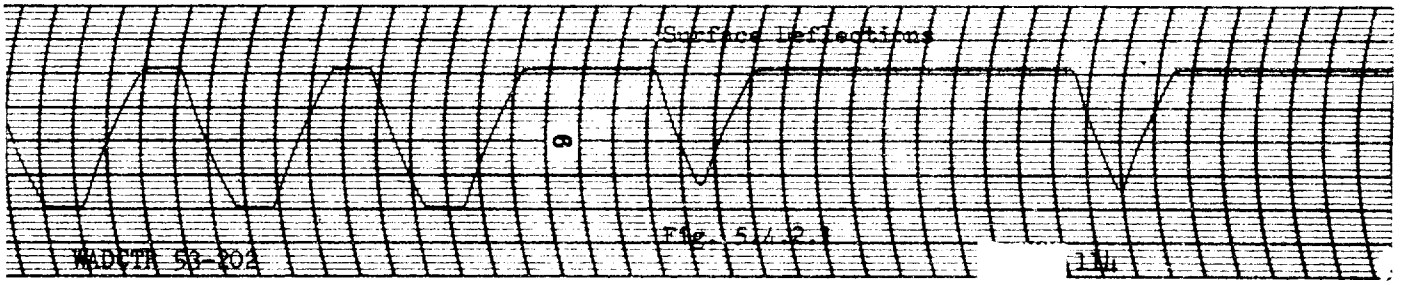
Surface Deflections
6
Fig. 5.4.2.1

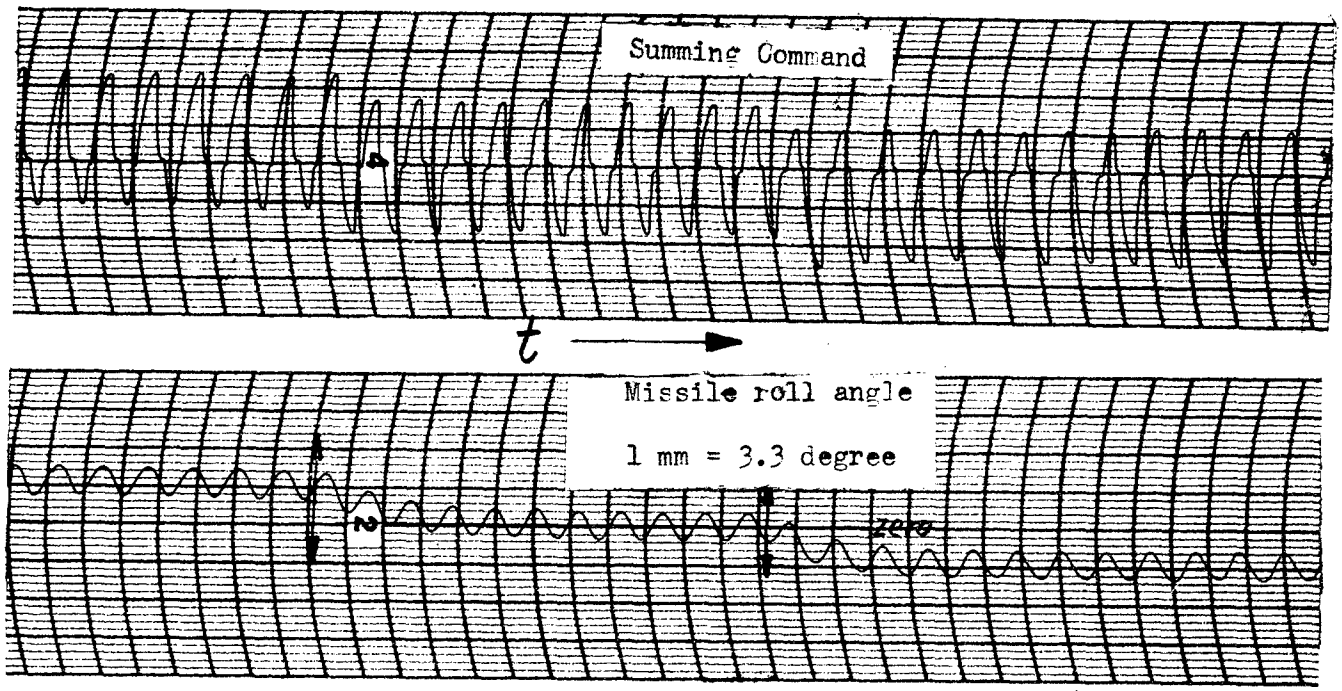

SYMMETRICAL CASE
Time Lag in Integrating Motor (T = 0.1 sec)
Dead Space in Summing Relay ±10 Volts
Ratio 1:0.5
25% External Disturbance
Surface Effectiveness 8 degrees/sec^2
per degree surface deflection

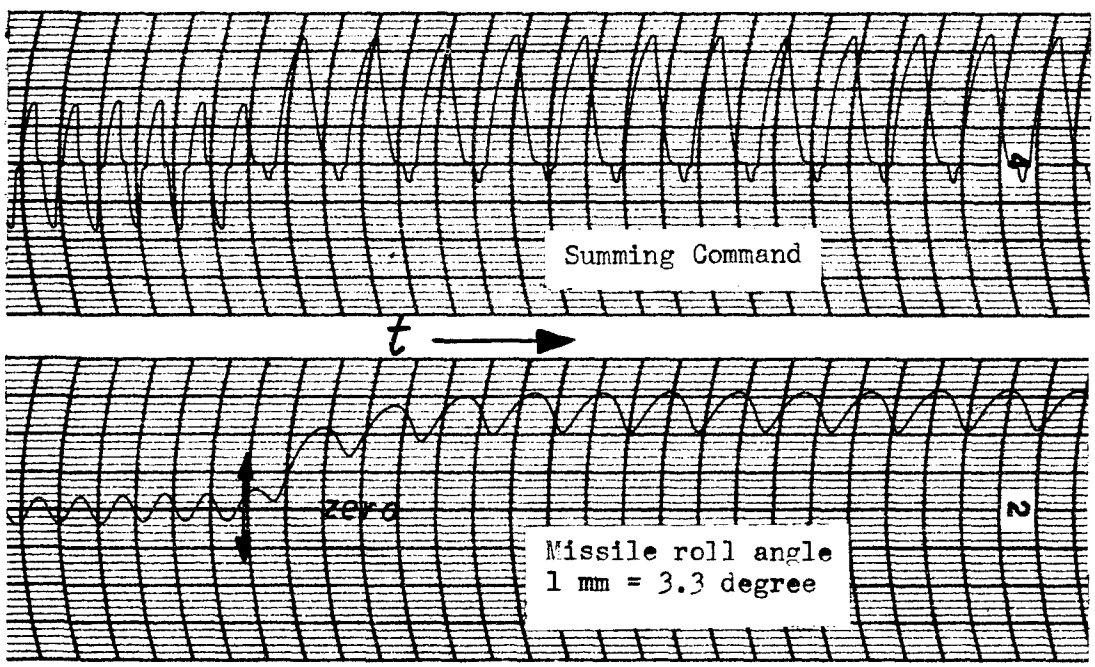

SYMMETRICAL CASE
Time Lag in Integrating Motor (T = 0.1 sec)
Dead Space in Summing Relay ± 10 Volts
Ratio 1:0.5
Surface Effectiveness 8 degrees/sec^2
per degree surface deflection
62.5 External Disturbance

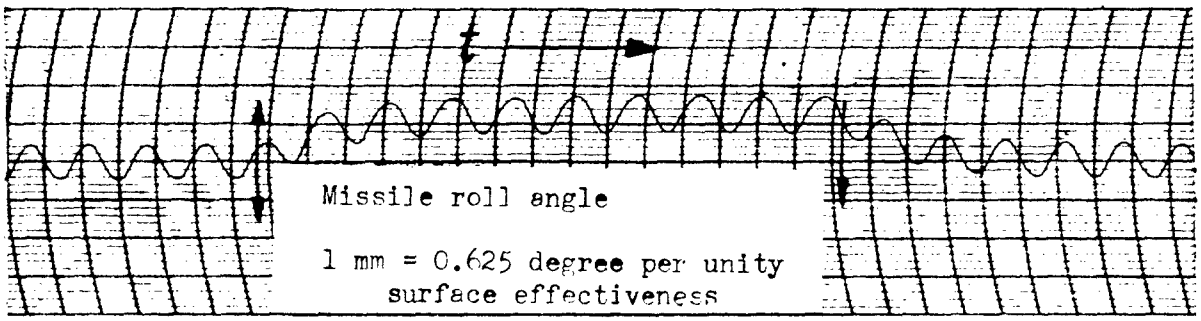

SYMMETRICAL CASE
Time Lag in Actuator (T = 0.1 sec)
Ratio 1:0.5
25% External Disturbance

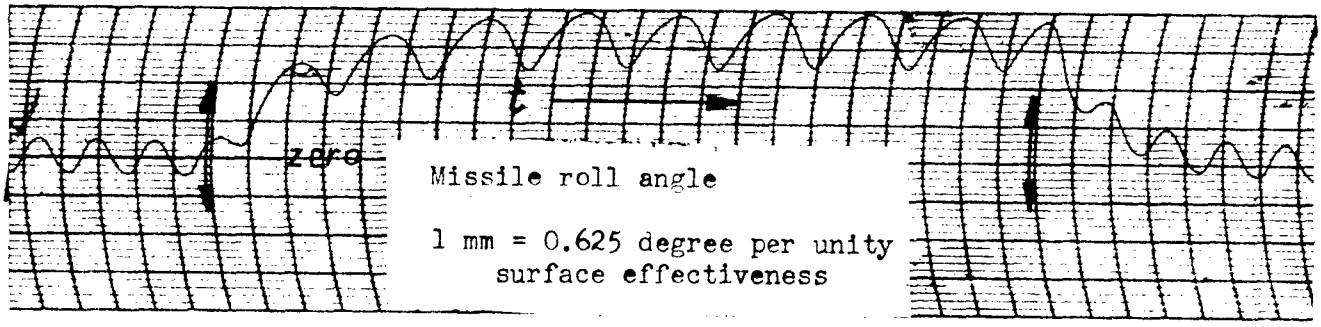

SYMMETRICAL CASE
Time Lag in Actuator (T = 0.1 sec)
Ratio 1:0.5
62.5% External Disturbance

Fig. 5.4.23

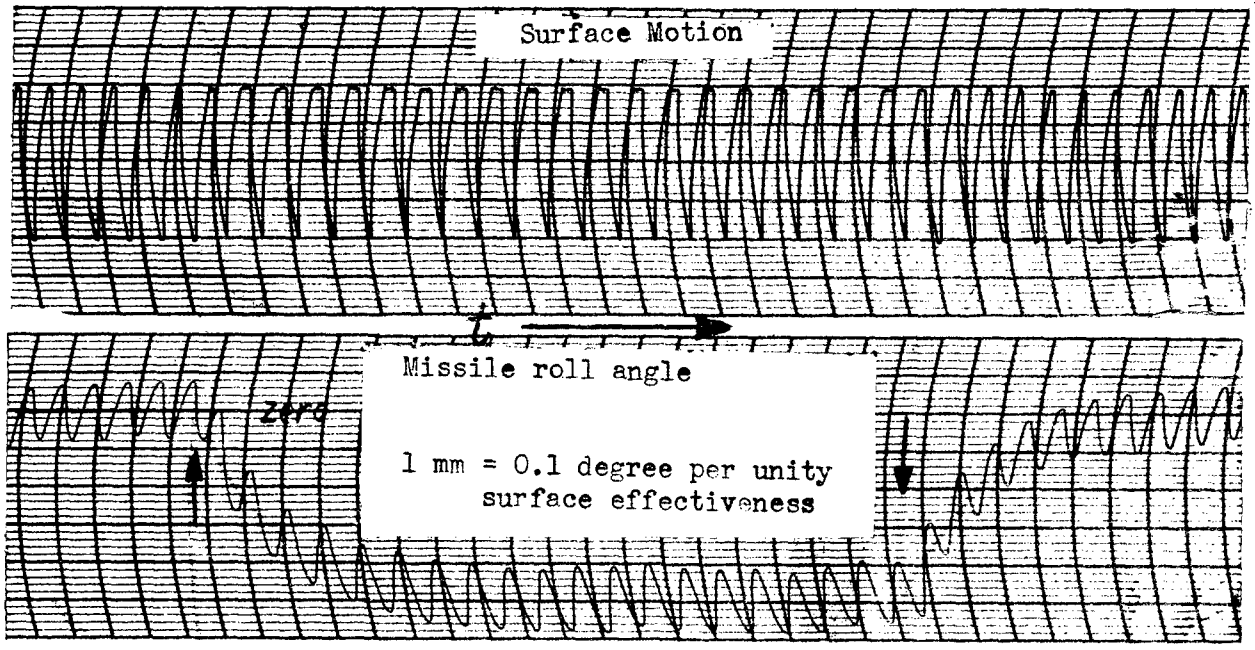

SYMMETRICAL CASE
RATIO 1:0.5
No Time Lag, No Dead Zone
25% External
Disturbance

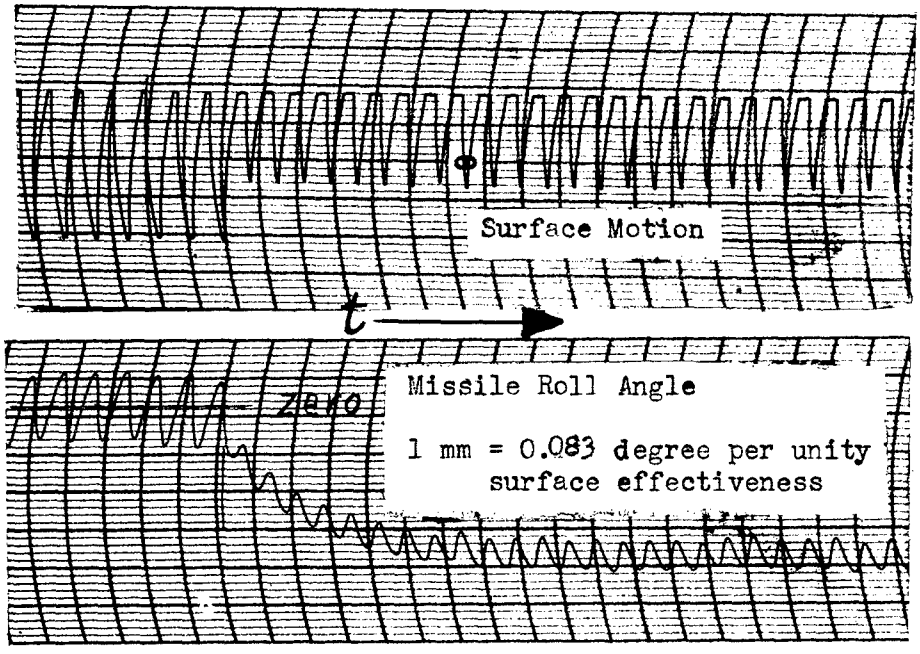

SYMMETRICAL CASE
RATIO 1:0.5
No Time Lag, No Dead Zone
62.5% External
Disturbance

q = 5 (Integrating Motor)

Gain Ratio I:0.5
Surface Effectiveness:
8°/sec² per I° aileron deflection
± 10V Deadspace in Relay

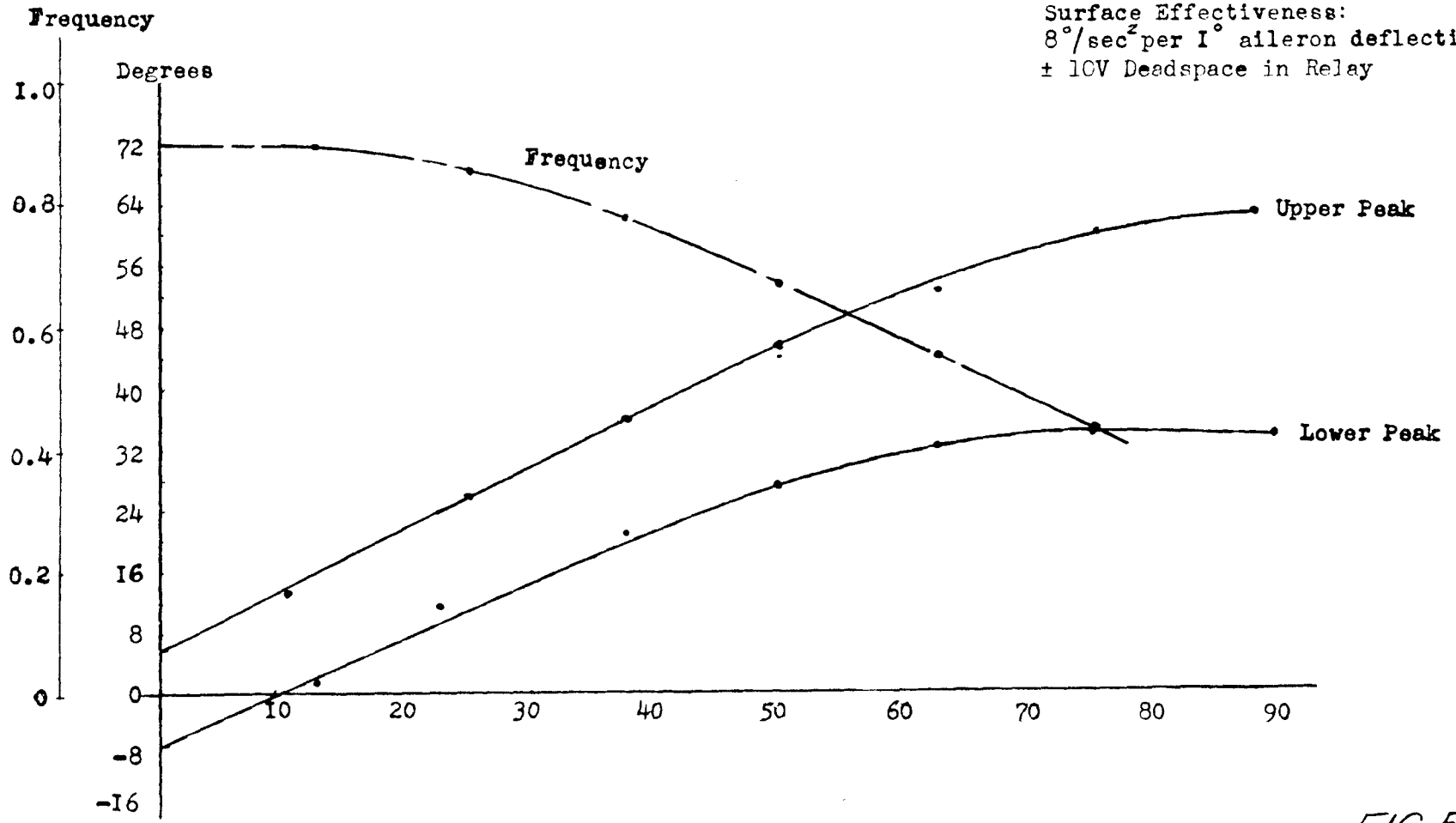

FIG. 5.4.3

Acceleration in Percent of Full Surface Deflection times Effectiveness

Symmetrical System
with asymmetry in the
Rate Gyro

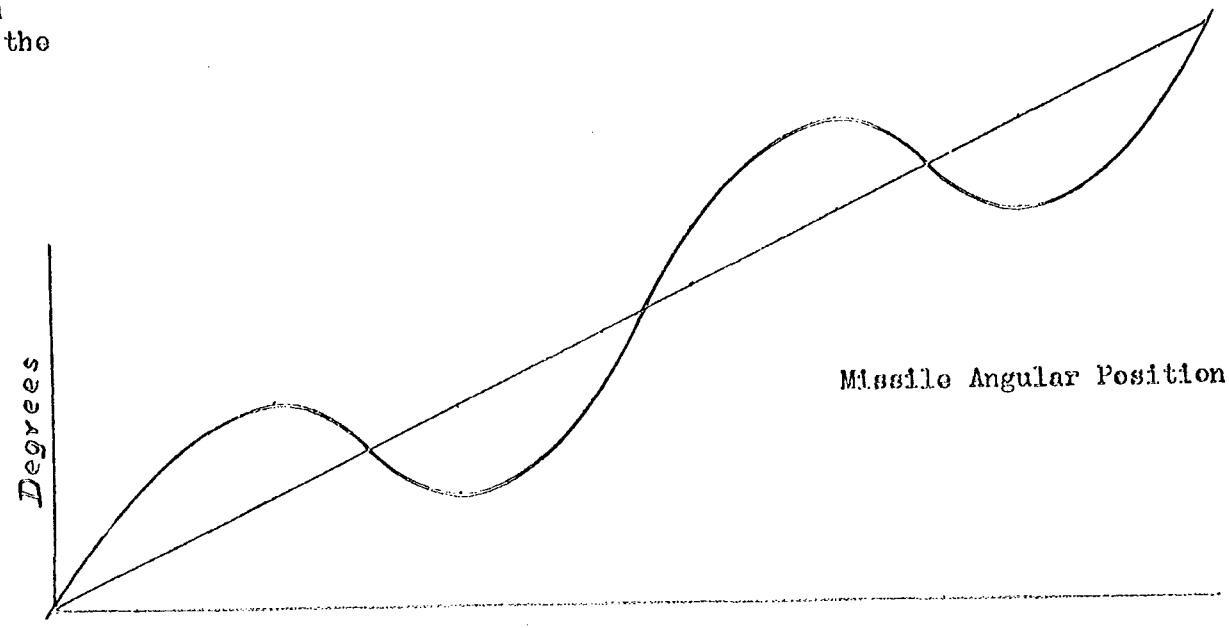

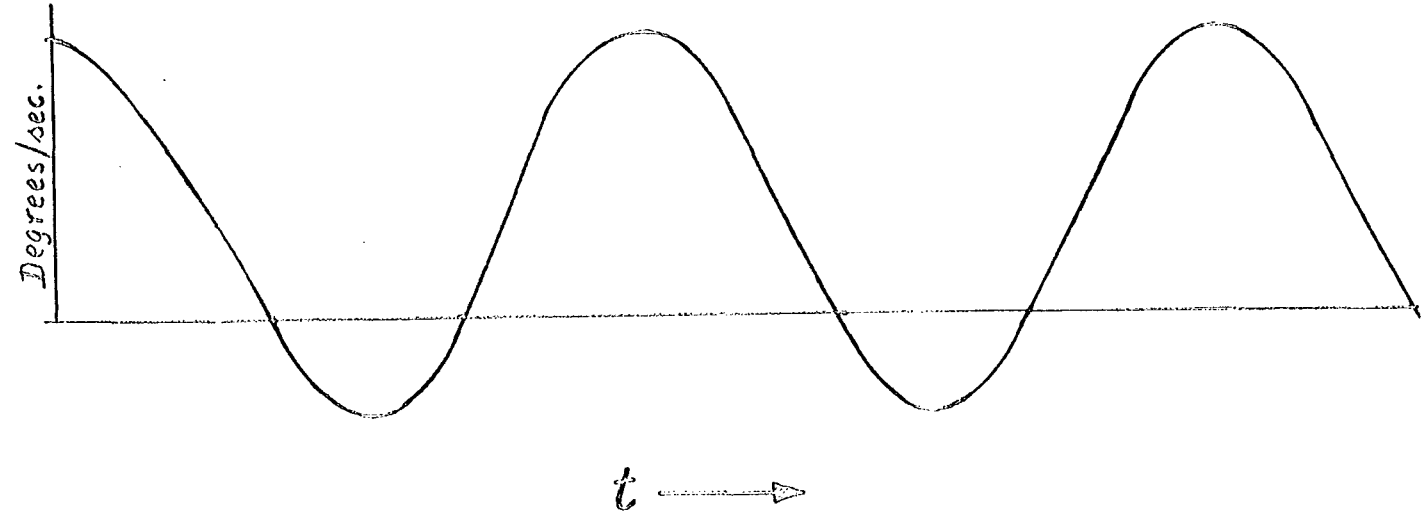

Missile Angular
Velocity

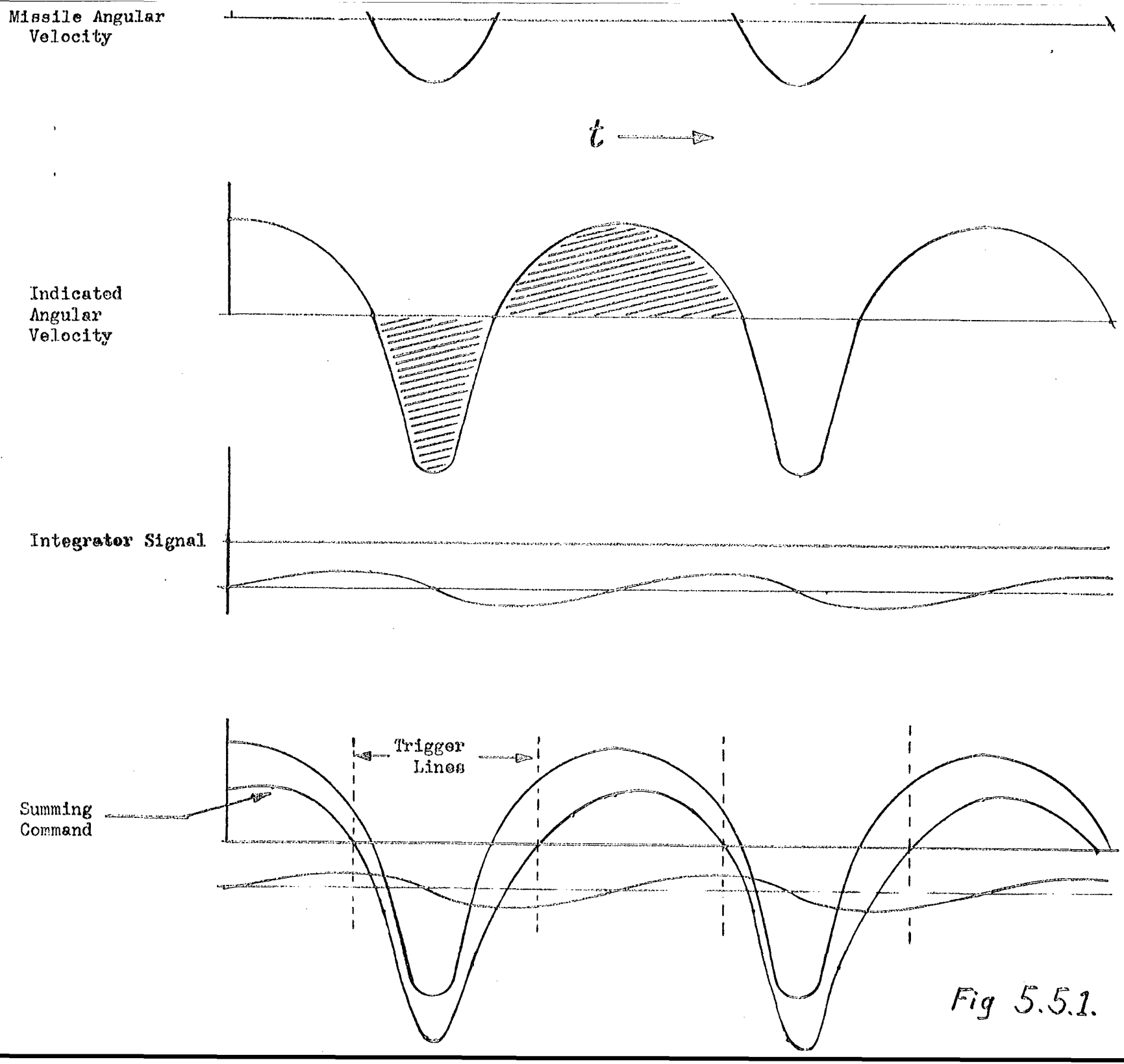
Missile Angular Velocity
t
Indicated Angular Velocity
Integrator Signal
Trigger Lines
Summing Command

Fig 5.5.1.

SYMMETRICAL SYSTEM WITH ASYMMETRY IN THE RATE GYRO 1:a = 1:1.85

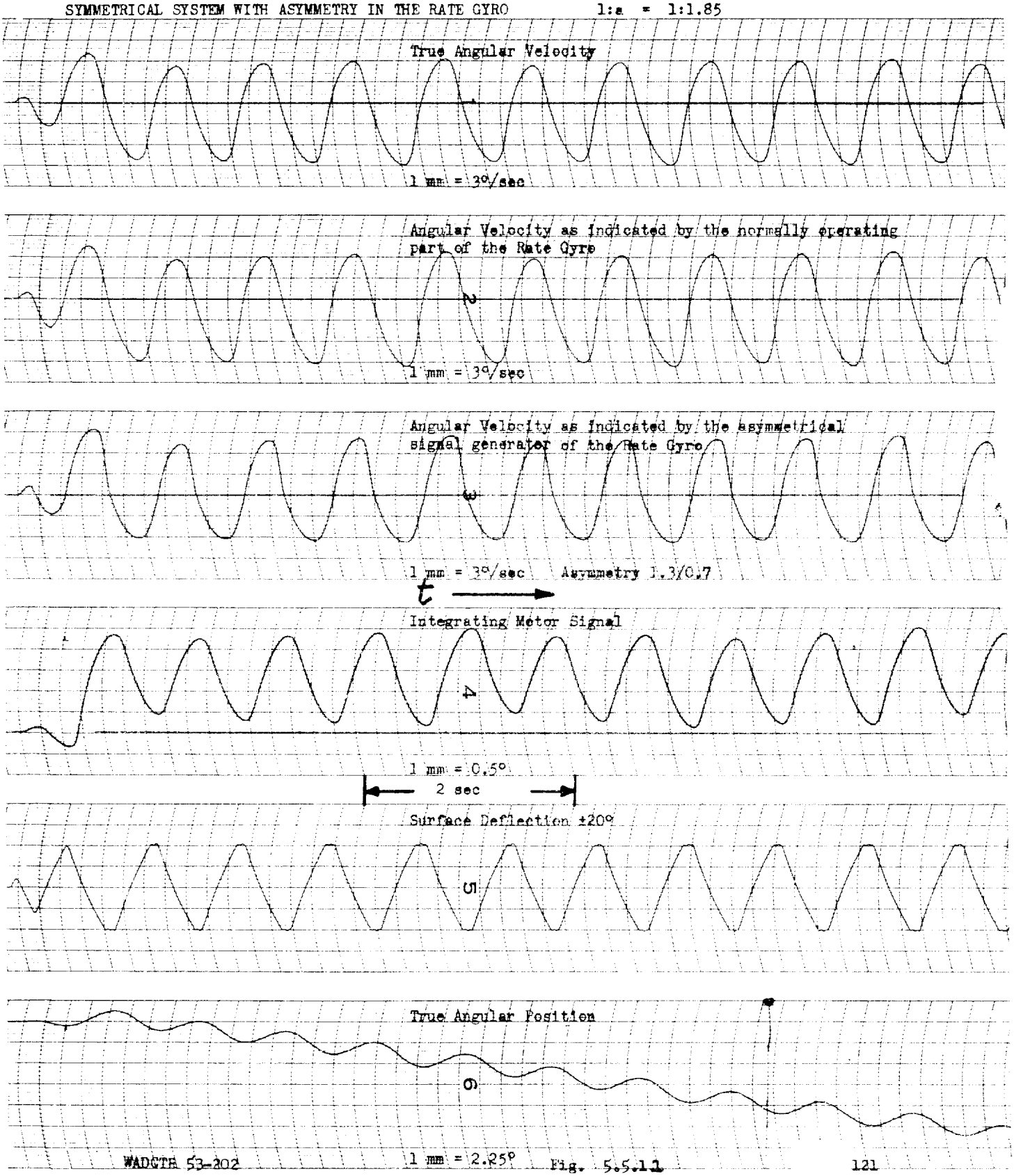

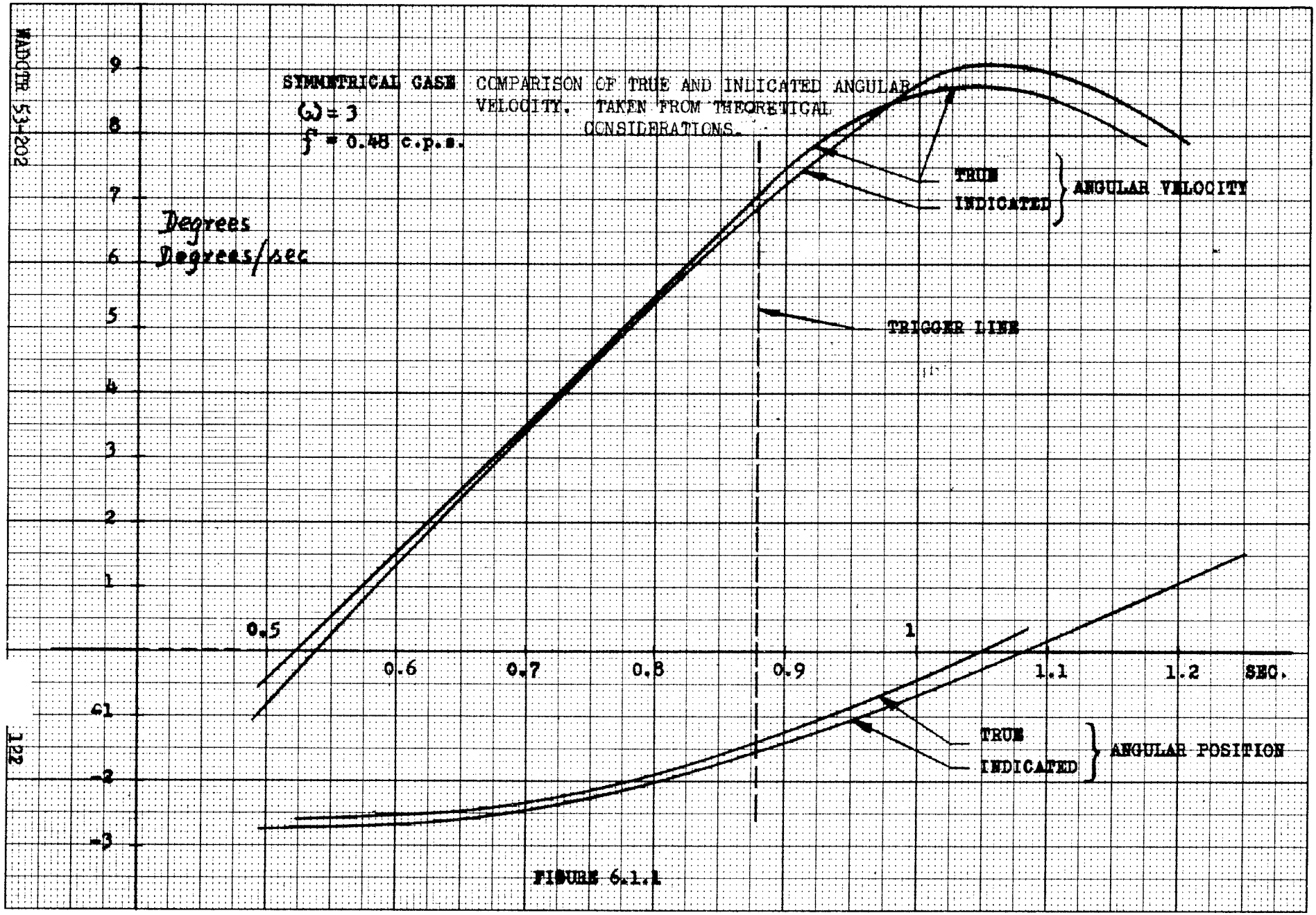
MADDEN 53-202
SYMMETRICAL CASE
ω = 3
f = 0.48 c.p.s.
COMPARISON OF TRUE AND INDICATED ANGULAR VELOCITY, TAKEN FROM THEORETICAL CONSIDERATIONS.
Degrees
Degrees/sec
9
8
7
6
5
4
3
2
1
-1
-2
-3
TRUE
INDICATED
ANGULAR VELOCITY
TRIGGER LINE
0.5
0.6
0.7
0.8
0.9
1
1.1
1.2
SEC.
TRUE
INDICATED
ANGULAR POSITION
122

FIGURE 6.1.1

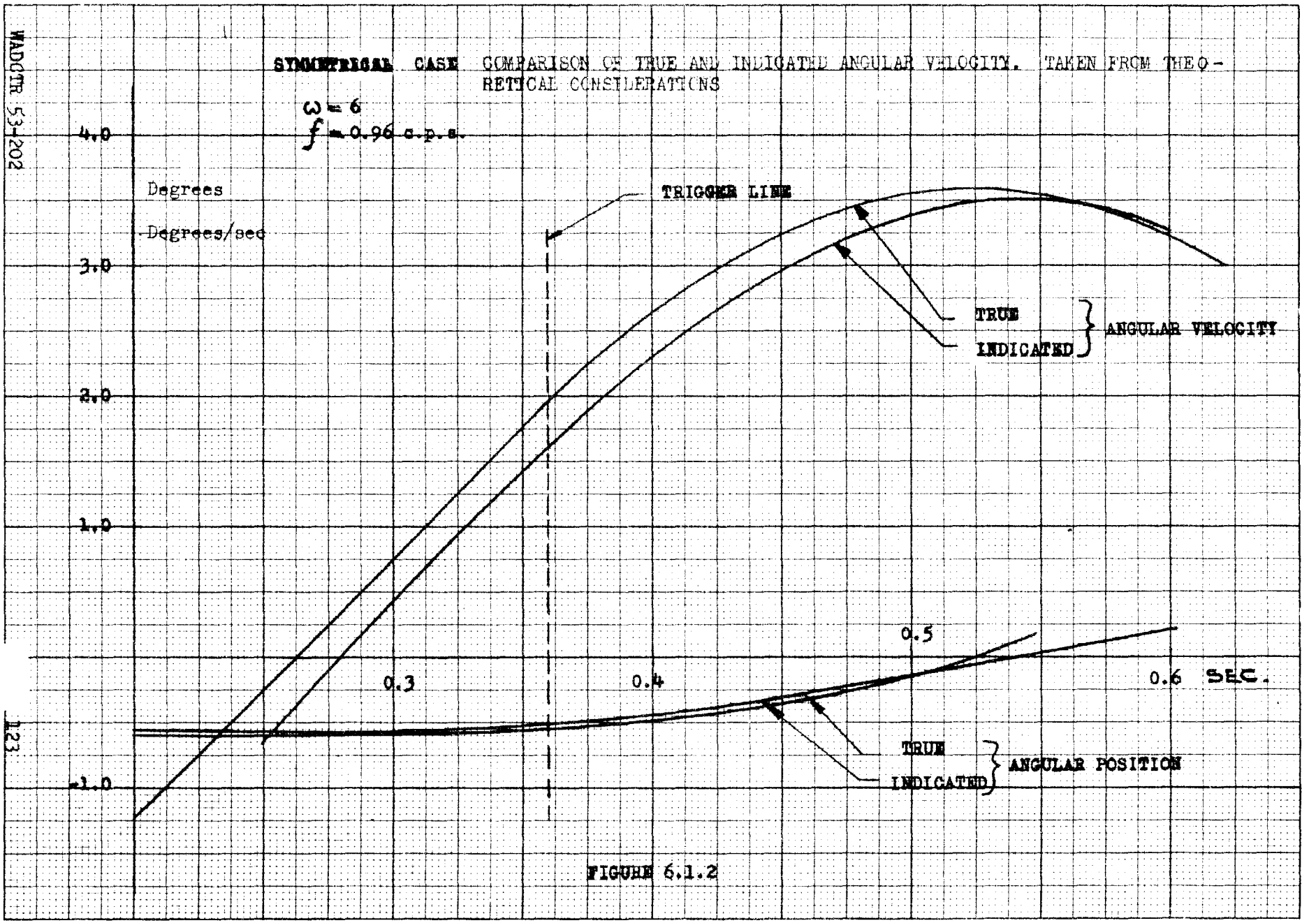
SYMMETRICAL CASE COMPARISON OF TRUE AND INDICATED ANGULAR VELOCITY. TAKEN FROM THEORETICAL CONSIDERATIONS
ω = 6
f = 0.96 c.p.s.
4.0
Degrees
Degrees/sec
3.0
2.0
1.0
-1.0
TRIGGER LINE
TRUE
INDICATED
ANGULAR VELOCITY
0.3
0.4
0.5
0.6 SEC.
TRUE
INDICATED
ANGULAR POSITION

FIGURE 6.1.2

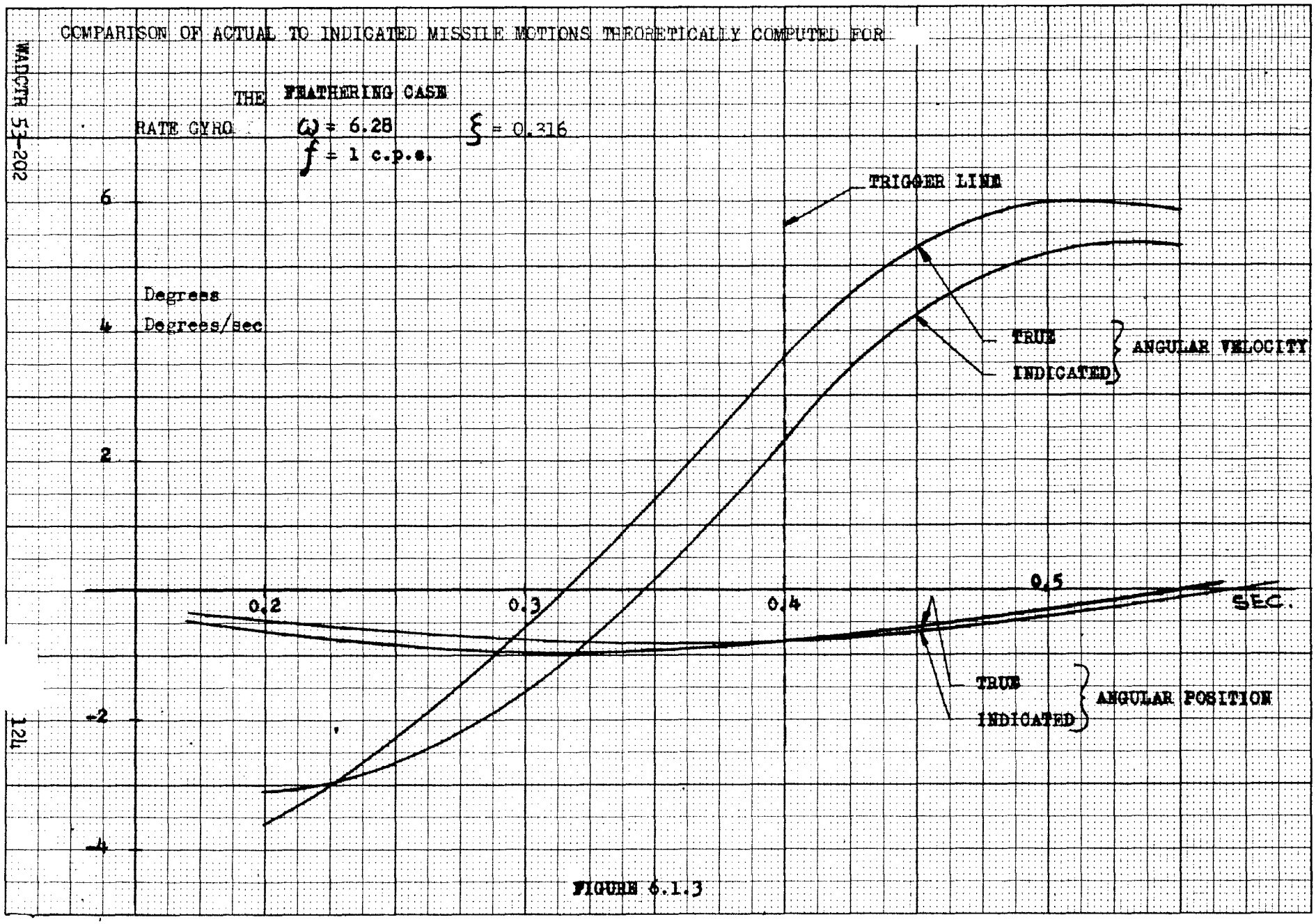
COMPARISON OF ACTUAL TO INDICATED MISSILE MOTIONS THEORETICALLY COMPUTED FOR
THE FEATHERING CASE
RATE GYRO
ω = 6.28
f = 1 c.p.s.
ζ = 0.316
WADCTR 53-202
124
6
4
2
-2
-4
Degrees
Degrees/sec
TRIGGER LINE
TRUE
INDICATED
ANGULAR VELOCITY
TRUE
INDICATED
ANGULAR POSITION
0.2
0.3
0.4
0.5
SEC.

FIGURE 6.1.3

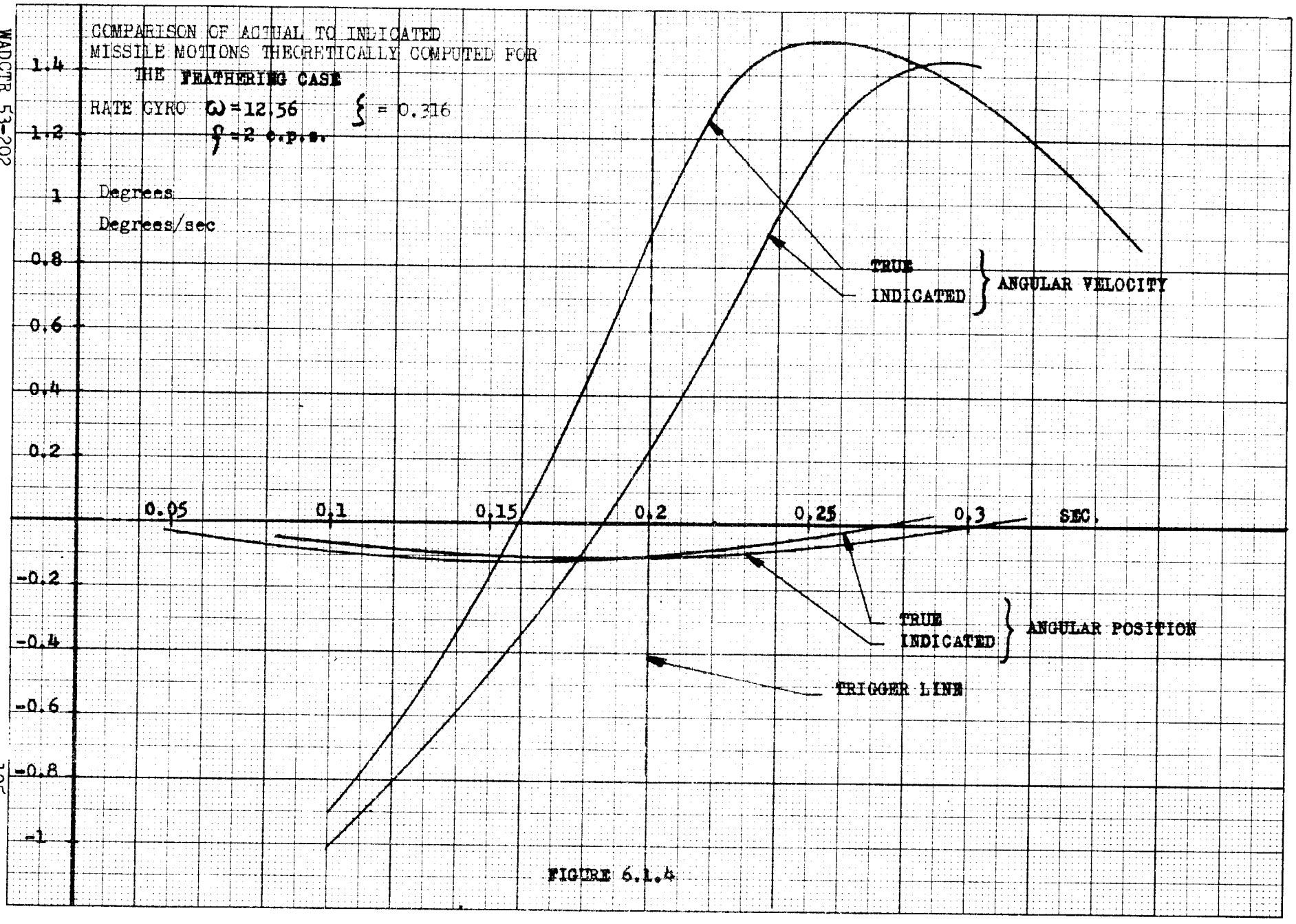
COMPARISON OF ACTUAL TO INDICATED
MISSILE MOTIONS THEORETICALLY COMPUTED FOR
THE FEATHERING CASE
RATE GYRO ω = 12.56 ζ = 0.316
f = 2 c.p.s.
Degrees
Degrees/sec
1.4
1.2
1
0.8
0.6
0.4
0.2
-0.2
-0.4
-0.6
-0.8
-1
0.05
0.1
0.15
0.2
0.25
0.3
SEC.
TRUE
INDICATED
ANGULAR VELOCITY
TRUE
INDICATED
ANGULAR POSITION
TRIGGER LINE

FIGURE 6.1.4

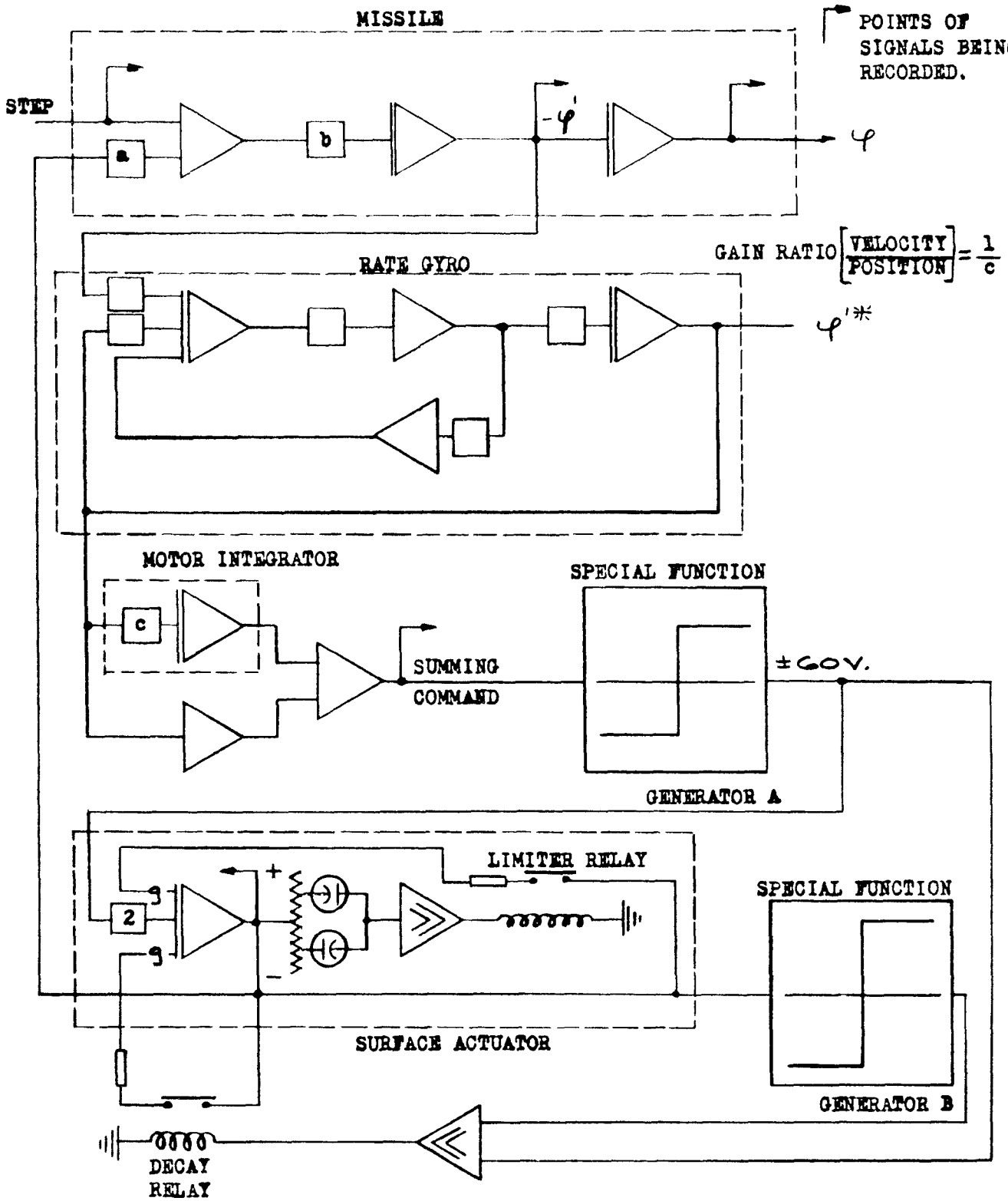

WADCTR 53-202

FIGURE 6.2.1

REAC SIMULATION OF FEATHERING SYSTEM
WITH RATE GYRO f_n = 5 c.p.s.
ζ = 0.316

FREQUENCY VERSUS GAIN RATIO

FOR DIFFERENT VALUES OF DAMPING RATIO (RATE GYRO)

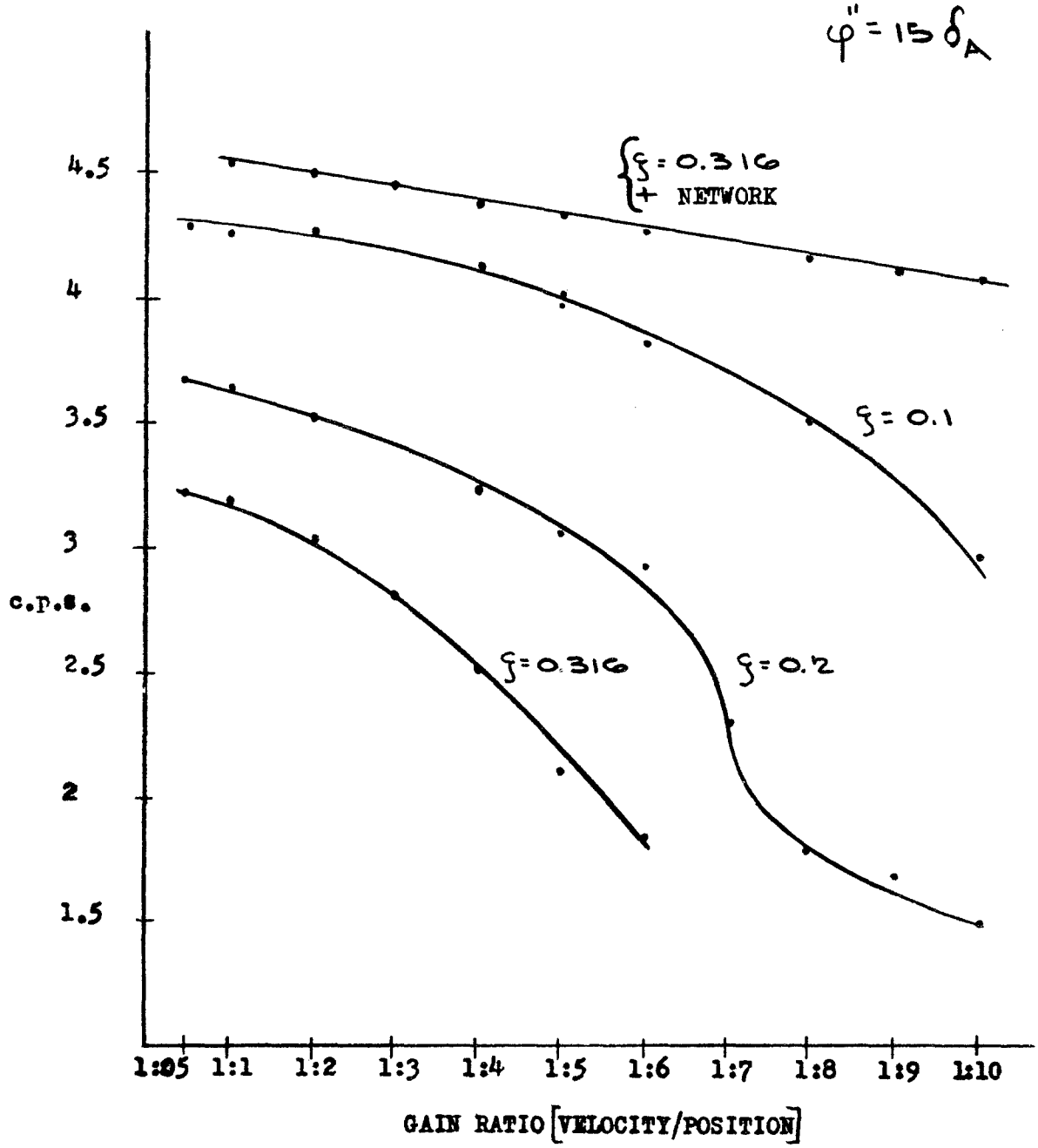

FIGURE 6.3.1.

LEAD NETWORK

(BETWEEN RATE GYRO OUTPUT AND SUMMING COMMAND FORMING COMPONENT OF CONTROL SYSTEM)

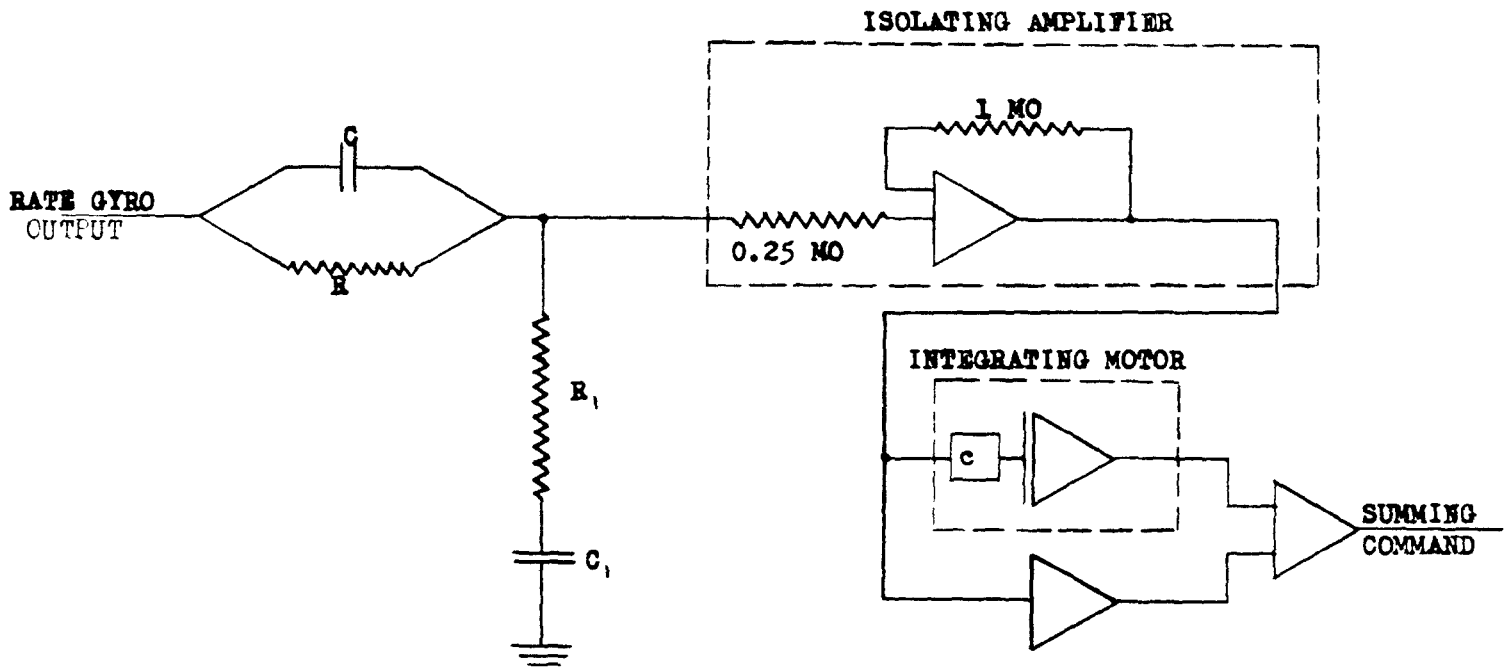

C = 0.7 μF R = 1.2 MO

C_1 = 0.01 μF R_1 = 0.01 MO

FIGURE 6.3.2

DISPLACEMENT AMPLITUDE VERSUS GAIN RATIO
FOR DIFFERENT VALUES OF DAMPING RATIO OF RATE GYRO

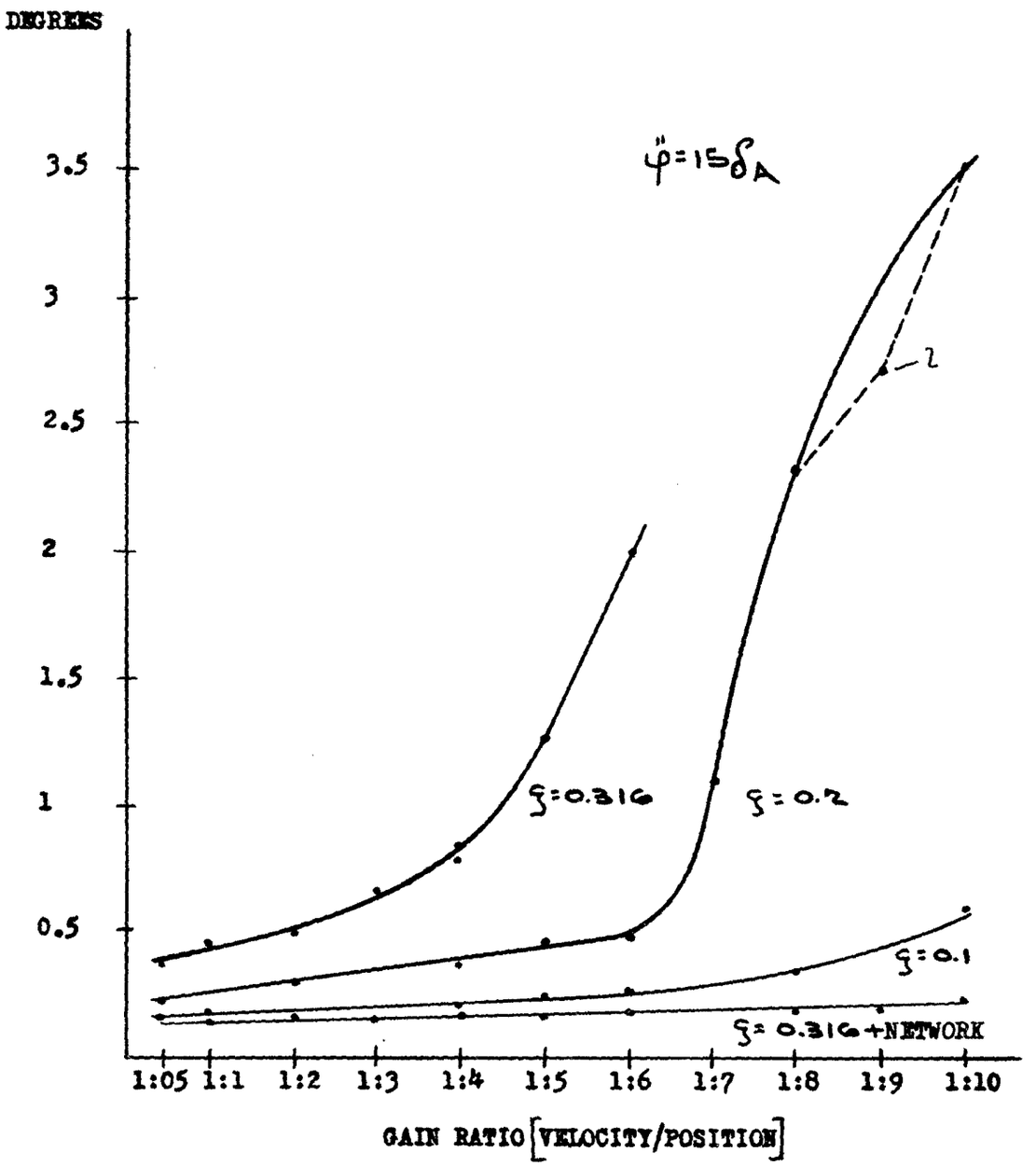

FIGURE 6.3.3

AMPLITUDE OF TRUE (—✕—) AND INDICATED (—•—) ANGULAR VELOCITY VERSUS GAIN RATIO FOR DIFFERENT VALUES OF DAMPING RATIO OF RATE GYRO (f_n = 5 c.p.s.)

(FEATHERING CASE)

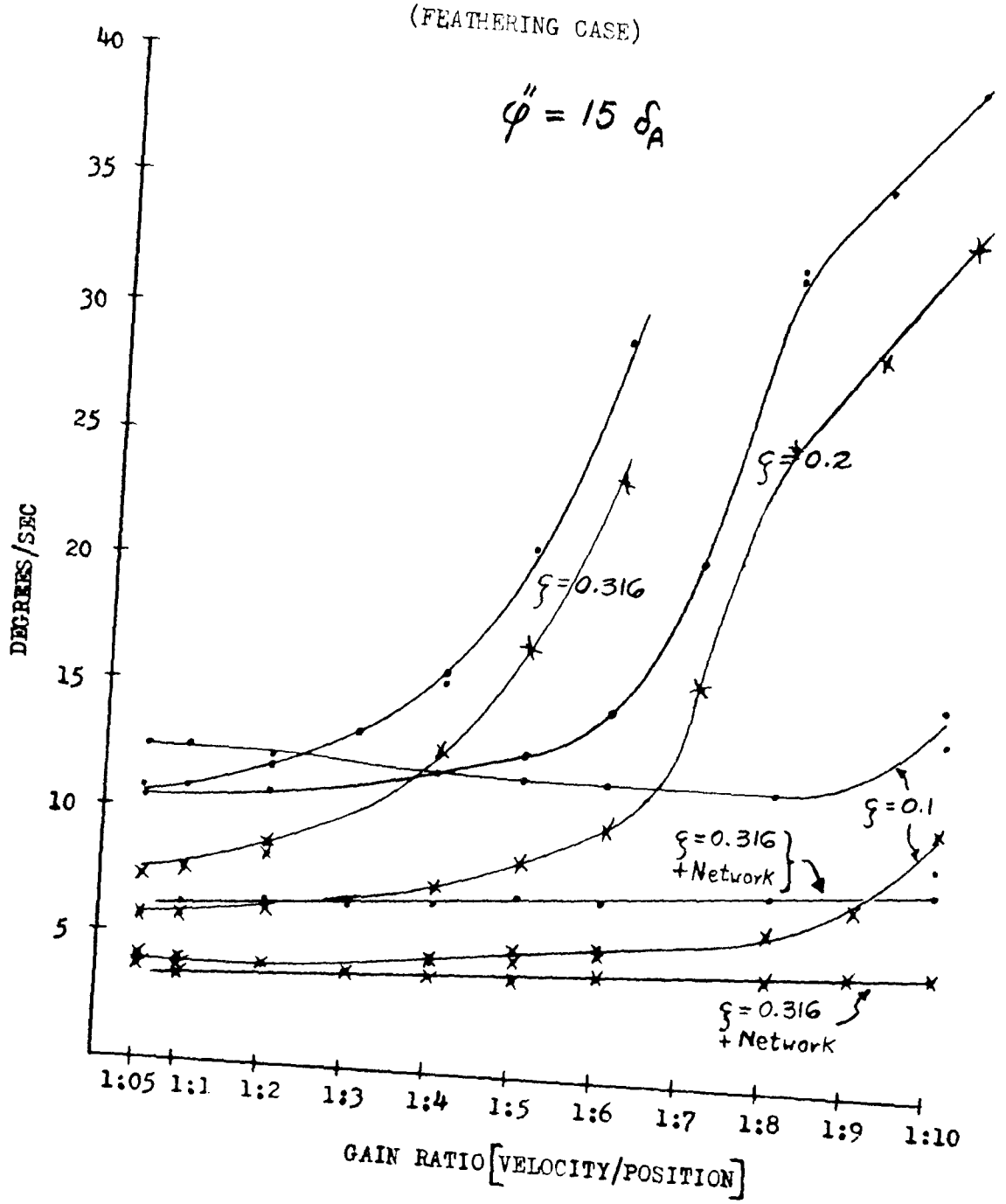

FIG. 6.3.4

AMPLITUDE RATIO OF $\frac{indicated}{true}$ ANGULAR VELOCITY VERSUS FREQUENCY RATIO FOR DIFFERENT VALUES OF ζ = DAMPING RATIO OF RATE GYRO

× TAKEN FROM RECORDS

— CALCULATED FOR SINUSOIDAL OSCILLATION

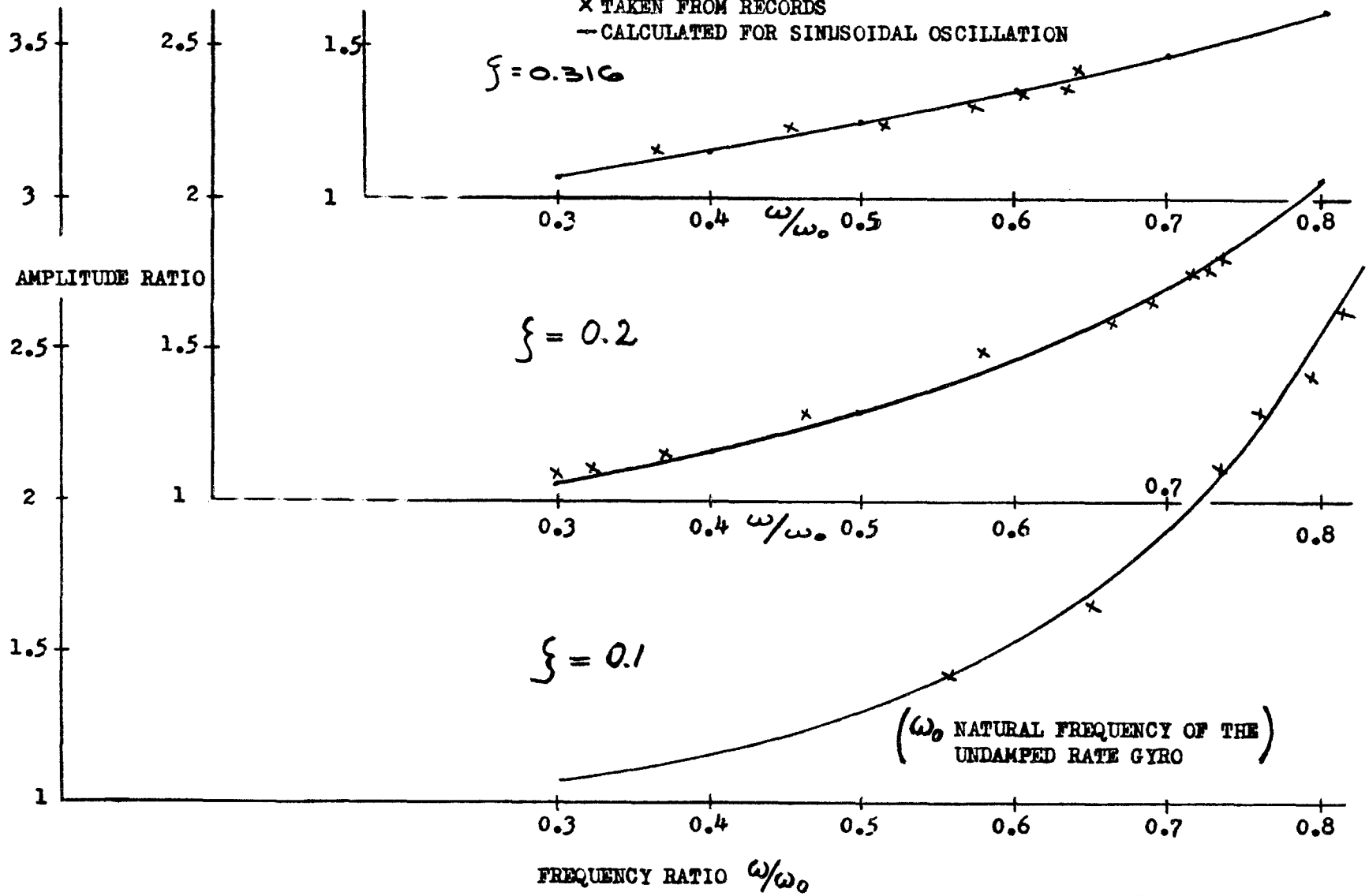

Fig. 6.3.5

FEATHERING SYSTEM
TRUE ANGULAR POSITION VERSUS DAMPING RATIO

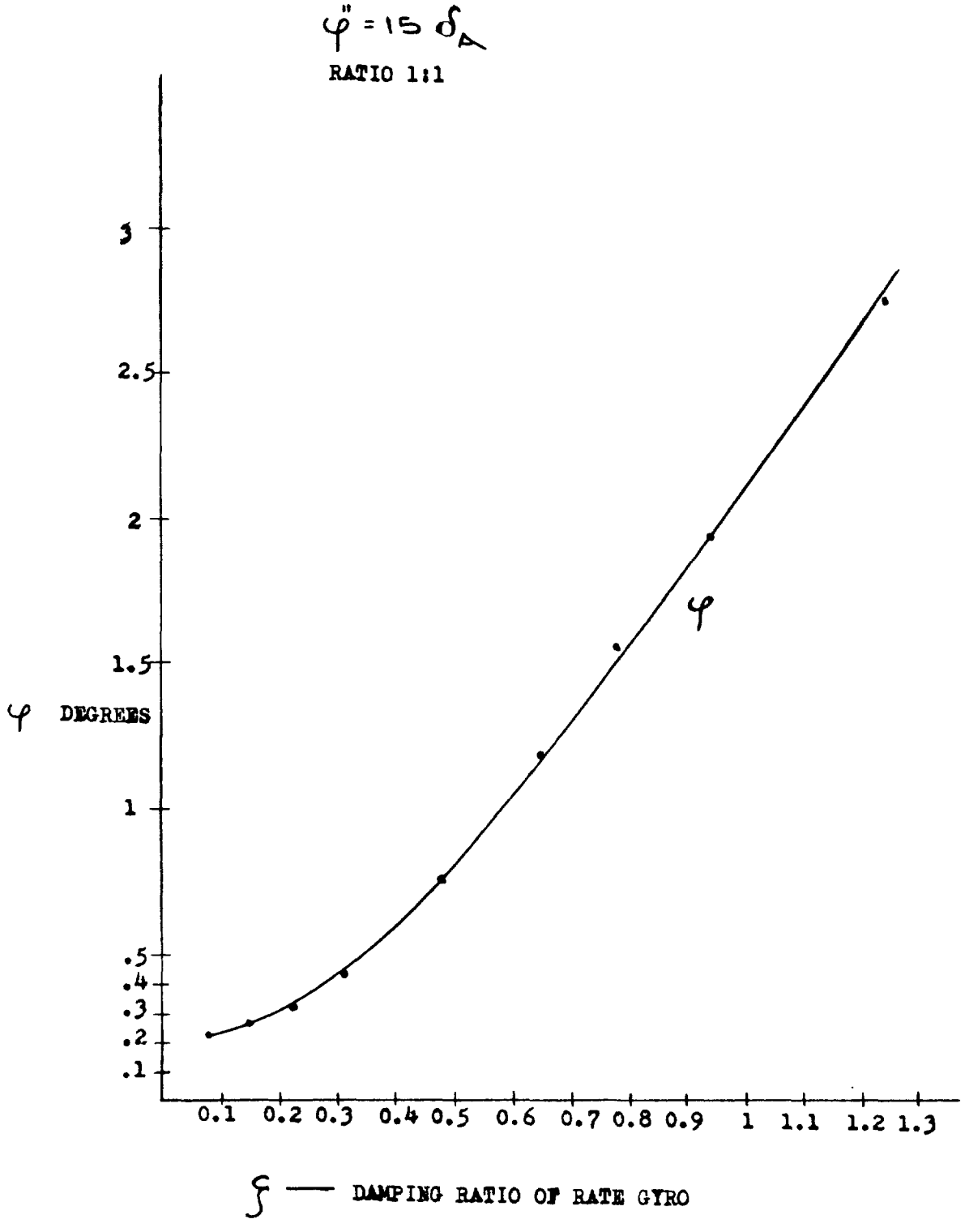

FEATHERING SYSTEM

TRUE ($\dot{\varphi}$) AND INDICATED ($\dot{\varphi}^*$) ANGULAR VELOCITY VERSUS DAMPING RATIO

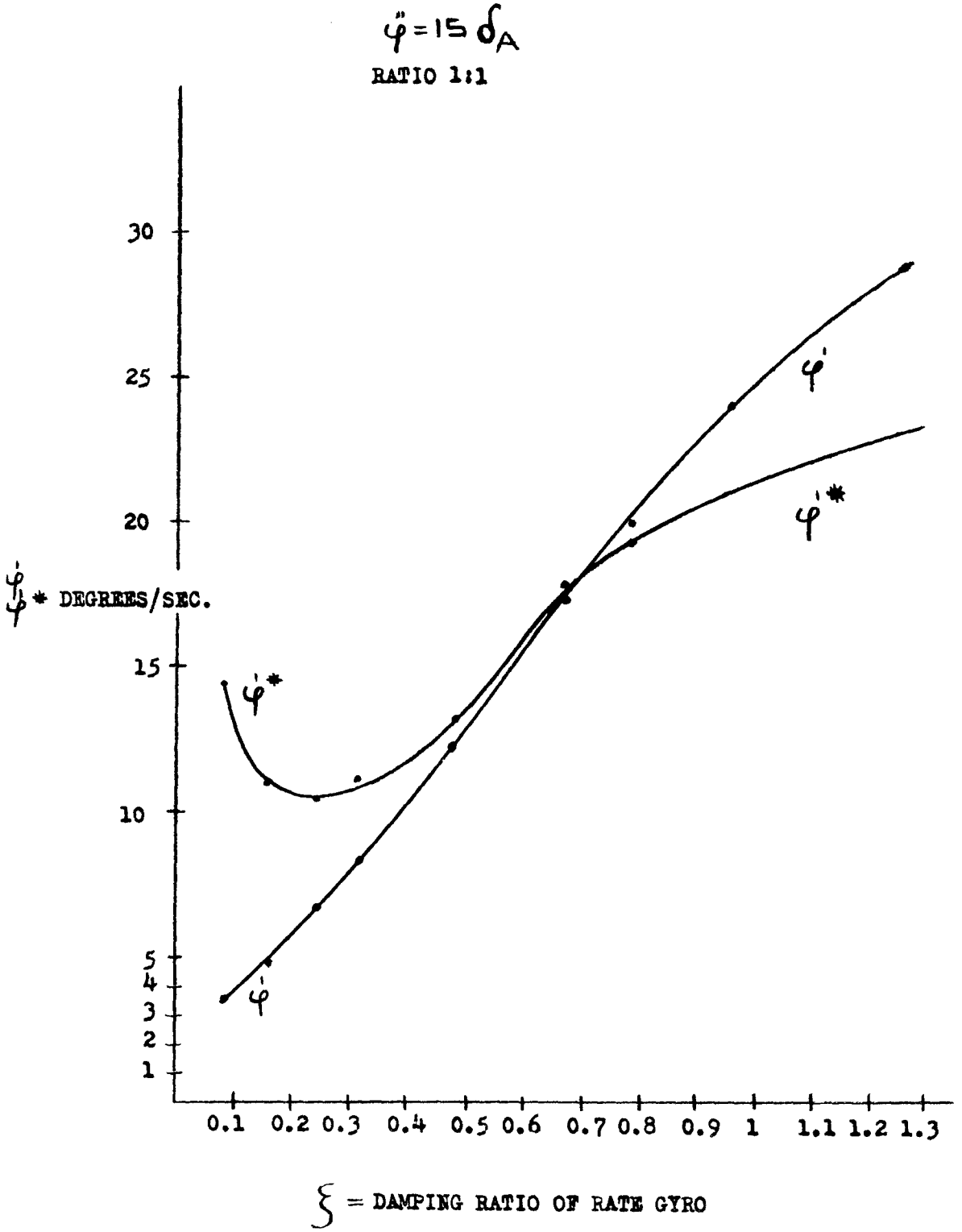

FEATHERING SYSTEM
FREQUENCY VERSUS DAMPING RATIO

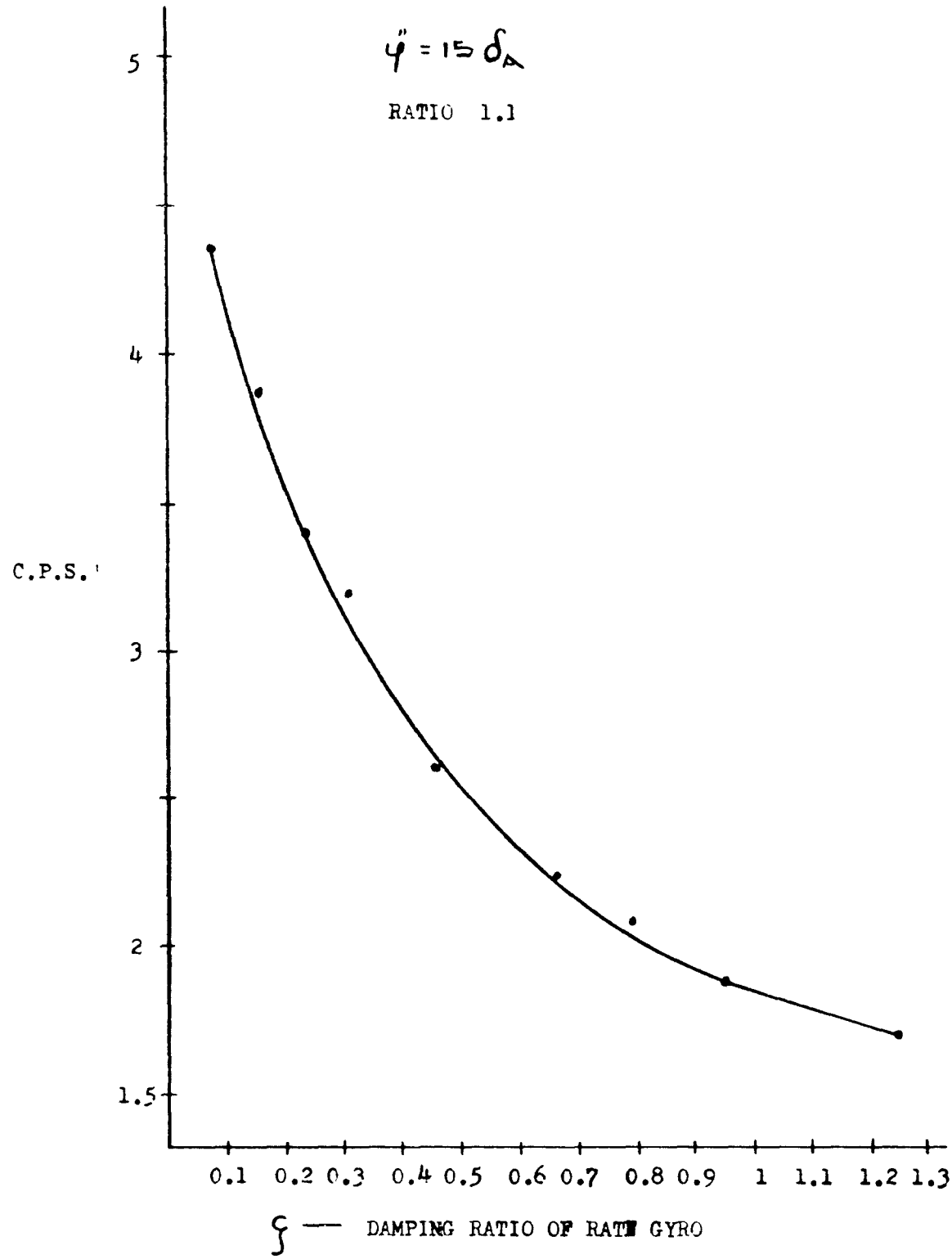

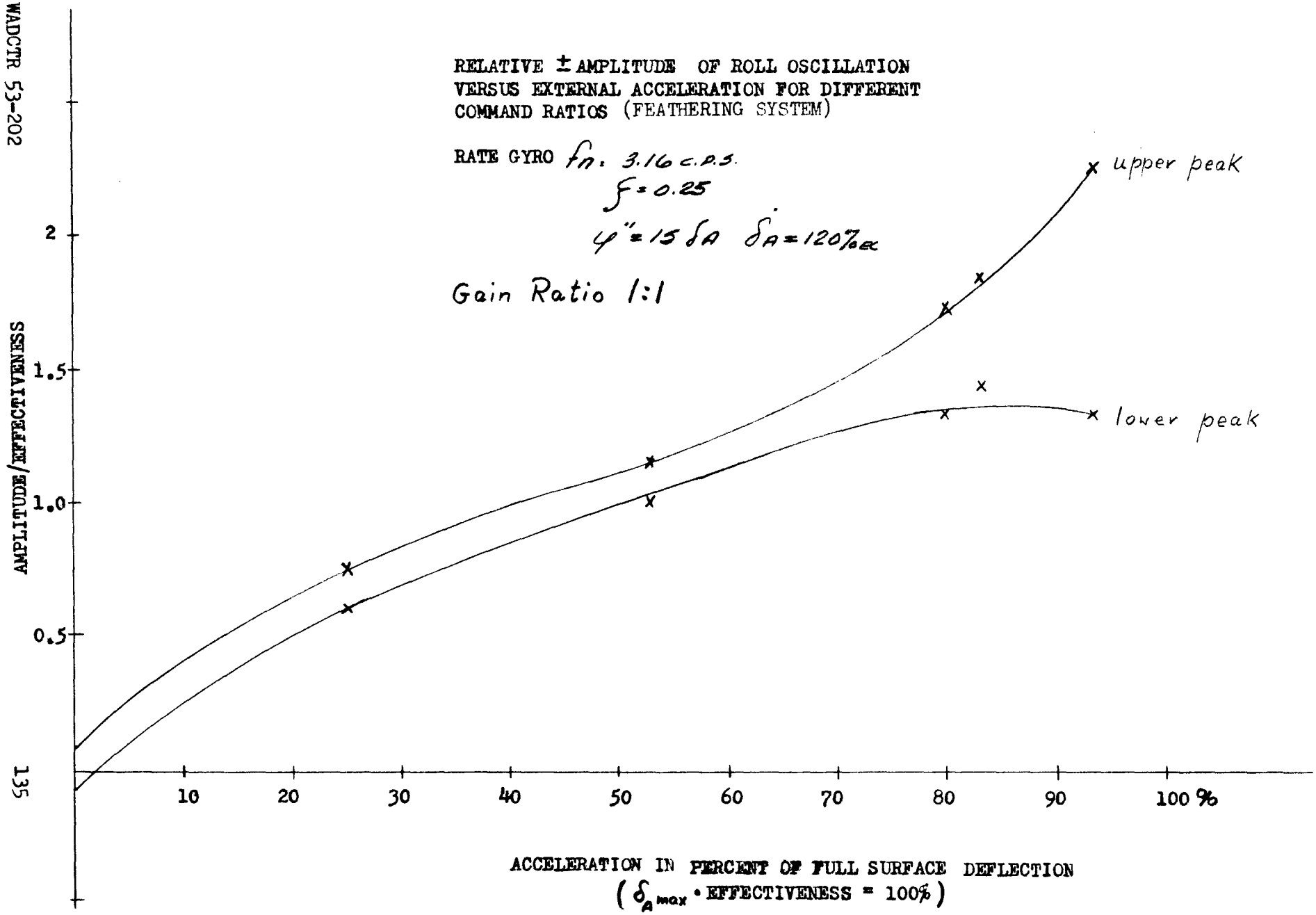
RELATIVE ± AMPLITUDE OF ROLL OSCILLATION VERSUS EXTERNAL ACCELERATION FOR DIFFERENT COMMAND RATIOS (FEATHERING SYSTEM)
RATE GYRO fn. 3.16 c.p.s.
ζ = 0.25
φ'' = 15 δA δA = 120°/sec
Gain Ratio 1:1
upper peak
lower peak
AMPLITUDE/EFFECTIVENESS
2
1.5
1.0
0.5
135
10
20
30
40
50
60
70
80
90
100 %
ACCELERATION IN PERCENT OF FULL SURFACE DEFLECTION
(δA max • EFFECTIVENESS = 100%)

FIG. C.3.7.1

RELATIVE ± AMPLITUDE OF ROLL OSCILLATION
VERSUS EXTERNAL ACCELERATION FOR DIFFERENT
COMMAND RATIOS (FEATHERING SYSTEM)

RATE GYRO f_n = 3.16 c.p.s
$\zeta = 0.25$
$\varphi'' = 15\,\delta_A$ $\delta_A' = 120°/sec$
Gain Ratio 1:2

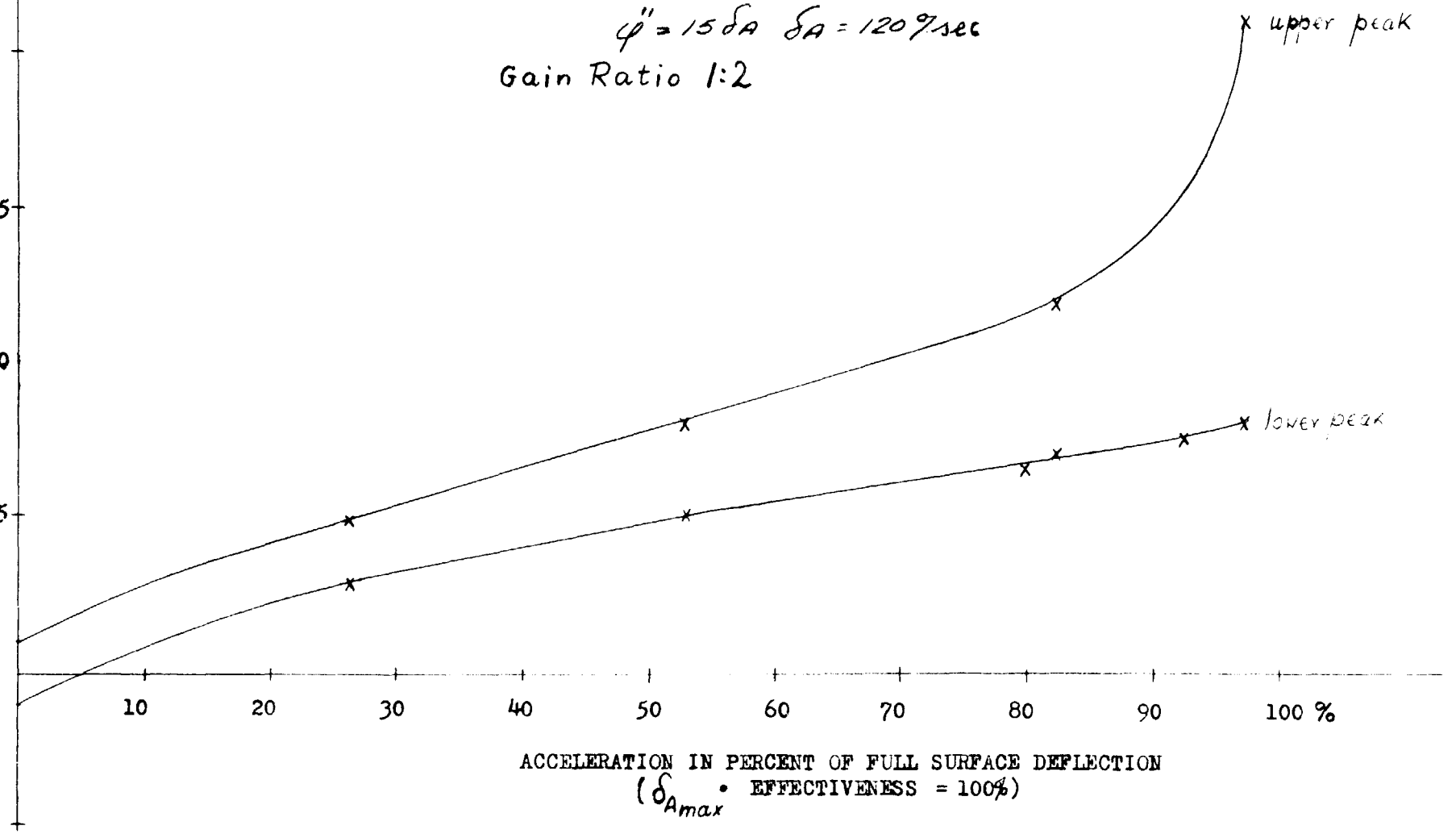

AMPLITUDE/EFFECTIVENESS

ACCELERATION IN PERCENT OF FULL SURFACE DEFLECTION
($\delta_{A\,max}$ • EFFECTIVENESS = 100%)

FIG. 6.3.7.2

RELATIVE ± AMPLITUDE OF ROLL OSCILLATION VERSUS EXTERNAL ACCELERATION FOR DIFFERENT COMMAND RATIOS (FEATHERING SYSTEM)

RATE GURO $f_n = 3.16$ cps

$\zeta = 0.25$

$4'' = 15\delta_A$ $\dot{\delta}_A = 120°/sec$

GAIN RATION 1:4

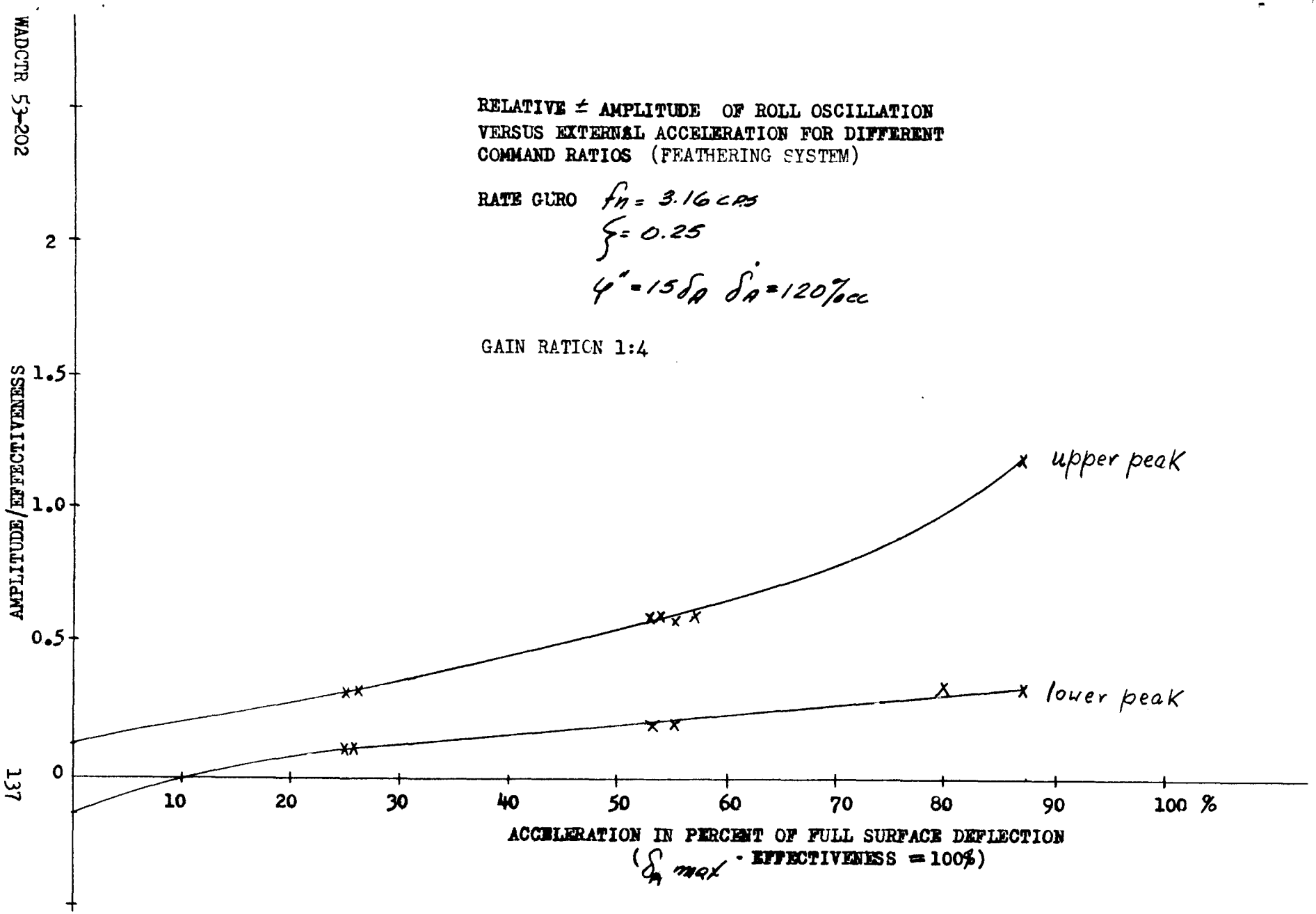

FIG. 6.3.7.3

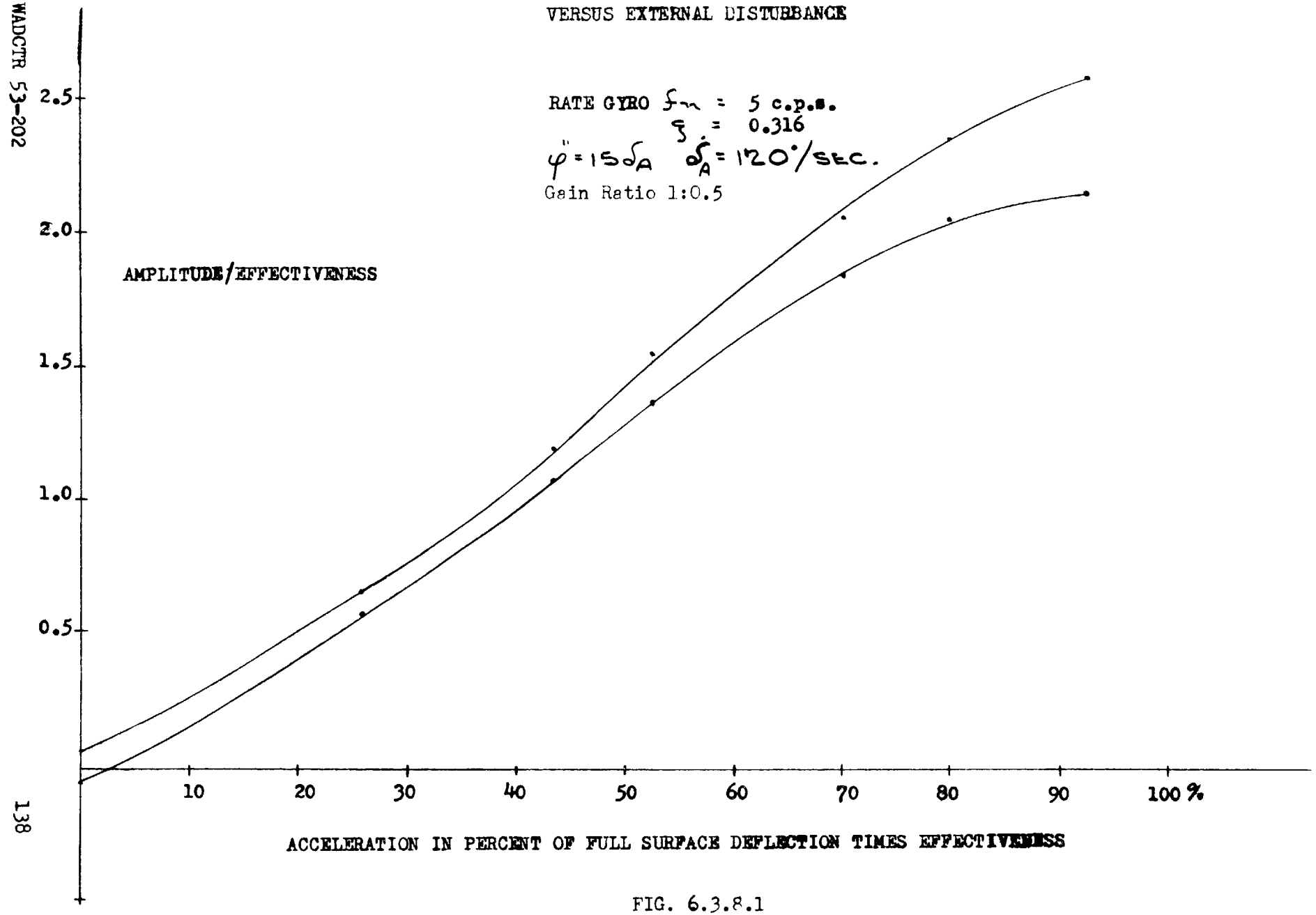
RELATIVE ± AMPLITUDE OF ROLL OSCILLATION
VERSUS EXTERNAL DISTURBANCE
RATE GYRO f_n = 5 c.p.s.
ζ = 0.316
$\ddot{\varphi} = 15\delta_A$ $\dot{\delta}_A = 120°/sec.$
Gain Ratio 1:0.5
AMPLITUDE/EFFECTIVENESS
2.5
2.0
1.5
1.0
0.5
10
20
30
40
50
60
70
80
90
100 %
ACCELERATION IN PERCENT OF FULL SURFACE DEFLECTION TIMES EFFECTIVENESS

FIG. 6.3.8.1

RELATIVE ±AMPLITUDE OF ROLL OSCILLATION
VERSUS EXTERNAL DISTURBANCE

RATE GYRO f_n = 5 c.p.s.
ζ = 0.316

$\ddot{\varphi} = 15\,\delta_A$ $\delta_A = 120°/\text{SEC.}$
Gain Ratio 1:1

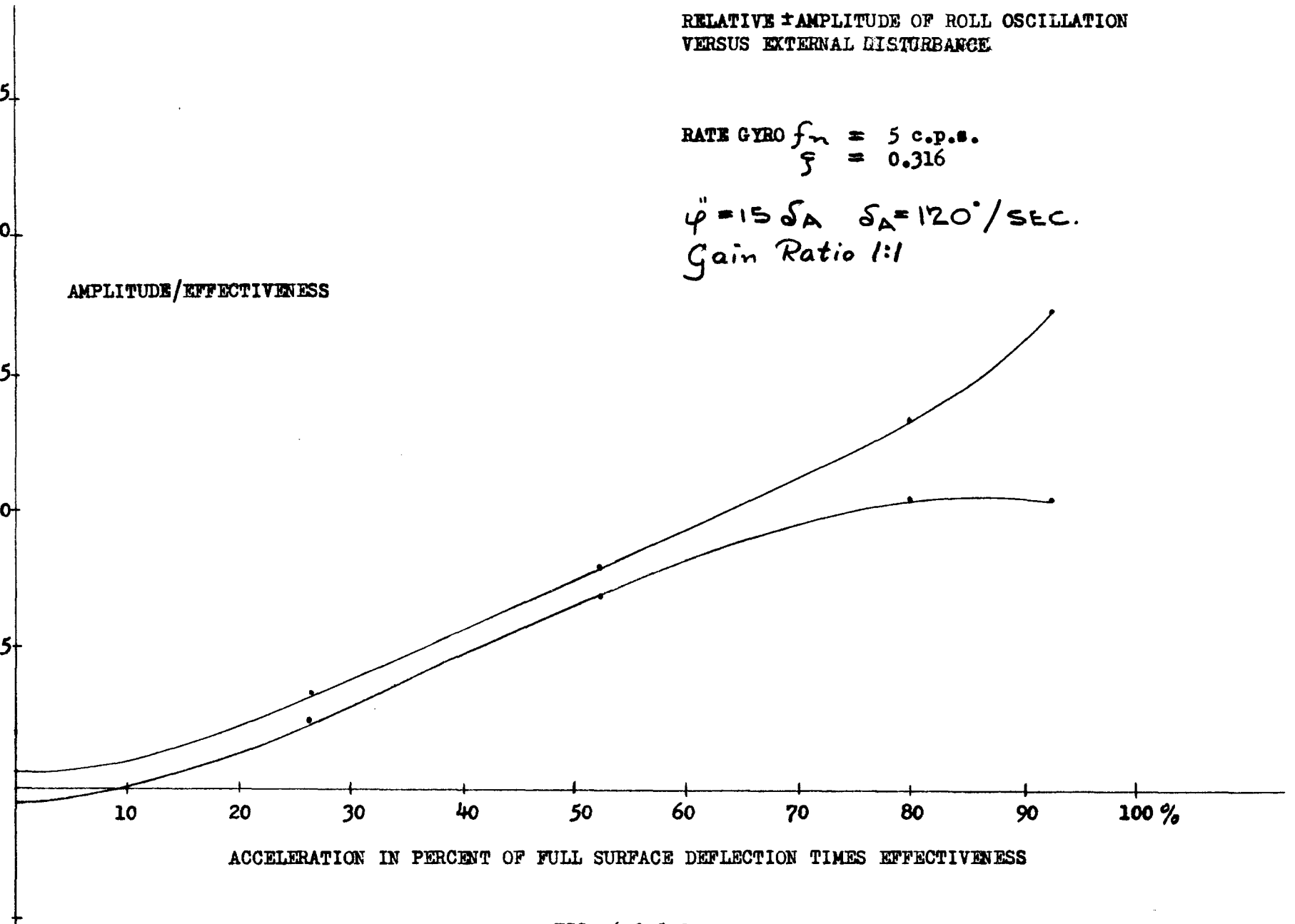

FIG. 6.3.8.2

RELATIVE ± AMPLITUDE OF ROLL OSCILLATION
VERSUS EXTERNAL DISTURBANCE

RATE GYRO f_n = 5 c.p.s.
ζ = 0.316

$\ddot{\varphi} = 15\,\delta_A$ $\dot{\delta}_A = 120°/sec.$

Gain Ratio 1:2

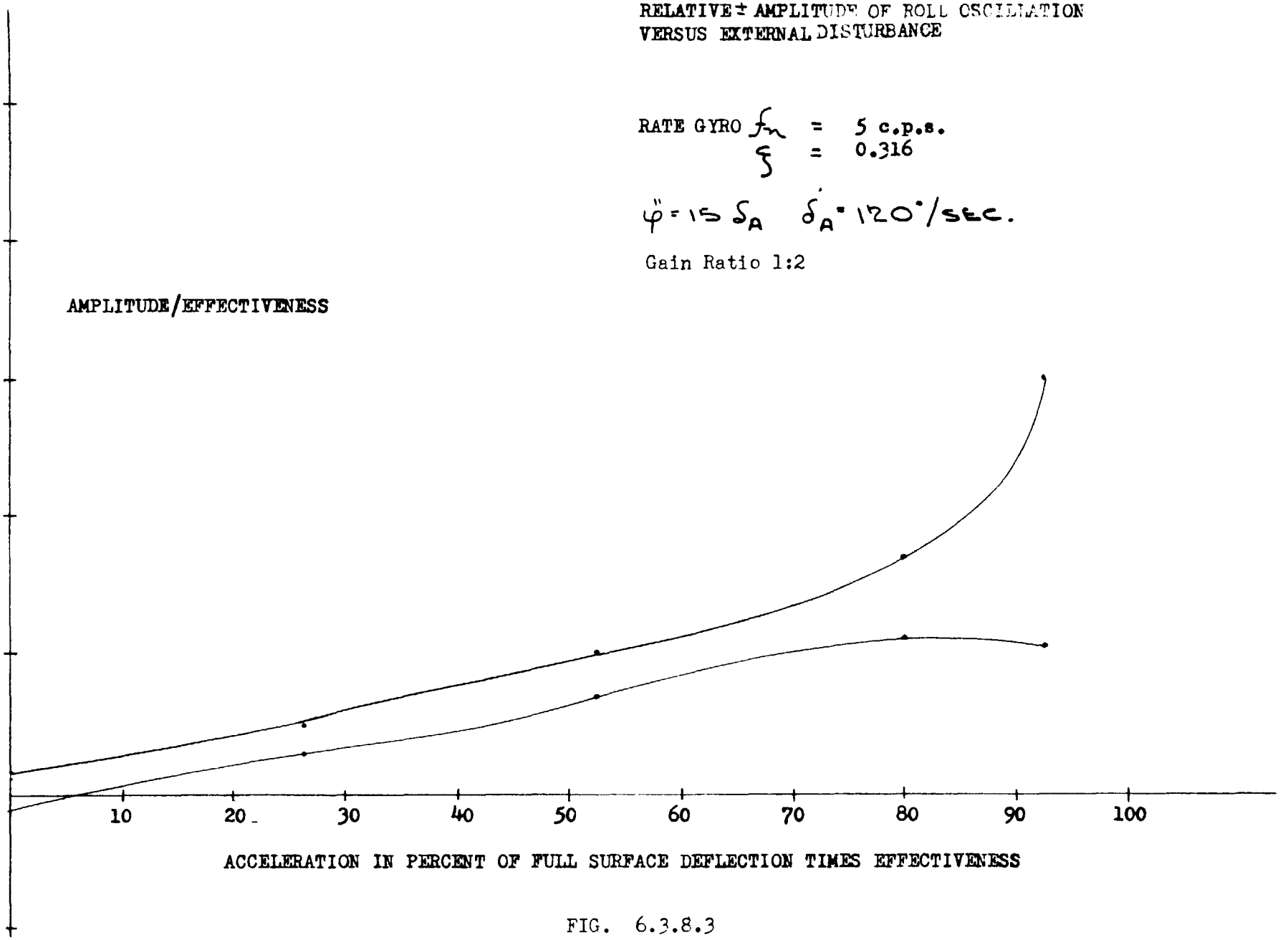

FIG. 6.3.8.3

FEATHERING SYSTEM

RELATIVE AMPLITUDE OF ROLL OSCILLATION
VERSUS EXTERNAL DISTURBANCE

RATE GYRO f_n = 5 c.p.s.
ζ = 0.316

$\ddot{\varphi} = 15\,\delta_A$ $\dot{\delta}_A = 120°/SEC.$

Gain Ratio 1:4

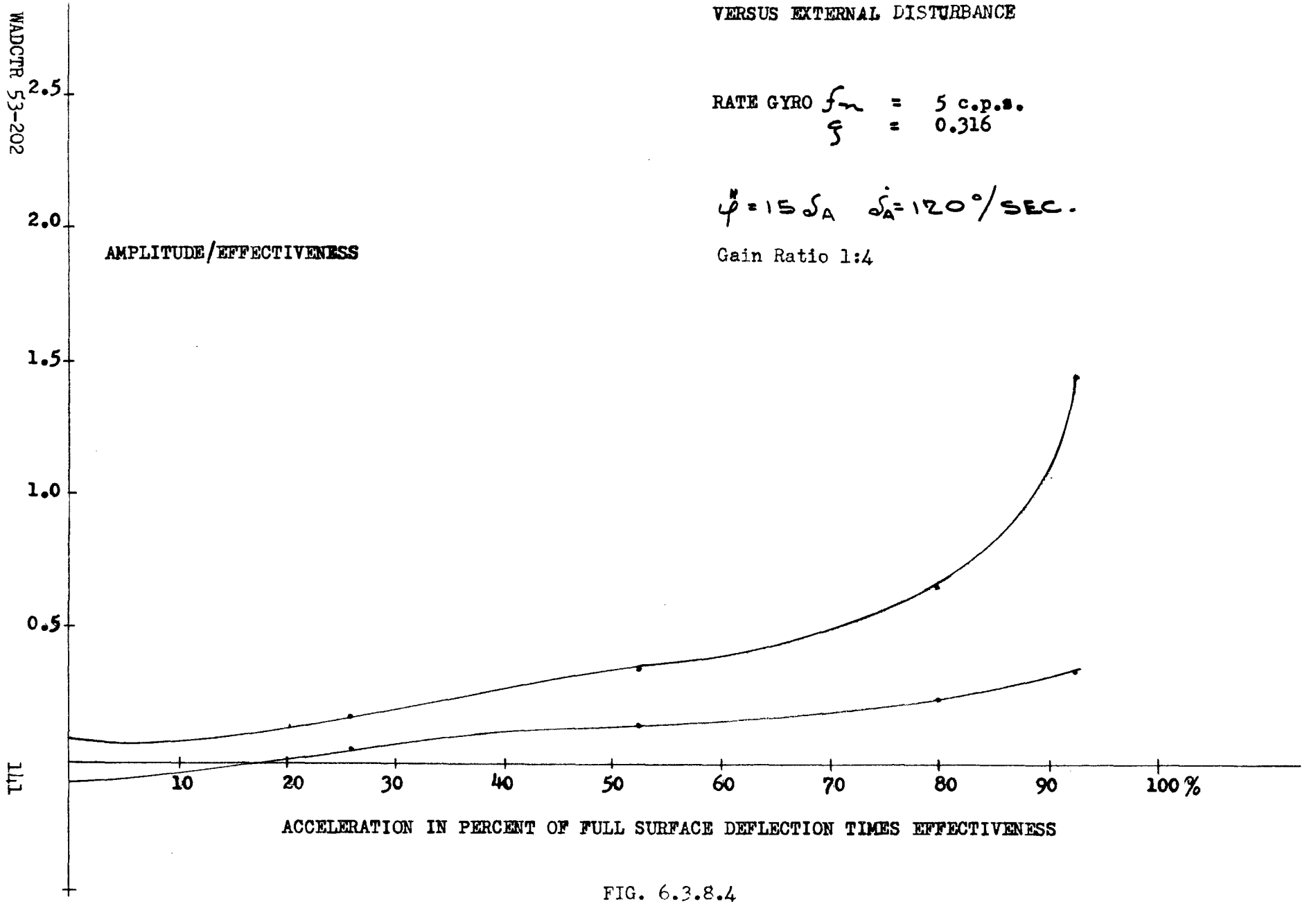

FIG. 6.3.8.4

FEATHERING SYSTEM

RELATIVE † AMPLITUDE OF ROLL OSCILLATION
VERSUS EXTERNAL DISTURBANCE

FEATHERING SYSTEM

RATE GYRO f_n = 5 c.p.s.
ζ = 0.316

$\ddot{\varphi} = 15\,\delta_A$ $\dot{\delta}_A = 120°/SEC.$

Gain Ratio 1:8

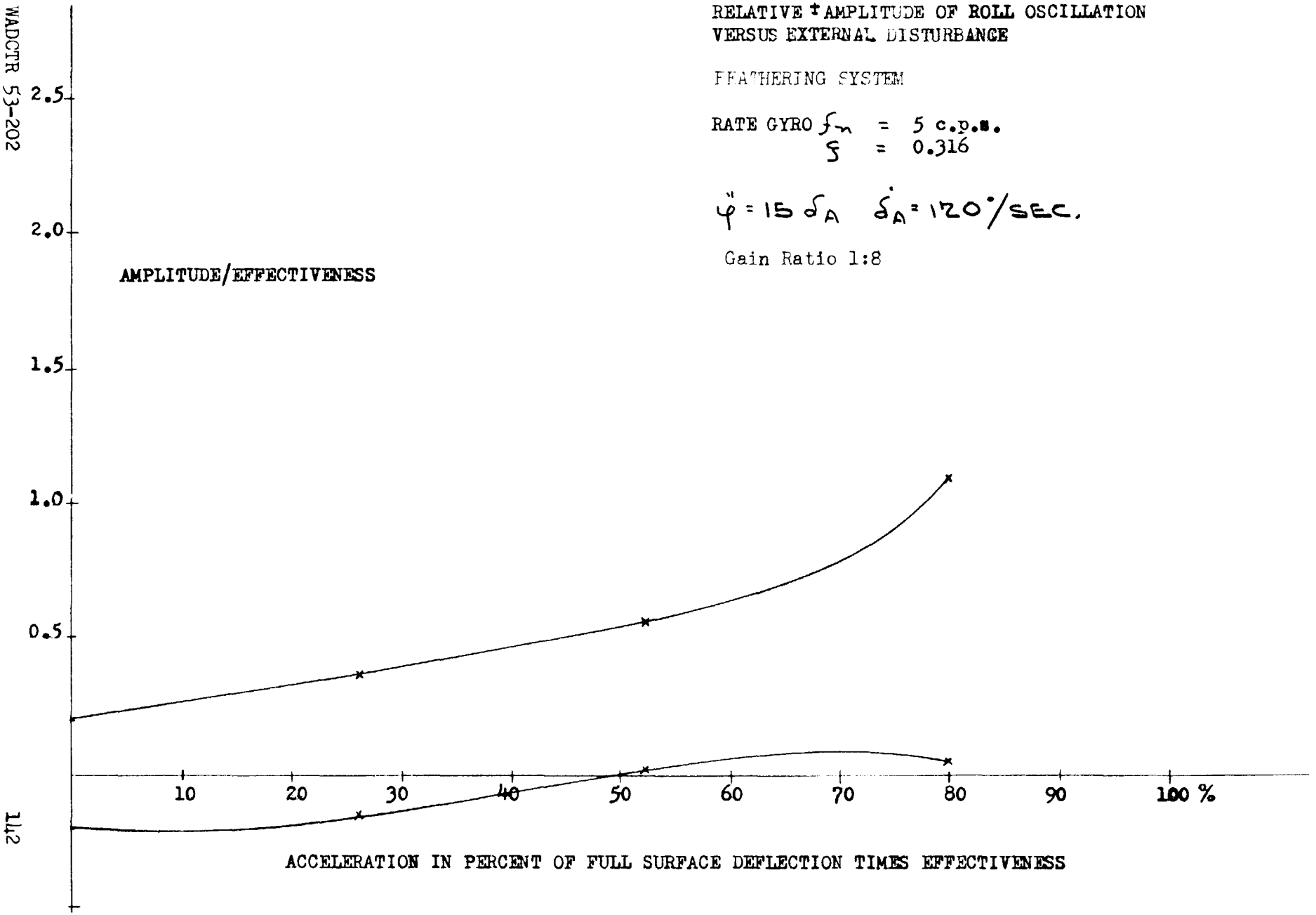

FIG. 6.3.8.5

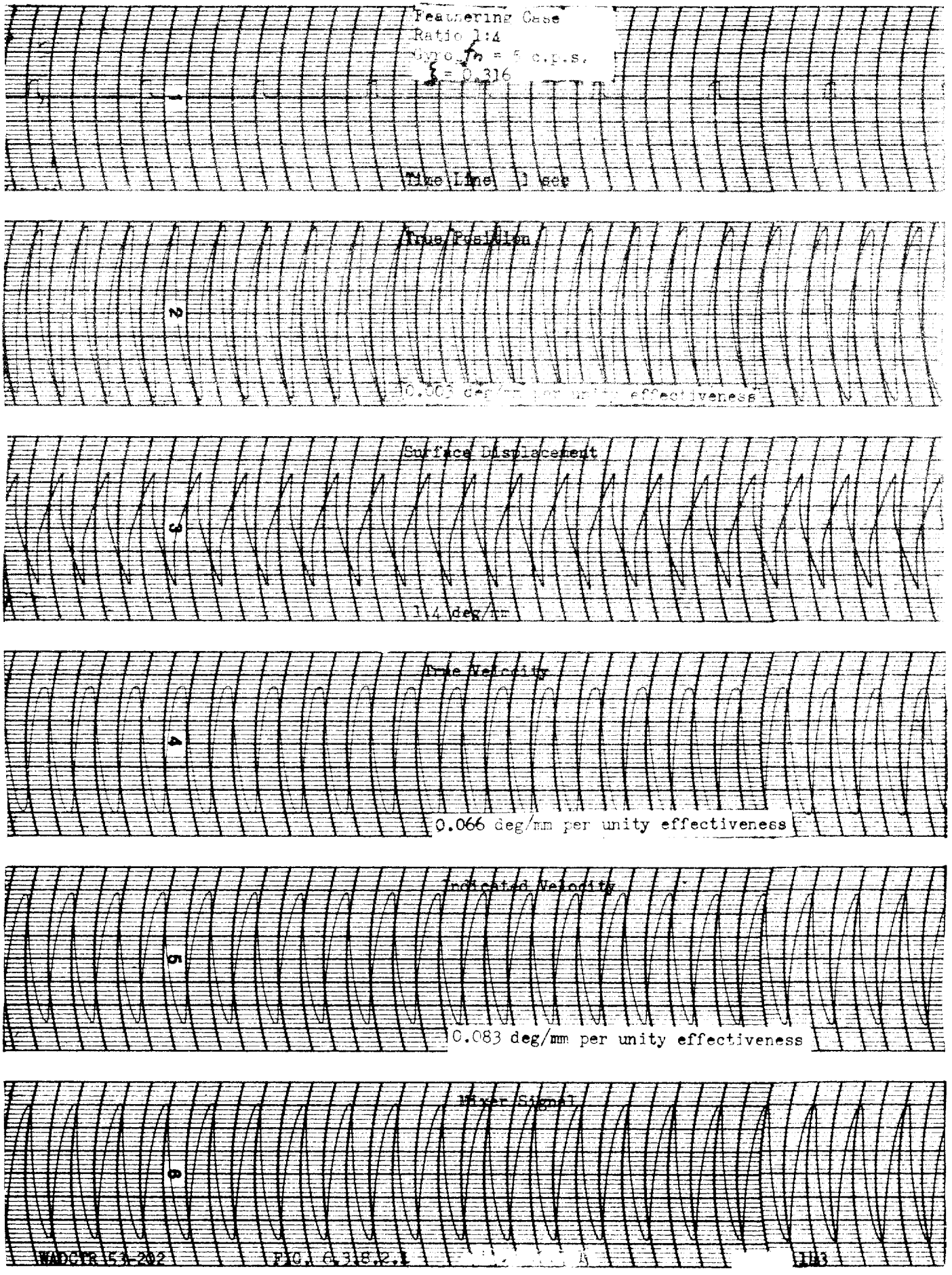
Feathering Case
Ratio 1:4
Gyro f_n = 5 c.p.s.
ζ = 0.316
1
Time Line 1 sec
2
True Position
0.303 deg/mm per unity effectiveness
3
Surface Displacement
1.4 deg/in
4
True Velocity
0.066 deg/mm per unity effectiveness
5
Indicated Velocity
0.083 deg/mm per unity effectiveness
6
Mixer Signal

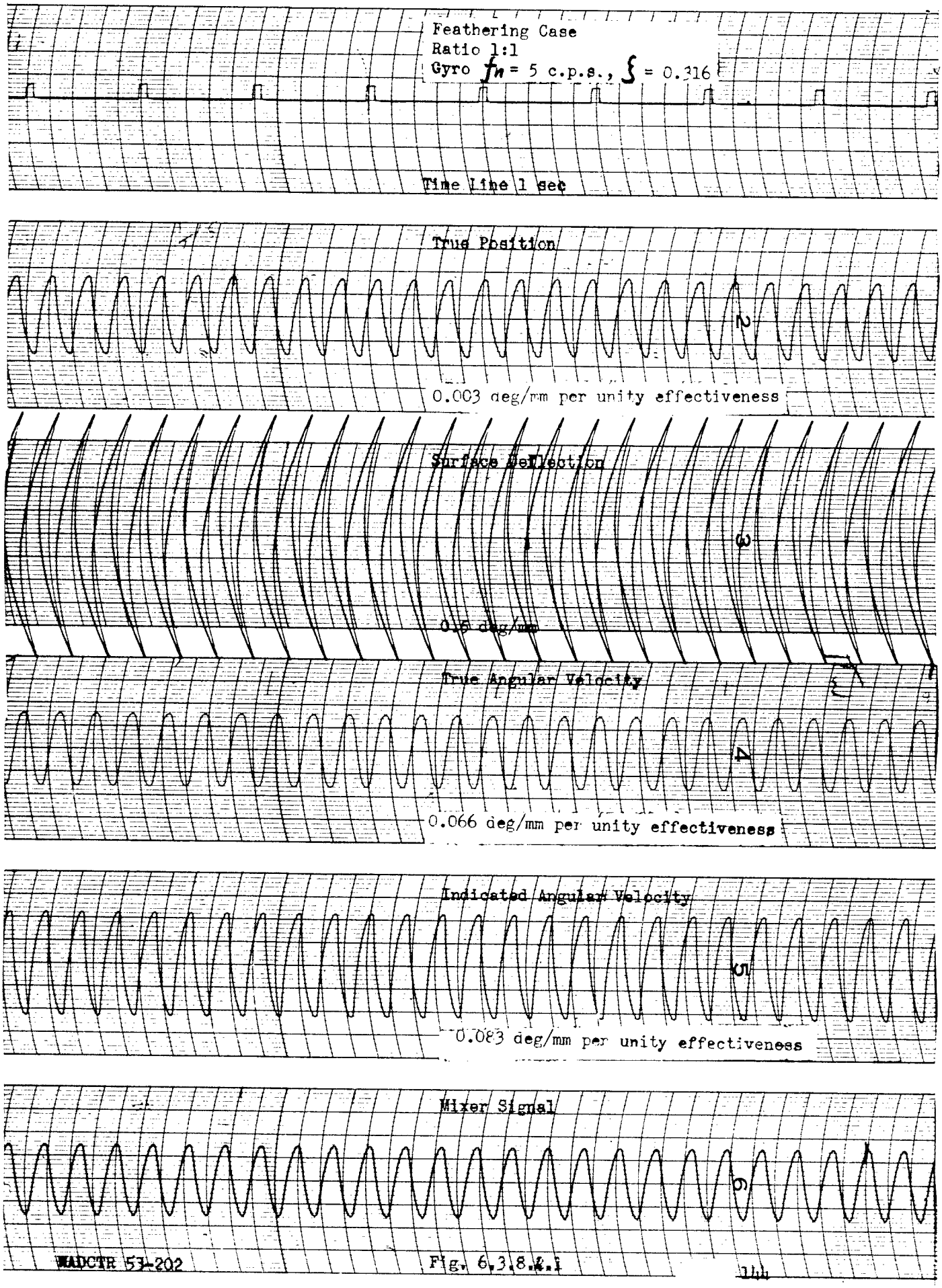
Feathering Case
Ratio 1:1
Gyro f_n = 5 c.p.s., ζ = 0.316
Time line 1 sec
True Position
2
0.003 deg/mm per unity effectiveness
Surface Deflection
3
0.6 deg/mm
True Angular Velocity
4
0.066 deg/mm per unity effectiveness
Indicated Angular Velocity
5
0.083 deg/mm per unity effectiveness
Mixer Signal
6

RELATIVE ± AMPLITUDE OF ROLL OSCILLATION VERSUS EXTERNAL DISTURBANCE. TIME DELAY IN INTEGRATING MOTOR T=100m-sec.

RATE GYRO $f_n = 5$ c.p.s.

$\zeta = 0.316$

$\varphi'' = 15\delta_A$ $\delta_A = 120°/\text{sec}$

Gain Ratio 1:1

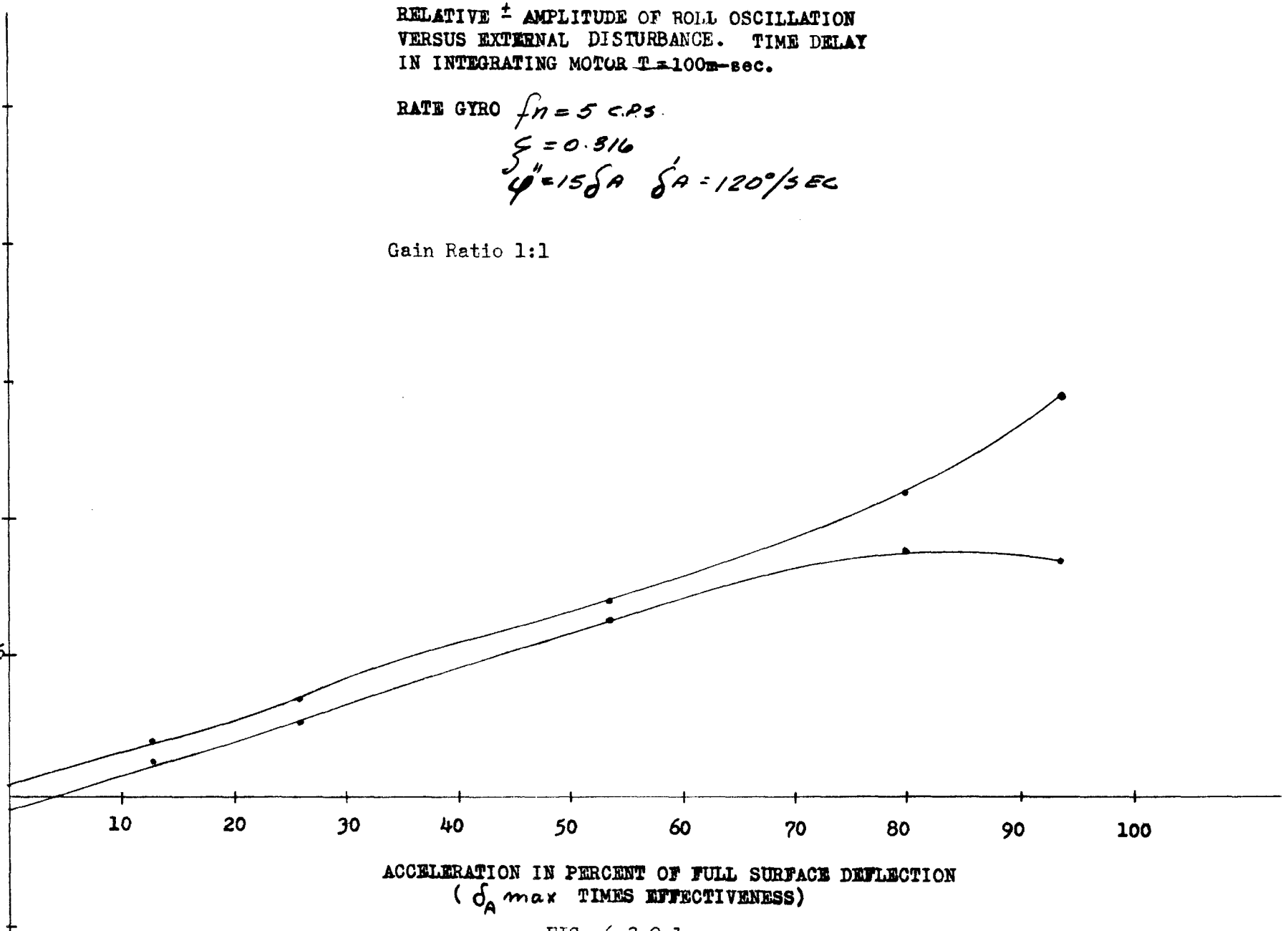

FIG. 6.3.9.1

RELATIVE ± AMPLITUDE OF ROLL OSCILLATION VERSUS EXTERNAL DISTURBANCE. TIME DELAY IN INTEGRATING MOTOR T = 100m-sec.

RATE GYRO f_n = 5 cps.

$\zeta = 0.316$

$\ddot{\varphi} = 15 \delta_A$ $\dot{\delta}_A = 120°/sec.$

Gain Ratio 1:2

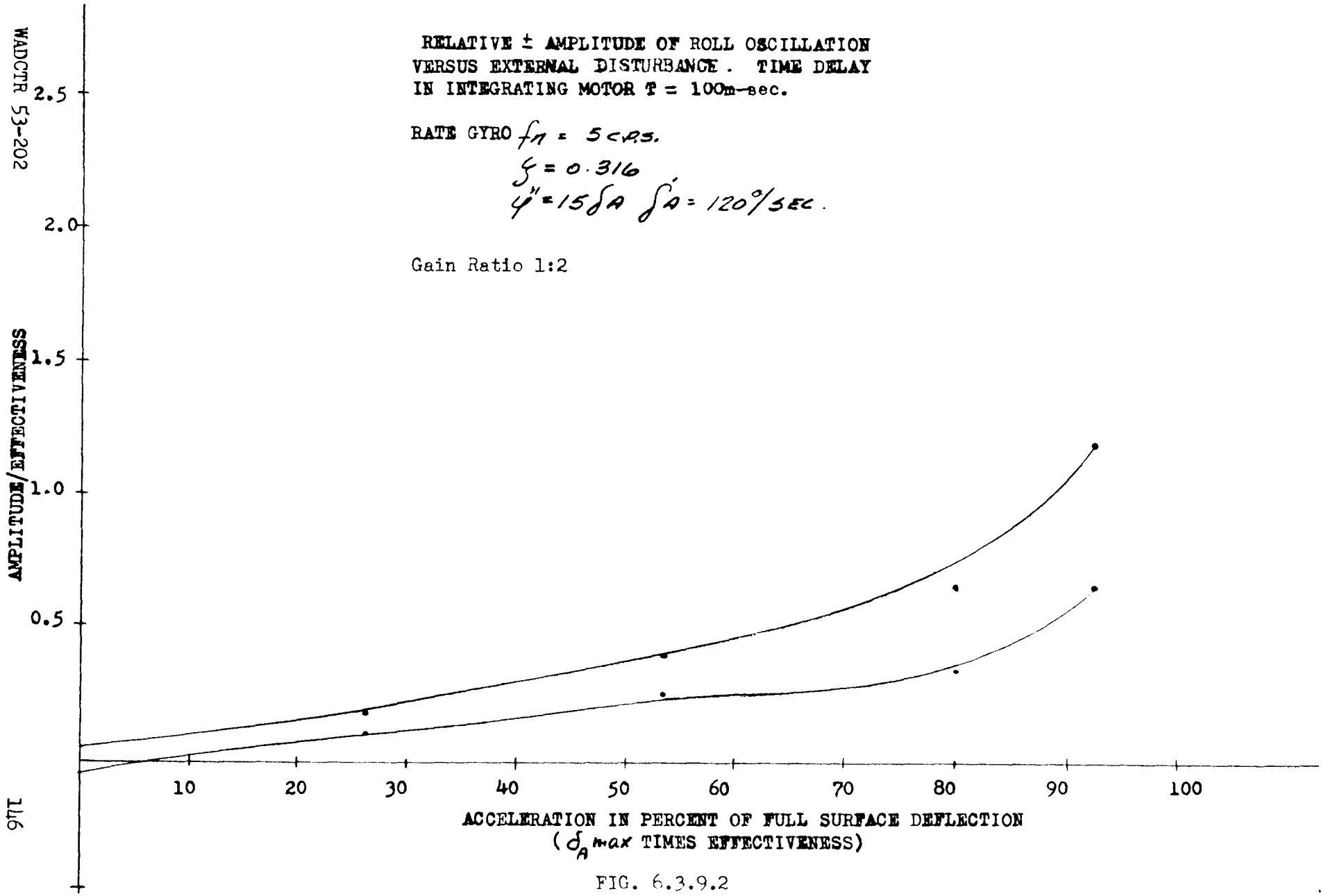

FIG. 6.3.9.2

RELATIVE ± AMPLITUDE OF ROLL OSCILLATION
VERSUS EXTERNAL DISTURBANCE. TIME
DELAY IN INTEGRATING MOTOR T=100 m.sec

RATE GYRO f_n = 5 C.P.S.
ζ = 0.316

$\ddot{\varphi} = 15\delta_A$ $\dot{\delta}_A = 120°/sec$

Gain Ratio 1:4

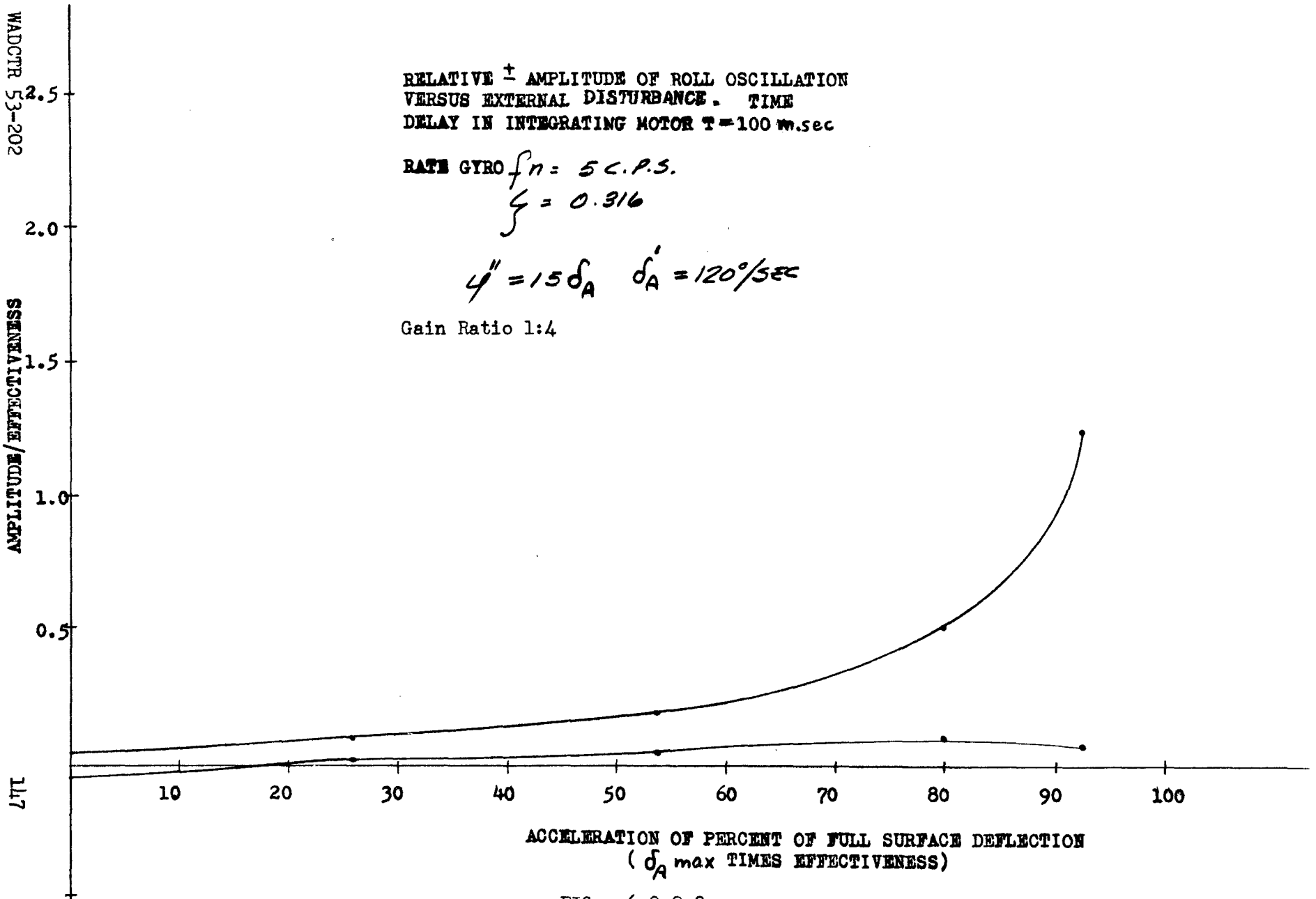

FIG. 6.3.9.3

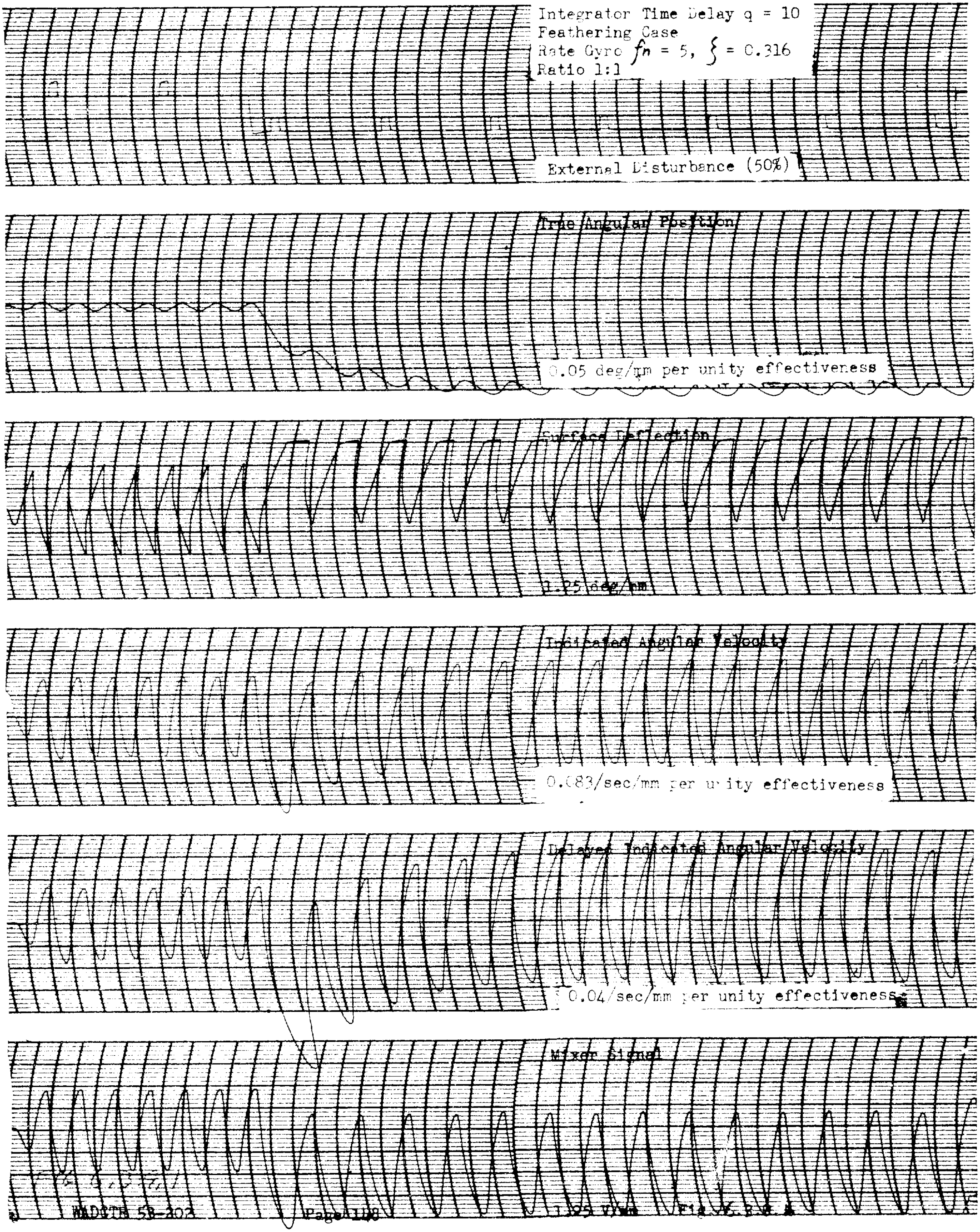
Integrator Time Delay q = 10
Feathering Case
Rate Gyro fn = 5, ζ = 0.316
Ratio 1:1
External Disturbance (50%)
True Angular Position
0.05 deg/mm per unity effectiveness
Surface Deflection
Indicated Angular Velocity
0.083/sec/mm per unity effectiveness
Delayed Indicated Angular Velocity
0.04/sec/mm per unity effectiveness
Mixer Signal

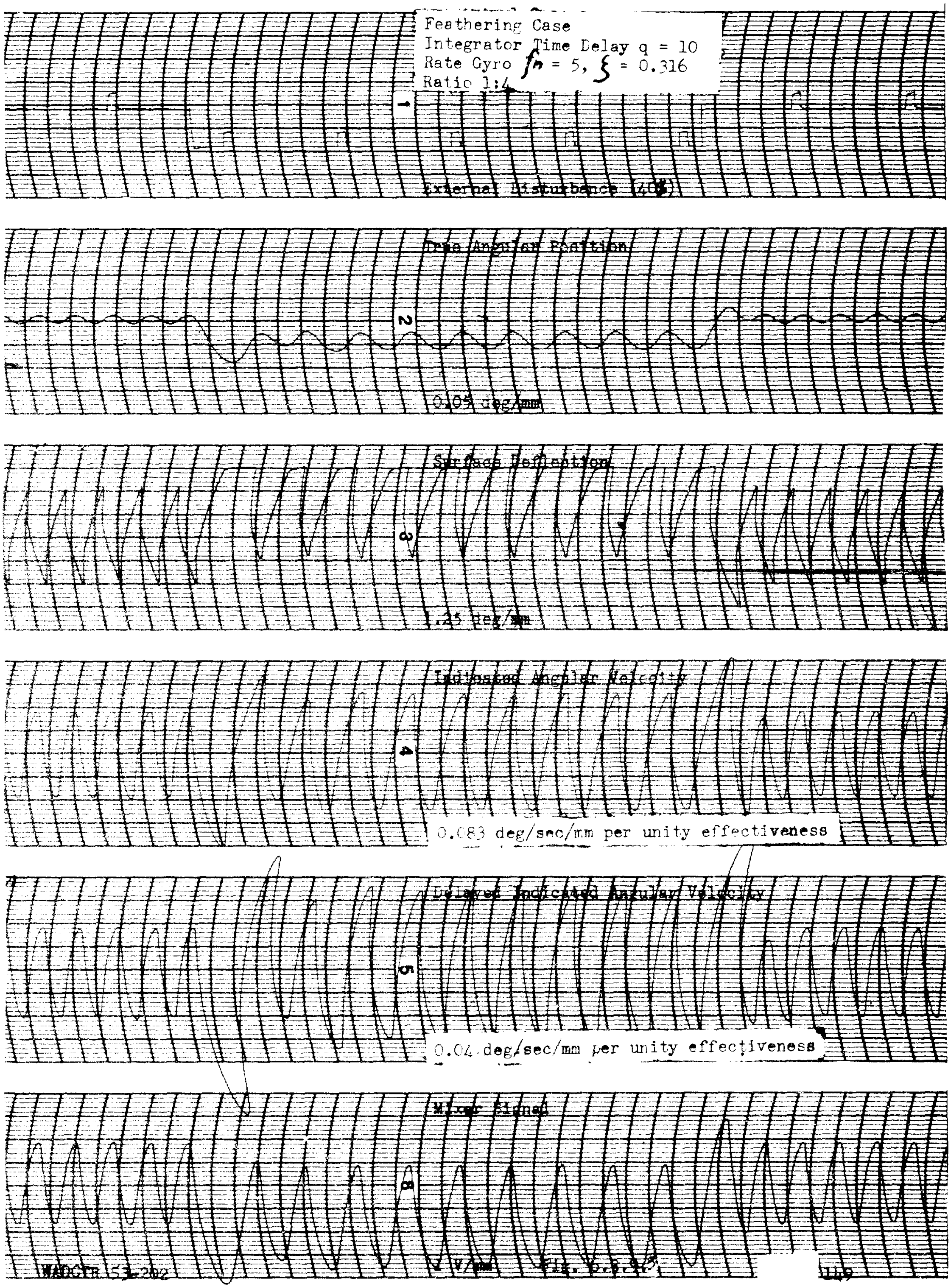
Feathering Case
Integrator Time Delay q = 10
Rate Gyro fn = 5, ζ = 0.316
Ratio 1:4
External Disturbance
True Angular Position
0.05 deg/mm
Surface Deflection
1.25 deg/mm
Indicated Angular Velocity
0.083 deg/sec/mm per unity effectiveness
Delayed Indicated Angular Velocity
0.04 deg/sec/mm per unity effectiveness
Mixer Signal

FEATHERING CASE

± AMPLITUDE OF ROLL OSCILLATION VERSUS EXTERNAL DISTURBANCE

TIME DELAY IN ACTUATOR
T = 0.010 sec

RATE GYRO f_n = 5 c.p.s.
ζ = 0.316

RATIO $\left[\frac{\text{VELOCITY}}{\text{POSITION}}\right]$ = 1:4

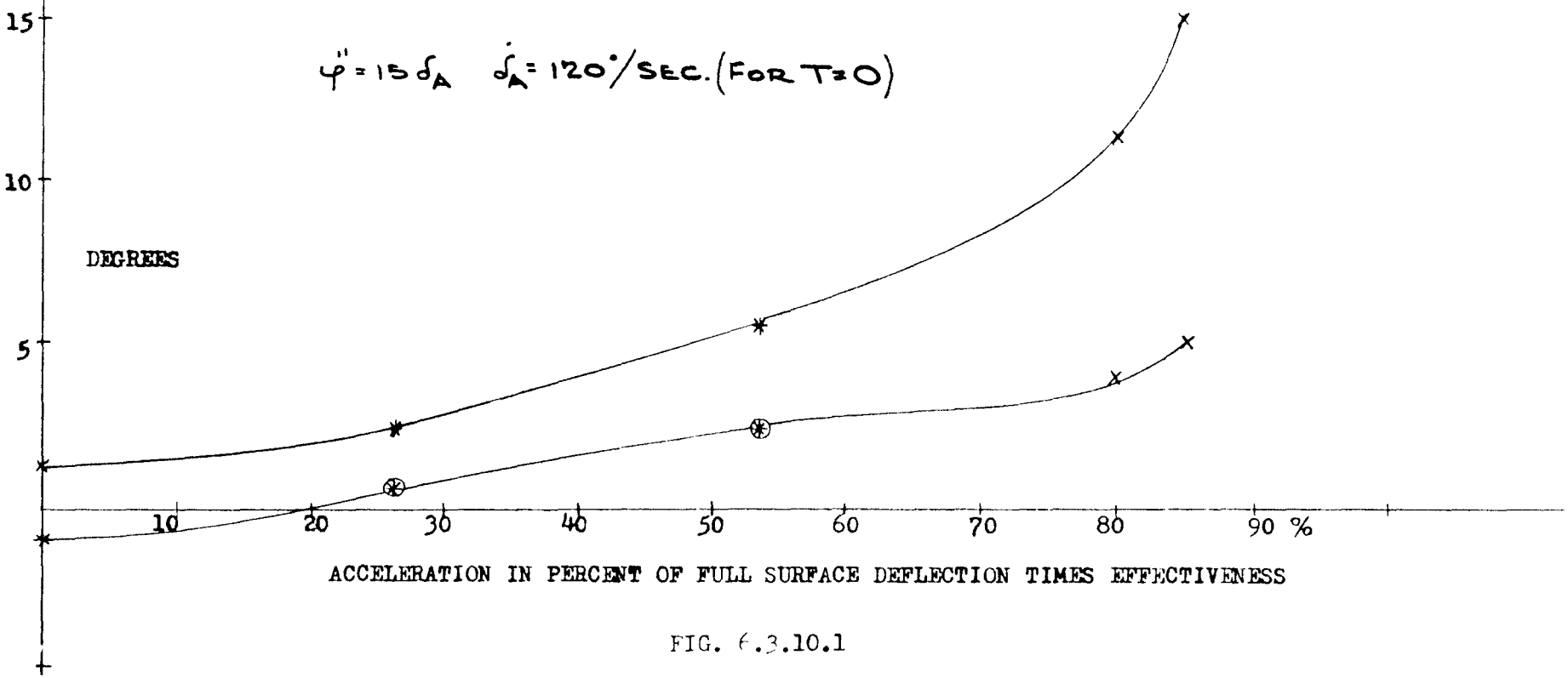

FIG. 6.3.10.1

FEATHERING CASE

± AMPLITUDE OF ROLL OSCILLATION VERSUS EXTERNAL DISTURBANCE

TIME DELAY IN ACTUATOR $T = 0.02$ sec

RATE GYRO $f_n = 5$ c.p.s.
$\zeta = 0.316$

RATIO $\left[\frac{\text{VELOCITY}}{\text{POSITION}}\right] = 1:4$

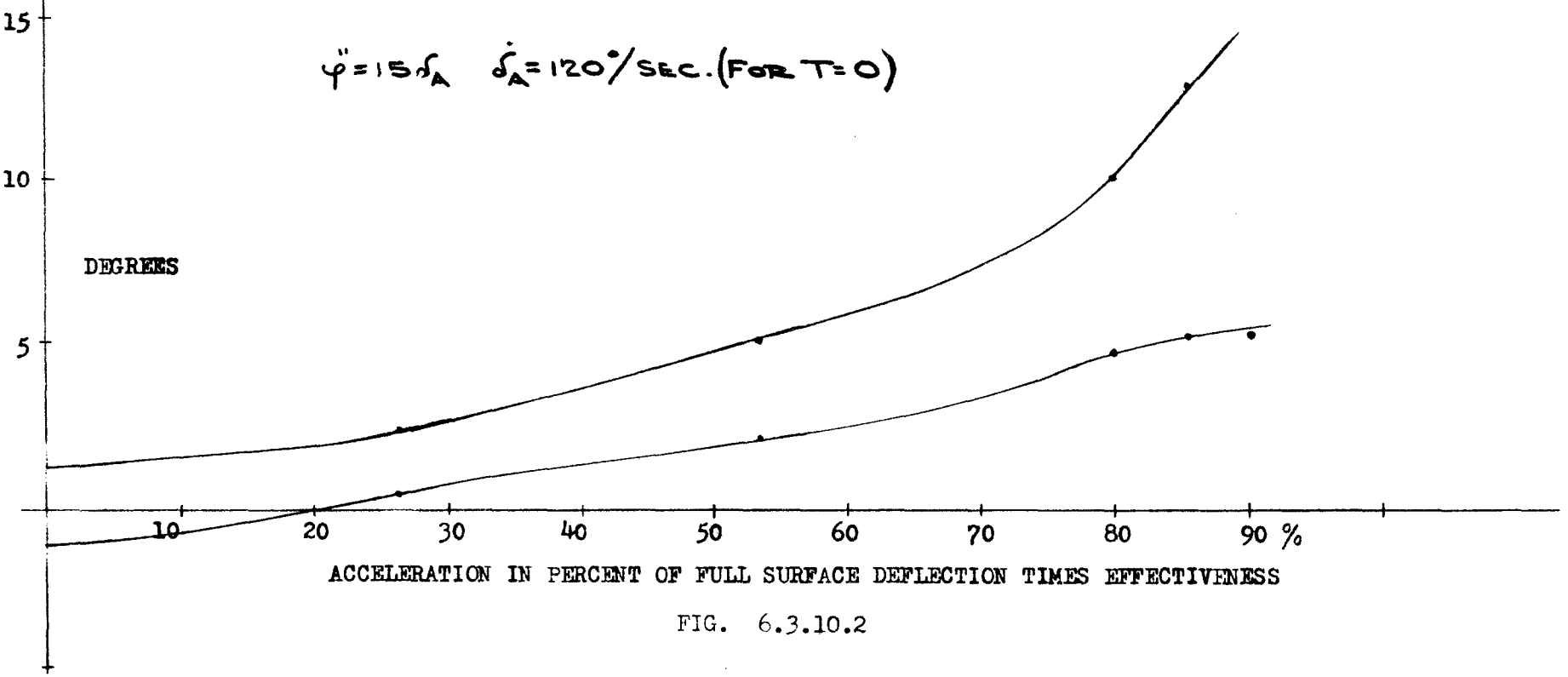

FIG. 6.3.10.2

FEATHERING CASE

±AMPLITUDE OF ROLL OSCILLATION VERSUS EXTERNAL DISTURBANCE

TIME DELAY IN ACTUATOR
T = 0.020 sec.
RATE GYRO f_n = 5 c.p.s.
ζ = 0.316

RATIO $\left[\frac{\text{VELOCITY}}{\text{POSITION}}\right]$ = 1:4

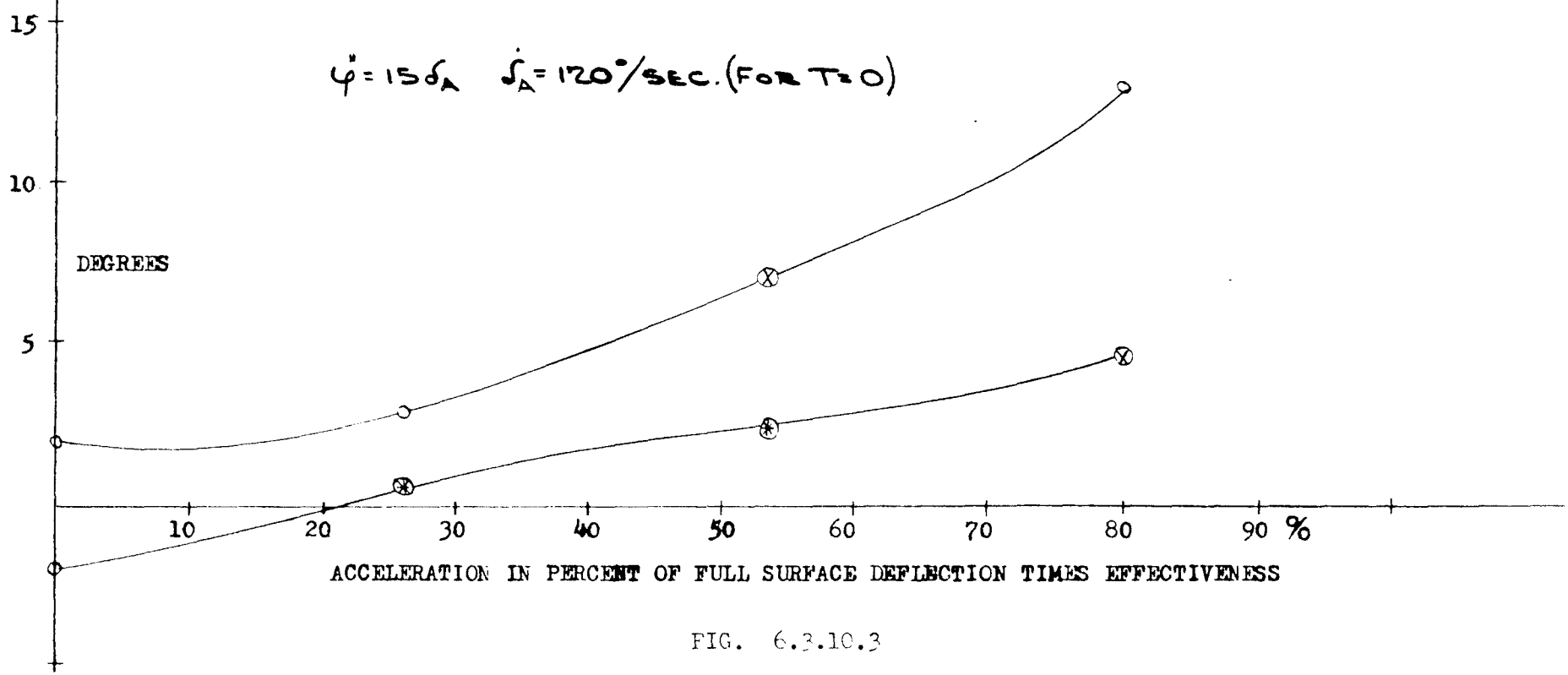

FIG. 6.3.10.3

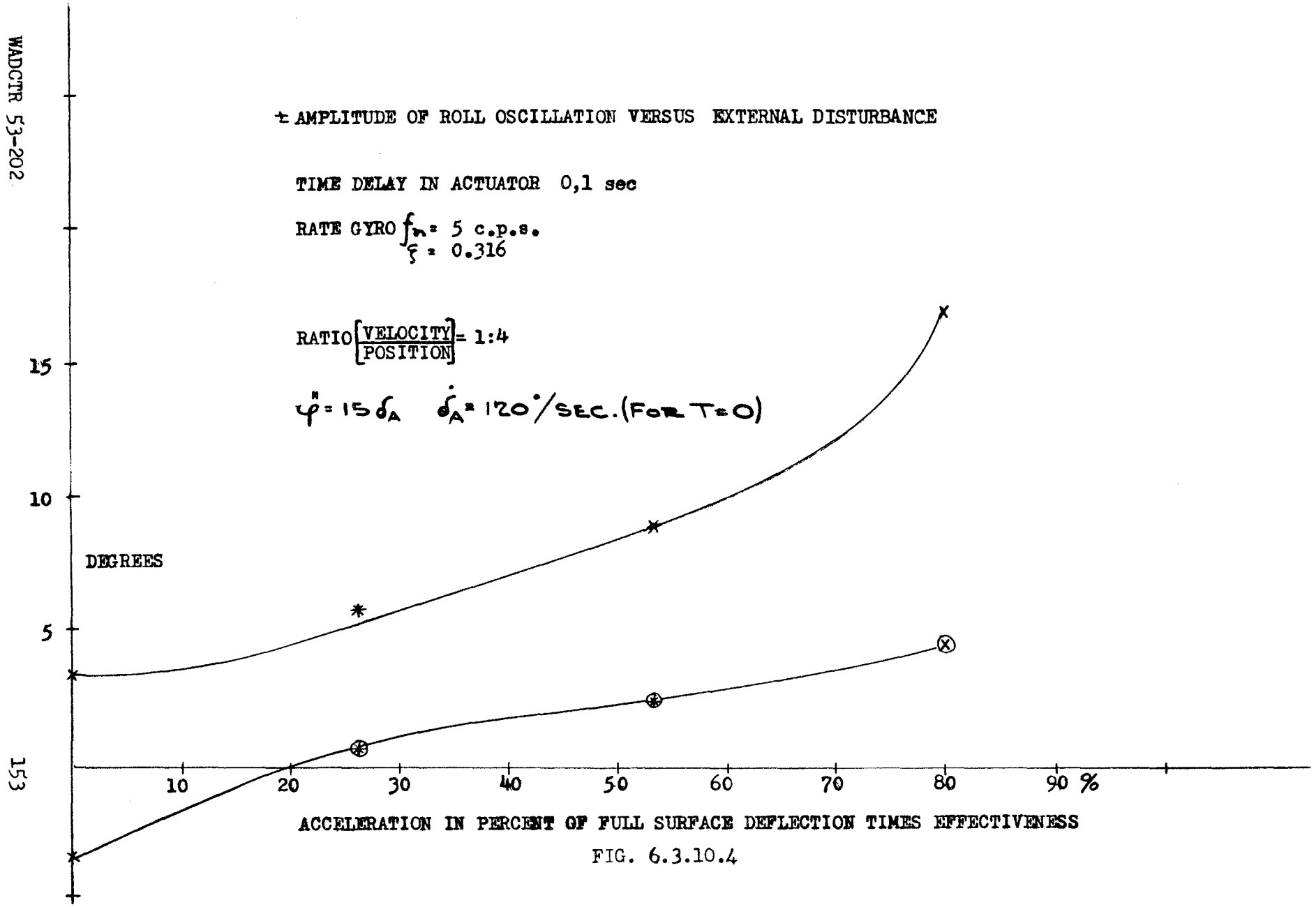
± AMPLITUDE OF ROLL OSCILLATION VERSUS EXTERNAL DISTURBANCE
TIME DELAY IN ACTUATOR 0,1 sec
RATE GYRO f_n = 5 c.p.s.
ζ = 0.316
RATIO [VELOCITY / POSITION] = 1:4
$\ddot{\varphi} = 15\,\delta_A$ $\dot{\delta}_A = 120°/SEC.$ (FOR T=0)
15
10
5
DEGREES
10
20
30
40
50
60
70
80
90 %
ACCELERATION IN PERCENT OF FULL SURFACE DEFLECTION TIMES EFFECTIVENESS

FIG. 6.3.10.4

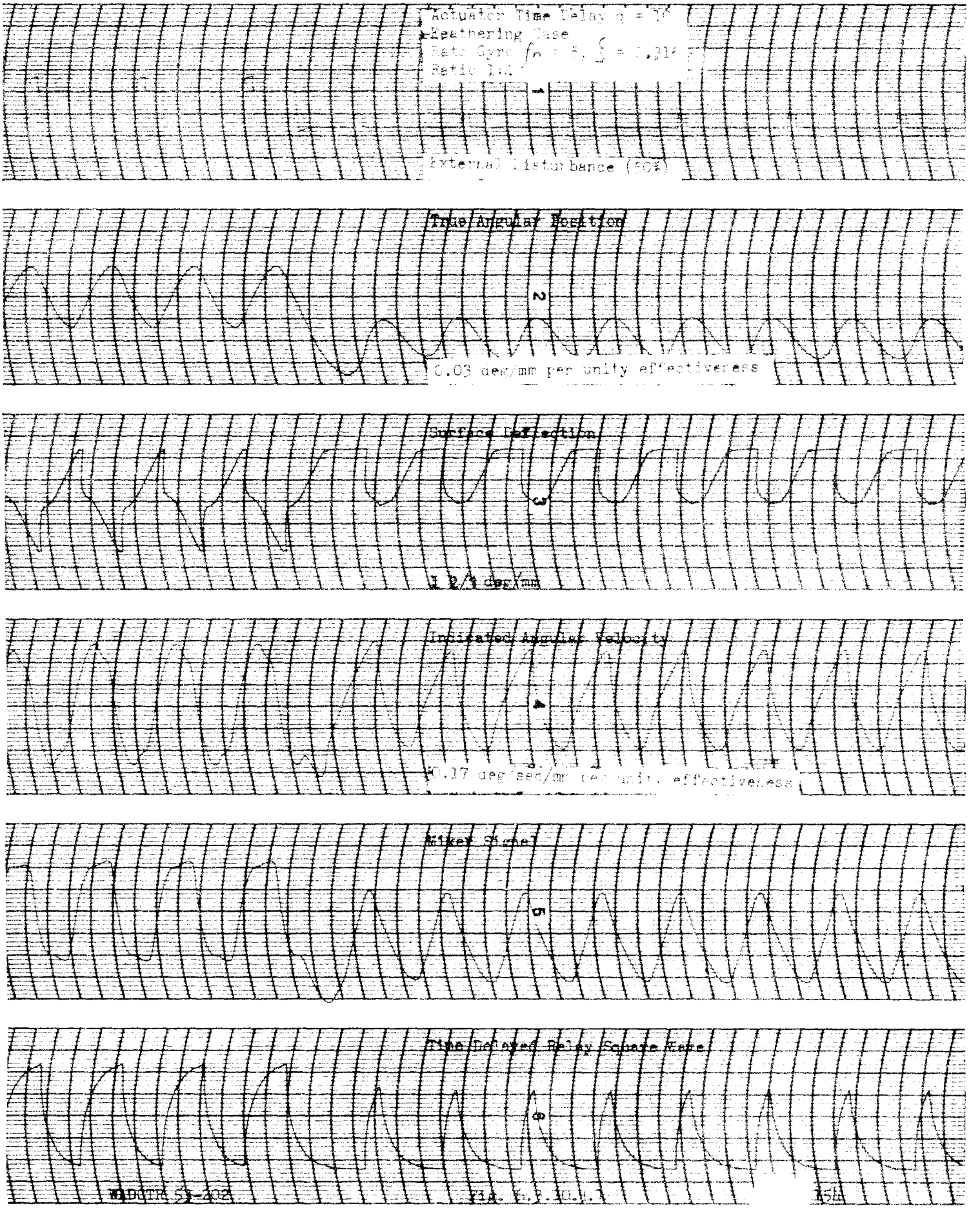
Actuator Time Delay τ = .1
Feathering Case
Rate Gyro fn = 5, ζ = .314
Ratio 1:4
1
External Disturbance (60#)
True Angular Position
2
0.03 deg/mm per unity effectiveness
Surface Deflection
3
1 2/3 deg/mm
Indicated Angular Velocity
4
0.17 deg/sec/mm (per unity effectiveness)
Mixer Signal
5
Time Delayed Relay Square Wave
6

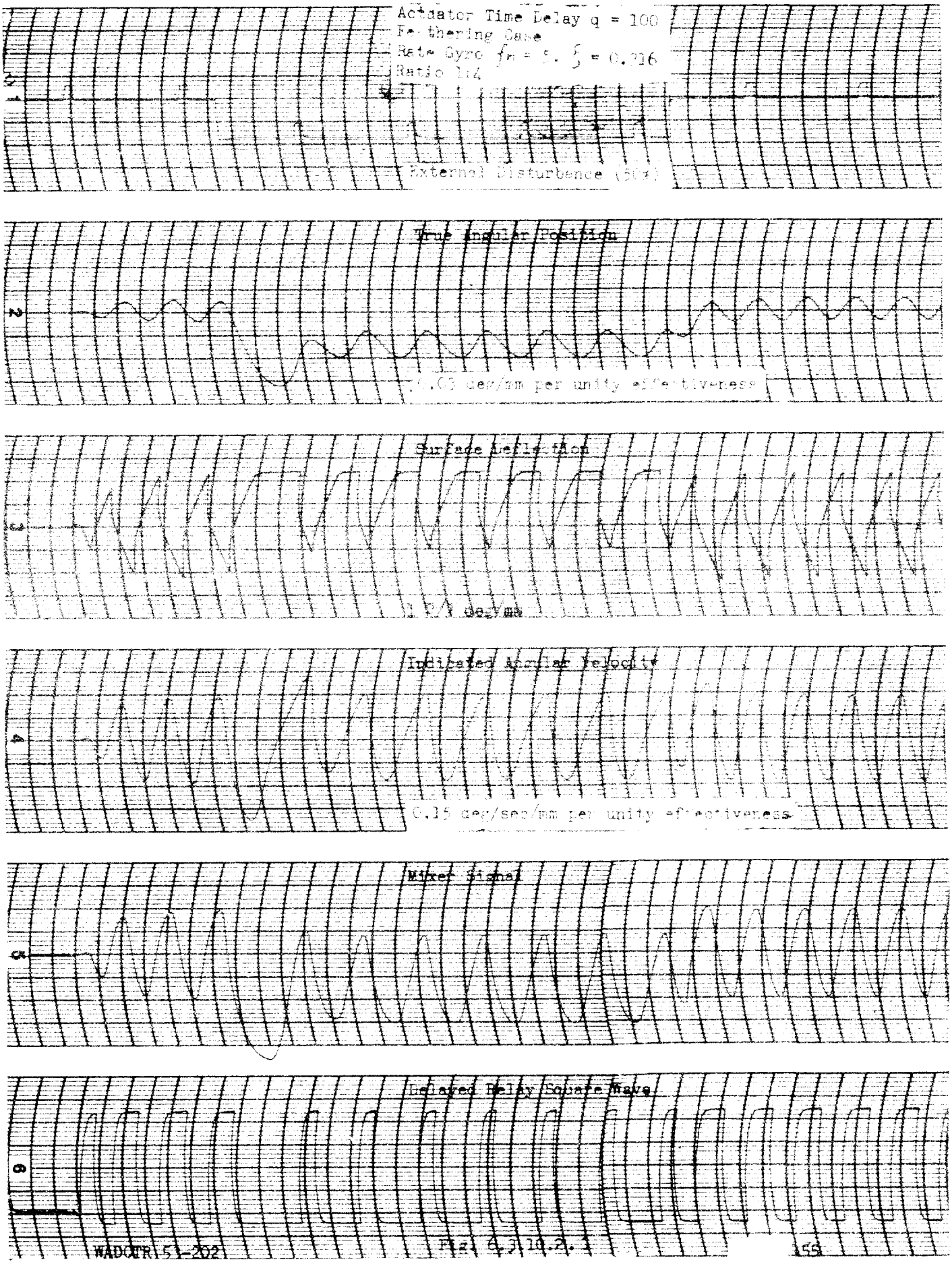
Actuator Time Delay q = 100
Feathering Case
Rate Gyro f_n = 5, ζ = 0.216
Ratio 1:4
External Disturbance (50%)
1
True Angular Position
2
1.0 deg/mm per unity effectiveness
Surface Deflection
3
1.0 deg/mm
Indicated Angular Velocity
4
0.15 deg/sec/mm per unity effectiveness
Mixer Signal
5
Delayed Relay Square Wave
6